Unwritten Procedural Modeling with the Straight Skeleton

This thesis has been composed by the student —
Tom Kelly

Submitted in fulfilment of the requirements for the degree of
Doctor of Philosophy

School of Computing Science

College of Science and Engineering

May 2013

Available online http://goo.gl/whgo6j

Abstract

Creating virtual models of urban environments is essential to a disparate range of applications, from geographic information systems to video games. However, the large scale of these environments ensures that manual modeling is an expensive option. Procedural modeling is a automatic alternative that is able to create large cityscapes rapidly, by specifying algorithms that generate streets and buildings. Existing procedural modeling systems rely heavily on programming or scripting — skills which many potential users do not possess. We therefore introduce novel user interface and geometric approaches, particularly generalisations of the straight skeleton, to allow urban procedural modeling without programming.

We develop the theory behind the types of degeneracy in the straight skeleton, and introduce a new geometric building block, the mixed weighted straight skeleton. In addition we introduce a simplification of the skeleton event, the generalised intersection event. We demonstrate that these skeletons can be applied to two urban procedural modeling systems that do not require the user to write programs.

The first application of the skeleton is to the subdivision of city blocks into parcels. We demonstrate how the skeleton can be used to create highly realistic city block subdivisions. The results are shown to be realistic for several measures when compared against the ground truth over several large data sets.

The second application of the skeleton is the generation of building's mass models. Inspired by architect's use of plan and elevation drawings, we introduce a system that takes a floor plan and set of elevations and extrudes a solid architectural model. We evaluate the interactive and procedural elements of the user interface separately, finding that the system is able to procedurally generate large urban landscapes robustly, as well as model a wide variety of detailed structures.

Ron Poet, Peter Wonka, Paul Cockshott & Pascal Müller:
for letting me build some crazy things.

The Crow Road:
for keeping me sane while building them.

Table of Contents

List of Figures

Chapter 1

Introduction

1.1 Motivation

Figure 1.1: *Hour glasses at the London Science Museum.*

We may ask ourselves how we would create a single model that could create all of the hour glasses in Figure 1.1. This is the goal in *procedural geometric modeling* – we have no definitive way to do this today, but in this document we hope to take some steps towards a solution.

Whilst a standard 3D work flow might allow a user to create a single hour glass of a specific dimension and design, a procedural modeling system might let a user create an algorithm that produces a glass of any given dimension.

Procedural geometric modeling (*PGM*) is a field studying algorithms that compute geometry. A procedural model consists of a sequence of parametrised operations that are able to automatically construct a variety of geometric forms.

The additional level of abstraction offered by PGM has significant benefits over single-instance modeling, but introduces a number of challenges. The advantages of PGM

include:

- An arbitrary quantity of geometry can be created to describe a virtual environment in constant time; the time it takes to construct the procedural model.
- The removal of the existing restriction that the size of a virtual environment is proportional to the time spent creating it.
- The quality of the environment is consistent at no additional cost.
- Procedural geometry tools could lead to runtime environment generation. A virtual world can be generated as the user explores it, giving an experience with more variety and less repetition to the user [97].
- Procedural methods offers the potential to generate content that reacts to various stimuli. For example it could respond to current hardware availability, to users' level of expertise, the length of their attention span, or the medium on which it is presented.

One particular application that has become a testbed for the concepts of PGM is urban modeling. In 2010, half of the people in the world lived in cities, and this fraction is increasing. Cities form the backdrops to large portions of our lives; the way they are designed, how they look, how we think about them, and how we get around them directly affects us all. With the rise of computer graphics, creating cityscapes in virtual worlds has become a common task in a wide range of disciplines such as architecture, city planning, 3D cartography, video games and cinema.

However, creating virtual representations of cityscapes is expensive. At the crudest level, paying an artist to attach a door-handle to every door in every building in a town is costly. Alternately we may obtain 3D city geometry by reconstructing photographs, but obtaining the photos is difficult, and the results often have a lot of noise. Furthermore, the cities that we wish to model may not yet exist, may have only existed before the invention of photography, or be entirely fictional. PGM offers a solution to these issues by promising to generate large quantities of characteristic geometry very quickly. The real world applications of urban procedural modeling are growing, recent examples include —

- Masdar is a new city, designed and built entirely on undeveloped land outside Abu Dhabi. The initial project is intended to be completed in 2015 and will cover $10^6 m^2$[266]. Given the large quantity of architecture that had to created, one of the designers turned to PGM, in the form of CityEngine[66] to design the Swiss Quarter of the city[67].

- Video games can use procedural technology to create new locations as the player explores. For example Dwarf Fortress [78] generates the terrain, structures and inhabitants of a virtual world procedurally. In this situation the key advantage is that a player may continually explore and discover unique structures, that neither they, nor anyone else, have seen before.

- When the first *Superman* movie was filmed in 1978 computer graphics were in their infancy. To give the appearance of Superman flying, Christopher Reeve was composited on top of footage from New York City, as a stand in for the fictional city of Metropolis. In contrast the 2013 release of *Man of Steel* portrayed the same fictional city, this time generated using the PGM tools Houdini[219] and CityEngine[103]. The advantages of PGM in this situation is that an entirely unrecognisable yet realistic fictional city could be created. Additionally, because the model was digital it could be realistically destroyed by a physical simulation of the alien invaders.

Given the promise of PGM, it makes sense to question why it isn't the standard technique for geometry creation. Designing procedural models is more complex; the designer must not just design a single item of geometry, but a continuum. Current state-of-the-art systems rely extensively on programming paradigms for users to construct useful and powerful procedural models. In summary, the drawbacks of current PGM include —

- Designers must undertake the more complex task of designing a class of geometry, rather than a single instance.

- Traditional artists are not familiar with classical methods of describing algorithms, such as programming languages.

- Traditional software engineers do not possess a classically trained sense of aesthetic.

- There are a large number of use cases of PGM, with each likely to require different solutions.

In this thesis we are concerned with removing several of these drawbacks, specifically the requirement that current PGM systems require considerable programming expertise.

1.2 Hypothesis

We propose that a geometric construct, the *straight skeleton*, and its generalisations, are a powerful technique for the creation of PGM systems that are accessible to people without programming skills. Systems exploiting these skeletons and variations thereof are able to generate large scale, varied and highly realistic results within the domain of urban procedural modeling.

1.3 Contributions

Our contributions to the corpus while examining the above hypothesis include:

- A simplification of existing straight skeleton events, the *generalised intersection event*.
- A novel skeleton, the *mixed weighted straight skeleton*.
- A method and evaluation of a system for procedural modeling of city lot shapes using the straight skeleton.
- A method and evaluation for the procedural modeling of architectural shells using the MWSS.

The papers written in the course of this thesis were:

- *Interactive Architectural Modeling with Procedural Extrusions*[121]
- *Procedural Generation of Parcels in Urban Modeling*[252]

1.4 Overview

To lay the ground for this work Chapter 2 examines existing work, and describes the properties of existing procedural systems. We continue to analyse the straight skeleton in Chapter 3 and to apply the skeleton to the problem of urban procedural modeling in Chapters 4 and 5.

The following chapter samples the wide range of tools available for the generation of 3D geometry. In particular we observe that an offset mechanism driven by the straight skeleton is a powerful accompaniment to a written programming language. This insight lead us to examine skeletons in greater detail.

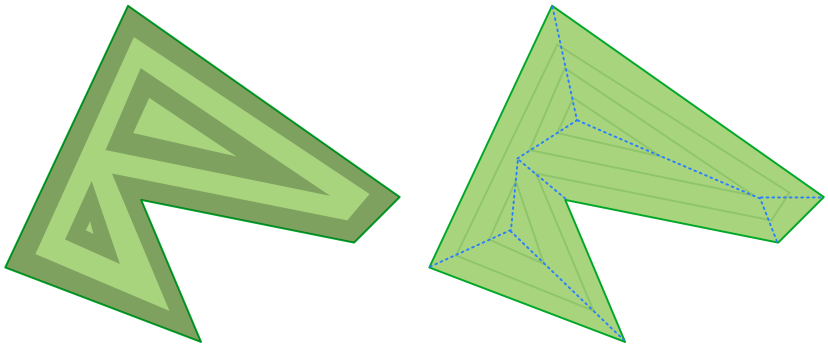

Figure 1.2: *Left: A shrinking polygon. Right: The arcs of the straight skeleton (blue) are formed by tracing the edges of the shrinking polygon.*

The straight skeleton is a geometric construct that subdivides a 2D shape, as introduced in Fig. 1.2. In Chapter 3 we analyse this construct and develop the theory behind the types of degeneracy encountered when computing the straight skeleton. By relaxing the constraints on this structure we introduce a novel variation, the mixed weighted straight skeleton. In addition we introduce a simplification of existing skeleton events, the generalised intersection event. These skeletons have interesting non-trivial properties, such as being able to split concave shapes into two, introducing holes into faces, and leaving behind "arcs" which form part of the centrelines of a shape. It is these emergent properties that we found we could exploit to create an expressive range of procedural geometry.

The first application of these properties is to the problem of subdividing city blocks to many parcels of land. We introduce the first complete algorithms and evaluation of block subdivision within computer graphics. In addition, we demonstrate how subdivision can take place without additional end user programming by presenting a parameterised algorithm that utilises the straight skeleton, as illustrated in Fig. 1.3. The results of this system are presented at the end of Chapter 4, and evaluated favourably again real-world subdivisions and existing block subdivision schemes.

The second application is the creation of solid architectural models. By using a novel generalisation of the straight skeleton, Chapter 5 demonstrates how to create complex architectural models, containing features such as buttresses, chimneys, bay windows, columns, pilasters, and alcoves. We introduce two user interfaces, one for the interactive specification of such geometry, and another for the procedural generation architectural models from floorplans over wide areas, as shown in Fig. 1.4. The system is evaluated both for its expressiveness, by modeling a wide range of existing architecture, and robustness, by automatically generating a large cityscape.

We conclude in Chapter 6, arguing that procedural geometric modeling without written programming languages is possible using the straight skeleton. Systems exploiting these

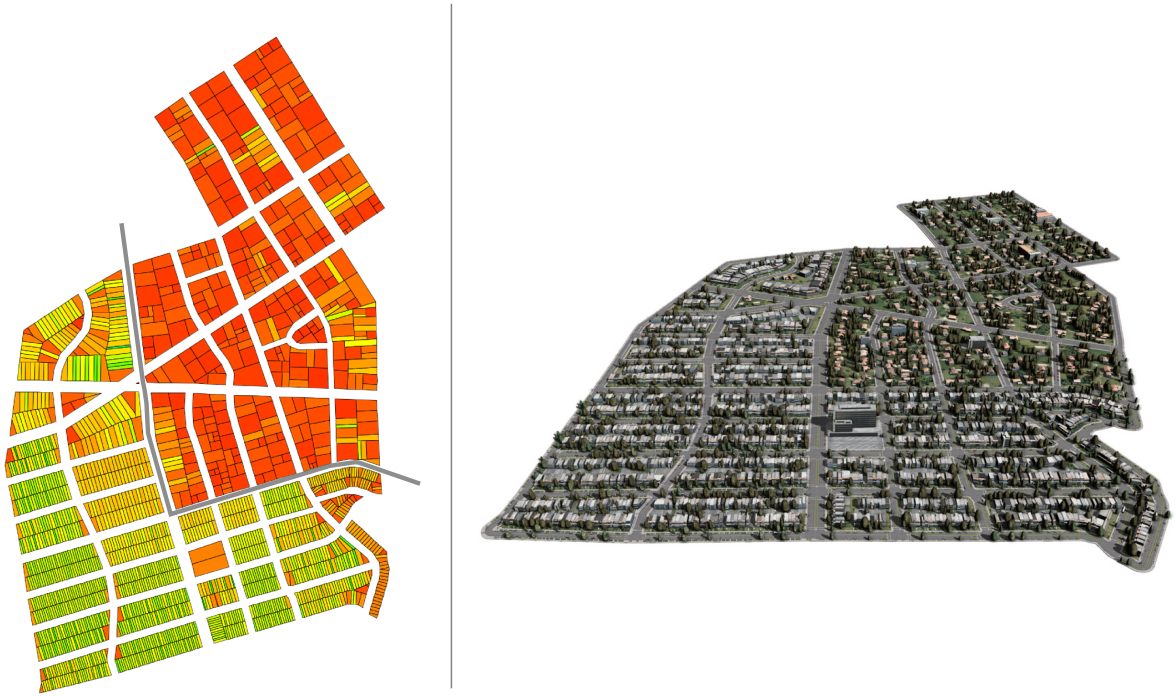

Figure 1.3: *The results of our parcel subdivision algorithm within CityEngine. Left: The parcel subdivision generated with both skeleton (bottom left of grey line) and OBB (top right) techniques; the colouring denotes relative area. Right: the result of the urban procedural modeling pipeline within CityEngine.*

Figure 1.4: *We present an interactive procedural modeling system that is able to model difficult architectural surfaces, such as roof constructions. This figure shows procedural extrusions applied to 6000 floorplans synthesised from a GIS database of Atlanta. Procedural trees were added for decoration.*

skeletons and variations thereof are able to generate large scale, varied, and highly realistic results within the domain of urban procedural modeling.

Chapter 2

Readings: A Spectrum of Proceduralisation

This chapter introduces some of the technical background of procedural modeling within the field of graphics. Procedural modeling is a broad subject that borrows from many established fields; we give an overview of the subject's context within a broad spectrum of proceduralisation.

This spectrum leads from general purpose languages to a specific instance of a model. At one extreme we visit general models that are able to create a wide variety of geometry, for example a programming language (not to be confused with a single program in a language) is capable of creating any geometry we can describe. As we progress we visit models that only work within a specified domain or produce models similar to an example. At the most specific end of our spectrum we visit "models" that are only single instances, such as a 3D mesh of a bunny.

A general language can describe any computable geometry, while an instance is a single, unchanging, object. However an instance is ready to use, while a language takes considerable specialisation to create any results. Furthermore, an instance requires no intelligence on the part of the user and guarantees good results, while a fully general language requires lots of intelligence and provides no assurances as to the final quality of the geometry.

In line with the content of the thesis this section will provide an emphasis on those techniques relevant to urban procedural modeling, although context is provided by sketches of the surrounding topics. We begin by examining the most general geometry production systems — languages, grammars and their variants, before moving onto the more specific combinatory modeling approaches, simulation and inverse procedural modeling techniques. The most specific techniques form the end of our spectrum — shape deformation and 3d tools.

```
public void paint( Graphics2D g )
{
  int count = 1;
  do
  {
    g.rotate( Math.PI/2 ) ;
    g.scale( 1+ (count/100.),1+ (count/100.)) ;
    for (double d : new double[] {0, Math.PI})
    {
      g.rotate( d );
      g.translate( -50, 0 );
      g.draw( new Arc2D.Double( -5, -5, 10, 10, 90, 180, Arc2D.OPEN ) );
      g.translate( 50, 0 );
    }
  } while (count++ < 20);
}
```

Figure 2.1: *A small example of a 2D geometric program in Java.*

There are two common uses of the word *model* in PGM — to represent some system that may create some geometry ("a grammatical model of architecture"), and to refer to the geometry itself ("the 3D bunny model"). In this chapter we will attempt to only use the former description, reserving *model* as a synonym for *system* to avoid confusion.

2.1 General Purpose Programming Languages

We first encounter an extreme – the general purpose programming language. Predominantly these languages are text-string based and Turing complete[245], such as FORTRAN[114], Haskell[110] or Java[86], Fig. 2.1. Appropriate libraries and interfaces allow these languages to create descriptions of geometric objects.

Being general, these languages can describe any computable geometry. However doing so is quite complex, especially for users unable to write programs. In particular a random string is most likely not a valid program, while a particular random program will be unlikely to create geometric output.

There are a wide variety of libraries available to generate geometry via a general purpose programming language. Many of the original library functions were intended to interface with graphics hardware such as OpenGL[270], others were languages for realistic rendering, such as RenderMan[247]. More recently higher level interfaces have emerged such as Open Inventor[262] and the Generative Modeling Language[105] (GML). Havemann introduced GML to construct procedural graphical primitives via Euler operations to generate meshes, which may be interrupted as multi-resolution

$$
\begin{array}{lcc}
N & = & A, B \\
\Sigma & = & a, b \\
S & = & A \\
P & = & \begin{array}{|ccc|}
\hline
\text{A} & \rightarrow & \text{Bb} \\
\text{A} & \rightarrow & \text{a} \\
\text{B} & \rightarrow & \text{Ab} \\
\hline
\end{array}
\end{array}
$$

Figure 2.2: *A Chomsky type 3 grammar that produces a regular language. A rule $x \rightarrow y$ indicates that the symbol x may be replaced by the symbol y.*

string	via rule		
A		S	
Bb	A	$\rightarrow$	Bb
Abb	B	$\rightarrow$	Ab
Bbbb	A	$\rightarrow$	Bb
Abbbb	B	$\rightarrow$	Ab
abbbb	A	$\rightarrow$	a

Figure 2.3: *The derivation of a string in the language defined in Fig.2.2. The language defined is the symbol* a*, followed by an even number of the symbol* b*; there are an infinite number of strings in this language.*

subdivision surfaces. GML has been applied to several procedural domains such as Gothic windows[106], castles[81] and underground infrastructure[155].

2.2 Formal String Grammars

Procedural modeling has been strongly influenced by the study of grammars. There are a wide range of grammars, each with different properties[44, 204], however a geometrically useful subset is given by the Chomsky hierarchy[42]. A formal grammar is a concise definition of a language. A language is a (often infinite) set of all the allowable strings of symbols from a fixed alphabet. Eventually we will introduce geometric interpretations of these strings for PGM, but formal grammars are concerned with the generation of these strings alone. The range of languages expressible by formal grammars are a subset of those recognisable by the general languages, a specialisation within our procedural spectrum.

A formal grammar consists of a set of non-terminal symbols, N, a set of terminal symbols, Σ, a set production rules, P, and a start symbol, $S \in N$. An example is given in Fig. 2.2.

The initial string consists of a single character, S, which is repeatedly altered by the production rules. During this manipulation the current string consists of a mix of

Chomsky designation	rule format	language name
type 3	$n_1 \rightarrow \sigma_1$	(left) regular
	$n_2 \rightarrow n_3\sigma_2$	
type 2	$n_4 \rightarrow \phi_1^\bullet$	context free
type 1	$\phi_2^\bullet n_5 \phi_3^\bullet \rightarrow \phi_2^\bullet \phi_4^\bullet \phi_3^\bullet$	context sensitive
type 0	$\phi_5^\bullet \rightarrow \phi_6^\bullet$	recursively enumerable

Figure 2.4: *The Chomsky hierarchy of grammars.* $\sigma_x \in \Sigma$, $n_x \in N$ *and* $\phi_x \in \Sigma \cup N$. *Repeated elements from a group are marked* $^\bullet$.

terminal and non-terminal symbols. When only terminal symbols remain in the string the production terminates. The final string is a member of the language defined by the grammar. We evaluate the earlier example in Fig. 2.3.

Different classes of languages can be defined by different forms of production rules. The example in Fig. 2.2 is a *type-3* grammar in the *Chomsky hierarchy*. A type-3 language may replace a single non-terminal symbol, with either a terminal symbol, or a non-terminal symbol followed by a terminal.

Type-3 grammars define the set of *regular* languages. A more expressive grammar may be allowed to replace the symbol with a longer string (a type-2 language), examine the context of the single symbol to be replaced (type 1), or replace any string with any other (type 0). Chomsky named this increasingly powerful hierarchy of grammars as types 2, 1 and 0, as shown in Fig 2.4. Each expresses a super-set of the languages of the previous type by relaxing the restrictions on the context of the replaced symbols.

There are a wide variety of other string rewriting systems[124]. For example, if we remove the distinction between terminal and non-terminal symbols, and the requirement for a single starting symbol, then we instead have a *semi-Thue process*[49]. Another variation is a *parallel grammar*, which applies a rule to every symbol in the string with each iteration. If we use a parallel context sensitive grammar over a symbol set consisting of the binary digits, then we have cellular automata[268], a popular example of which is Conway's *game of life*[80]. 3D cellular automata have been used to create procedural models of creeping plants[90]. Alternately every production rule in a grammar may manipulate attributes associated with a specific instance of a symbol, leading to *attributed grammars*[126]. Finally we may operate on graphs, instead of strings, leading to the concept of *graph-grammars*.

2.3 Graph Grammars

Graph Grammars specialise the concept of string grammars to include a topological element. Instead of replacing a symbol or string, we replace a node or sub-graph of a

graph. Therefore a graph grammar defines a language (a set of) of graphs.

Pfaltz and Rosenfeld introduced graph grammars as *web grammars* in their 1969 paper[186], although their terminology is no longer in popular use. In a similar manner to formal string grammars, the paper describes production rules as triples consisting of a *left* target graph, a replacement *right* graph, and an *embedding function*.

This embedding function describes how the edges to and from a sub-graph of the host matching the left graph will relate to edges in its replacement, the right graph. However, the paper by Pfaltz et al. does not define the structure of this embedding statement, rather descriptions are given in prose. There are a large number of such embeddings function and much of the remainder of the theoretical work on graph grammars concerns itself with the different forms this embedding function may take.

For our purposes a graph, γ, consists of a set of nodes and edges between these nodes. The set of nodes, P, is labelled by a finite alphabet, V. As with string grammars, these labels are either in the set of terminals, Σ, or non-terminals, N. The set of directed edges, E, consists of pairs in (p_1, p_2) where $p_1, p_2 \in P$, and are optionally labelled from V.

A graph grammar is a 4-tuple, $G = (V, N, \gamma_0, R)$, where γ_0 is the initial graph and R is a set of production rules. A production rule $r = (\gamma_l, \gamma_r, E)$, consists of the left and the right graphs, and an embedding function, E.

As with formal string grammars, the host graph is initially γ_0, and production rules are applied until no more nodes or edges with non-terminal symbols exist. A simple graph grammar is given in Fig. 2.5, defining a simple lattice-like language of graphs. However, without well defined embedding functions several questions are unanswered. For example, as each rule is applied, are any edges from the host graph to the right hand side of the graph created? or how are edges to the removed left graph treated?

The two main competing approaches to embedding functions are set-theoretic and algebraic. The algebraic approach utilises category theory to define gluing functions[62], while the set-theoretic approach utilises set-expressions to define the embedding function, typified by [169]. We refer the reader to the citations for the full details, but demonstrate a single production rule from each in Fig. 2.6 and Fig. 2.7.

As with string grammars, there are a large number of variations on the theme of graph grammars. L-systems (Sec. 2.4) inspired *parallel graph grammars*[61]. These divide the graph into covering subgraphs, each of which matches the right hand side of one production rule; each rule is then applied at the same time, in parallel with one another. *Negative application conditions*[170, 94] specify situations in which a particular rule should not be applied. *Programmed graph grammars*, as introduced by

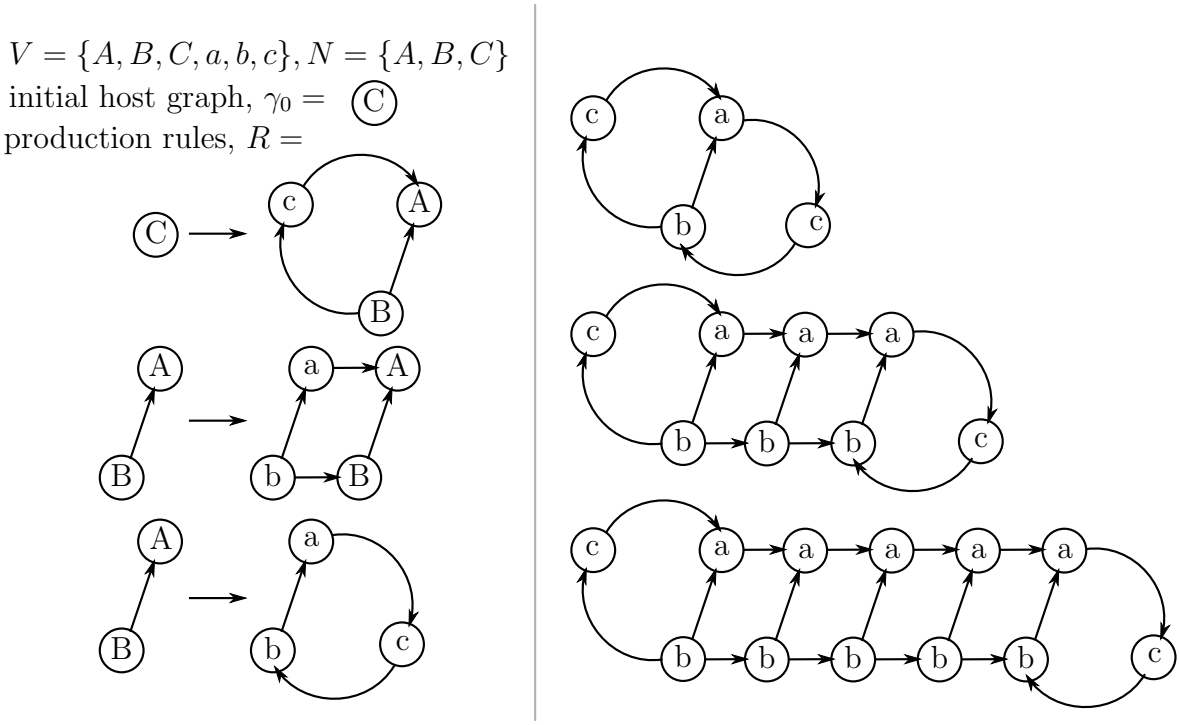

Figure 2.5: *Left: an overly simple graph grammar, overlooking embedding rules. Right: several graphs in the language defined by this grammar. Note edge labels are not shown here.*

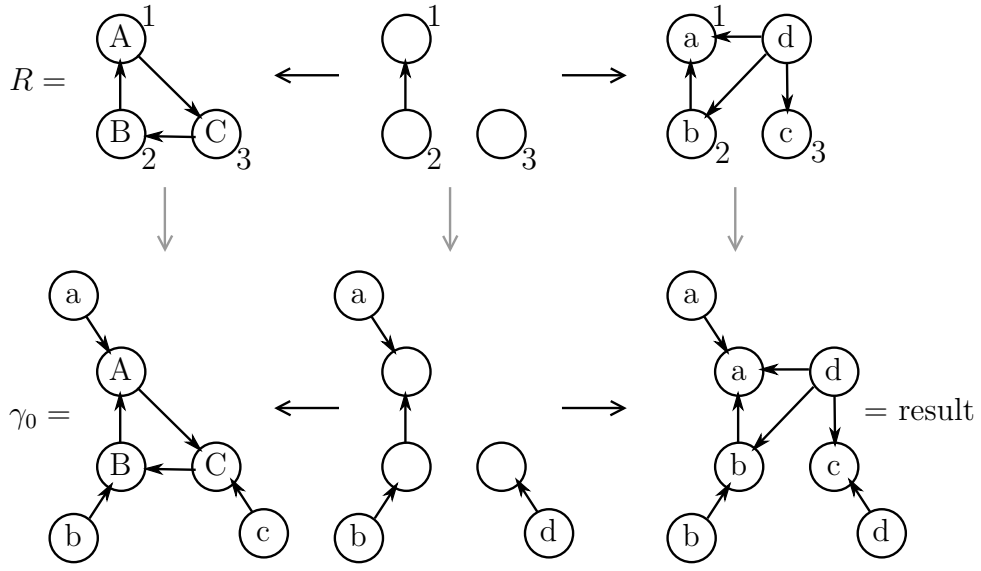

Figure 2.6: *The application of an set-theoretic production rule, R, using the double pushout method[62]. Note that numeric values establish node identity in these diagrams. Top row: the two stages in the production rule. Top left: the left graph to match. Top middle: any nodes to be renamed have their labels removed and edges to be deleted are removed. Top right: the new labels and edges are applied. Bottom: the application of R to a graph (bottom right).*

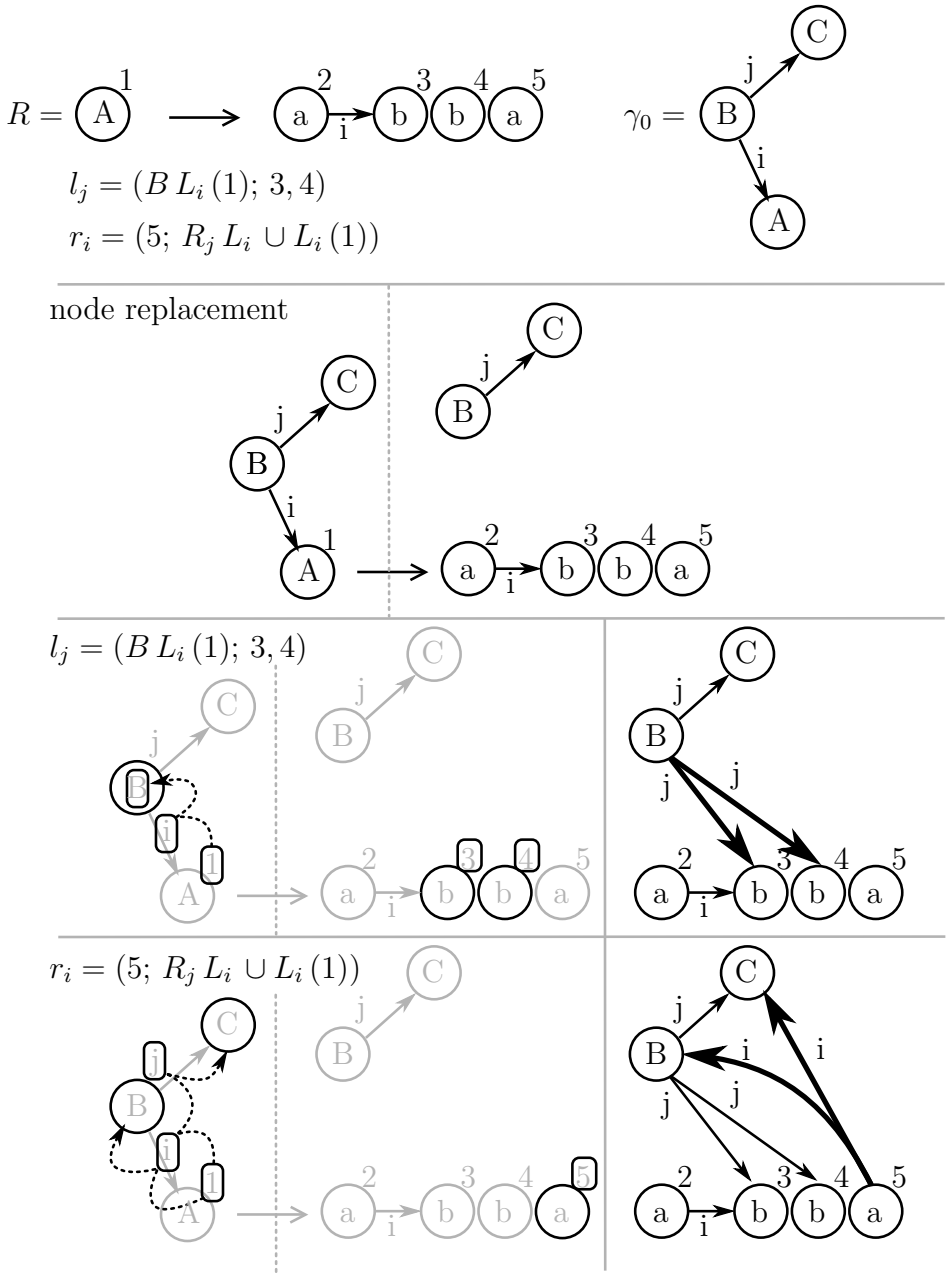

Figure 2.7: *The application of an algebraic production rule using the system specified by Nagl[169]. First row: the rule, R which consists of the left graph, the right graph, and the embedding components l_j, r_i. Numeric node identities are given outside each node in the rule. The graph we will apply the rule to is γ_0, replacing the node labelled A with the right graph (second row). Third row: the application of the embedding l_j creates new edges by walking over the graph (dashed arrows). The origin of the walk is the node with identity* 1*, traversing all outbound edges labelled i and filtering for nodes labelled B. The destinations are the nodes with identity* 3 *and* 4*, the new edges are shown in bold. The embedding r_i proceeds similarly, except the $\cup$ operator performs two walks to use as the destinations. The resulting graph is given in the bottom right.*

Göttler[88], take this concept further and replace the set of production rules with a list of production rules to be applied sequentially, via conditional statements or loops.

Unfortunately identifying matching subgraphs in graphs (to identify the portion of graphs to be replaced) is an instance of the computationally NP-complete *subgraph isomorphism* problem. While there are situations where this complexity is alleviated, such as in the case of planar graphs[64], this complexity may be a reason that graph grammars are not widely used in PGM. Another problem is that graph grammars are no more expressive than string grammars as there is an encoding of any graph in string form (typically an adjacency matrix). This string representation may be manipulated in equally expressive ways via a type 0 string grammar.

In spite of these shortcomings there are several graphical applications of graph grammars, such as the design of technical diagrams[87], production of system flow diagrams [56], the design of a visual languages[91] and CAD-systems[92]. In particular graph grammars offer a topological-oriented description of the otherwise geometry oriented shape-grammars[279], introduced in Sec. 2.5.

2.4 L-Systems

Lindenmayer-systems[142] introduced a *parallel* string replacement grammar in 1968, specifically motivated by the study of plant growth. Unlike the sequential model described by Chomsky, every biological cell in a plant may divide simultaneously. To simulate this, a production rule is applied to every symbol in the string concurrently.

Meanwhile in the 1980's the computer graphics field was producing tree models, these were lacking a formal grammar, such as the tendril-like forms in [119], or the detailed models of specific varieties of trees in [27]. In 1986 L-systems were combined with graphical techniques[193] to produce a graphical interpretation of a grammar's language. This combination of a string grammar and a turtle became synonymous with the term *L-system*. In binding their domain to graphics, and usually botany, L-systems are a more specialised system than formal grammars, the first true procedural geometric modeling system we examine.

A basic L-system specifies a *parallel* string replacement grammar, a number of iterations, a starting string, and a turtle interpreter to create graphical output. Unlike grammars their output is a single result, rather than a language. We define an example L-system in Fig. 2.8,

The string replacement grammar doesn't contain any terminal symbols, and is parallel in that at every derivation step every symbol in the string is replaced by a matching rule.

n	=	8
δ	=	90°
initial string	=	F
production rule	=	F → F+FF+

Figure 2.8: *The description of a simple L-system.*

F
1: F+FF+
2: F+FF++F+FF+F+FF++
3: F+FF++F+FF+F+FF+++F+FF++F+FF+F+FF++F+FF++F+FF+F+FF+++

Figure 2.9: *The first three terms in the evaluation of the string grammar of Fig. 2.8.*

The grammar also differs from a formal string grammar in that there is no distinction between terminal and non-terminal symbols. Instead, a fixed count of parallel rule applications occur, Fig. 2.9, after which the string is interpreted by a *turtle*.

A turtle uses this string to create geometry by evaluating one symbol of the string at a time, using a left-to-right ordering. The turtle's 2D location and rotation is manipulated by each symbol in turn, creating geometry as a side effect, Fig. 2.10. Typical mappings for symbols are F to move the turtle a unit length in the forwards direction creating a line segment as it moves, + or − to rotate the turtle an angle, δ, clockwise or counter-clockwise respectively, [to store the turtle's current location and orientation on a stack, and] to restore it's location and orientation by popping the top location from the stack.

To summarise, a simple L-system is defined by an initial string, S, a number of rule applications, n, a set of production rules, P and a rotation angle, δ.

An extension to these basic L-systems is *context sensitivity* for the string grammar, reminiscent of a move from a type 2 formal grammar in the Chomsky hierarchy to type 1. For example to state that a b between an a and a c should be replaced with a d we would use the notation:

$$a \langle b \rangle c \rightarrow d$$

For example, given the context sensitive L-system in Fig. 2.11, we may evaluate the string grammar as in Fig. 2.12, and finally produce our geometric output, Fig. 2.13.

The result from these systems is generally pleasing given the compact description, and simulates a discrete form of growth as successive evaluations occur. The book *The Algorithmic Beauty of Plants*[194], from which this example was taken, gives a very detailed introduction to the modeling of flora using L-Systems.

A basic L-system has several limitations, including a lack of environmental sensitivity,

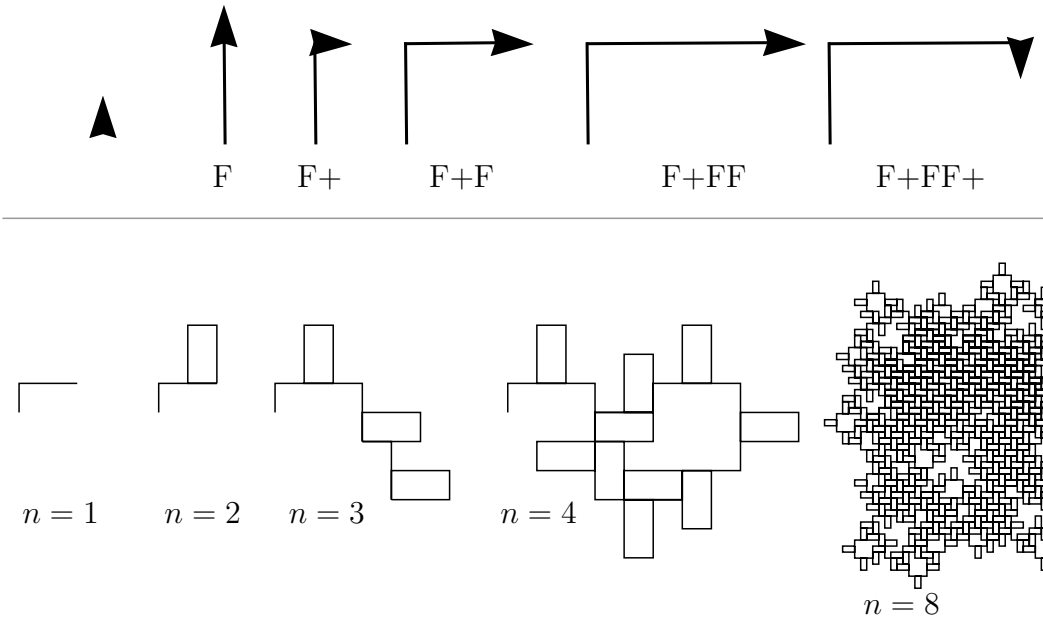

Figure 2.10: *Top, left-right: incrementally constructing a graphical interpretation of a string using a turtle. Bottom: the turtle's evaluation of terms 1,2,3,4 and 8 of the L-system in Fig. 2.8*

n	=	39
δ	=	22.5°
#ignore	=	+-F
initial string	=	F1F1F1

production rules =

0	⟨	0	⟩	0	→	1
0	⟨	0	⟩	1	→	1[-F1F1]
0	⟨	1	⟩	0	→	1
0	⟨	1	⟩	1	→	1
1	⟨	0	⟩	0	→	0
1	⟨	0	⟩	1	→	1F1
1	⟨	1	⟩	0	→	1
1	⟨	1	⟩	1	→	0
⋆	⟨	+	⟩	⋆	→	-
⋆	⟨	-	⟩	⋆	→	+

Figure 2.11: *A self-sensitive string grammar (example 1.31,b from TABOP[194]).*

F1F1F1
1: F1F0F1
2: F1F1F1F1
3: F1F0F0F1
4: F1F0F1[-F1F1]F1
5: F1F1F1F1[+F0F1]F1
6: F1F0F0F0[-F1F1F1]F1
7: F1F0F1F1[-F1F1][+F1F0F1]F1
8: F1F1F1F1F0[+F0F1][-F1F1F1F1]F1
9: F1F0F0F1F1F1[-F1[-F1F1]F1][+F0F0F0F1]F1
10: F1F0F1[-F1F1]F1F0F0[+F0[+F0F1]F1][-F0F1F1[-F1F1]F1]F1

Figure 2.12: *Some statements given in the language. The evaluation of the grammar given in Fig. 2.11 for the first 10 iterations.*

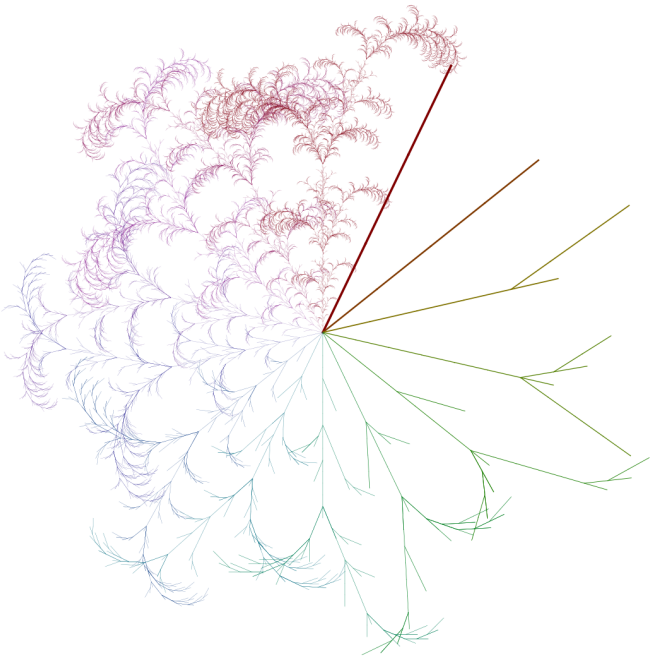

Figure 2.13: *The turtle evaluations of the different L-Systems given by* $n = 0, 3 ... 36, 39$*, as computed in Fig. 2.11. Consecutive systems are evaluated in a different frame, rotated clockwise from vertical. Each evaluation is drawn a factor of* 0.7 *times smaller than its predecessor.*

initial string: $A(0,0)$
production rules:
1 : $A(x,i) \rightarrow S(x)B(x,i)A(x+\Delta, i+1)$
2 : $S(x) \rightarrow @R(0,1,0,0,0,1) + (Y(x))\&(P(c))F(\delta(x))$
3 : $B(x,i) : \{$
if $(i\%2 == 0)\ \theta = 0;$
else $\theta = 90;$
$\} \rightarrow [/(\theta)L(x,i)R(x,i)]$
4 : $L(x,i) : \{$
if$(i\%2 == 0)\{$
$angle = \varphi_L(x);$
$length = h_L(x);$
}else{
$angle = (\varphi_L(x) + \varphi_R(x)) * 0.5;$
$length = (h_L(x) + h_R(x)) * 0.5;$
$\} \rightarrow$ [+ (angle) Organ (length)]
5 : $R(x,i) : \{$
if$(i\%2 == 0)\{$
$angle = \varphi_R(x);$
$length = h_R(x);$
}else{
$angle = (\varphi_L(x) + \varphi_R(x)) * 0.5;$
$length = (h_L(x) + h_R(x)) * 0.5;$
$\} \rightarrow$ [/(180) + (angle) Organ (length)]

Figure 2.14: *A parameterised programmable L-system from[13] to model the biological phenomena of decussate phyllotaxis. The necessity of referring to the previous iteration adds considerable complexity.*

non-realistic rendering and a complex grammar editing process. To overcome these, L-systems have been periodically extended. The remainder of this section explores some of these extensions and their applications:

- *Context sensitive.* As described above, symbol replacement can occur based on the surrounding elements.
- *Stochastic.* Each production rule is given a corresponding probability with which it occurs on each iteration[276]. For example the branching characteristics of a tree may be encoded in a stochastic L-system[196], or the choice of which building to place on a given parcel of land[180] may be made stochastically. While a basic L-system is deterministic in that it always creates the same output, a stochastic L-system may produce different output every time it is evaluated.
- *3D.* By using a three dimensional turtle, instead of the two dimensional standard, three dimensional geometry can be created. For example, [195] uses a two-axis rotation system to manoeuvre the turtle in 3D, while using L-system rules to determine the developmental cycles.
- *Parametric.* Here each symbol is given a set of parameters, and a replacement can only take place if a logical statement associated with the parameters is true [100]. Parametric L-systems are comparable to the parallel case of attributed formal grammars[126]. These parameters can model the flow of morphogens such as genes or hormones[34].
- *Table.* These use a variable table of production rules to simulate step-changes in the applicable rules. For example one table may model the plant in a winter (non-flowering) state, and another the summer (flowering) state.
- *Map.* This early approach to produce a graphical interpreter for L-systems uses a parallel grammar to manipulate a geometric graph as "cells"[141]. Because this system works directly on geometry it is unnecessary to interpret the results using a turtle. Map L-systems are a geometric analog of graph grammars, see Sec. 2.3.
- *Environmentally sensitive.* There has been a large quantity of work to allow L-systems to interact with their virtual environments. Table-L-systems provide a discrete phase-transition in response to external stimuli, while context sensitive L-systems give only topological self-sensitivity. L-systems that are physically constrained by their environment are introduced by [196], although the effect of the plant on the environment are not modelled. To address this issue, bidirectional information exchange is introduced by [167], using physical simulations to

describe the availability of water and light to developing foliage and root systems. Geometrically self-sensitive L-systems are used by Parish[180] to generate road networks; these modify a production rule with both global goals and local geometric constraints.

As they have been extended to overcome their limitations, L-systems have become increasing complex. One case study is that of phyllotaxis, the pattern that plant organs (leaves or flowers) form around the stem; in particular decussate phyllotaxis alternates between pairs of leaves at 90°. It is instructive to compare an L-system for a phenomena such as decussate phyllotaxis from Fig. 2.14, to the same description in a general purpose language, Fig 2.1. It becomes clear that it is more complex to represent this phenomena in parallel production systems than in Java. This suggests an issue for the designer of the L-system in comprehending the consequences of an edit to an L-system. To address this usability issue, there is limited work to reconstruct L-systems from an image representations [220, 210] or user sketches[13], avoiding the issue of writing grammars altogether.

The above argument suggests L-systems are an over simplification of botanical systems, that are not gracefully extended to all observed plant models. It is strengthened by recent research into *physical simulation* to model the Auxin hormones that cause phyllotaxis[216]. More generally, algorithmic botany has moved away from L-systems, towards deeper physical simulations such as the simulation of tropisms in [179] or geometric simulation of the apical meristem (growing tip of a plant shoot) in [171].

There are similarities between programming an L-system and *multicore* (parallel) programming. In particular the current string is reminiscent of the *shared state* of some parallel models of computing, and developmental delay[195] is similar to *message passing*. The similarities suggest that some of the problems of multicore programming may be present when designing large L-systems. These may include synchronisation issues, dead and live locks, as well as race conditions.

2.5 Shape Grammars

In the previous sections we have examined grammars that are formed by production rules over strings of symbols (formal grammars and L-systems), as well as graphs. In contrast, *shape grammars* consist of production rules that match and replace certain *shapes* in a figure. The high level description of the grammar remains the same — a start state is given, and production rules transform it to a shape in the language; however the states and rules are expressed as shapes rather than graphs or symbols.

Stiny and Gips created the concept of shape grammars in 1971[227]. They have since been used in a relatively unchanged form to design a wide range of procedural models within academia. We may position shape grammars in our spectrum of proceduralisation by noting that like L-systems they are constrained to the construction of geometry. They are also Turing complete[84].

In comparison to L-*systems*, shape *grammars* are indeed grammars. They specify a language, a set of valid statements, but do not say which specific sentence should be generated at a particular evaluation. The order of the rules applied may be determined manually or automatically depending on the application.

The formalism behind a shape grammar eventually[223] came to consist of a set of shapes, S, a set of symbols, L, an initial labelled shape, γ_0, and a set of production rules, R; each production rules takes the form $\alpha \rightarrow \beta$. The left hand side, α, specifies zero or more labelled shapes, $(S,\ L)^*$, that are matched against the current shape. The right hand side, β gives a labelled or unlabelled replacement, $\in\ (S,\ L)^+ \cup S+$. As with the previous grammars, we begin with γ_0, applying rules until all symbols have been removed. At this point the current shape, γ is an element in the language defined by the grammar.

In contrast to L-Systems, the production rules are not applied in parallel to all matching instances, rather in a serial manner reminiscent of Chomsky grammars[41]. Given the lack of restrictions on the context of the shape, we may see similarities to a type-0 Chomsky grammar.

An example of a very simple façade shape grammar is given in Fig. 2.15, left, using the symbols $L = \blacktriangle, T$. We show the evaluation of one shape in the language in Fig. 2.15, right, by repeated production rule application until no symbols remain. Various other shapes in the language are shown in Fig. 2.16.

A single grammar production rule can often be matched to an infinite number of positions on the current shape by matching *subshapes*. For example a rule containing an arc may be positioned at an infinite number of points around a circle, as in Fig. 2.17.

Given this flexibility of rule application, it is a natural that the categorisation of the different varieties of shape-grammars concerns itself with the mechanism for matching α against the current shape, γ, the *subshape problem*. Common variations include:

- the shapes that may be matched — such as only lines, rectangles or curves in 2D or 3D,
- the type of matching that occurs — whether only whole shapes (such as rectangles), or *subshapes* (such as one corner of a rectangle), may also be matched. The

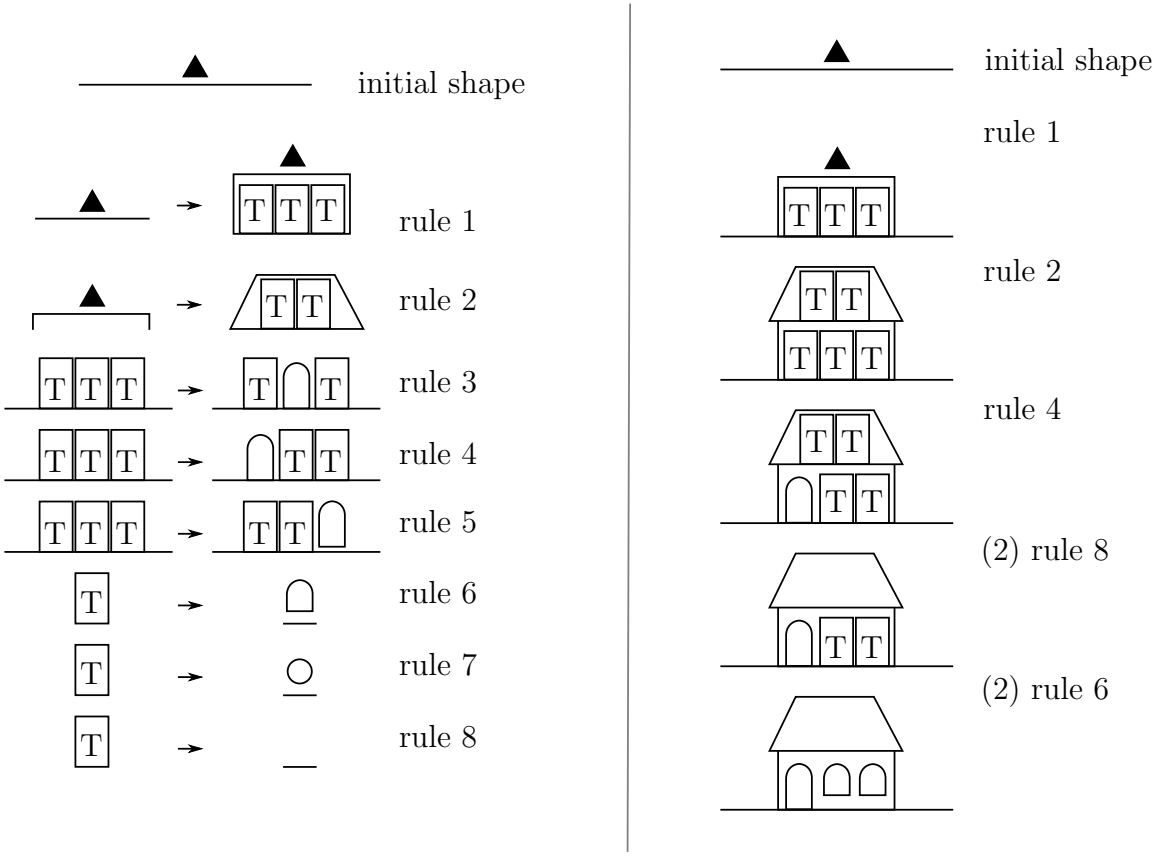

Figure 2.15: *Left: We introduce a shape grammar consisting of 8 shape rules. The shapes on the left of each arrow may be replaced by the shapes on the right of the same arrow. Right: An example derivation of this shape grammar that creates a bungalow. The number of applications of a rule are specified in parentheses.*

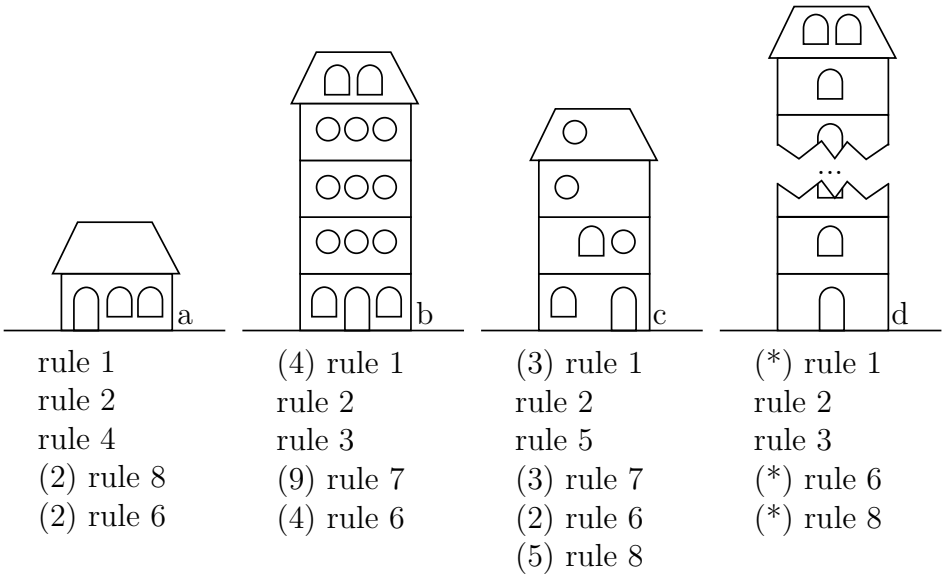

Figure 2.16: *Four evaluations of the shape grammar given in Fig. 2.15, with the rules that created them.*

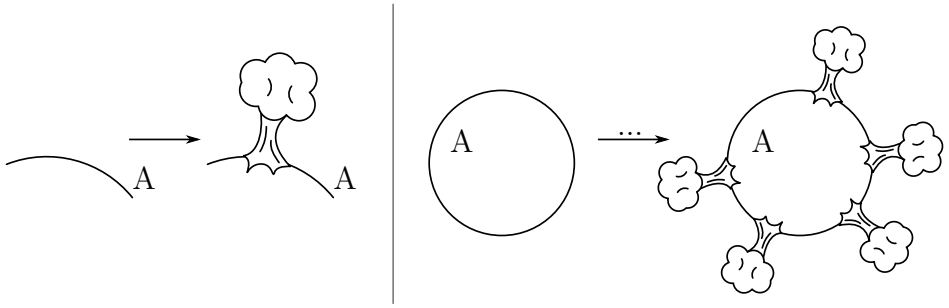

Figure 2.17: *Left: A shape grammar production rule that positions a tree on an arc. Right: If we allow subshape matching under rotation we may position trees at an infinite number of locations on a circle. We show the result of several applications of the production rule upon a circle.*

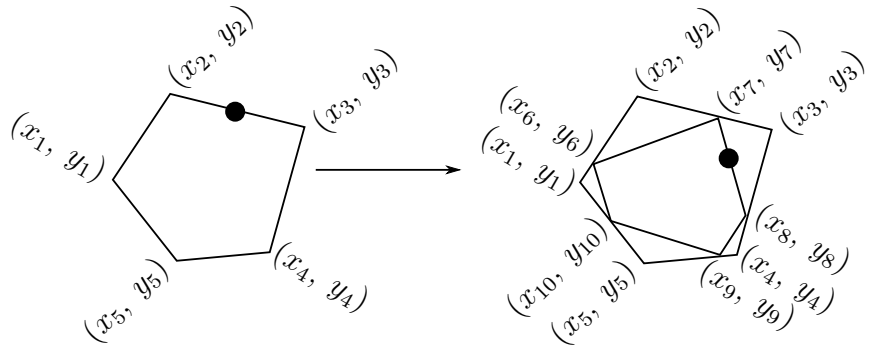

Figure 2.18: *A single parametric shape grammar production rule inspired by[223]. The accompanying schemata might specify that the new point* $(x_6,\ y_6)$ *lies on the line between existing points* $(x_1,\ y_1)$ *and* $(x_2,\ y_2)$*, and similarly for the other new points. This parametrisation permits a language of nested pentagons to be defined.*

advantage of subshape matching is that it allows more "emergent" (unexpected) shapes to be generated,

- the transform we are allowed to apply to *alpha* to locate a match — such as isometries, rigid transforms or affine transforms, and
- whether any parametrisation of α is allowed.

These *parametric shape grammars*[223] are variants which allow the arbitrary parametrisation of production rules. We show an example parametric rule in Fig. 2.18. There are no computational limits placed on these rules, and are typically expressed in the corpus by prose[222], or omitted entirely[72]. These parametrisations can be also used to limit the repetition of rules, for example by adding area or height conditions.

The computational complexity of finding potential matches of α in the current shape, γ, the subshape problem, is well studied. The matching of whole labelled shapes has

a linear computational complexity in the number of the current shapes. Therefore there are well developed algorithms and systems for matching rectilinear[131, 130] and curved 2D shapes. However parametric subshape recognition is NP-hard[279], even in the case of a rectilinear shape vocabulary. This has not stopped implementations of the parametric case in 2D[153]. The theory of shape recognition in 3D is addressed by [132], against straight line figures only, while [37] introduces an implementation that limits their use to circles and arcs. The issue of subshape matching with general curves and surfaces in 3D is still unaddressed in the literature.

Despite these complexity issues, shape grammars have been widely applied in academia. The initial examples were artistic drawings[227] and 2D architectural plans[225]. These were extended to 3D isometric plans of houses, generated using parametric shape grammars[128]. 3D shape grammars are less common, and tend to be simple, such as modeling historic soft drink bottles[37]. A wide range of applications have been found for shape grammars include modeling the morphospace of chair-backs[125], Harley Davidson motorbikes[198], and coffee machines[3].

A subtlety of shape grammars are their termination criteria. The language specified by the grammar does not contain all possible evaluations of rule sequences, but only those shapes that do not contain symbols. There are sequences of production rule applications in Stiny's well cited Palladian grammar[225] that lead to dead-ends in which the grammar can never terminate, Fig. 2.19. Of particular issue is the fact that there are no guarantees as to how many times we might have to evaluate statements in the grammar before a valid result in the language is generated.

The lack of a mechanism to specify situations in which a rule cannot be applied causes additional difficulties with self intersection and termination (*negative application conditions* in graph grammar terminology). A shape grammar rule with a β that is a superset of the corresponding α gives rise to an infinite language. We present an example in Fig. 2.16d, in which the façade may be indefinitely tall. This poses the problem of how to stop a sequence like this from intersecting other geometry, especially in non-parametric shape grammars.

Because of the requirement for shapes in the language to not contain symbols, and the infinite nature of certain shape grammars, we may characterise shape grammars as a search through some shape-space. The order of search can either be manually defined (as in most of the corpus) or automated to produce figures automatically[89]. Regardless of the mechanism for choosing rules, sequences of rules will behave in one of the following ways:

- All symbols will be removed, and a figure that the grammar describes will be produced.

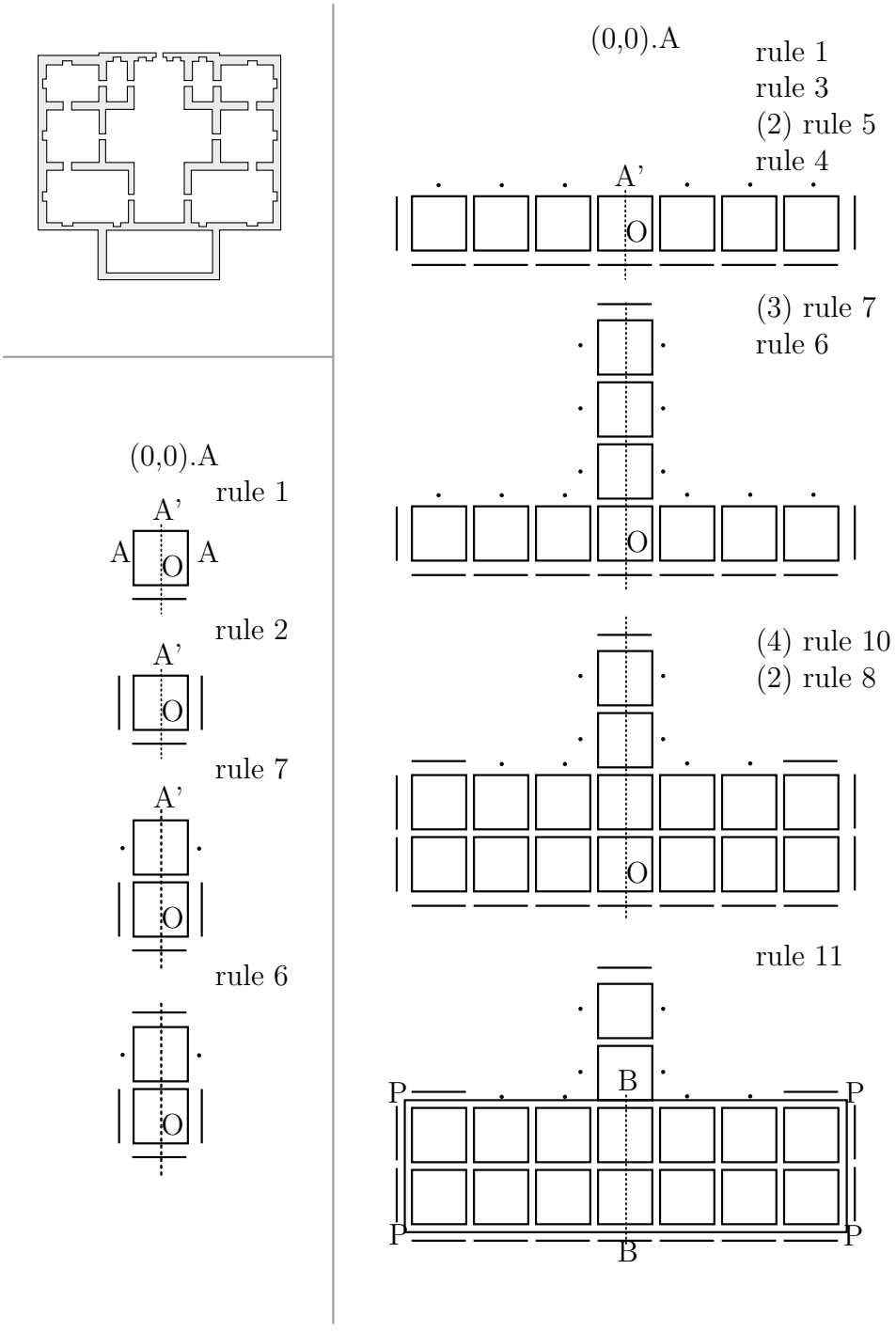

Figure 2.19: *Top Left: An example from Stiny's Palladian shape grammar[225]. Bottom left, right: Example rule sequences in the same shape grammar that lead to dead ends. After these rules, there is no way to remove the symbols* •*, or* O*, leading to evaluations of the grammar that are not in the language.*

- Symbols remain in the figure, but no further rules may be applied. The evaluation stalls at this invalid shape (Fig.2.19).
- The evaluation continues endlessly. Either by force or choice the sequence of applied rules is unending, and evaluation continues indefinitely. There are similar situations in formal grammars, graph grammars and L-systems.

Other common issues surrounding the use of shape grammars are well summarised by [84], for example

- the subshape and termination problems introduced above,
- the design of an adequate interface for the construction and application of shape grammars,
- the lack of robust implementations for parametrised shape grammars,
- the difficulty in application to non-linear geometry, such as curved surfaces,
- the lack of a standardised shape-description, and finally,
- the lack of production grade or commercial systems for working with shape grammars.

2.6 Split Shape Grammars

The computational complexity of classical shape grammars seems to have limited their use to small scale academic projects. However in 2003, Wonka et al. created a specialisation of shape grammars, *split shape grammars*[269], with lower complexity. To simplify their computation, these extend set grammars, initially within a 2D domain of labelled nested shapes and using only whole-shape matching. These grammars have been shown to be well suited to large urban environments, and façade generation in particular.

As the name implies, a split shape grammar consists of production rules that take a labelled shape and split it into a number of covering labelled shapes. Unlike a shape grammar these labels are categorised as terminal or non-terminal. This delegation of area to subsequent rules continues down a hierarchy until only shapes with terminal symbols remain.

A principle assumption is that this hierarchical split operation is well suited to the generation of designed structures. There is ample justification for this assumption in the

literature of early urban modeling pipelines, such as the book *A Pattern Language*[9], which introduces a hierarchy of 35 guidelines for the design of of urban areas, ranging from "major city structures" and "common land" to "structure of the floor and walls" and "furnishing":

"The elements of this language are entities called patterns. Each pattern describes a problem which occurs over and over again in our environment, and then describes the core of the solution to that problem, in such a way that you can use this solution a million times over without ever doing it the same way twice."

The book is representative of the architectural literature in that it purports to present solutions to urban design problems, without providing sufficient details for an computational implementation, for example:

"Pattern 10...Do this by means of collective regional policies which restrict the growth of downtown areas so strongly that no one downtown can grow to serve more than 300,000 people."

This hierarchical split approach to urban languages presented by *A Pattern Language* is quite pervasive in the computer graphics literature, with examples such as [70], [97], [11], and [180] using variations on the theme of a hierarchical urban decomposition.

Returning to Wonka's 2003 paper[269], we observe that this concept of a strict hierarchy in urban design is exploited to simplify shape grammars.

Compared to shape grammars, split shape grammars have the advantages of fast computation and no dead-ends during the evaluation. The subshape problem is bypassed by using a set grammar[224] in which matching takes place based on a whole shape and a symbol. This removes the emergent behaviour of subshape matching, but permits finding all possible shape matches in time linear to the size of the existing figure. While certain split shape grammars may be evaluated endlessly, if they do terminate they are guaranteed to supply a valid shape.

Müller et al.'s later influential paper, *Procedural Modeling of Buildings*[164], extends the concept of a split shape grammar to 3D and introduces a written formalism for split shape grammars, *CGA Shape*. The system has gained widespread use and notoriety as it has been successfully commercialised[66].

A CGA Shape grammar consists of an initial labelled shape and a set of production rules, each with a certain priority. All the applicable rules with the highest priority are executed before others; this priority mechanism is exploited to produce differing

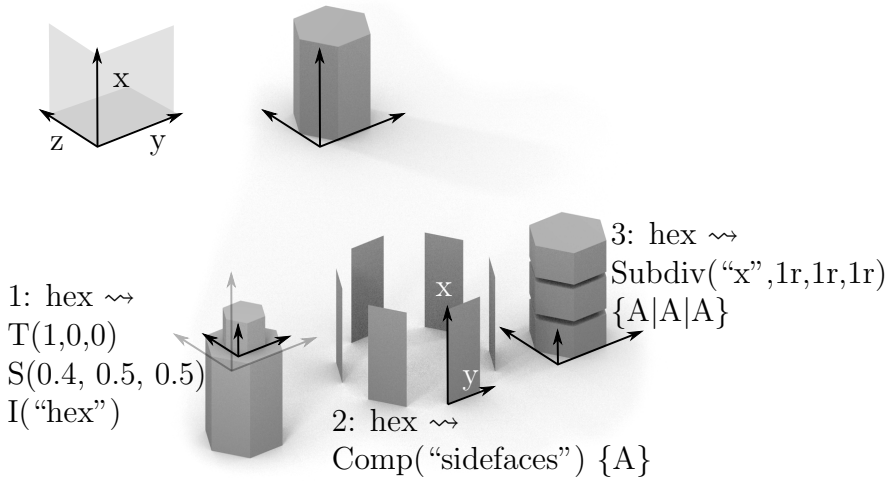

Figure 2.20: *The current scope in a CGA Shape grammar defines a frame and extent for the production rules. Given the initial 3D scope, shown in the top left, and the initial geometry, top middle, we show the result of three production rules. Rule one translates and scales the frame before adding another hexagonal prism of dimension specified by the transformed frame. Rule two performs a component split, creating 2D faces, giving them each their own 2D frame. Rule three subdivides the current shape along the x axis into 3 equally high prisms, and matching scopes.*

geometry based on the required level of detail. Models with higher details are generated by executing rules with lower priority.

To define the reference frame for the production of geometry, a scope is introduced that defines a frame, as well as an extent, as in Figure 2.20. This is reminiscent of an L-system's turtle. When geometry is created, the scope defines the size, location and orientation. When the current shape is split, the scope defines the orientation and number of splits.

A production rule of a given priority in CGA Shape consists of a unique ID, a parametric symbol to match on, an optional condition, a labelled successor shape that is generated, and a probability with which the rule will be applied: *id: predecessor : cond* ⇝ *successor : prob.* The successor operation has an involved syntax that is able to manipulate the scope via transforms, splits, repeats and dimension reduction. A 2D example is given in Fig. 2.21. The condition is used to limit the applicability of the rule, for example to shapes of a certain size, or if certain occlusion conditions are met. These occlusion queries form a domain-specific environmental sensitivity that is used, for example, to stop the production of windows occluded by roof geometry. This is the only context sensitivity available in the system.

Split shape grammars have been successfully applied to the reconstruction of several historical sites such as Mayan ruins[168], the ancient Roman city of Pompeii[163, 58]

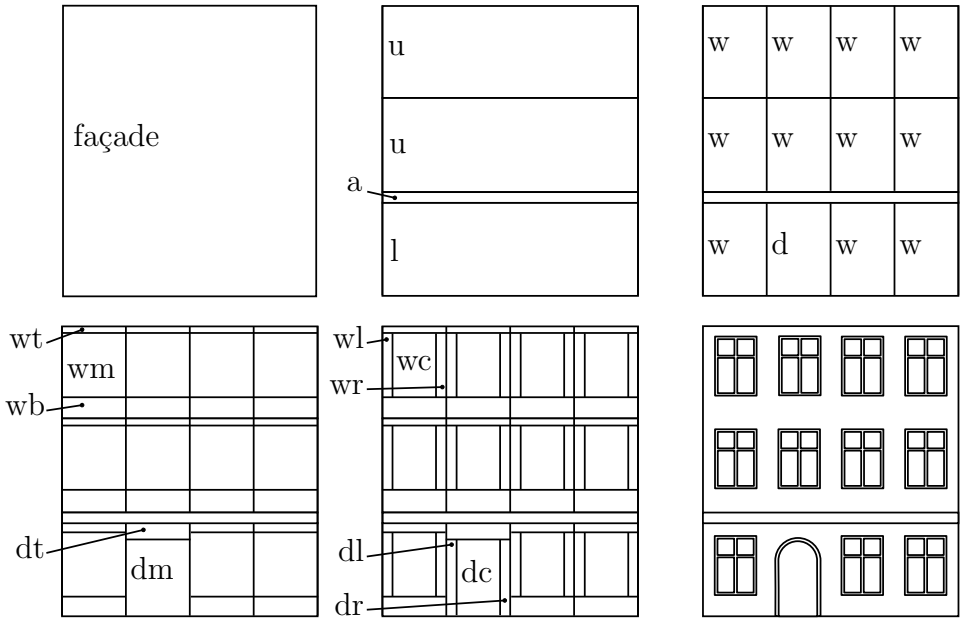

1: façade ⇝ Subdiv("X", 2, 0.2, 1r, 1r){l|a|u|u}
2: u ⇝ Repeat("Y", 1.5){w}
3: l ⇝ Subdiv("Y", 1.5, 1.5, 1.5, .1.5){w|d|w|w}
4: w ⇝ Subdiv("X", 0.3, 1r, 0.1){wt|wm|wb}
5: d ⇝ Subdiv("X", 1r, 0.3){dt|dm}
6: wm ⇝ Subdiv("Y", 0.15, 1r, 0.15){wl|wc|wr}
7: dm ⇝ Subdiv("Y", 0.15, 1r, 0.15){dl|dc|dr}
8: wc ⇝ I("window")
9: dc ⇝ I("door")

Figure 2.21: *The production of a façade in CGA, top, via the given grammar, bottom. Rule 1 splits the façade into 3 floors and a architrave (top middle). Rules 2 & 3 create repeating windows and doors according the floor (top right), while rules 4–7 further refine the window and door positions. Rules 8 & 9 position geometry to create the doors and windows (middle right).*

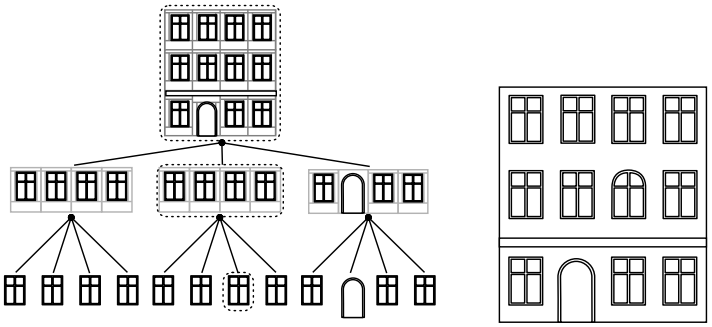

Figure 2.22: *The instance locators of Lipp et al. [144] identify a component by its position in a derivation tree (left). After each production rule the index referred to (dashed lines) can be stored relative to the start, middle or end of the split sequence. The instance locator can be used to store modification to a procedural object, such as a modification to the style of a window, right.*

and Malay houses[206]. Novel uses of split shape grammars include the presentation of uncertainty in archaeological findings by presenting several derivations of a grammar[96], and animatable articulated objects structures[112].

Writing the production rules for split grammars is somewhat involved and required specialist knowledge. Several attempts have been made to simplify the process. The first presents the production rules as a graph[183], giving an understanding of the relationship between application possibilities of the rules. However using this system requires the user to comprehend the underlying grammar before using it. An alternative is given by Lipp et al.[144], who allows the user to construct a grammar by editing an example instance. By constraining the modeling tools to those that may be translated to production rules, the user is able to quickly produce a PGM without interacting with the grammar itself. When a user edits a single feature in an example instance, this edit must be encoded into the grammar, in a persistent manner. To do this Lipp introduces *instance locators* to store user edits in a split shape grammar, Fig 2.22.

Strict hierarchy and *over-compartmentalisation* can cause problems when working with shape grammars[107]. For example sharing information about the number of elements in a façade, as in Fig. 2.23, left. Additional difficulties are caused by problems placing objects over two or more disjoint portions of the hierarchy, as in Fig. 2.23, right. In these situations it is necessary to re-write the grammar to add a new shape, or to add some portion of the shape to two separate portions of the hierarchy. Recently work has begun to address this issue by creating connection patterns between portions of two different shape grammars[129]. The problem of over-compartmentalisation is uniquely critical to split shape grammars; while some shape grammars do use such a hierarchy[225], many do not[146, 128].

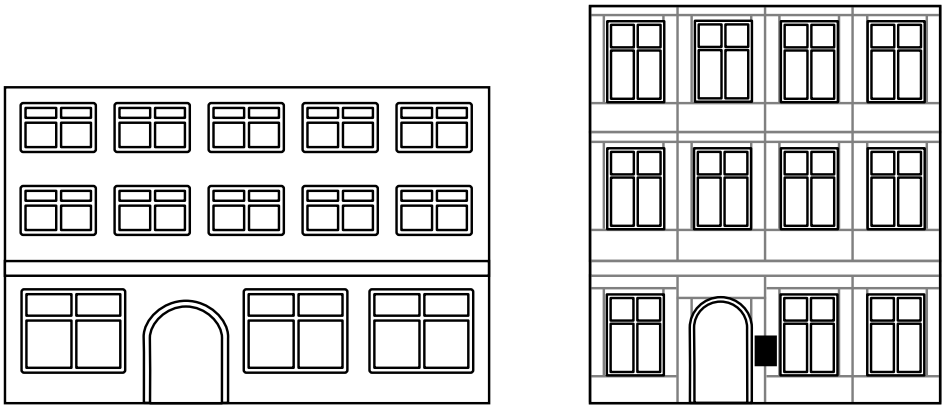

Figure 2.23: *Left: The strict hierarchy may cause problems for coordinating features, as in this evaluation of the grammar of Fig. 2.21, showing a lack of synchronisation between the ground floor and upper windows. Right: The over-compartmentalisation means that it is impossible to place some features that cross over the hierarchy's bounds, such as positioning an intercom near the door (black rectangle).*

2.7 Data Flow Programming

Data-flow graphs are a model of parallel computation introduced as an alternative to the classical von Neumann model.

Written imperative programming languages are typically a 1D sequence of symbols which explicitly sequence instructions. This ordering of instructions is typically associated with the von Neumann model, which executes a single instruction at a time. In contrast, a parallel model of computation may execute many instructions concurrently.

To schedule the execution of a single instruction, a general requirement is that the instruction's inputs are available — whether they have been entered by the user or calculated by a previous instruction. The necessity of the inputs' availability creates a dependence of the following instruction on the previous instructions' execution, and may be represented as a data flow from the previous function to the next, as in Fig. 2.24. In this way data flow languages are declarative, allowing the executing system's scheduler to determine the order of operations given the data flow constraints.

We introduce data flow languages, and in particular graphical data flow languages for geometry as a typical example of a general non-written PGM system, before looking at an example commercial application. The topic of data flow programming occupies a wide range of our procedural spectrum. A data flow language with loops may be Turing complete, and has many applications from parallel programming to task scheduling. However there are a number of implementations that are graphical and geometrical — their user interface is a graphical graph editor, and their output is geometrical. These are the use cases that are of most interest to PGM, being of similar generality to shape grammars, being concerned with the graphical domain.

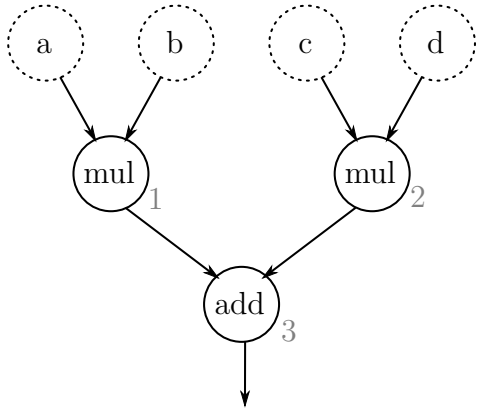

Figure 2.24: *A data flow graph that calculates ab+cd given the mathematical convention that multiplication instructions are performed before addition. The circular nodes are instructions, while the directed edges are the data flows. An inbound edge is an input to the instruction, while an outbound edge is a use of the output. Each instruction requires that all of their inputs be present before calculating an output. For example instruction 3 requires both instruction 1 and instruction 2 to be complete. However the order of the operations are not specified in a data flow graph, so the execution order may be 123, 213 or instruction 1 and 2 may be executed in parallel before 3.*

There are several varieties of data-flow graphs in the literature, we shall briefly examine the *token based* model of Dennis from [54], introduced in 1974. Fig. 2.25 shows an example graph for generating nested rectangles, showing examples of splitting and combining data flow arcs. A token based data flow model models the arcs in data flow graphs as FIFO queues of tokens. Each token is associated with a value, in our example this value is either a rectangle or a Boolean. When a node has a token available on each of its inputs it removes these tokens from its input arcs, computes an output, and adds a token representing this output to any output arcs. The FIFO queues may be initialised with tokens before the system is executed (as Fig. 2.25e). Ensuring that the correct sets of input tokens arrive at the front of the FIFO queues at the same time is challenging for the user, as demonstrated by the involved select/distribute syntax of our example. This *sequencing issue* is one that will occur frequently in data flow graphs.

We note that the graph of Fig 2.25 can only be used for the generation of one figure at a time because of loops, negating the advantages of parallelism. This is somewhat mitigated by the use of tags[54, 259], in which each invocation of the graph uses tokens with different tags, allowing the same instruction node to execute on different sets of input concurrently.

An alternative data flow model offers a different way to mitigate the sequencing issue, by removing loops from data flow graphs. The *structural data flow* model[47] models arcs as arbitrary and possibly infinite data structures. As computations are completed,

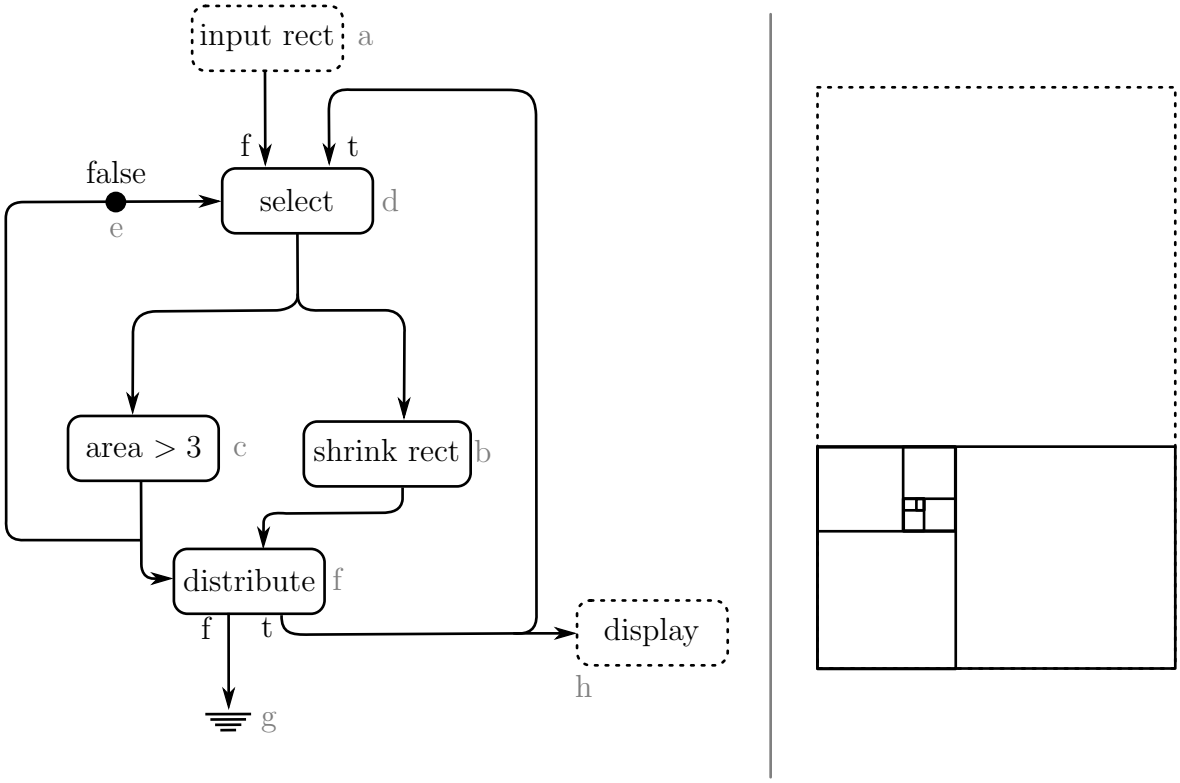

Figure 2.25: *A token based data flow graph (left) that generates nested rectangles (right). The data flow graph takes an input rectangle (a), shrinks and positions it (b) or terminates if the area is less than a constant (c), otherwise the sequence repeats itself. The sequencing issue of whether to take a new input rectangle, or iterate on the existing is addressed by the select and distribute nodes. The select node (d) outputs either the new input rectangle, or the result of a previous iteration, based on the horizontal input; it is initialised with a token of value false (e) to initially take a new input rectangle. The distribute node (f) sends the output of the shrunk rectangle to one of two locations, based on the result of the area test. It is either discarded (g), or output (h) and used in a subsequent iteration via the select node (d).*

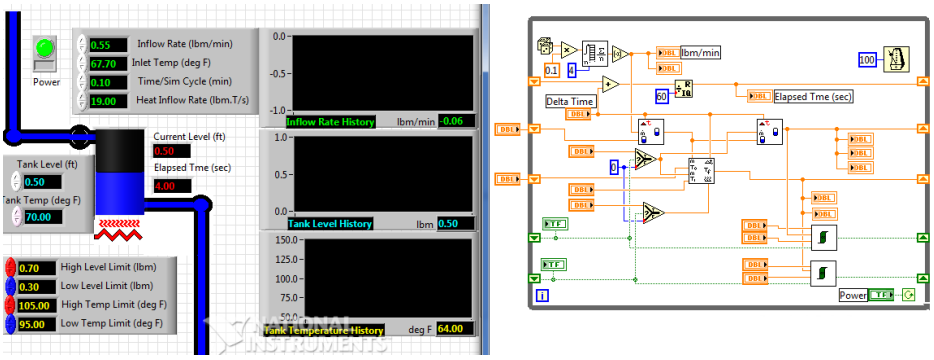

Figure 2.26: *A visual data flow diagram used for controlling the temperature of a virtual water tank.*

these data structures are updated, and their values used by subsequent nodes. Structural data flow diagrams do not require loops as the token based systems do, however this comes at the cost of storage; all computed values are retained by the data structures. Additionally nodes must be equipped with the logic to comprehend the, possibly involved, input data structures.

While textual systems, such as LAU[188] and CAJOLE[101], focused on parallelism and efficiency, another early justification for data flow programming was ease of use. Curiously the development of easy to use graphical user interfaces to data flow languages preceded these formal written languages. In particular Sutherland introduced a data flow editor[230] in 1966, 8 years before Dennis' work. This system used a light-pen to edit the structure of data flow graphs, and define functions by drawing nodes and arcs. There followed many graphical data flow research languages, with examples such as the Graphical data-driven Programming Language[48] and Grunch[50], a graphical interface to CAJOLE. Many of the graphical programs were more visually complex than their textural counterparts. In particular embedding a data flow graph into the plane often leads to the crossing (without connecting) of graph arcs, making reading the graph quite difficult. However this did not stop the use of graphical data flow languages in industry, with systems such as Prograph[152] for general programming and LabVIEW[113] as a digital laboratory, Fig 2.26.

There are several interesting diversions at this point that are beyond the scope of this chapter:

- Data flow graph editors cannot express anything more than a written language (at their most expressive they are still only Turing complete) despite their additional dimensions. However many authors make the claim that graphical programming is easier as it is more difficult to introduce syntax errors than when writing text based programs.

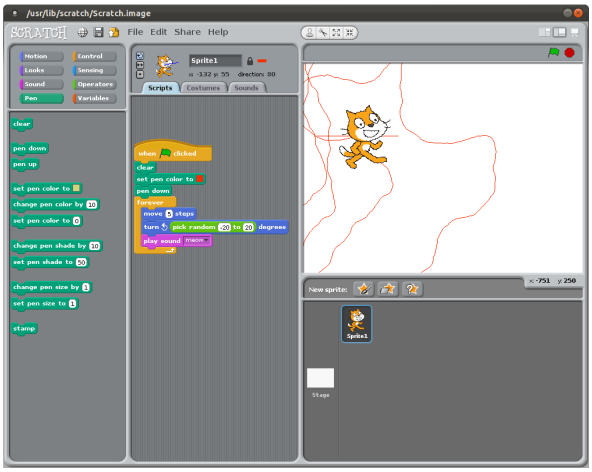

Figure 2.27: *A random walk (red line, top right) programmed in the Scratch visual programming language[200]. Statements are chosen from the palette on the left to be added to the program in the centre. The execution of the program is performed by the cat sprite in a turtle-like manner, top right. Note that invalid expressions may not be programmed, for example there is no attachment point to add a further operation after a "loop forever" statement.*

- There are a significant number of graphical editors for imperative programming[234, 85]. These exploit the ease of use of graph-based systems to appeal to, for example, those new to programming. For example Scratch[200] shown in Fig. 2.27 is able to create geometry. These control graphs describe the sequence of operations, rather than the data dependencies, usually allowing side effects and mutable data structures which data flow programming largely avoids.

- We may create graph based graphical visualisations of many aspects of a program. For example the data structures may be modelled by the *Unified Modeling Language* (UML) or we may animate the flow of data[209]. These are analytical, not generative, applications of graphs to programming.

As graphical hardware advanced it became clear that the graphical editing of data flow programs was a good candidate for creating geometric programs. To clarify, not only is the program edited graphically, but also creates geometric output. These systems provide a widely used example of PGM without written programs, albeit under another name.

The Fabrik Programming Environment[149] allowed 2D graphics, user interfaces, and their elements, such as scroll bars, to be constructed within a dataflow environment, but suffered from "poor performance". Conman[95] utilised data flow graphs on more complex graphics hardware to create 3D objects. A user of the system could construct nodes that interact with the user, allowing user interface sliders, 2D curve editors, and arbitrary scripts to create 3D objects. Later Lovejoy et al. used the Prograph data

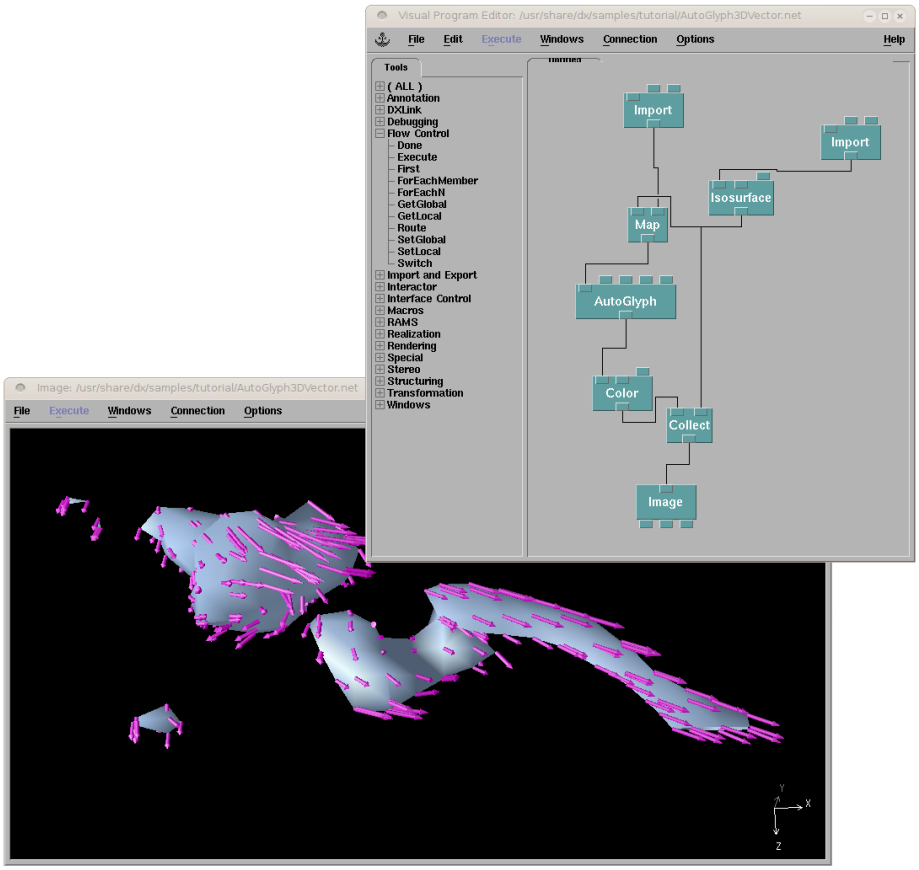

Figure 2.28: *An example of data flow being used to configure the visualisation of a surface via OpenDX. The two paths the data takes through the graph construct the isosurface and surface velocity, before combining them into the single 3D view.*

flow language to control a 2D turtle[148], and Abram et al. use data flow languages to visualise 3D data[2]. More recently, data-flow as a programming paradigm has seen use in the graphics literature. For example, the strict hierarchy and lack of side effects in split shape grammars can be modelled as a visual graph[183]. In [24] a message-passing approach, reminiscent of data-flow programming, is used to connect otherwise disjoint L-systems.

Perhaps more significantly, the data flow model is used extensively in recent commercial software; *3D modeling packages* frequently utilise some form of data flow graph as an alternative to scripting languages. Both Alias' Maya's *Hypergraph* and Blender's *Nodes* use data flow graphs to describe causality within complex kinematic systems, and the relationships between different texture channels. OpenDX[237] uses data flow graphs to allow users to quickly visualise data sets of a wide variety of types, as in Fig 2.28. The hierarchical compartmentalisation makes shape grammars a target for data flow graph editors, as implemented in CityEngine[66]. A more general dataflow programming system is given by the likes of Generative Components[25] or Grasshopper[46].

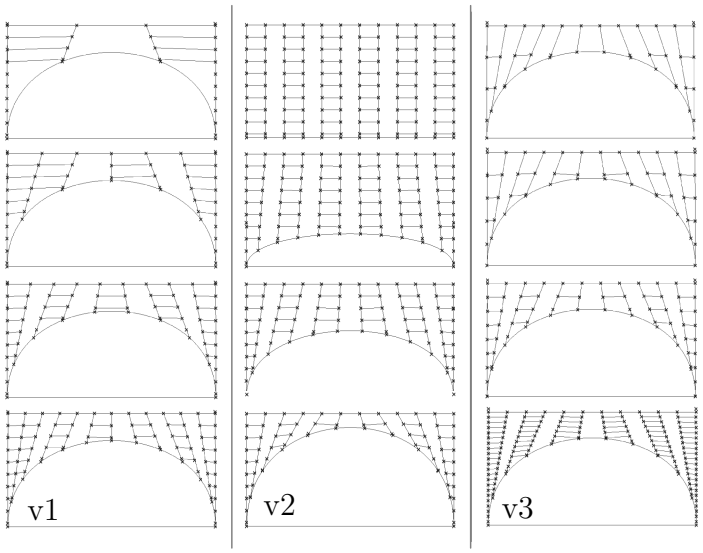

Figure 2.29: *The result of varying the parameters $v1, v2$ & $v3$ in the Grasshopper parametric model of Fig. 2.30.*

To conclude this discussion of data flow graphs we introduce details of Grasshopper to give an indication of the typical tools available in these languages. Grasshopper uses a structural data flow graph to describe procedural geometry. We give an example of a Grasshopper data flow graph in Fig 2.30, to create the geometry of a procedural truss bridge in Fig 2.29.

The structures transmitted along the arcs are nested lists, each nested to a depth specified at compile time. Because only lists with the same nesting depth can be used as inputs to the same function, Grasshopper's UI indicates the nesting depth by the type of line between nodes (undecorated, double or dashed lines for single elements, lists-of-elements or lists-of-lists-of-elements respectively), as in Fig 2.30. To address the sequencing issue, when an operation node takes more than one input Grasshopper specifies several data-matching techniques, demonstrated in Fig. 2.31, based on the number of evaluations of the operation — either the shortest, longest, or product of the sizes of the inner most list. In addition there are a number of operations for re-ordering or selecting elements from the data structure, marked by $*$ in Fig. 2.30. However they are only able to manipulate elements in the inner-most list; more complex patterns require writing programs to order the nested lists.

As an aside we note that data flow programming in no way alleviates the standard numerical computation issues, as witnessed by the removal of a small delta in two places of the computation, marked ‡ in Fig. 2.30.

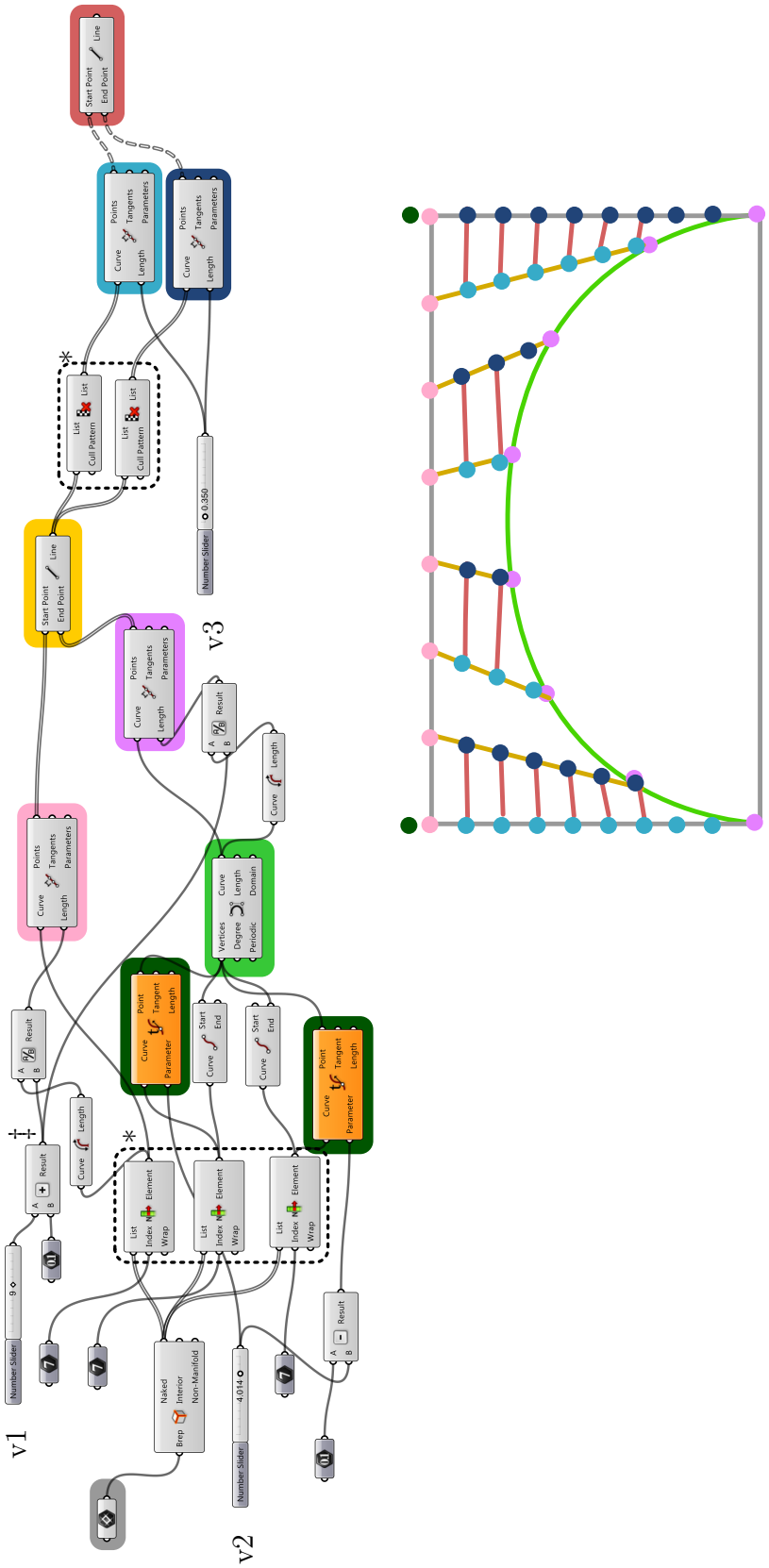

Figure 2.30: *Top: A graphical geometric data flow graph in Grasshopper. The model is controlled by three numeric parameters $v1, v2$ & $v3$, controlling the number of vertical beams, the curve of the arch and the number of horizontal beams respectively. Bottom: The truss structure generated, colour coded to indicate the graph nodes that created the geometry, starting with the grey rectangle input to the system (top, far left).*

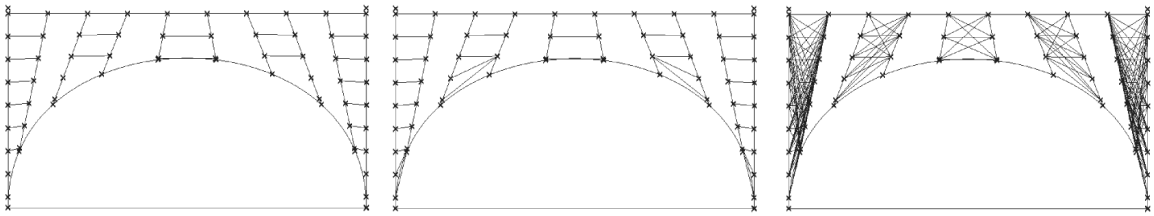

Figure 2.31: *Data matching in Grasshopper. When joining the horizontal truss members, three techniques are offered — Left to right:* Shortest list*,* longest list *and* cross reference*.*

2.8 Simulation Approaches

Creating grammars to describe man made objects is somewhat natural, as we are able to encode the design process that a human may go through to create an object. However there are many non-designed artifacts that we may wish to model in a procedural manner, for example terrains, the historical growth of cities or damage to trees and plants. *Simulation* approaches to procedural modeling involve the imitation of observed processes to approximate the interactions within a model, and between the model and its environment.

Simulation is used in a wide variety of ways to create geometry; we have already seen examples of grammars simulating the growth of plants using L-systems[51] and complex systems via data flow graphs[113]. We might even consider that searching through grammar derivations is a simulation of the human design process. This section explores a collection of systems that have simulation in common.

A very simple form of simulation are *cellular automata*; a specific example is provided by *Conway's Game of Life*[80] in which every simulation step updates a 2D array of cells (boolean values) using very simple rules. As illustrated in Fig. 2.32, these simple rules are executed in parallel on every update step, possibly changing the value of a cell. Despite the simplicity of the rules, different starting values for the cell yields a wide range of persistent and varied forms.

Attempting to program Conway's Game of Life for a particular purpose is often quite involved, however it delights in the unexpected behaviours that may be observed as the simulation progresses. These unexpected or *emergent* behaviours have been better studied in simpler still automata, such as those 1D systems studied by Wolfram[267]. Fig. 2.33 shows certain very simple rules creating complex patterns. There are 256 similar sets of rules, and this example is one of two examples that exhibit these emergent properties, generating aperiodic, non-local structures.

Emergent behaviour seems to be very powerful as it produces intricate patterns from

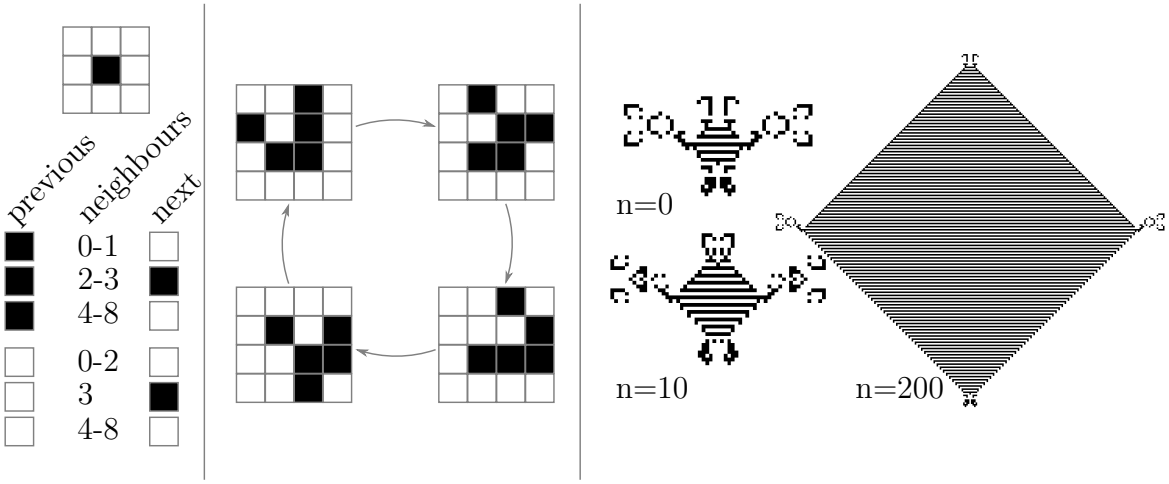

Figure 2.32: *Left:* Conway's Game of Life*[80] simulation takes place on a 2D grid, the transition from a living (black) to a dead (white) state occurs based on the current state and the eight neighbours (top). Middle: The glider pattern, which self-propagates along a diagonal as the simulation progresses. Right: A space-filling pattern by Hartmut Holzwart, at simulation steps 0, 10 and 200.*

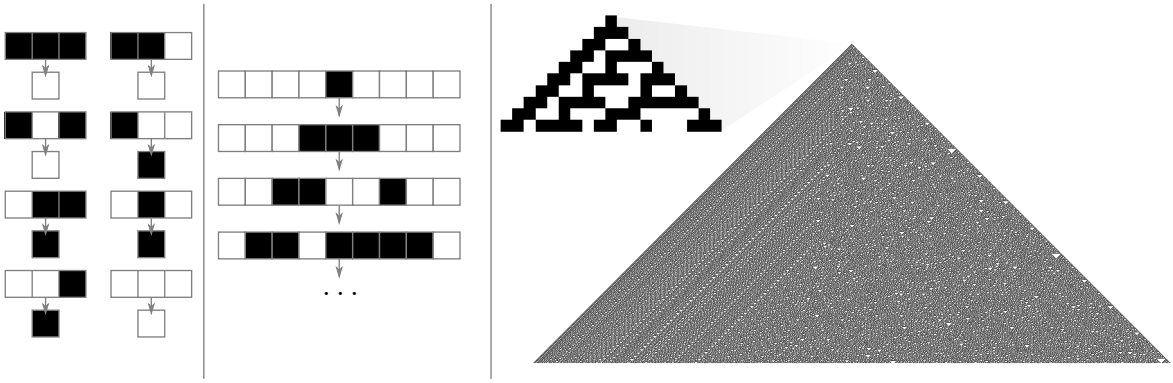

Figure 2.33: *A Wolfram cellular automata defines a transition over a 1D sequence of cells who are either alive (black), or dead (white). Left: In this particular case "rule 30" specifies these eight transitions given a context of three cells (the cell to the left, the cell itself and the cell to the right). Middle: When applied in parallel these rules mutate a start state consisting of a single black cell in a deterministic manner. Right: We may repeat this procedure a large number of times to generate an complex emergent system of local structures throughout the right hand side of the pyramid.*

very concise descriptions. For these reasons simulation seems to lie on a cusp on our spectrum of procedural modeling. Those general models that we have already examined, may exhibit emergent behaviour, while those that follow are less likely to. However, by definition, emergent behaviours are not intended. It is difficult to engineer these system with particular properties; perhaps the only way of working with these systems is to have a large library with known behaviours, and to select the system with the most desirable properties.

Turing's work on emergent patterns in physically based simulations[244] suggests that this library approach may be the one favoured by natural selection; appropriating emergent patterns into situations where they are evolutionary advantageous. However these approaches have not found much traction in the computer graphics and procedural modeling mainstream. Examples are limited to corpora to texture synthesis [154] and the physical simulation of plants. Smith et al. construct a time-based 3D growth simulation of the meristem (growing tip of a plant's shoot) in [216]. By modeling the flow of growth hormone auxin through this region, and the geometric changes that it produces, the model produces a realistic geometry demonstrating several modes of Phyllotaxis.

As well as simulating the processes within a plant, there is also a body of work that simulates the environment surrounding a plant. 3D (*voxel*) cellular automata may be used to model the intersection, proximity and occlusion of a plant[90]. Traumatic events, such as branches breaking may be modeled as step events during the simulated growth of a plant[51]. The growth of a tree through a volume can be simulated as a space colonisation algorithm[205] while structural simulation can create balanced trees[104]. Finally some systems simulate the interaction between both internal and external factors; for example work by Prusinkiewicz et al. growth[167] simulates both the plant-state, via L-systems, and exogenous factors such as the availability of daylight and water.

Another frequently simulated domain are cities. Many systems exist for modeling land use, populations and travel costs within cities[255, 212]. Mostly these use grids of data points, or fixed-structure cells to represent design and layout, some even use cellular automata to model these processes[8, 108].

The introduction of PGM to urban modeling simulations has allowed the creations of detailed visualisations of the resulting cityscapes that change over time. Typically geometric city simulations follow the same procedural urban modeling "waterfall" pipeline as time-static procedural cities[180], an example of which is given in Fig. 2.34. *Major roads*, such as motorways and A-roads provide access to a *quarter*, an area with particular characteristics. Access within the quarter is provided by *minor* B-roads. The area

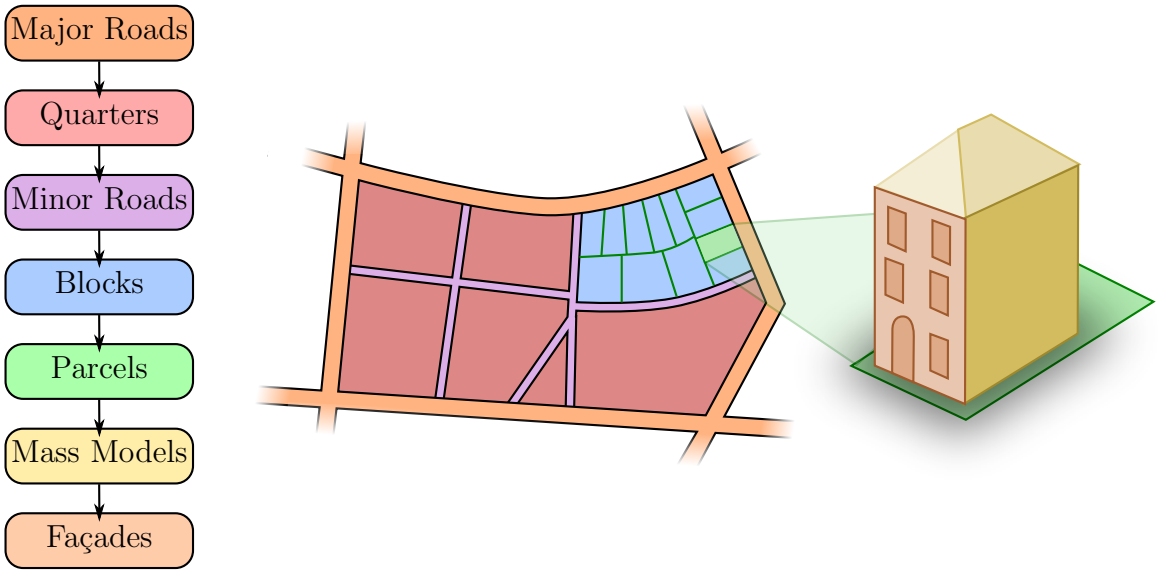

Figure 2.34: *A typical urban modeling pipeline, similar to [260] and [250].*

between B-roads becomes *blocks*, which are further split into *parcels* of land. Finally buildings are positioned on the lots — the 3D geometry described by *mass models*, each face of which is then assigned a façade. When working with discrete time-step simulations, as in the 2D model by Vanegas et al.[249] or 3D model by Weber et al.[260], it is necessary to repeat this course to fine hierarchy with every time step. Examples of Weber's resulting land-use and transport map are given in Fig. 2.35.

This concept of a single pipeline is a gross simplification of the processes that occur within a real city, in which many other factors are considered — for example major roads must take into account and avoid historical buildings. However the waterfall pipeline is a computationally efficient system with proven results. A system that allows for interactive feedback between users of the simulation and the system itself is presented by Vanegas et al.[251]. The user may edit values in the simulation using a paintbrush tool, after which the simulation then commences and the system brings the underlying behavioural and urban models back into equilibrium under the new assumptions. This is a useful urban planning tool for quickly examining the results of decisions, such as building new roads in neighbourhoods.

A further use for simulation at the building level is for the investigation of the physical strength of a system. For example we may wish to:

- identify the safe range of parameters in a parametric model, such that our building is able to support itself[264].
- design a truss structures to support certain loads[215].

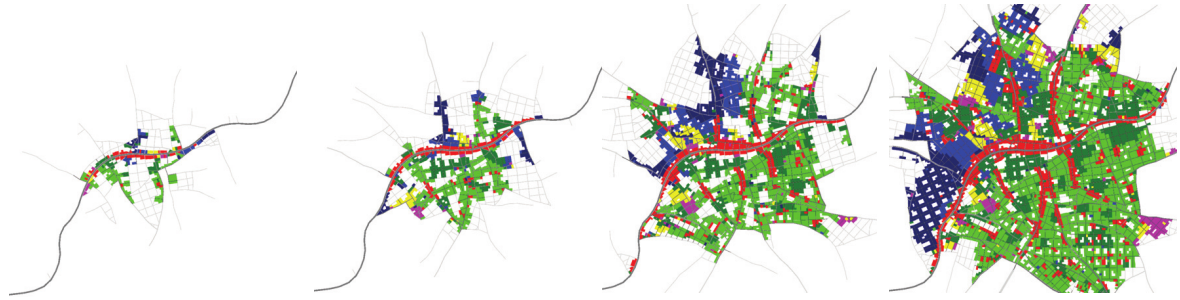

Figure 2.35: *The work of Weber et al. (©2009) simulating the geometric growth of a city[260].*

- find self-supporting free-form surfaces[254] that are sufficiently strong to be constructed.
- build furniture that is both stable and durable[246].

Each of these systems allow the user to specify a model and then simulation is used to search for physically stable variation. This approach blends artistic human design elements with automated reasoning about the properties of such a design.

Finally we find systems that use simulation for interior design. Two recent systems attempt to position a given set of furniture in room by maximising an evaluation function. Merrel et al.[158] encode various interior design guidelines, such as the distance chairs should be from one another to permit conversation. Starting from a user suggestion, the system is able to find a solution that accommodates these guidelines. Alternately Yu et al.[278] learn pairwise relationships between items of furniture from several examples, and include occlusion constraints to ensure clear paths between doorways. Both of these systems simulate a walk through an evaluation function by *Markov Chain Monte-Carlo* sampling. While this is perhaps not simulation in the classical sense, it may be seen as simulating a human designer's exploration of the design decisions.

2.9 Inverse Procedural Modeling

As we have seen, the creation of procedural models is quite involved, requiring considerable knowledge of grammars and languages. Recently there have been attempts to generate procedural models from real world examples, the process of *inverse procedural modeling*. As with much of the shape grammar literature, the focus has been on applications to the urban environment.

The data from the input examples may have been captured via multiple cameras and terrestrial or aerial LiDAR (LIght Detection And Ranging, Sec. 2.12 contains further

details); therefore it may contain significant quantities of noise. Identifying features in this data is the first challenge, for urban environments in particular repeated features are of significant importance. Recent techniques[159, 184] for identifying such features in noisy data cluster the transforms between similar local features to determine prevalent transforms. To reduce noise in the input data, RANSAC[71] is a popular algorithm, and is utilised by GlobFit[138] to clean meshes making assumptions about features such as planar surfaces, repeated distances and shared angles. Finally we can form descriptions of 3D meshes as a tree of such patterns and symmetries[258] for compression and error correction.

The grammar extraction techniques presented in this section mainly use the models derived to compress data, rectify noisy captured data, or to extrapolate data to fill holes. There has been relatively little work to re-target the extracted procedural models to create novel geometry.

Before we examine systems that derive entire grammars themselves, we note that there is a quantity of work on fitting parametric models to existing data. In the field of urban layout reconstruction Aliaga et al.[12] learn descriptive parameters for a road network via statistical analysis; this is then used to create new road maps. Alternatively a template shape grammar may be parameterised to match input from vision techniques[151].

The construction of grammars from examples has proved difficult, and the majority of solutions rely on meta-heuristic techniques to search for a suitable candidate. Typically these techniques repeatedly manipulate the grammar and compare the current results with the noisy input data. In early work, Dick et al.[55] fit a grammar from several images using a *reversible jump Markov chain Monte-Carlo* technique. The grammar used is relatively simple — a set of walls formed the model, and each wall having a set of associated decorations. The work is notable as it was able to reconstruct unseen portions of buildings. Another system that uses a simple grammar and rjMCMC is that of Ripperda et al.[202, 203] who utilise *minimum description length* of the derived grammar as an evaluation criteria. By simplifying the grammar to an assignment of a parameterised mass model to a number of quads covering the floor plan, [133] successfully used rjMCMC to reconstruct large cities from aerial data.

More generally, rjMCMC has been recently used to force the derivation of an arbitrary stochastic context free grammars to posses some specific qualities[232]; for example the silhouette of a derived tree to some specified shape.

An alternative meta-heuristic for creating grammars are evolutionary algorithms. Simon et al.[213] exploit a *Pareto* evolutionary algorithm to evolve a façade shape grammar matching a number of images. In this system the appearance from multiple views,

and the depth correspondence form the evaluation (evolutionary fitness) function.

An incidental generation of grammars occurs in several places in the urban reconstruction literature. As [99] and [22] typify, the grammar complements the bottom-up landmark cluster analysis with a top-down grammatical description of the scene, enhancing feature extraction. An alternative approach[239] is to only apply the bottom-up clustering analysis, using the grammar to describe the properties derived from the input data.

To avoid the need for meta-heuristics entirely Müller et al.[165] use the concept of mutual information to identify repeating patterns in images of façades. The presence of strong horizontal or vertical lines is used to determine the split-locations to generate a CGA Shape grammar. This leads to a compact representation of the façade that can be manually extrapolated to 3D. Another assumption that simplifies the construction of grammars is that of a Manhattan World[248], in which all objects are orthogonal polyhedra.

Müller's automated extraction of façades is one example of using the extracted grammars to re-target content. In this case the resulting façade could be re-sized arbitrarily. Another example is *Style Grammars*[11]; a building grammar is created from 3D geometry, such that it may be retargetted to a different floorplan or height. This system works principally by analysing the 1D patterns of sequences within a shape-grammar like environment to predict a split rule for the resulting grammar. Finally Vstava et al. extract L-systems from 2D vector designs by identifying similar components and then analysing the transforms between them[220]. These L-systems may then be edited to create unique new designs.

Inverse procedural modeling has the potential to create models that may be retargetted to model novel situations, such as constructing buildings of different heights or floor plans. However the results are, by design, derivative of the examples provided. For this reason we may consider inverse procedural techniques to be more specific than general purpose or simulation systems, yet more general than geometry capture or modeling systems.

2.10 Combinatory Modeling

A subset of the inverse procedural modeling techniques that have an emphasis on usability are *combinatory modeling* techniques. Combinatory modeling assembles subcomponents of example objects to create unique new geometries. These techniques fall into one of three broad categories based on the level of input that the user is required to supply.

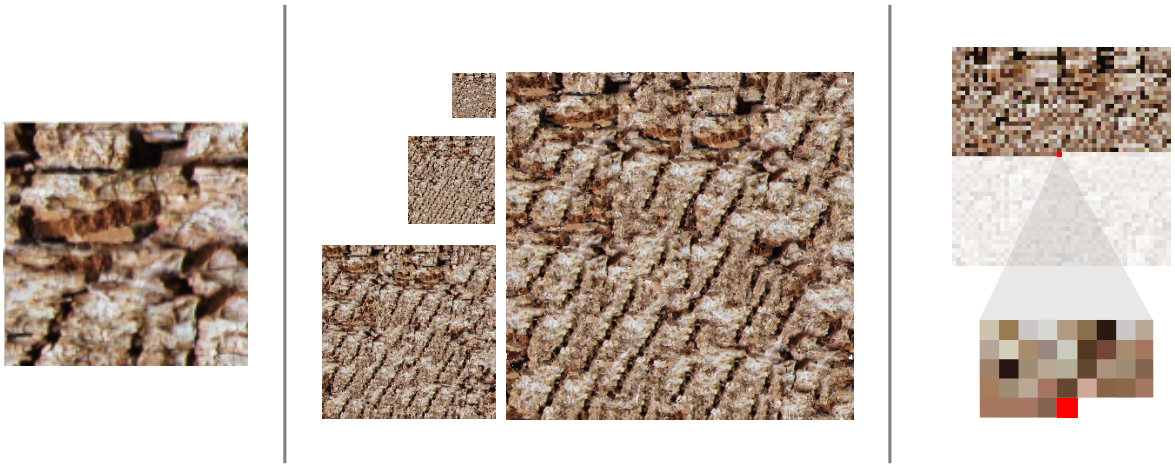

Figure 2.36: *Texture synthesis by the method of Wei et al.[261]. Left: An example tree bark texture. Middle: The results of the synthesis. Synthesising a pyramid of textures helps preserve large features. Right: Each pixel in a scan-line ordering of the new texture is synthesised in turn. The feature vector of the red pixel is shown in the bottom right, This will be compared to the example texture to identify a suitable colour for the pixel.*

Combinatory modeling obtains its procedural element from the choices made during automated assembly. When there is a choice of the choice of parts to attach, a range of designs may result. However, whatever algorithm is used to make the derivation choice, the result can only comprise subcomponents of the examples. For this reason combinatory modeling is a very domain specific technique in our procedural spectrum.

Early work in combinatory modeling was inspired by the 2D case of synthesising textures. Given an example texture in the form of a bitmap, *texture synthesis* aims to generate additional bitmaps that are at the same time characteristically similar to the input and yet unique. As in Fig. 2.36, the standard technique is to grow an image from an example texture by combining pixels from the example in a novel order, based on their neighbourhood. To synthesise a certain pixel adjoining the patch, local pixels from the patch form a feature vector. This is compared against all possible vectors in the example texture to find the best match[59, 261].

Variations of texture synthesis include *image quilting*[60], which creates a reasonably coherent grid of overlapping square texture tiles from the example texture. A minimum error cut then determines the exact boundary through the overlapping pixels. An alternative approach is to ensure that the tiles are always positioned in such a way that adjacent borders do not contain discontinuities. An example of this approach is Wang tiles[43].

When attempting the synthesis of 3D mesh-based geometry, local features, such as those in texture synthesis, have been successful in reconstructing small missing patches

of meshes[208] using iterative refinement of nearest neighbour search and blending techniques. The synthesis of entire objects has been attempted by tiling 3 space with compatible cuboids, with early examples using *Wang Cubes*[211]. Later examples by Merrell et al.[156] use learnt adjacencies between neighbouring cuboids. Merrell extended his work to arbitrary meshes[157], from which common adjacencies are extracted, and a backtracking search constructs a new model consistent with these adjacencies. The system is able to create a large quantity of architectural models with only a single mesh as input, and no further user interactions. However the work with tiling geometry retains the limitation that only transformations allowed by the tiling, rather than arbitrary transforms, are present in the output.

Domain specific tools use specialised techniques to relax this limitation and consider non-local portions of the geometry when combining portions of meshes. Two notable examples by Aliaga et al. synthesise city layouts, and façades. The first system[11] extracts statistics about the roads and parcels in an example city layout and and uses them to synthesise new portions of a city. The gaps between the roads are filled with textured parcels generated using a Voronoi tessellation; the textures for these parcels are taken from similar shapes from the example, and morphed to fit. Given a segmented 3D façade the second system[11] decomposes it into a simple split grammar by identifying 1D patterns, which can be retargetted to new geometry or floor plans. More recently work has taken place to allow "intertwined" 1D sequences of elements over such a façade, allowing for more irregular elements to be represented in a retargettable fashion[140].

To overcome tiling limitations general symmetry analysis techniques have been developed [159] to identify compatible (symmetrical) subcomponents and valid location sites, from an example model[30]. To address the subsequent issue of controlling which of several subcomponents is positioned at a certain site, systems such as those by Kalogerakis et al. introduce a probability based approach[118] which learns the conditional probability of certain classes of geometry being adjacent, and the spacial relationship between the parts. To gather these probabilities, a large number of examples with subcomponents are required, but the result is a realistic combination of those subcomponents. For example when working with a corpus of aeroplanes, propellers are not combined with jet-engined chassis.

In contrast to these unsupervised combinatory modeling techniques, *interactive* combinatory modeling of arbitrary meshes is addressed by Funkhouser et al.[75]. This work introduces a tool-chain to allow the user to quickly create detailed models using subcomponents from existing libraries. A shape-based search finds components in a database, and both positioning and mesh blending tools are provided to the user to align and attach those subcomponents to the existing model. This work is later ex-

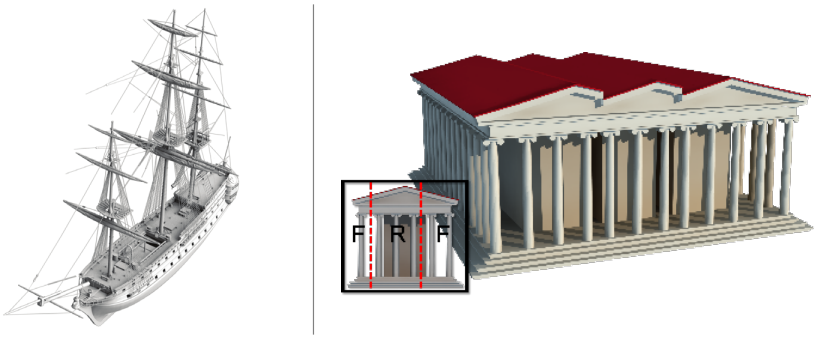

Figure 2.37: *Two geometry errors with combinatory modeling systems. Left: From [118], the rigging of this novel boat is not attached to the deck because there is no mechanism to deform subcomponents. Right: From [140], if subcomponents are not carefully selected it is easy for the large scale geometry to contain undesirable patterns, such as the roof on this model of the Parthenon Images ©their respective authors.*

tended to search for 2D sketched profiles of shapes in a library[135]. Other systems specialise in the interactive synthesis by example of repeating 1D systems[176] and the use of genetic programming to inspire the exploration of subcomponent-space[272].

An obvious limitation of combinatory approaches is that they are only capable of imitating local and global patterns that have already been observed. While these systems are very successful in combining geometry in new and interesting ways, they are also limited by various geometric cases, where geometric continuity is required between the subcomponents, as demonstrated in Fig. 2.37.

2.11 Shape Deformation

Moving towards more specific procedural modeling techniques we may decide to only manipulate existing geometry, rather than attempting to design geometry from first principles . *Shape deformation* is the continuous manipulation of an existing geometry. Typically these models create a range of designs as they deform a shape, and so are a more general procedural tool than geometry construction techniques.

Recent work has begun to explore the overlap between combinatory and shape deformation techniques. Bokeloh et al. continued their work on identifying symmetry[29] to exploit these repetitions to deform models, typically architectural, that contain duplicated elements. These repeats are often reminiscent of combinatory modeling techniques. For example [30] resizes a repeating 1D sequence by repeating symmetrical elements, either chosen randomly, or by a user. An alternative interface is given in [31] which introduces *sliding dockers* as user positionable handles to deform meshes with repeating elements. An underlying elastic deformation is combined with constraints

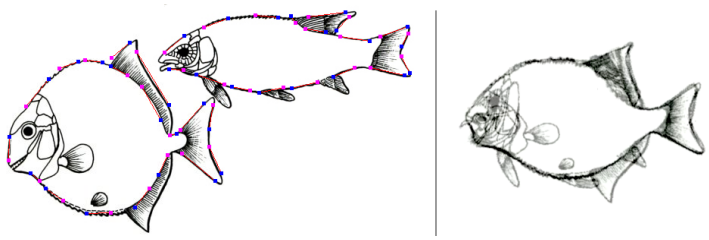

Figure 2.38: *An example of the 'morphing system of Beier and Neely[23]. Left: Two images (black) and their control points (pink, blue). Right: The result of a 50% warp between the two.*

to preserve observed symmetries, such as straight lines or 1D repeating patterns. The most recent system in Bekeloh's series of papers [32] uses a linear system to maintain basic relationships, after factoring out 1D or 2D repeating elements.

The first 2D image *warping* method was created by D. Smythe for the movie *Willow*[217] in 1988; it was used to smoothly deform a goat into an ostrich, and finally a tortoise. The user specifies the location of key points between the images by positioning a grid, and the system would create an image at a certain interval between the examples, allowing the features to flow to different locations smoothly. To achieve this effect the grid was smoothly interpolated between the two states, and the content of the meshes blended. A similar technique was presented in 1992[23], that used discrete handles instead of a grid, that weighs each pixel's location relative to each handle. An example is given in Fig. 2.38. A recent system by Igarashi et al. has a different goal; to allow an image to be deformed as rigidly as possible[111]. This is applied to examples to allow the interactive animation of images. A pair of linear solvers allow a mesh to retain a physical rigidity, while being retargetted to a new shape. An alternative image deformation technique is image resizing. *Seam carving* is a 2D technique to resize images, whilst retaining the most important features[21]. By discarding low-energy seams from an image, the most interesting features of an image can be retained, at the cost of global distortions.

One of the earliest system to deform 3D objects was created by Sederberg[207]. This scheme, analogous to the 2D system of Smithe, utilises a 3D lattice positioned over the object to be deformed. By moving the points of this lattice, the geometry within can be smoothly reshaped without introducing discontinuities. This technique is global, in that the entire mesh is deformed when a lattice point is manipulated. Another global technique[33] allows the user to position handles on the 3D mesh. After moving these to a new location the system deforms the mesh such that it again touches the handles.

One issue with global deformations is that it is difficult for two physically local sections of geometry to have different deformations without interference. For example, when

deforming the middle finger of a hand, it is likely that the index finger will also be repositioned. A response to this was a local deformation — *skeleton based* deformation techniques, in which portions of a 3D mesh are deformed in response to only a subset of the skeleton. Different portions of the mesh are associated with different portions of the skeleton, allowing for nearby verticies to be manipulated by entirely different deformations. There are many different methods for defining a skeleton —

- In early work[136] the bones that comprise the skeleton are coordinate frames defined by the user.
- Later systems[26, 277] use the medial axis of the mesh to define a skeleton as a "shrunk" version of the mesh that can be animated and reconstructed.
- Lastly we may analyse a mesh to discover mechanical joints, and the joint limits that may be present[273], to associate the correct portions of the skeleton with the mesh.

One issue that is common to most deformation techniques, but skeleton based deformation in particular, is the undesirable self-intersection of the mesh under aggressive editing. Various approaches have been suggested to address this issue, including changing the weights near a sharp bend in the skeleton[136], or deforming the mesh based on self-proximity[277].

Both the local and global techniques examined so far have been unable to identify and preserve the symmetries and patterns present in man-made objects. To this end, there have been several recent efforts to create tools specifically targeted to the deformation of man-made objects. For example Cabral et al.[35] resize meshes using constraints that specify that the angles must remain constant, and the edge lengths must remain as similar to the original as possible. These linear systems can then be solved at interactive rates to allow urban geometry to be resized by a number of user-placed handles. iWires[77] instead analyse the geometry of the given object, to extract a number of wire-like handles that can be used to deform the object. The analysis reveals the symmetries between the wires visible in the shape, and these may then be retained under user edits. Given a model that has a number of constraints, such as orthogonality or planarity, Habbecke et al[93] present a method for deformation when the user drags an arbitrary vertex. A combination of a linear model and *compressed sensing* are used to ensure as few verticies as possible are moved.

Some mesh representations, such as *planar quad* (PQ) meshes, have underlying constraints on the location of verticies. PQ meshes require that all the faces of a mesh are planar quads, and are useful when, for example, we wish to build curved glass roofs

from a patchwork of planar tiles. Yang et al[274] introduce a framework for deforming such meshes by exploring a high dimensional space. This space is bounded by the given constraints, and may be explored via 2D maps. The resulting mesh is found by projecting back to 3D.

As a form of deformation *parametric* modeling is an often-overlooked subject in both general academia and computer graphics[105]. *Computer aided design* (*CAD*) systems are used to design 3D geometry in many industries. Typically these operate on similar principles to geometrical modeling, but with the end goal of producing domain specific results, such as AutoCAD[18] for standard-compliant architect's plans, ArcGIS[17] for maps, or Mastercam[218] for *computer numerical controlled* (*CNC*) fabrication machines. *Parametric modeling* is an extension to CAD to consider the design of elements where parameters may vary, producing a range of objects, as in procedural modeling. This offers a way for a draftsman to encode domain knowledge into a model[14]; as they work the designer specifies which measurements are parametric, and the constraints that are necessary for each measurement. As with PGM, there is no standard format for parametric components[134].

An example of a deformation technique that is typically used to create a single instance of a 3d mesh is *digital sculpting*. Commercial projects such as zBrush[187] and Mudbox[20] provide the best example of this technique — users are able to manipulate a 2.5D or 3D mesh by drawing strokes on the surface to mark the location of deformations. Typically users can push and pull the surface, as when sculpting a real-world deformable material, such as clay. These tools are used widely by 3D mesh artists to create highly detailed models, for example, reconstructing extinct animals from their fossil remains[221].

2.12 Geometry Construction

Towards the most specific end of our procedural spectrum the systems we examine do not create true procedural models, but only create a single geometric instance, such as a 3D mesh. Typically every new geometric instance will require significant human interaction. We begin our overview of this expansive subject by looking at some examples of domain specific geometry modeling tools, then sample some geometry capture methods, and finally examine 3D mesh construction techniques.

An overwhelming variety of domain specific geometric modeling tools are available. Chen et al. exploit tensor field editing systems to design street networks in an urban environment[38], exploiting the literature on the subject to build a novel urban geometry design tool. The *Arches*[185] framework presents a novel representation of terrains,

as well as sculpting and editing tools to manipulate the mass of of rocks, or introduce features such as cracks. Another domain that has been approached is to allow the easy modeling of flexible objects[257], by reducing the degrees of freedom that such objects have in an intelligent manner.

Freeform architectural surfaces are characterised by large smooth curved areas, that are not regular geometric structures. The work in graphics on these surfaces is largely connected to modeling these surfaces as 3D meshes, with each face, having certain physical properties. The faces are often constructed of planar glass sheets, often quadrilateral. These surfaces are well represented by PQ meshes, but many mesh editing techniques do not guarantee these planarity properties. One approach by Pottman et al. is to optimise a given thin PQ mesh such that each quad is within some planar tolerance[147], another is to allow the user to explore the space of such meshes[274]. The generation of thick, offset, surfaces to PQ meshes is studied in later work[190]. Instead of PQ meshes, we may wish to construct our freeform surfaces from bendable strips of flexible material[192], or use such strips to create geodesic patterns[191]. These techniques use elements of simulation to create one-time models, with a typical example being the simulation of a cost function for the physical manufacture of the mesh faces[63]. The authors present a cost function based on the reuse of face shapes and deviation from the specified design.

A quantity of work aims to reconstruct 3D objects from 2D plans[275]. We may, for example attempt to interpret 2D vector plans, typically created by CAD software, into plausible 3D objects. Lewis et al.[137] introduce techniques to re-structure plans in such a way as to make the data suitable for extrusion. However if we only possess a bitmap image of the plan, without any of the meta-data associated with vector plans, a range of machine vision techniques must be used to identify the different features[57]. These techniques have also been used for rapid video-game environment construction[73].

Academic projects also explore sketch based deformation techniques, such as Keraut et al.[123] who utilise *shape from shading* techniques to allow users to construct 3D meshes from their 2D drawings of an object lit from several angles. More recent work allows users to deform 3D meshes by sketching the position of highlights or silhouettes[83]. An alternative to sketch based deformation, is the photo based approach of Xu et al.[271], who use a photo to deform a 3D mesh to replicate the form of a certain 2D image. This is achieved by decomposing the symmetry of the mesh and re-aligning it to the silhouette given in the photograph.

Utilising 2D images to aid in 3D geometry synthesis forms an extensive sub-field of geometry capture from sources such as single photographs, sets of photographs, LiDAR and GPS data. In Sec. 2.9 we explored several systems that exploit a procedural

model as a reconstruction tool; there is considerable overlap between such systems and the geometry reconstruction techniques given here that reconstruct a static 3D mesh. A thorough treatment of this spectrum of reconstruction techniques is given in[166], although we now give an overview.

Manual reconstruction from a single photograph is quite unconstrained and so relies on domain specific information to produce useful results. Early attempts[109] required further human assistance and exploited assumptions about objects always touching a known floor to infer depth. More recent attempts exploit domain specific properties, such as the strong rectilinear nature of façades[165], or the symmetrical nature of a certain class of buildings[116] to automatically reconstruct geometry.

Given several photographs we may reconstruct a 3D point cloud over the surface of a building, using techniques such as *structure from motion*[53]. To construct accurate meshes from a low number of images, together with user interaction, one approach is to use such 3D data as a mesh modeling aid. The *Façade*[52] system pioneered this approach, using several images, with edges identified by the user, to reconstruct the geometry from basic blocks. Another approach is given by Sinha et al.[214] who allow the user to sketch polygonal faces that are then fitted to the recovered 3D point cloud using the *RANSAC* algorithm. This is then followed by automated texture extraction from the source images. A similar vision approach is used in [177] to reconstruct a coarse 3D representation of a building site, such that the user can sketch the walls of a building on embedded 2D planes.

To perform fully automatic reconstruction, we may make assumptions about the geometry in the scene. For example Werner et al.[263] assume an architectural scene with a few principle edge directions. To automate reconstruction from general images, generally a larger set of images are required. For example, an automated version of the Façade system uses dense polygonal reconstruction from several photographs[189]; this is sufficient detail to reconstruct a coarse mesh of a single building. Larger scale reconstructions require using hundreds or thousands of photographs to reconstruct urban areas in fine detail. Gathering sufficient data for these approaches is challenging, with researchers using image-sharing websites[4], crowdsourced calibrated capture[115] and novel games[242] to collect a sufficient number of images covering the geometry to be reconstructed.

An alternative to optical photography is LiDAR reconstruction. LiDAR uses laser range finding to plot a depth-map of some geometry. Common examples include street level LiDAR for façade reconstruction[197], and aerial LiDAR for urban[280] or forest environments[161].

The industry default 3D mesh creation techniques are mesh construction tools, these

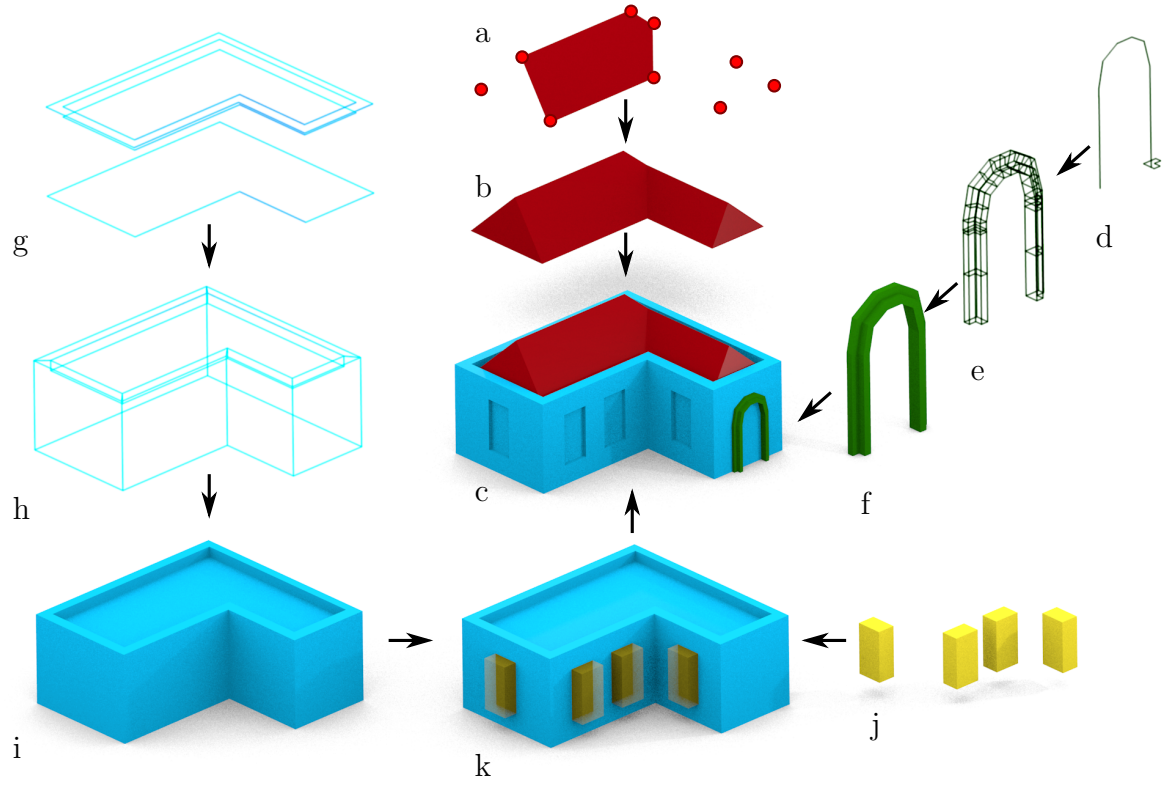

Figure 2.39: *A slightly contrived mesh construction workflow to create a house (centre). The walls, windows, door and roof are created using lofting, constructive solid geometry, bevelling and manual modeling tools respectively.*

have become ubiquitous, with commonly used commercial packages such as Maya[19], Blender[74] and Sketchup[240]. In the most part this chapter has been discussing more general alternatives to these techniques, however this tool chain is used to create the majority of 3D geometry in use today.

A typical workflow to create a 3D mesh of a house in a is show in Fig 2.39. To create the roof (Fig 2.39, ab), a user may manually add verticies (red points), and select groups of verticies to form faces. Rotational, translational and scaling tools allow these elements to positioned appropriately, (c). A door may be constructed using the *bevel* tool. A cross section and path are defined (d) using manual modeling techniques; an application of the bevel tool then sweeps the same cross section along the profile, creating faces (ef). The *loft* tool is similar but takes a list of curves with the same topology, but changing geometry (g) and creates solid faces between them (hi). The loft tool creates the walls of the house, but to inset the windows we use *constructive solid geometry* tools[238] to subtract the volume of a set of carefully positioned cuboids (j) from the result of the loft operation (k). We note that there is no correct choice of

Figure 2.40: *A single model by* Bob1938 *from the Timble 3D Warehouse[241], that was found using the search term "Victorian house". The time to find and download the model was 30 seconds, a significant improvement on many of the PGM systems presented in this chapter. ©Bob1938.*

tool for each geometric element. For example manual vertex construction could have been used for the entire mesh, or the walls could have been constructed via CSG over an appropriate set of cuboids.

However a wide variety of research is still undertaken to create meshes, here we only present a small sample. For example, given only a 2D sketch of a 3D object, reconstruction is an under constrained problem; a problem that *Structured Annotations*[82] approaches by asking the user to annotate a sketch to provide more constraints. Alternately *FiberMesh*[172] approaches construction using a sketch-and reconstruct cycle. A novel tool is the application of texture cloning to 3D to allow interactive mesh geometry copying from one mesh to another[231]. Finally Li et al.[139] address the issue of the manipulation of irregular verticies in near-PQ meshes to achieve aesthetic or structural benefits.

2.13 Digital Libraries

The most specific extreme of our spectrum of PGM contains libraries of objects. Given the range of geometry creation systems available it should be not surprising that repositories such as *TurboSquid*[243] contain upwards of 200,000 3D meshes.

Given such a variety of geometry, some search tools are required to allow users to locate the geometry they require. Most of the commercial websites such as *Trimble Warehouse*[241] or Turbosquid use text based search, an example result is show in Fig. 2.40. However searching large collections of 3D meshes remains a active research area. The seminal work in this area by Funkhouser et al.[76] indexes and retrieve meshes by sketches or example models. The rotation invariant properties of *spherical harmonics* are used to construct easily indexed feature vectors. An alternative feature descriptor

is given by [174], which uses the low frequencies of the depth map of the rendered object. The rendering stage ensures the system is robust to irregular meshes, such as those which contain holes. A different approach is to exploit the continuous variability in a set of models to allow users to explore the set of models interactively, as in [175]. For example, users navigate from one airplane mesh to another by indicating that they wish the wings to be further forwards on the fuselage. Recently *fuzzy correspondences* have been introduced as a technique for exploring a library of meshes uses regions of interest that the user specifies on an example model.

Because each model in the library has been manually created, they are free from many of the artifacts that recovered geometry may contain. Furthermore they are free from many technical concerns that come with many of the more general procedural systems, such as termination criteria in the case of shape grammars. However, the user faces several other issues in using this content — for example, given an existing lot in a city finding a house of the correct style to fit, depends on the contents of the library. Generating a large cityscape may require repeating objects from the library, or mixing meshes of different styles and level of detail.

2.14 Summary

In general there are many axes on which we can classify the work on procedural modeling, such as quantity of human interaction, or applicability to real-time situations. However in this chapter we have introduced one such axis — a continuum of procedural specialisation from the general purpose to the specific.

We have given examples examining the range of geometry that may be generated with each system. From general purpose programming languages, that only happen to be used for geometry creation, through complex grammar and inverse procedural techniques, to simply finding the closest possible item of geometry in a library. Unfortunately it is hard to make a quantitive argument about the trade off between power and ease of use over this spectrum. This is due to the difficulty in capturing ease of use information given the wide range of users' abilities (both programming and artistic), and in quantifying the range of results that a system can create. We may imagine some future work in which users create a model with each system in the spectrum, and we then evaluate the time it took the user, the fidelity, and the range of geometry the created model creates.

Complicating matters we have observed an increasing number of cross over systems in recent years — combining separate parts of this spectrum to increase the utility of the system. For example,

- grammars are used in urban reconstruction via inverse modeling to more tightly fit geometry.
- the 3D meshes created by tools can be positioned to form a facade using a shape grammar, that itself is implemented in a general purpose programming language.
- simulation is used to evaluate the results of L-systems to create models of trees.

Given the broad range of geometry synthesis systems available today, users would be well advised to find the most specific technique that has the required flexibility. For example a video game artist may wish to "synthesise a large set of alien tower blocks" with a shape grammar, a town planner may wish to "visualise this area of a city after a 10% increase in public transport usage" using simulation techniques, or residents may only care to "visualise the new statue outside the town hall" using mesh construction tools.

In our introduction we stated that in order to be useful, existing procedural systems required users to write computer programs. With this spectrum of proceduralisation, we can see a strong correlation between general, powerful systems and the requirement to write computer programs. The most general geometry creation techniques, Sec. 2.1 to 2.7, require users to program. The type of programming involved was quite varied; we have encountered systems that use a conventional language, a shape grammar, or a data flow graph to specify an algorithm. Conversely, the the most specific techniques, Sec. 2.8 to 2.13 do not require any programming. The user is able to generate a smaller variety of geometry, often confined to a single domain. However they are able to create models using a variety of easier to master techniques such as graphical editing (in the case of shape deformation or geometry construction), discrete selection (in the case of digital libraries or combinatory modeling approaches), or by selecting a number of parameters (in the case of simulation systems).

If we start from the premise that we wish to build a system that is as general as possible without writing a computer program in any form, we find the state-of-the-art in the middle of such a spectrum.

2.15 Approach

We wish to possess a system that is as expressive as a split shape grammar, or data flow programming system, but inspired by the types of user interface present in the simulation or inverse procedural modeling approaches. Inspiration for a such a system was forthcoming from Havemann's thesis[105]. This provides some convincing examples

that an offset mechanism driven by the straight skeleton was a powerful accompaniment to a written programming language. After studying a variety of man made objects inside and outside an urban environment, it became clear that some generalised offset mechanism could describe many features of man-made geometry.

The straight skeleton has a simulation-like definition, in which a 2D shape is shrunk until it disappears, leaving behind it a subdivision of the original shape. The output is promising because it was closely correlated to the input, and is quite predictable and easy to understand via a user interface. However the skeleton also had some interesting non-trivial outcomes, such as being able to split concave shapes into two, introducing holes into faces, and leaving behind "arcs" which form part of the centrelines of a shape. It is these emergent properties that we found we could exploit to create an expressive range of geometry.

Chapter 3 introduces our detailed examination of the straight skeleton, the kind of events that we observe as it shrinks, and the kind of degeneracies that occur if we are unlucky. We continue to examine how the straight skeleton can be generalised so that it becomes a more powerful modeling tool in more situations, whilst keeping its desirable properties.

Given a theoretical understanding of the geometry, we continue to apply the skeleton to the domain of urban procedural modeling. The urban domain has several properties which make it ideal for modeling with skeletons. Given the polygonal output required for many tool-chains used to create 3D environments, the straight edges of many architectural forms was appealing. Cityscapes also offer a more semantically and geometrically demanding domain than, for example flora — façades have constraints such as only locating doors at street level, and unlike procedurally generated botany, the self-intersection of buildings is undesirable. Finally the urban landscape is well documented, which facilitates easy to obtain reference material and comparisons.

Our first application of the straight skeleton to an urban domain was in identifying the centerline of city blocks so that they could be split into lots. Existing systems assumed a simpler model, in which the block was repeatedly split into two pieces, however such a system was unable to represent the characteristic centrelines. In Chapter 4 we examine a novel technique for the subdivision of city blocks using the straight skeleton. The straight skeleton is combined with geometric construction techniques to give a parameterised algorithm for city lot formation.

We continue into Chapter 5 to apply a generalisation of the straight skeleton to the construction of solid buildings that may be located within such lots. The similarity of the of the straight skeleton to a building's roof is exploited and extended to generate a wide variety of interesting architectural forms. Repeated applications of the

skeleton are guided by user defined plans and profiles to generate buildings. The generalisations of the skeletons that we introduce prove to be robust building blocks for a novel yet expressive system.The emergent properties of the skeleton gives very intricate forms simple constructive definitions. These forms prove to be robust enough for large scale cityscape generation, and capable of generating a wide variety of observed urban structures.

Chapter 3

Various Skeletons

This section contains both literature survey and novel components. As introduced in *Interactive Architectural Modeling with Procedural Extrusions* [121] I contribute both the general intersection event and the mixed weighted straight skeleton. Further contributions are the analysis of the weighted skeleton degeneracies, as "published" in a blog post, and the description of the pincushion problem.

The *straight skeleton* is a geometric subdivision of a 2D shape, based on the notion of "shrinking" the shape. In the following we will introduce the skeleton, its properties, degenerate cases, computational complexity, and how to construct it. We extend the standard definition of straight skeleton in several steps, introducing a hierarchy of several skeletons, each of which is a generalisation of the previous. These generalisations introduce additional degeneracies which we catalogue and suggest techniques to resolve.

Given the spectrum of geometry creation tools explored in Chapter 2, we were searching for an expressive yet simple to use tool that would lie in the centre of our spectrum of proceduralisation. It had to be general enough to create a width range of useful results, but easily controllable without the need for specialist training. As we stumbled upon the idea of offsetting geometry, and were introduced to existing results[105] relating to the straight skeleton modeling the roofs of buildings, it became clear that the skeleton had the potential of being a powerful modeling tool. The close relation between offsets and the straight skeleton, introduced in Sec. 3.2 formed a powerful argument for this particular geometric primitive having a wide range of modeling applications.

Discovering that the straight skeleton was also heavily used for roofs, we examined how the skeleton could be extended to a larger domain. In the first case we noted that the walls below a skeleton-created roof could be modelled either by an extrusion operation

or by the scaling the roof in the vertical direction until it became almost vertical. From this point we explored the generalisation of per-edge slopes in the skeleton. Because the definition of such a structure remained inherently simple and geometric the natural user interface wasn't programmatic, but instead visual.

In this chapter we examine the straight skeleton in detail and formally introduce a hierarchy of skeletons, each of which takes the same basic information as input, but expresses a wider range of geometric forms than the previous skeleton. In taking this approach we can technical problems underlying the key skeleton concepts of offsetting, or shrinking, a polygon.

3.1 Ways of Shrinking Polygons

There are many ways in which to shrink a polygon. Fig. 3.1 illustrates four published techniques which translate shrinking edges in a self-parallel manner. These techniques only vary in their treatment of reflex corners:

a) Given that each edge moves towards the inside of the polygon (green), parallel to itself (white arrows), a multitude of techniques can be imagined by changing the handling of the corners.

b) The *medial axis* [28]. A reflex vertex becomes a parabola as it shrinks, maintaining a constant distance from the original polygon. The medial axis itself is a skeleton defined as the set of all points within the polygon which are equidistant to two or more points on the boundary of the polygon.

c) The straight skeleton[6] (SS), moves reflex verticies with the intersection of the two adjacent edges. We investigate further properties of the straight skeleton in Sec. 3.2.

d) The *linear axis* [233] introduces *hidden edges* into reflex corners of the skeleton to approximate the medial axis using only straight line segments. These hidden edges immediately grow to "blunt" such verticies, reducing their "speed" as the polygon shrinks.

e) A weighted variation of the straight skeleton (*WSS*) was introduced by similarly timed later papers by both Eppstein and Erickson [65], as well as Aicholzer and Aurenhammer [7]. Both papers only give a passing mention to WSS and degenerate cases are not introduced. The edges of the WSS are assigned independent speeds for shrinking, which shall be examined further in Sec. 3.3.

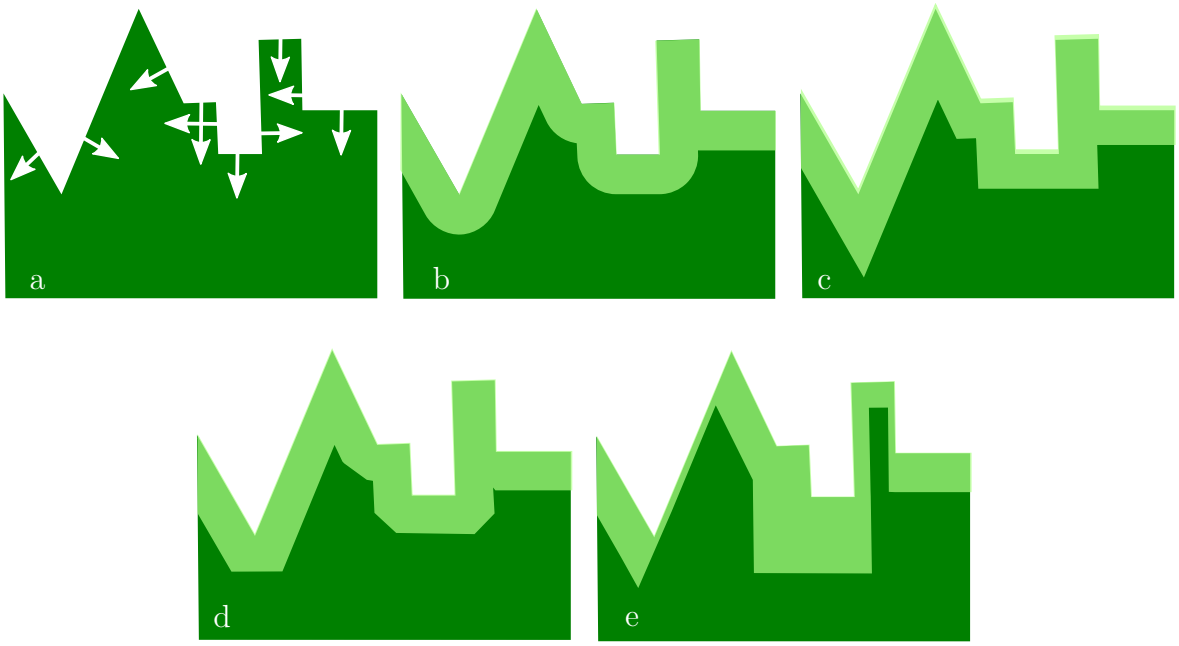

Figure 3.1: *Techniques to shrink a polygon (a). These include the medial axis (b), straight skeleton (c), linear axis (d) and weighted straight skeleton (e). The result of using each technique to shrink the polygon by a small distance is shown (the light green areas are lost to the shrinking process).*

Our interest here is in the straight skeletons (SS and WSS), as these structures do not introduce curved or additional edges, and, as demonstrated in Chapters 4 and 5, are well suited to modeling certain classes of man-made objects as 3D meshes.

3.2 The Straight Skeleton

Let us consider the growth of a crystal, as in Fig. 3.2. As Aichholzer observed in [7], if we were to watch such a crystal growing we would see that each face grows outwards in a self-parallel manner, and the edge between two such faces moves outwards as the intersection of these faces. Thijssen et al.[236] earlier explored the statistical properties of such growth in crystals, introducing a 2D proxy for the original 3D geometry, Fig. 3.3. This model of self-parallel growth is the reverse of the process that is performed to calculate the straight skeleton, which is calculated by the shrinking of a polygon.

The straight skeleton (SS) is a 2d graph of *arcs* generated from this shrinking of a polygon. Each of the edges of the polygon moves towards the interior at a constant speed in a self-parallel manner. Occasionally the topology of the polygon changes as we observe *events* such as an edge shrinking to zero length. As shown in Fig. 3.4, the movement of the corners of the decaying polygon trace out the "skeleton" itself. These arcs describe the path of the verticies as the polygon shrinks. Several examples are

Figure 3.2: *Composite grey cubit crystals of galena with purple cubic crystals of fluorite. Cave-in-rock, Hardin Co., Illinois, USA.*

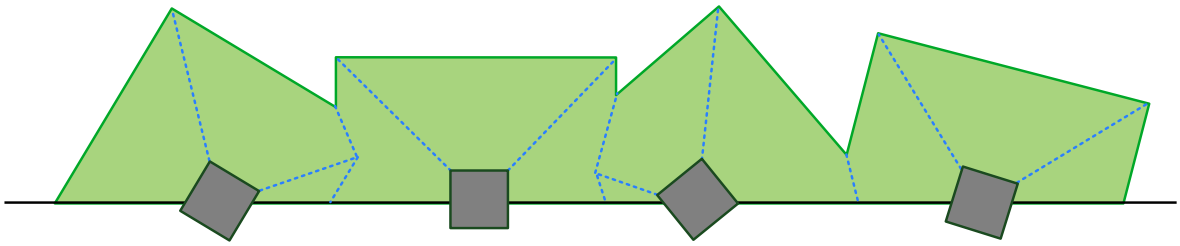

Figure 3.3: *Given a set of square seeds (grey) on a line, the polycrystalline growth moves outwards (green), and the movement of the corners traces out lines (blue).*

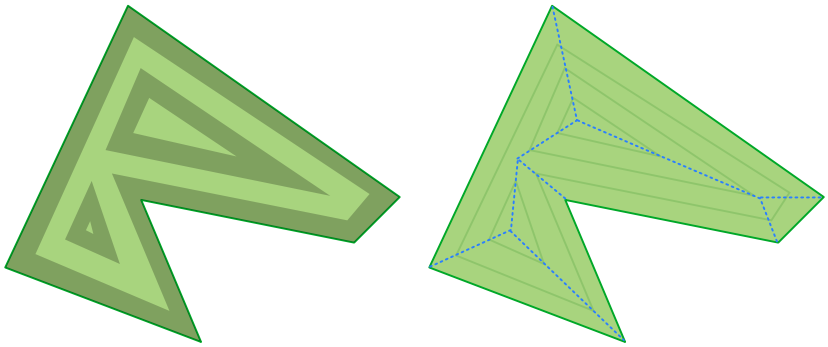

Figure 3.4: *Left: A shrinking polygon. Right: The arcs of the straight skeleton (blue) are formed by tracing the edges of the shrinking polygon.*

shown in Fig. 3.5.

3.2.1 Constructing the Straight Skeleton

The SS is a graph of straight edges in $\mathbb{R}^2$. However we can interpret it as a *terrain* – a set of faces in $\mathbb{R}^3$ which form a "landscape"[6], Fig. 3.6 right. This approach is taken as it allows a comparison between the standard, unweighted straight skeleton, and the various types of weighted straight skeletons (WSS), a generalisation introduced in Sec. 3.3. The terrain constructed touches the polygon on each edge, and the projection of the edges of the terrain onto the polygon forms the 2D straight skeleton.

The shrinking process is modeled as a sweep plane that rises with constant speed from the input polygon, carrying with it the evolving shape. Each edge of the polygon moves inwards with a constant speed relative to the sweep plane motion. The sweep plane rises and the polygon shrinks, encountering various topological events. Eventually the polygon shrinks to nothing and the skeleton is complete. The terrain approach allows the events to be modelled as the intersection of three planes, rather than three 2D edges, allowing the geometry of Chapter 5 to be constructed trivially.

To distinguish between the under constrained term "polygon" and a similar structure with additional constraints, we introduce a *plan*, Fig. 3.6. A plan is a planar partition (a straight line planar embedding of a planar graph) that divides the plane into finite *inside* and infinite *outside* regions. A plan is a set of polygons consisting of corners and edges, these are embedded in a plane parallel to the xy ("ground") plane, so that all corners of a plan have the same z (height) value. The jth polygon is described by n^j polygon corners $c_i^j \in \mathbb{R}^3$ with $1 \leq i \leq n^j$. Each corner c_i^j is connected to the next corner (according to the polygon orientation) by an *edge* e_i^j. The loops of edges are oriented counter-clockwise, but polygons describing holes are oriented clockwise. Additional bounded regions may be recursively located inside a hole. When discussing

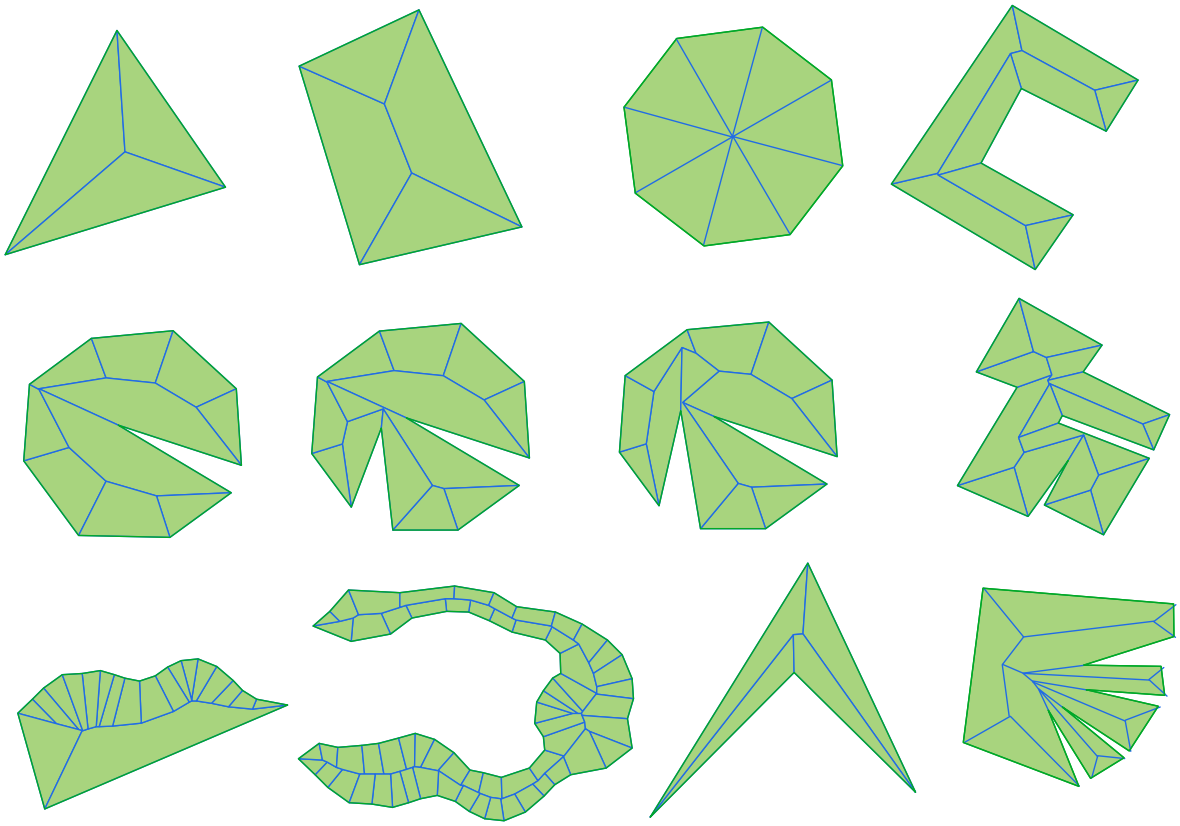

Figure 3.5: *A variety of polygons (green) and their straight skeletons (blue).*

plans, indices are treated cyclically, so that in a polygon with corners c_1^j, c_2^j, and c_3^j, the vertex c_4^j means c_1^j.

Unlike the medial axis, there is no trivial description as to whether a particular point within a polygon lies on the SS arcs. Instead, the skeleton is defined in the literature as the result of the process of shrinking a polygon. That is, the only description of the SS we have, is the algorithm for its construction.

To construct the skeleton, a sweep plane rises vertically from the *input plan*. This sweep plane carries with it an *active plan* that defines cross sections of the terrain.

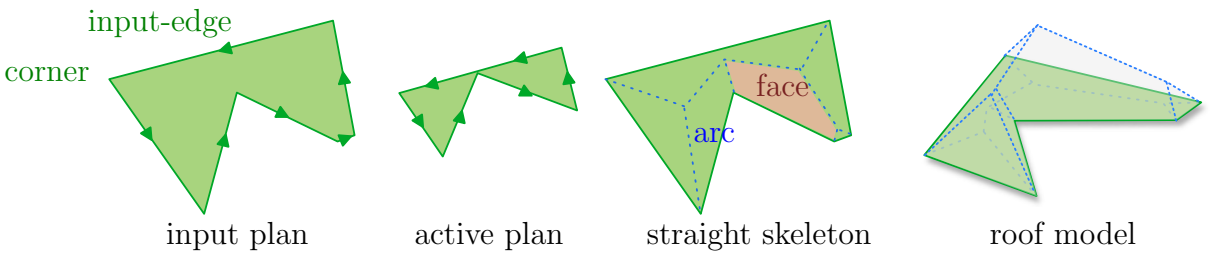

Figure 3.6: *Straight skeleton terminology. The input plan defines the starting state of the construction, while the active plan defines the state part way through the shrinking process. The final straight skeleton is a 2D graph consisting of arcs adjacent to faces. The roof model is an alternative 3D representation, the projection of which onto the ground plane forms the 2D straight skeleton.*

This 3D approach was first suggested by Eppstein et al. [65], although in spirit similar to the original 2D proposal by Aichholzer[6], with data structures inspired by Felkel and Obdržálek[68]. However we use our own notation for continuity. The output of the system is a series of *skeleton faces* that make up the 3D terrain. The edges between the faces are named *arcs* after Aichholzer et al.[6], a term that we shall use in both 2D and 3D interpretations of the skeleton.

As the SS is constructed, the sweep plane rises with constant speed, and the active plan shrinks. In the case of the basic straight skeleton every plan edge moves with a constant and uniform speed towards the interior of the polygon. As both the speed of the sweep plane and plane edges are constant, each plan edge remains within the same 3D plane. One of these *direction planes* is associated with, and intersects, every edge in the input plan. As both the speed with which the sweep plane rises and the movement of the edges is equal, the direction plane associated with each edge e_i^j forms an angle $\pi/4$ with the input plane. Each skeleton face lies in one of these direction planes. To obtain a steeper or shallower roof from the SS we may scale the faces in the Z direction appropriately.

At all times in this shrinking process we must ensure that the active plan remains *well formed*. That is:

- The enclosed region remains to the left of every directed edge.
- No edge intersects another edge, with the exception of touching the neighbouring edges only at shared corners.
- Every enclosed region has a positive, finite and non-zero area.
- There must be a finite number (zero or more) of such enclosed regions.

In the SS every active plan edge has the same constant, positive, speed. As the edges move, the corners remain defined by the intersection of the adjacent direction planes and the current sweep plane, as in the plans of Fig. 3.7. Therefore each corner in the active plan, c_i^j, moves between events with a constant, and often unique, speed and slope relative to the input plan.

Fig. 3.8 shows that as sweep plane rises and the active plan shrinks, the plan may become badly formed (red). To ensure that the active plan remains well formed, we detect when more than two or more edges intersect and we make topological changes to the active plan. We call these *events*; as introduced by Aicholzer et al. [6] there are two types of event:

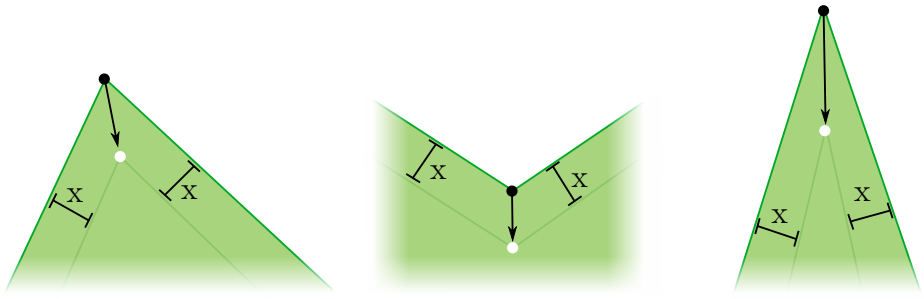

Figure 3.7: *As the active plan shrinks, the edges move with a constant speed. Several plans (left, middle, right) are shown (green), along with their shape at a later time (grey lines). In a certain time, every edge moves the same distance (x), but movement of the corners is defined as the intersection of the corners and so the distance moved typically varies. Very sharp reflex or acute angles between edges may cause corners to move with high speed (right). This speed approaches infinite as the interior angle approaches 2π from below, or 0 from above.*

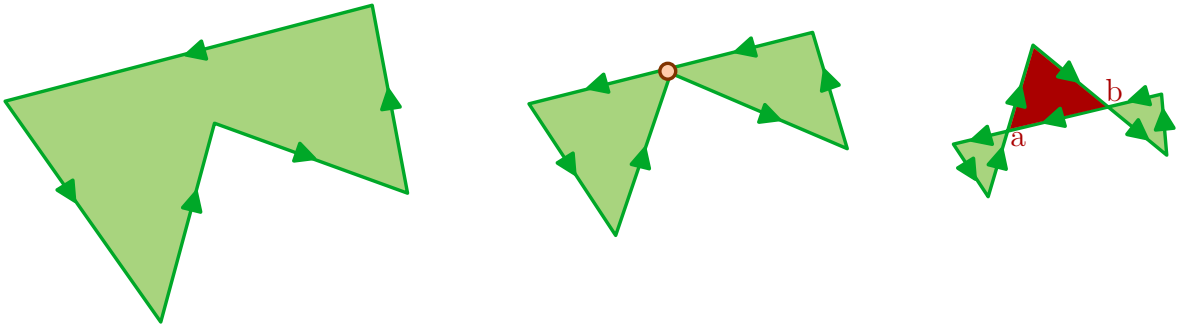

Figure 3.8: *Left: the anti-clockwise oriented input plan. Middle: The active plan at a split event (orange). Right: Without a split event, a portion of the active plan becomes badly formed. There are self-intersections at a and b, and the red region is defined by a clockwise loop; that is, the edges define an infinite inside region outside the red area.*

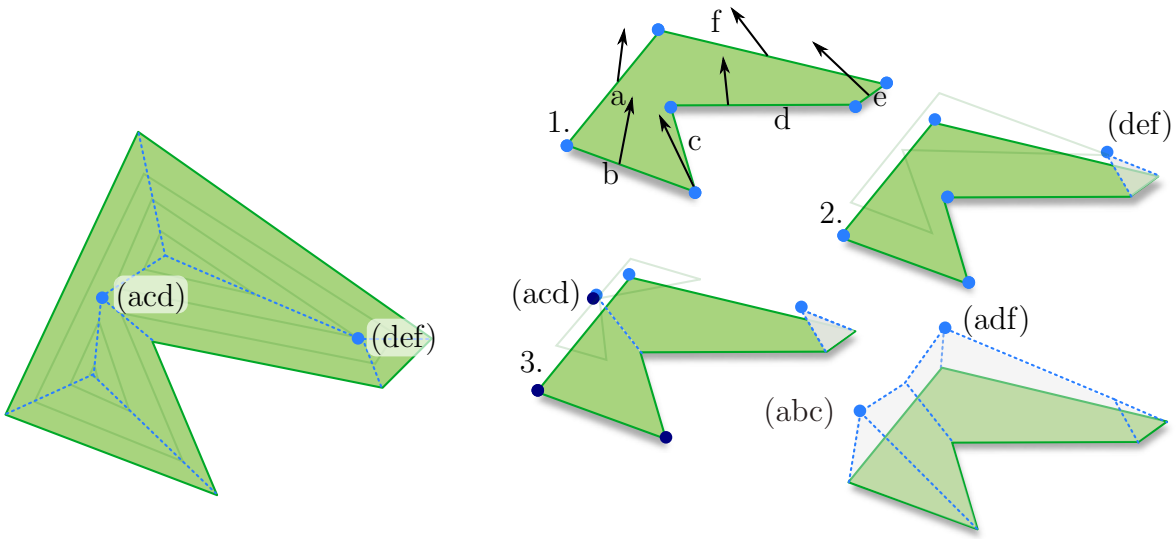

Figure 3.9: *Left: the straight skeleton is given by arcs (blue lines) tracing the verticies of a shrinking polygon (black lines). Each edge moves with a constant speed towards the interior of the polygon, and as it does the topology of the polygon changes in several different ways (dark green lines), during* events. *Right 1-3: The calculation of the SS is primarily a sequence of such events.*

- *Edge events* occur as the length of an edge shrinks to zero. When a plan edge shrinks to zero the direction planes defined by three consecutive (linked by corners) edges collide (Fig. 3.9, 2).
- *Split events* take place when two adjacent direction planes, and one non adjacent direction plane collide (Fig. 3.9, 3). These split the region bounded by the active plan into two parts.

.

We can describe these events in terms of the local plan around the direction plane

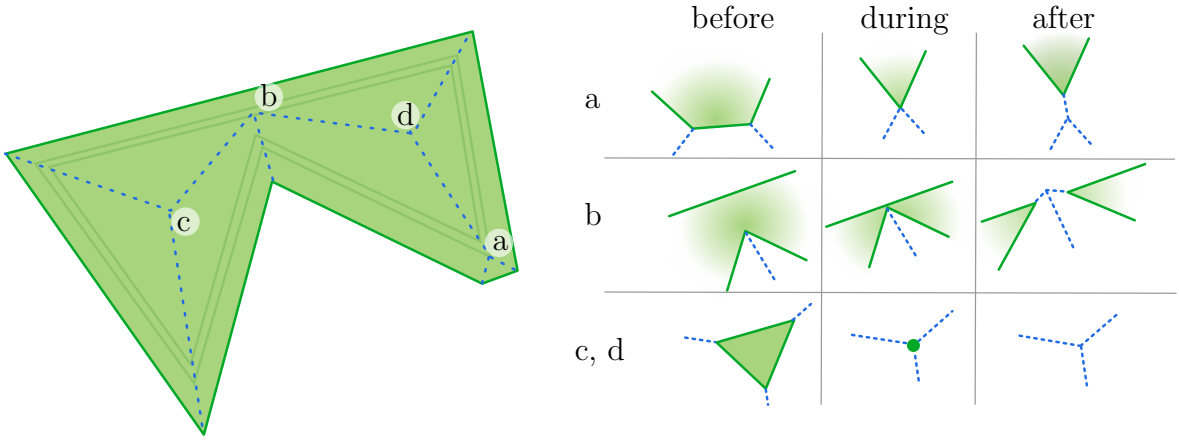

Figure 3.10: *Edge (a) and split (b) events that occur as a polygon shrinks. Peaks (c & d) comprise three co-sited edge events.*

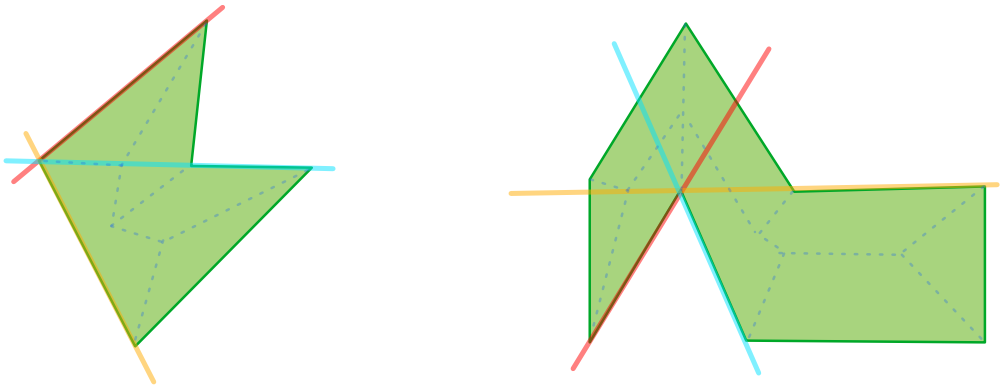

Figure 3.11: *The active plan in two configurations in which intersection of unbounded direction planes (intersection with active plan shown as red, cyan and orange lines) does not lead to an event as they occur outside the bounds of the associated edges.*

intersection point, Fig. 3.10. Here we see the local active plan region before, during and after edge events (a), split events (b) as well as peaks (c & d). As these peaks may be considered to be three edge events occurring together, we classify them as edge events.

Each of these events is witnessed by the intersection of three direction planes. However not all intersections between three unbounded direction planes indicate an event. As identified in Fig. 3.11, we must be sure that the faces intersect within the bounds of the associated edges on the active plan. Also of interest to optimisation is that at least one pair of adjacent plan-edges must be involved; an SS event consists of three edges, at least two of which must be adjacent.

Every event creates one or more output arcs, a portion of the boundary of a terrain face. Every arc is the boundary between two faces.

We present a crude algorithm in Fig. 3.14 that maintains this queue as new corners are introduced by events. We defer describing the event handling in detail until Sec. 3.2.4, noting that Felkel [68] simply gives a terse set of manipulations to the data structure in the case of edge or split events.

The active plan is stored in a data structure that holds the corners of each polygon in a doubly linked list, as illustrated in Fig. 3.12. There is such a list for every polygon and associated holes. Each corner, therefore, has a pointer to its next and previous corners (assuming counterclockwise order), as well as a pointer to its previous and next direction planes. The corner is a point in $\mathbb{R}^3$ at the lowest intersection of the adjacent plan edges. We may find the position of a corner in the active plan by intersecting the corner's next and previous direction planes with the sweep plane. Correspondingly, an edge on the active plan is given by the positions of two consecutive corners in the linked list. In this manner the linked list implicitly stores the active plan at the sweep

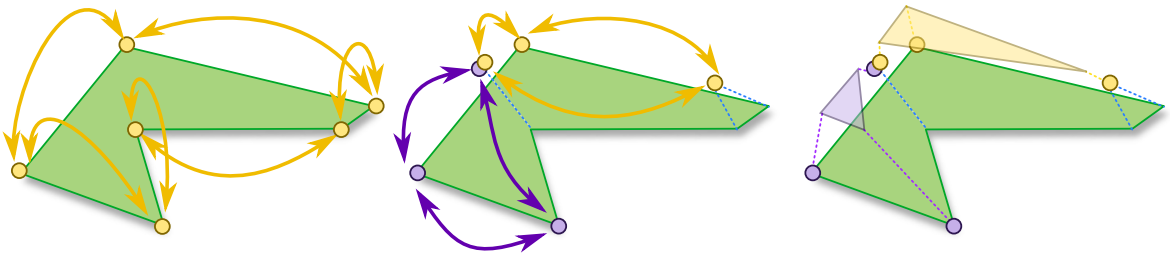

Figure 3.12: *Left: The initial set of corners (yellow circles) and points in the doubly linked list (yellow arrows) that make up the input plan. Not shown are the pointers to the adjacent direction planes. Centre: As the sweep plane rises, and various events occur the active plan may split. Corners are added and removed from the linked lists. Here two linked lists store an active plan with two polygons (yellow, purple lists). Right: By projecting the intersection of the corner's direction planes onto the sweep plan, we store the implicit active plan (purple, yellow polygons)*

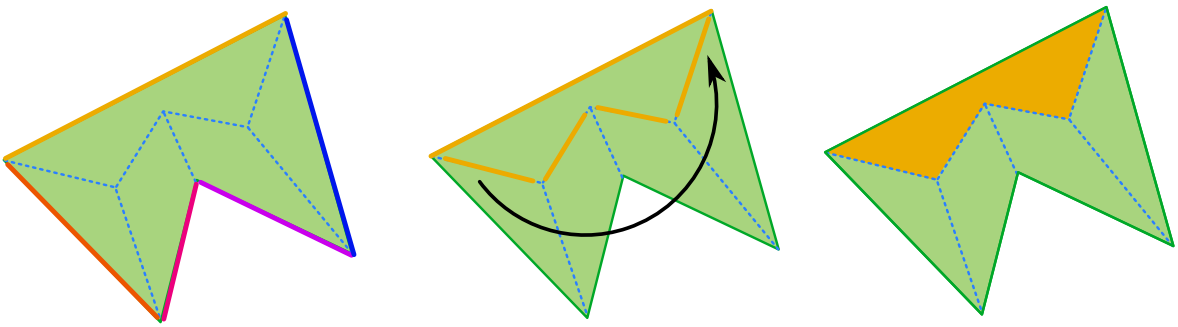

Figure 3.13: *Left: After all events have been processed, every arc is associated with two input plan edges. Middle: A single input plan edge has a set of edges, which may be traversed (right) in a counter clockwise direction to construct a face (right, orange).*

plane, via corners at or below the plane.

To simulate the rising sweep plane approaching events, a priority queue ordered by height (z) is kept, specifying triplets of edges colliding at a certain height. We assume that the queue only holds one event for each unique set of colliding direction planes. Before an event is processed, the algorithm checks that it is at or above the sweep plane, and within the current bounds of each face — previous edge events may even have removed the edges and their direction planes entirely. The details of the *HandleEvent* routine of Fig. 3.14 are introduced in the following section, which may add arcs to faces, and add or remove corners and edges from the active plan. Arcs are stored in a list associated with each input-edge; events add arcs to these lists. The algorithm continues until all events in the queue have been processed. After all events have been processed we traverse an input-edge's arcs in a counter clockwise direction to determine the 3D face. This process is illustrated in Fig 3.13.

Given a "random" or irregular input plan these two (split and edge) event types are the only features we are likely to see, Fig. 3.15. This is because the skeleton of irregular

```
Main begin
    Q = new priority queue;
    sweepZ = 0;
    foreach corner c in active plan do
        CreateGIEEvents ( c, Q );
    while !Q.empty() do
        event = FindNextEvent(Q);
        event.removePlanesNotInActiveplan();
        event.removePlanesOutOfBounds();
        if event.getPlanes().size() ≥ 3) and
        event.z ≥ sweepZ then
            newCorners = HandleEvent( event );
            sweepZ = event.z;
            foreach corner c in newCorners do
                CreateEvents(c, Q);
    foreach edge e in input plan do
        ReconstructFace (e);
end
CreateGIEEvents( corner c, queue Q ) begin
    p1 = c.nextEdge.getPlane();
    p2 = c.prevEdge.getPlane();
    foreach direction-plane p3 in the input do
        location = Intersect (p1, p2, p3);
        Q.insert (new Event(location, p1, p2, p3));
end
```

Figure 3.14: *Pseudo-code for the SS algorithm*

polygons rarely have events where more than 3 faces meet at one point.

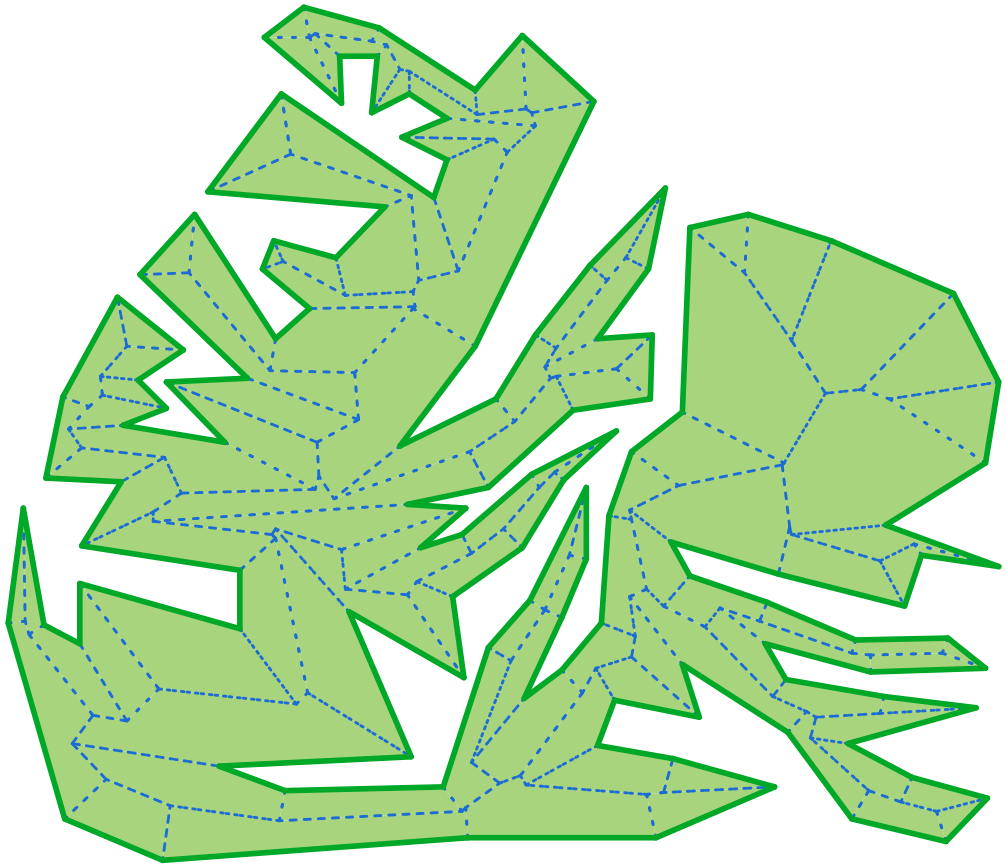

Figure 3.15: *The straight skeleton of a complex plan in which only three faces meet at every node in the graph.*

3.2.2 Computational Complexity of the Straight Skeleton

The algorithm presented in the previous section, Fig. 3.14, runs in a time complexity of $O(n^2 \log n)$, where the number of input plan corners is n. This is due to the observation that there are a maximum of n events that must each search for new adjacent planes to intersect ($O(n^2)$), and insert any new events into the priority queue ($\log n$). Filling the priority queue initially also takes $O(n^2 \log n)$ time.

Originally Aichholzer et al. presented a similar analysis in 2D[6], and a variation with a similar result[5]. These papers also prove the above lemma stating the number of events is $O(n)$. It is also given that calculating the SS of a convex polygon is possible in $O(n \log n)$ time since an edge on the active plan will only intersect with its neighbours. The higher complexity in the concave case is caused by the propagation of reflex verticies, and the requirement to identify which other edge they intersect with.

The following year Aichholzer and Aurenhammer[7] introduced an elegant method that triangulates the active plan.The key observation is that every event is witnessed by a shrinking triangle reaching zero area and collapsing, Fig 3.16. By keeping a list of triangles, ordered by their collapse time, the propagation of the offset (wavefront) is simulated. This would give a linear time complexity, except that the collapse of certain triangles does not signify an event. Due to an inability to place a non-trivial bound on these *flip* events, the algorithm has a total time complexity of $O(n^3 \log n)$. Recent research has lead to strong evidence that such an algorithm delivers $O(n)$ performance in practice[178].

Eppstein and Erickson[65] introduced the sweep-plane component used in the previous algorithm to construct a 3D terrain. This was augmented by a powerful closest-pairs data structure and advanced ray-casting techniques to give a sub-quadratic time complexity of $O(n^{1+\epsilon} + n^{8/11+\epsilon} r^{9/11+\epsilon})$, where r is the number of reflex verticies, and ϵ is a arbitrarily small constant controlling time/space trade off. Given that r is of order $O(n)$, and as ϵ approaches 0, a time complexity of $O(n^{17/11})$ is achieved.

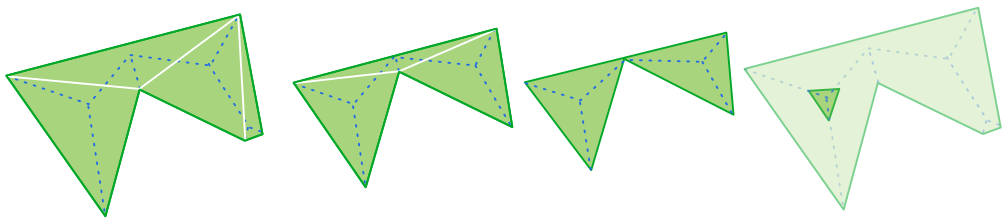

Figure 3.16: *Aicholzer introduced a triangulation based algorithm[7] for the calculation the Straight Skeleton in 1996. As the shape shrinks, the events (above; left to right) are each witnessed by a collapsing triangle in the triangulation (bordered by white lines). By ordering the triangles by their collapse time, it is possible to identify a correct sequence of events.*

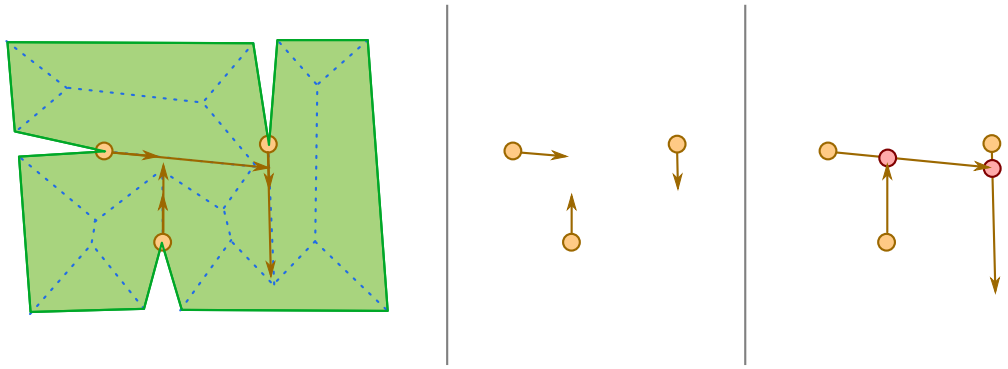

Figure 3.17: *Eppstein's motorcycle[65] graph divides the polygon (left) into concave regions, considering only the reflex verticies (orange points) and their propagation (orange line) with time. These propagation lines may not be crossed by another vertex, if they do the vertex terminates (red points). The time complexity of constructing such a graph is introduced as $O(n^{3/2})$. The resulting tessellation of the polygon may then be used as an acceleration structure when constructing the straight skeleton.*

Eppstein and Erickson also introduced a model of the problematic reflex verticies - that of calculating the *motorcycle graph*. A brief introduction is given in Fig. 3.17. Chen and Vigneron[40] continued this work to produce an algorithm that isolates parts of the skeleton based on the motorcycle graph. Chen's algorithm to calculate the motorcycle graph in a time of $O(r\sqrt{r}\log r)$ leads to a randomised algorithm to calculate the skeleton with a lower bound of $O(n\log^2 n + r\sqrt{r}\log r)$.

Recently Huber et al. introduced a robust, implementation-oriented approach with time complexity $O(n^2 \log n)$, which exhibited $O(n \log n)$ in practice. The algorithm introduces additional Steiner verticies to account for the effects of reflex verticies.

3.2.3 Straight Skeleton Degenerate Events

Thus the algorithm presented in Sec. 3.2.1, in line with the literature, is applicable to general input plans, however in contrived *degenerate* situations, we may see complex arrangements of active plan edges intersecting at a point. The previous work leaves these events badly defined; here we detail several observed situations: *loops of two*, *many edges colliding* and *parallel consecutive edges*. In contrast, the following Sec. 3.2.4 will introduce a *general intersection event* which calculates a well-formed active plan after all events – edge and split events, as well as the degenerate cases introduced here.

The literature is limited in its discussion of events. The original work by Aichholzer[6] describes split and edge events, but does not describe an algorithm to compute them. Eppstein[65] presents the *many edges colliding* degeneracy, under the classification *vertex events*, but does not detail an algorithm to resolve them. Only the work by

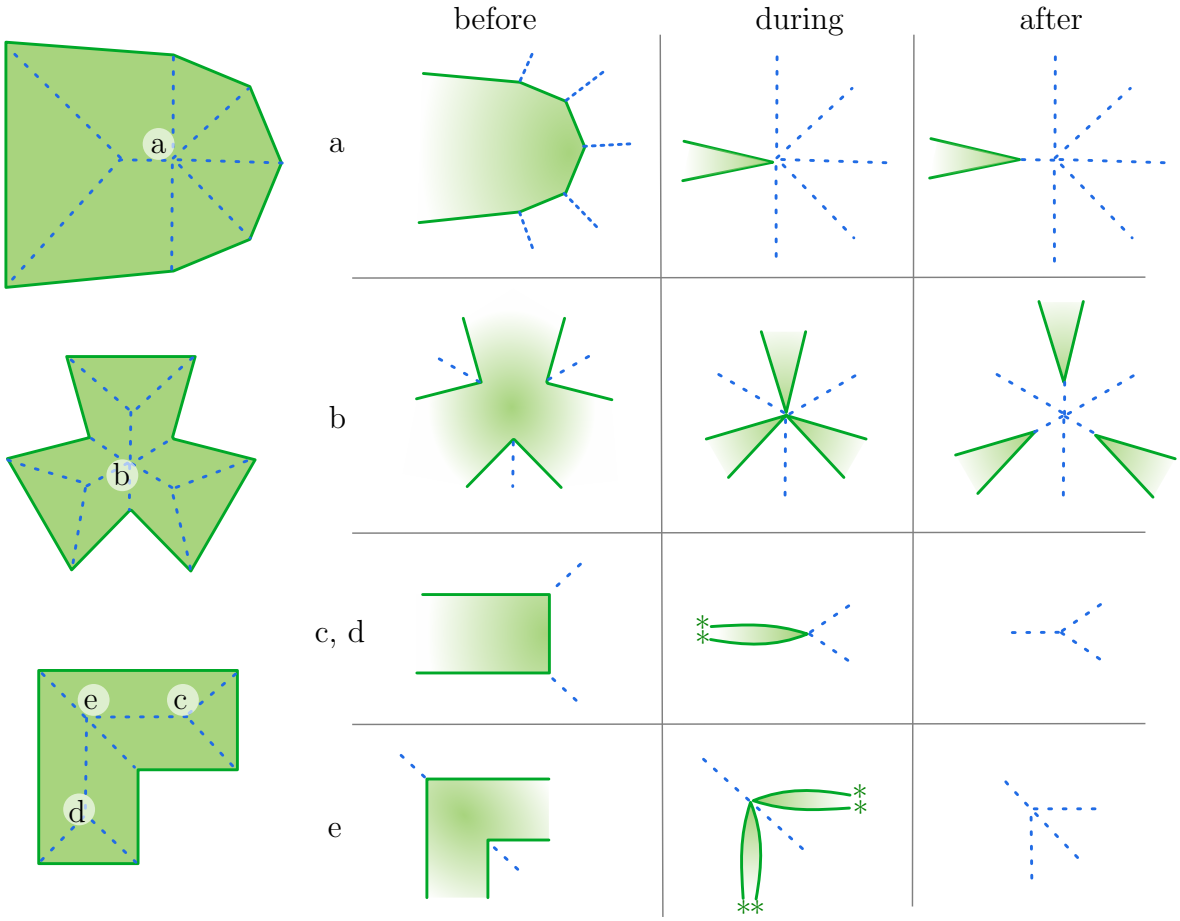

Figure 3.18: *In degenerate situations, more than three edges will collapse at one time (a,b & e). We also note that sometimes the active plan collapses to a* loop of two *(c,d & e). We show these coincident edges as curved lines, with asterisks.*

Felkel[68] explicitly addresses the topology manipulation at events, but then does not discuss degenerate events, beyond a special check for *loops of two*. As we introduce generalisations of the straight skeleton, these degenerate events and the algorithms used to resolve them become more important.

Fig 3.18, c,d and e, shows one degenerate case in which the active plan becomes a region with only two edges and zero area, a *loop of two* degeneracy. A more involved example is shown in 3.19. After all the events at a certain height, parallel edges may cause the active plan to become partially or entirely composed of these zero-area regions. Felkel at al.[69] require a special case to identify and remove these degeneracies.

Another type of degeneracy occurs as four or more plan edges collide at a point, the *many edge degeneracy*. Several connected edges may intersect at the same time, as illustrated in Fig 3.18 a, in which only the first and last edges exist after the event, as the intermediate edges shrink to zero length. Alternatively we may see reflex verticies in the input plan form several connected sets of edges involved in a single event, as in Fig 3.18, b. These types of events are ignored in some of the earlier work[6], introduced

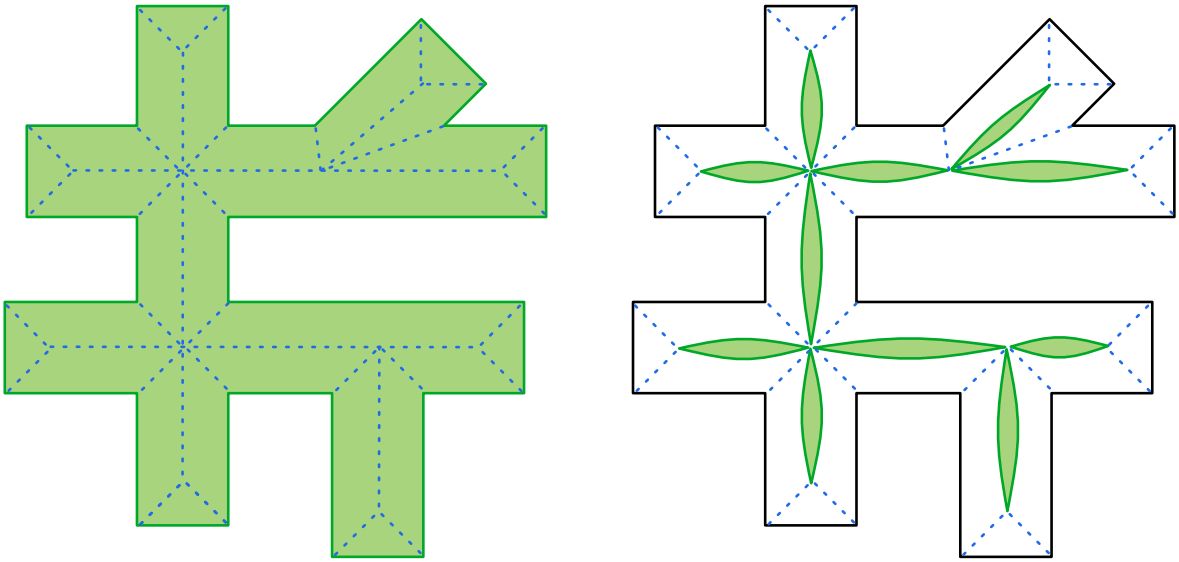

Figure 3.19: *A more complex example of a straight skeleton, left, that creates a zero area plan, right. Note that the curved line segments are in reality straight, but again drawn as curved segments to represent the topology.*

as a third type of *vertex* event in [65], and dramatically changes the expected time complexity of the algorithm in [40].

A final degenerate case occurs when adjacent, yet parallel, edges in the active plan become consecutive, the *parallel consecutive edge* (PCE) degeneracy. Fig. 3.20 demonstrates such a case. Because we have defined the movement of corners over the active plan, the intersection of the adjacent direction planes, the intersection of parallel collinear edges neighbouring a corner is a line, rather than point, causing a special case to arise. Existing work[6] leaves the outcome undefined. It appears that there are two resolutions techniques applicable to this degeneracy:

- The *separate* solution shown in Fig. 3.20, left-centre. After the PCE, the faces remain separated by an arc. This approach maintains a single face for every edge in the input plan. However defining the movement of such a vertex is problematic as the adjacent direction planes are coincident.

- The *merge* solution illustrated in Fig. 3.20, right-centre. When a PCE occurs, the two faces are joined together. This has the advantage that no vertex is created with parallel adjacent edges. However this removes the one-to-one mapping between the edges in the input plan and the output skeleton faces.

In the unweighted case a further resolution is to define a special case for this situation. In this case the corner would move perpendicularly to both the neighbouring plan edges, towards the interior of the plan. This is inelegant, and is not able to generalise to the weighted case in Sec. 3.3.

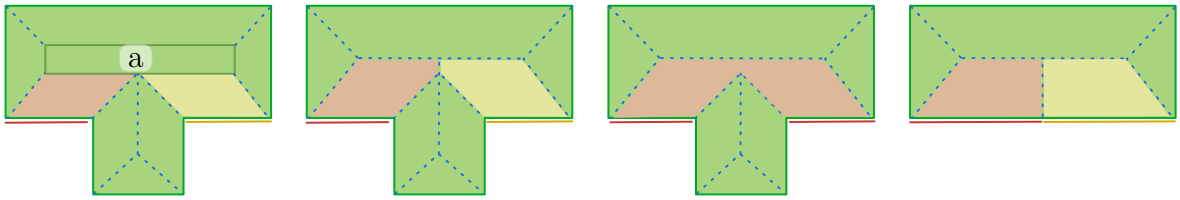

Figure 3.20: *Left: The PCE problem: What is the resolution to the event marked a? Left-Centre: The separate rule. Right-Centre: the merge rule. Right: When there are PCE in the active plan, a resolution must still be applied to determine the initial direction and speed of the corner.*

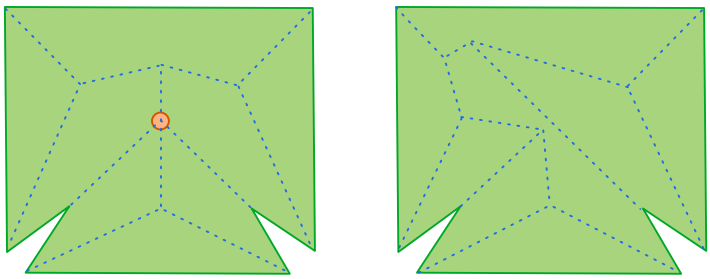

Figure 3.21: *Figure from [65], demonstrating that perturbing the sequence of events at a point (orange), rather than solving them together, may lead to wildly different results (left).*

It is interesting to note that [6] seems to exclude such PCE in the input, however there is no easy way to tell if parallel edges will become consecutive as the skeleton is constructed. By symmetry we would expect to see PCEs in the input computed using the same solution, as illustrated in Fig. 3.20, right.

The PCE resolution technique chosen in a given SS implementation will depend on the desired properties of the resulting skeleton.

In order to process any of these degenerate events it may be suggested that we perturb the active plan slightly. However, as in Fig. 3.21 from Eppstein and Erickson[65], there are situations in which small perturbations cause undesirable large changes in the resulting skeleton. In this situation two input reflex corners form a third reflex corner during evaluation. It is therefore necessary for a single event to process collisions between many direction planes. The earlier Fig.3.5, bottom right, gives another example where successive pairs of reflex corners meet, are resolved, and carry on to create additional reflex corners.

3.2.4 The Generalised Intersection Event

This section demonstrates that we can unify the split, edge and vertex events into a *generalised intersection event* (GIE). This avoids the involved categorisation in the

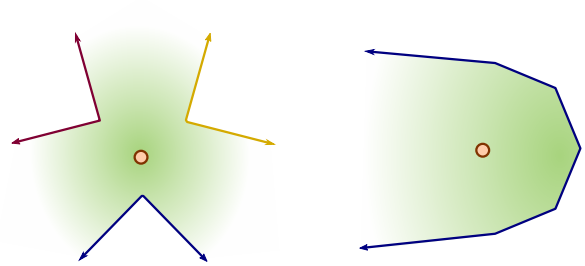

Figure 3.22: *Two regions of active plans corresponding to Fig. 3.18b on the left and Fig. 3.18a on the right. We can group the active plan edges involved in an event into chains (red, yellow and blue edges) by asking which edges are consecutive in the linked list data structure.*

literature and allows a single algorithm to compute well formed results, even when events contain loop of two, PCE or many edge degeneracies.

The GIE is consistent with the split and edge events observed on the active plan.

We begin by defining *chains* of edges that are involved in an event, Fig. 3.22. A chain is a list of consecutive edges that are colliding at the event. They are ordered corresponding to the edge's direction. These form the partial boundary to our possibly bounded topological disc region of the active plan that is collapsing at the event.

In the case of the SS we can order the chains themselves around the event's location, Fig. 3.23 d. That is the chains themselves may be ordered in a cyclic list. We can note that after an event the last edge in the preceding chain, and the first edge in the following chain become adjacent, Fig. 3.23 c and e.

The intuition behind the GIE is that at an event's location, an inside area on the active plan collapses and transitions to an outside area. As this occurs, adjacent chains that before bounded interior regions split in two, with the two halves of adjacent chains now bounding an exterior region. These newly created chains do not intersect each other as their single shared vertex is moving away from the event's location, in a unique direction. This direction is bounded by the two edges of the new chains, as in Fig. 3.23 d, and ensures a solution free of self-intersections. Therefore, our algorithm first removes edges that shrink to zero length, and then "cycles" the chains in such a manner to bound the interior regions.

To resolve an event using the GIE we firstly pre-process the edges involved in the clustered intersection events into a set of *chains*. A chain defines a connected portion of the active plan boundary involved in the event. A chain, h^i, is a list of consecutive active plan edges, $\epsilon^i_1 ... \epsilon^i_{hmax_i}$. A cyclic *chain list*, b, contains all such chains, $h^1 ... h^{bmax}$ (we assume a cyclic index). The chain list is ordered by the edge's orientation around the intersection. After this pre-processing we perform the following sequence of steps, a pseudocode summary is given in Fig. 3.26.

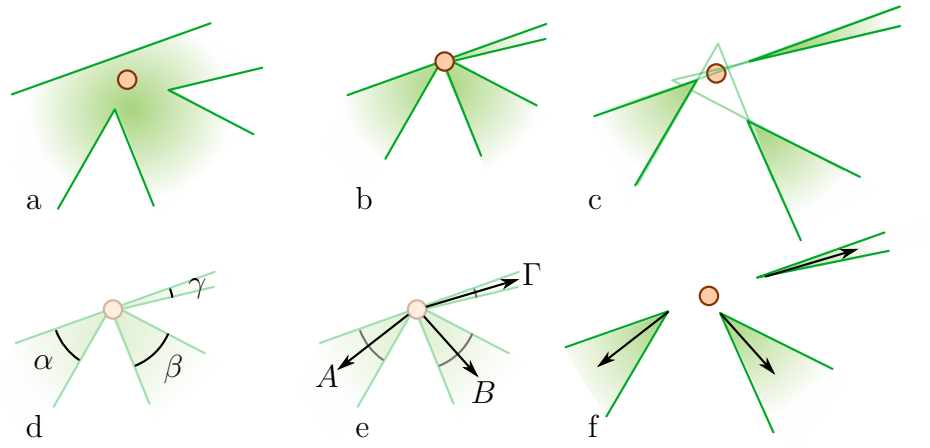

Figure 3.23: *As three chains approach an event (a, orange), we can imagine the active plan at the event (b), or the degenerate plan if no event takes place (c). We observe that the last edge in the previous chain and the first edge in the following chain become adjacent, also that every chain is split into two (f). Given that the angles between adjacent chains (d, α, β & γ) may not overlap and that all edges are moving towards the interior, the directions of the new inter-chain verticies (e, A, B & Γ) are unique and non-intersecting. Hence the new topology (f) does not self-intersect.*

- *Intra chain step* (Fig. 3.24): Within each chain, any edges in the middle (not the first or the last edge in a chain) shrink to 0-length and are removed from the active plan. Formally, we remove all interior edges from a chain h^i, leaving only the start, ϵ^i_1, and the end, $\epsilon^i_{hmax_i}$, of the chain. That is, if $hmax_i \geq 3$, then edges $\epsilon^i_2..\epsilon^i_{hmax_i-1}$ are removed from the active plan, being replaced by a new corner at the event location, connecting the end of ϵ^i_1 to the start of $\epsilon^i_{hmax_i}$.This leaves only chains of length one or two remaining.

- *One chain step:* Chains of 1 edge are split at the location of the event. All chains are now of length 2.

- *Inter chain step* (Fig. 3.25): We split each each chain into two and connect the start of the last edge in the previous chain to the end of the first edge in the following chain. The chains therefore swap an edge with their neighbour; all chains remain of length two. Formally the inter-chain stage takes place between each adjacent pair of chains, h_x and h_{x+1} in the cyclic chain list b. For each pair of adjacent chains we create a new corner at the event location and connect the start of the last edge in the proceeding chain, $\epsilon^x_{hmax_x}$, and the end of the first edge in the following chain, ϵ^{x+1}_1. Finally the inter-chain stage finishes by removing any unreferenced corners from the active plan.

- *PCE step:* We resolve any newly parallel consecutive edges according to the merge or separate solutions.

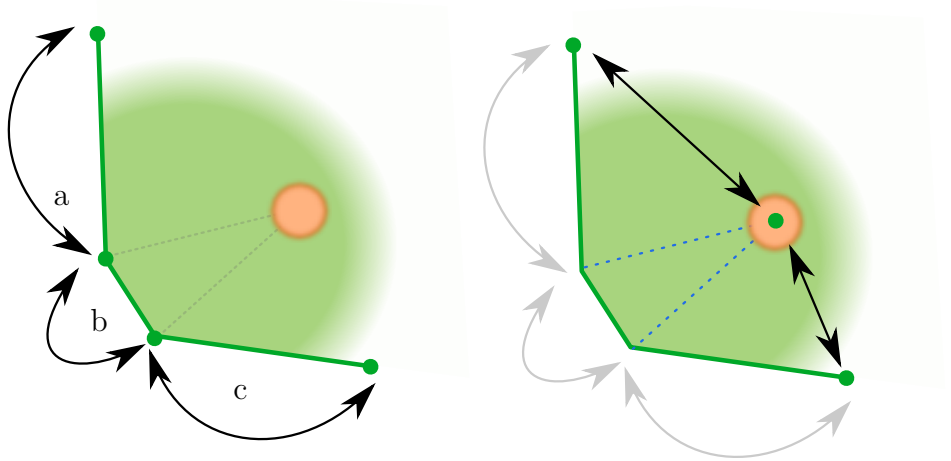

Figure 3.24: *The intra chain step removes all edges in the interior of a chain, joining the first edge to the last. Left: The edges a,b and c intersect at the orange point. The corner's next and previous pointers are shown (black arrows). Right: New arcs are added from the old corners to the intersection location (blue lines), and the pointers are manipulated to remove the central edge, b.*

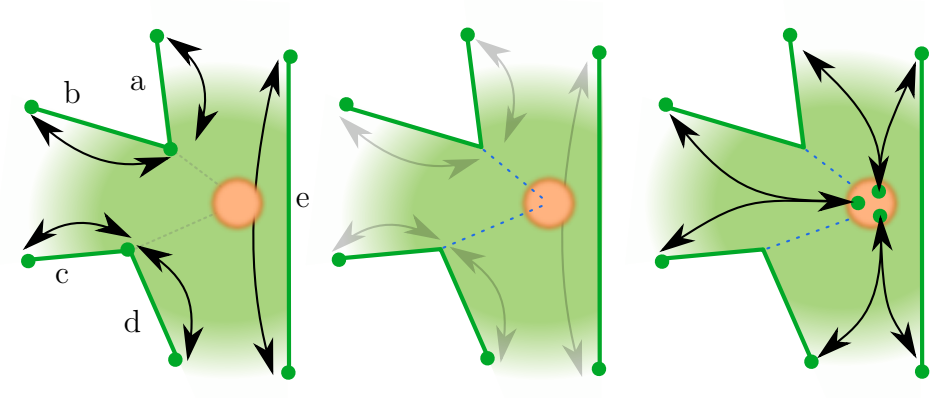

Figure 3.25: *An intra chain manipulation followed by an inter chain manipulation, colouring as Fig. 3.24. Left: the active plan before the event. Middle: Additional arcs are created during the intra chain stage. Right: The pointer manipulations swap edges with their neighbours around the intersection point.*

Because more than three planes may meet at a single point, we must modify the *FindNextEvent* routine of Fig. 3.14 to search Q for all co-sited events. The new event contains all directions planes that intersect at one point. Because Q is ordered by sweep plane height, we are able to find such planes efficiently.

```
HandleEvent( EventCluster ec ) begin
    RemoveAllInactiveEdgesFromCluster( ec );
    chainList = BuildEdgeChains( ec );
    if chainList.countEdges() < 3 then
        return;
    /*intra chain stage*/
    foreach chain chain_j in chainList do
        foreach consecutivePairOfCorners c_k, c_l in chain_j do
            AddSkeletonArc(ec.location, c_l);
            c_l.inactive = true;
    PerformOneChainStep();
    /*inter chain stage*/
    foreach consecutive chain_j, chain_k in chainList do
        c1 = firstCornerOfLastEdgeOf chain_j;
        c2 = firstCornerOfSecondEdgeOf chain_k;
        cnew = createNewCorner( ec.location );
        cnew.prevDirectionPlane = c1.nextDirectionPlane;
        cnew.nextDirectionPlane = c2.nextDirectionPlane;
        InsertCornerBetween( cnew, c1, c2 );
    PerformPCE();
    return newCorners();
end
```

Figure 3.26: *Algorithm for the generalised intersection event.*

The single GIE event with PCE handling allows the active plan to remain well-formed after both collisions with more than three edges involved, and successfully handles the loop of two situation, as in Fig. 3.27.

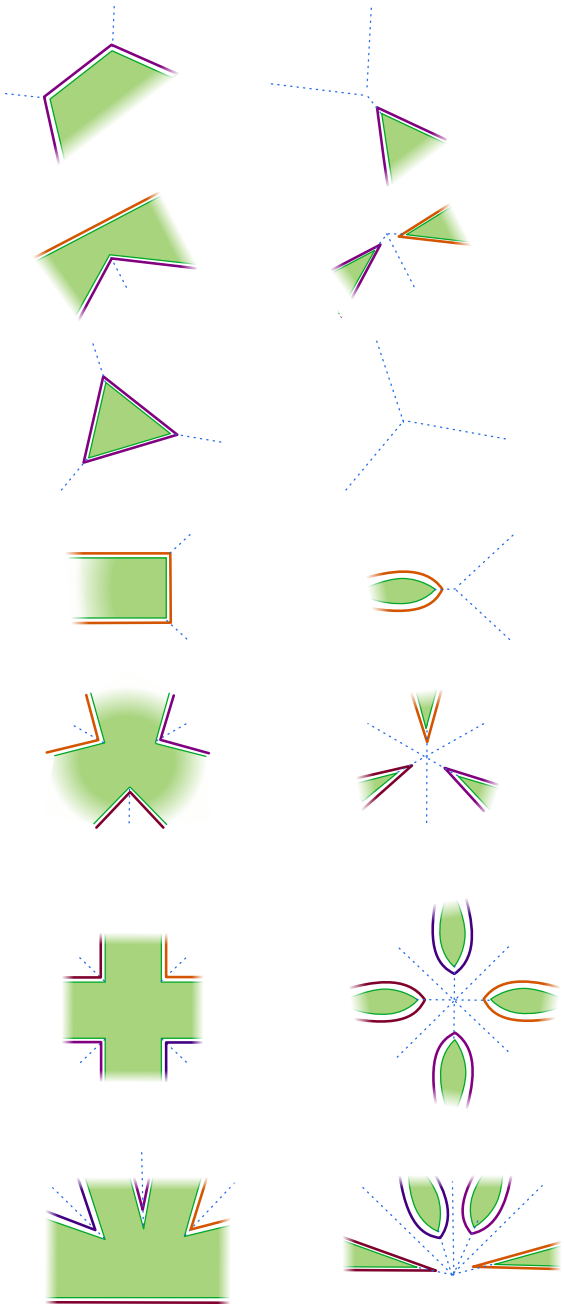

Figure 3.27: *The results (right column) of applying the GIE to several different types of situation (left column). From the top: an edge event, a split event, a peak event, one pair of collapsing non-parallel edges, a three chain situation, four pairs of collapsing non-parallel edges and an event that includes a straight line and parallel edges. Bold solid coloured lines show chains both before and after.*

3.3 The Positively Weighted Straight Skeleton

The positively weighted straight skeleton (PWSS) is a variation of the straight skeleton. Each edge is allowed to move with an independent speed towards the interior the bounded region as the sweep plane rises. The PWSS was introduced in [7] and [65] as *the weighted straight skeleton*, however for reasons that will become clear in the next chapter the naming convention in this document has been altered. Neither of these publications investigate any of the new features and degeneracies that may occur with the weighted skeleton. Later work[16] addresses only the convex cases.

The increased degrees of freedom that varying the edge speeds introduces, again leads to a new class of degeneracies. As with the SS, there are a class of PWSS-like constructions which are similar, except in their behaviour when certain borderline events arise. We have already seen one example in the case of the SS, the parallel consecutive edge degeneracy, which can be solved using either the merge or separate rules. The new class of degeneracies that occur in the PWSS are a generalised version of these SS PCE events.

3.3.1 Introduction

To enable independently weighted edges we must introduce another degree of freedom for every edge in the input plan, e_i^j. This is an *angle*, θ_i^j, which measures the angle between the vertical (perpendicular to the input plan), and the direction plane, Fig. 3.28. As the edges may not move over the active plan with unbounded speed, we enforce the limit $0 \leq \theta < \frac{\pi}{2}$.

Because of the etymology of straight skeleton terminology we use the terms *angle* and *weight* interchangeably to refer to the speed of propagation of an edge in the active plan.

The construction of the PWSS is identical to the SS for nearly all events. However it is instructive to note that the resulting skeletons may have different properties. For example, as shown in Fig. 3.29, the skeleton faces may contain holes. This necessitates a new approach to constructing the faces of the terrain, in which we traverse all arcs that have been created and assigned to an input edge. As in the SS case, we traverse the face boundary counter clockwise, starting from the input plan edge. Finally all remaining arcs are traversed, and oriented, in a counter-clockwise manner on the associated direction plane to form holes.

Compared to the faces of the unweighted skeleton, the faces of the PWSS have a more complex geometry. For example, Aichholzer proved in [6] that every face of the SS

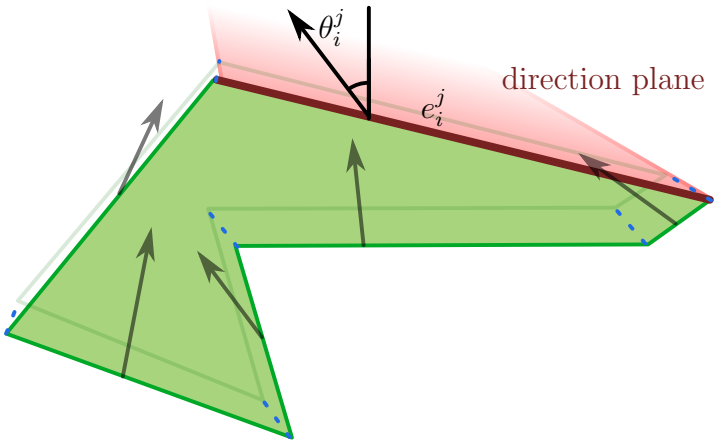

Figure 3.28: *In the PWSS, every input edge is associated with an angle that defines the slope of the associated face.*

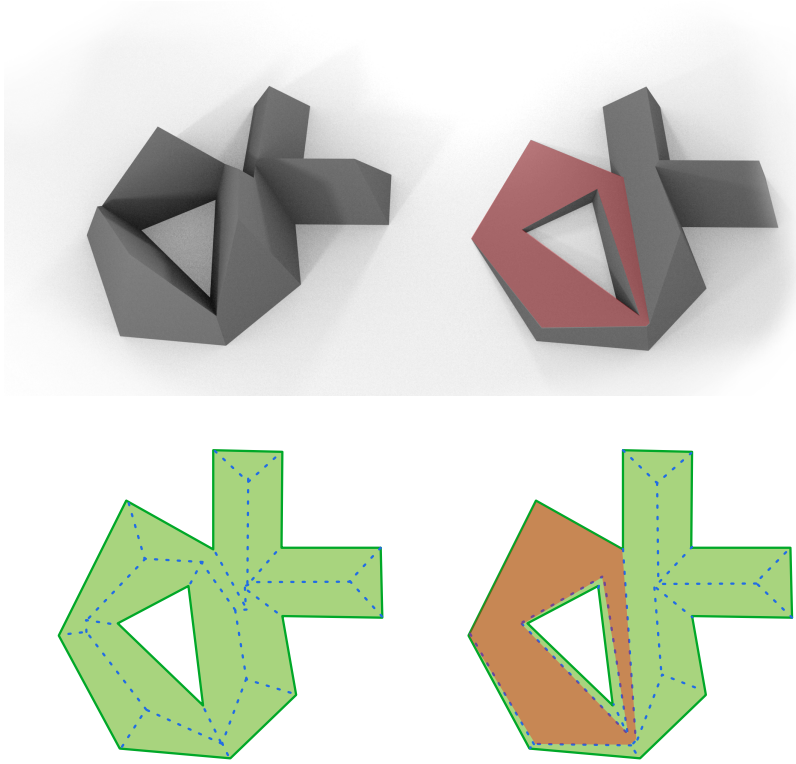

Figure 3.29: *Top: The 3D terrains or roof models of two skeletons. Bottom: Their corresponding 2D PWSSs. Left column: An unweighted skeleton. Right: A PWSS in which one face (red) has a shallow angle which causes it to contain a hole.*

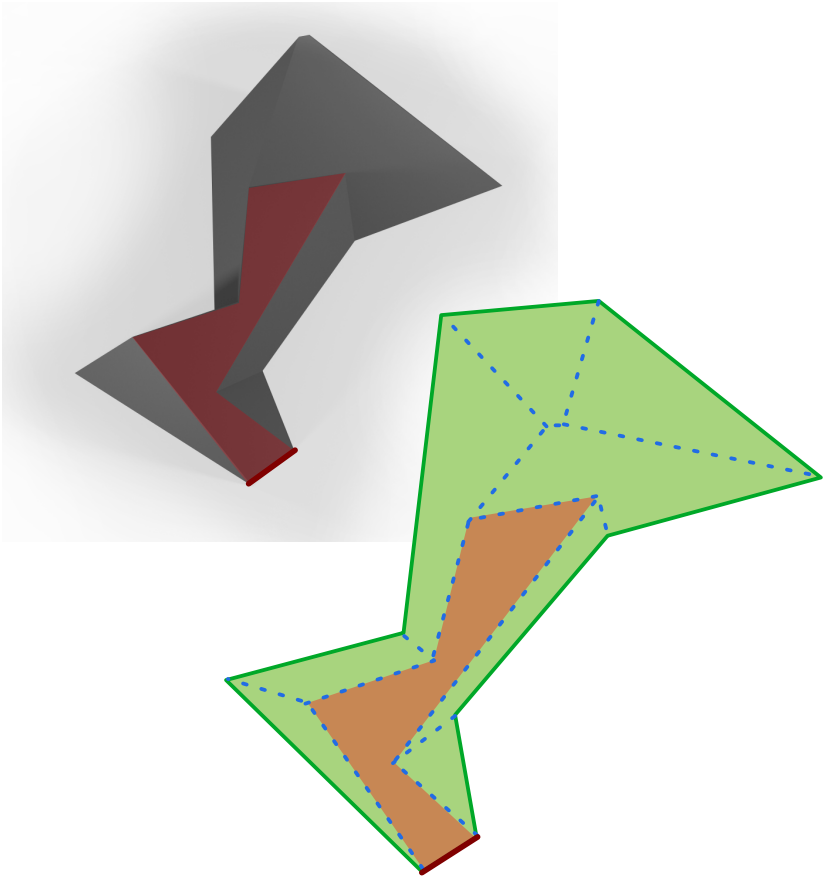

Figure 3.30: *A PWSS in which a face (red area) is non-monotone with respect to it's associated input plan edge (red line).*

is monotone with respect to the edge that lies on the input plan, however this is not the case with the PWSS. Fig. 3.30 introduces an input plan in which reflex corners and steep angled edges combine to cause a shallow edge to become non-monotone with respect to its edge.

Although degenerate cases do not occur frequently, the additional degrees of freedom that the PWSS has over the SS allows more input plans to become degenerate, given particular direction plane angles. The output of all possible PWSSs are are a superset of all possible SS; the possible PWSS events are also a superset of the SS events. As with the SS, given a random input plan, we are likely to see only events involving three edges. However, the degenerate cases become more intricate, and must be addressed on a global scale. It is hard to defend the use of the PWSS when a complete algorithm for all possible plans cannot be given, and so we continue to introduce, and suggest resolutions to, these PCE-like events.

3.3.2 The PCE event revisited

The parallel consecutive edge problem of the SS can again be observed in the PWSS. Recall that this degenerate case arises when two (or more) neighbouring edges in the active plan become colinear upon the sweep plane. This happens, for example, when edges previously separating the colinear edges are eliminated, via the intra-chain step of the GIE.

A PCE event may occur in the same manner as in the SS, as in the earlier Fig. 3.20, as well as new situations introduced by the varying edge speeds. The input plan edges which cause the degeneracy no longer need to be colinear since a faster moving edge may catch up a slower edge in the PWSS. Therefore there are a larger range of input plans that lead to PCEs in the PWSS than the SS, as illustrated in Fig 3.31.

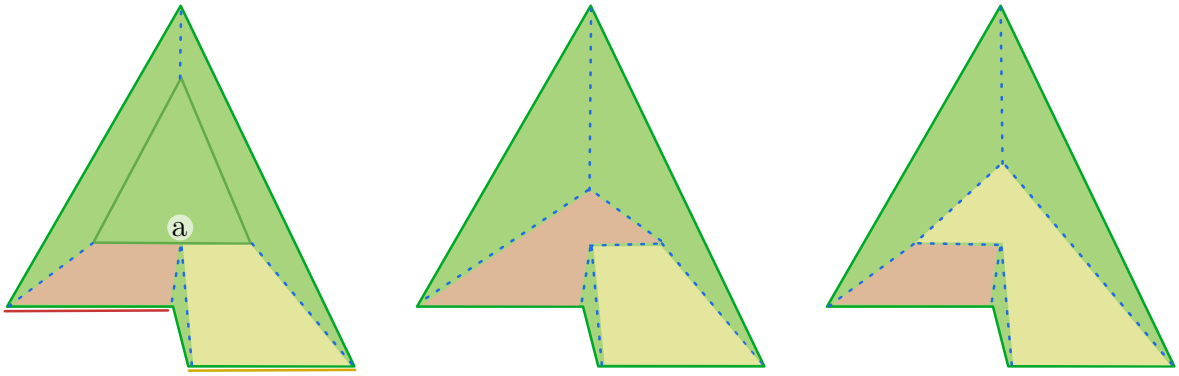

Figure 3.31: *A plan that leads to a PCE, a. The algorithm must choose between the red (middle figure) or yellow (right figure) faces to dominate.*

If the two neighbouring and colinear edges bound different sides of a region, the output is an arc. This arc is a roof-ridge and the computation proceeds as normal – at the opposite end of the ridge the two edges will collide again. This is not a degenerate event; we can distinguish the regular "roof ridge" case from a degenerate event by examining the relative directions of the directed edges in a plan. However, when the edges have the same orientation (they bound the same side of a region) we are not able to determine the direction of the subsequent arc, Fig. 3.31. The intersection of the adjacent direction planes is a horizontal line, parallel with the sweep plane, which causes the direction of the new corner to be under-constrained. For example in Fig. 3.31, left, it is unclear, at point a, whether the corner should move to the left, or the right.

It is unhelpful to examine situations where the edges are nearly parallel for guidance. As the angle between the edges approaches $\pi/2$ from different directions, we get suddenly different results. Either one or the other edge will be predominant. This singularity means that the limiting case is of little help when resolving the degeneracy.

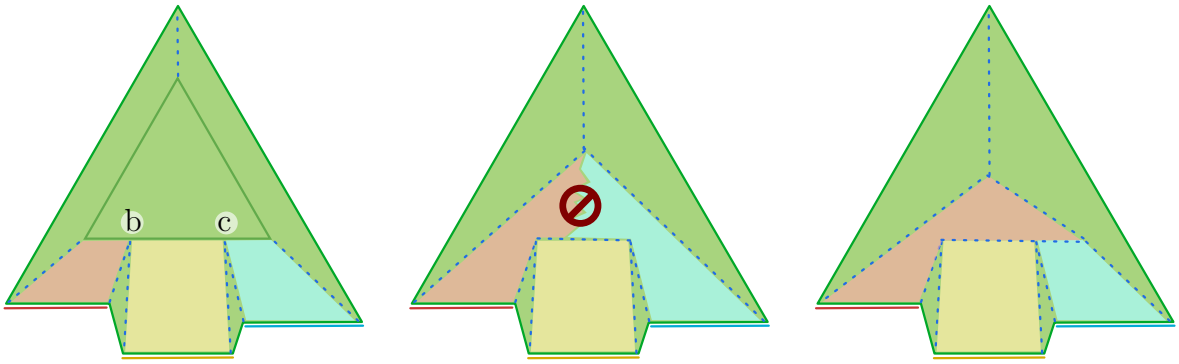

Figure 3.32: *A PCE that requires global coordination to resolve. If the events at b and c do not coordinate, we may end up with non-enclosed regions on the plan (middle). To address this issue one edge is globally determined to dominate, right.*

To complicate matters further, more that two edges may become parallel and consecutive upon the sweep plane at a single height. If these events are addressed separately, we may create further PCE degeneracies, leaving a poorly defined skeleton face, Fig. 3.32 middle. Therefore the PCE degeneracies need to be solved consistently and globally. This requirement for a global solution sets the PWSS apart from the SS, which can be constructed from local events that occur at a single point.

Our strategy to resolve this degeneracy replaces the set of PCEs with one or more of the approaching edges, which share a single angle. We take inspiration from our merge resolution of the unweighted SS PCE to combine these skeleton faces.

Given a set of edges that form the PCE degeneracy, $\{e_n^j\} \in PCE$, and their angles, $\{\theta_n^j\}$, we identify one angle, $\Theta = f(\{\theta_n^j\}) \mid e_n^j \in PCE$. The edges and faces associated with Θ, are merged, and the remaining edges and faces are removed from the active plan.

To select this angle, Θ, we propose using a priority scheme, f, derived from the angles of the edges. This scheme selects one or more edges with the same angle. We then use the SS merge solution (Sec. 3.2.3) to combine these faces, and remove the others. Fig. 3.32, illustrates the case in which each angle is unique, whilst Fig. 3.33 demonstrates a situation in which Θ is shared between two edges.

Typical priority schemes for f are:

- *volume maximising* (lowest θ), or
- *volume minimising* (highest θ).

The choice of ordering scheme, f, very much depends on the application for which the PWSS is being used for. This PCE resolution method is the most convenient of a large

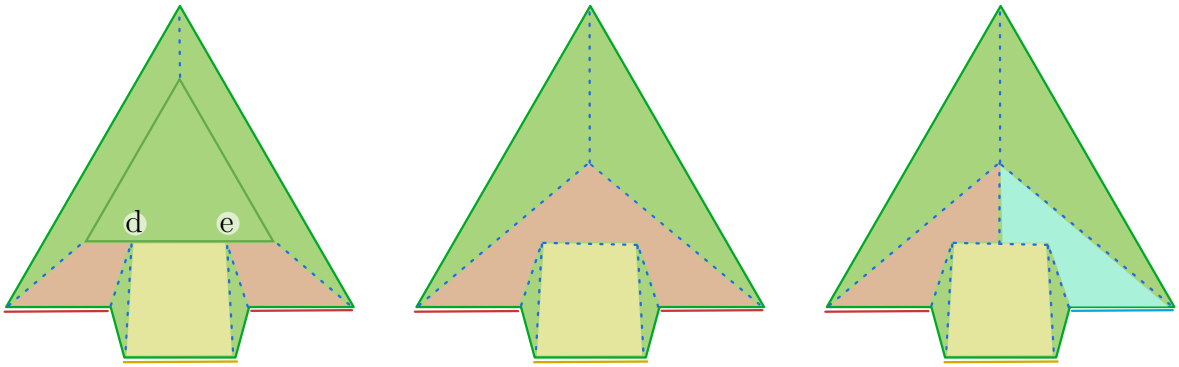

Figure 3.33: *Left: A PCE degeneracy with two edges sharing an angle (red), and a shallower edge (yellow). Middle: Using the scheme f =* volume maximising*, Θ is chosen to be the angle of the red edges. Therefore the two red edges and their faces are merged, and the yellow face is removed. Appropriate arcs are added to the output. Right: There are many alternate consistent resolution systems apart from the one presented here.*

number of alternatives. We can imagine other schemes, Fig 3.33, right, but find ours is a simple and practical approach.

3.4 The Negatively Weighted Straight Skeleton

In passing we may also note that the same degeneracies and techniques are applicable to the negatively weighted straight skeleton (NWSS), an example of which is show in Fig. 3.34 left. This skeleton is the dual of the PWSS, representing an ever-growing polygon. We omit further details of this structure here due to its similarity to the PWSS. Indeed, we obtain the same 2D skeleton by taking the PWSS of weighted polygon, and the NWSS of the same polygon with each edge's direction reversed, a situation illustrated in Fig.3.34, right.

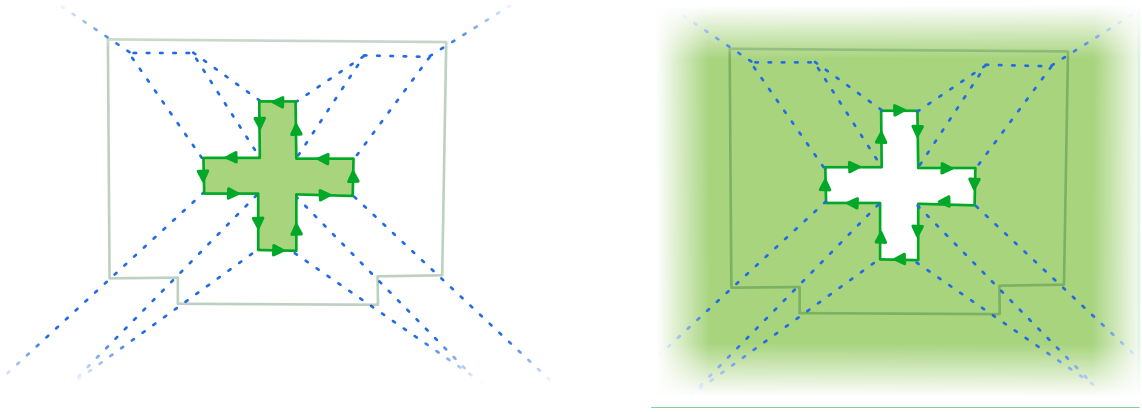

Figure 3.34: *Left: A negatively weighted straight skeleton (NWSS), in which every edge, e_i^j is associated with an direction plane specified by an angle $\theta_i^j \leq 0$. Right: The skeleton constructed is identical (barring degeneracies) to a PWSS in which every edge's direction is reversed, and θ_i^j is negated.*

3.5 The Mixed Weighted Straight Skeleton

The final variation of the SS we will introduce is the *mixed weighted straight skeleton* (MWSS). This new structure allows the angle of the direction planes, θ, to be positive or negative over edges in a single plan. Thus regions of the active plan can shrink inwards or grow outwards. Once again the increased degrees of freedom introduce new types of degeneracy. This section introduces some of the issues surrounding these *point degeneracies*, presents an algorithm for simplifying them, and introduces one theorem as to the solution of such cases.

As in the PWSS case, θ is limited in the MWSS to avoid infinitely fast edges on the active plan, allowing only $-\frac{\pi}{2} < \theta < \frac{\pi}{2}$. Therefore a $\theta < 0$ implies that an active plan edge is moving away from the interior of the polygon, a $\theta = 0$ implies an edge that does not move, and a $\theta > 0$ implies an edge is moving towards to interior of the polygon. Fig. 3.35 gives an example of both a PWSS and MWSS.

The MWSS enables a wider variety of 3D terrains to be defined; the set of skeletons definable are a superset of the SS, PWSS and NWSS schemes. For example the active plan can grow, as well as shrink, or can be a mixture of both. Therefore certain MWSSs may not terminate after the final event; the enclosed area may continue growing indefinitely as the sweep plane rises. It is an open problem to determine if a given MWSS will terminate if it contains any values of $\theta < 0$, without executing the skeleton algorithm itself. Fig. 3.36 gives an example in which the resolution of a borderline case differentiates between an non-terminating skeleton, and a terminating one.

As with the PWSS, the active plan can split as the sweep plane rises. But as Fig. 3.35 shows, like the NWSS, MWSS regions can merge.

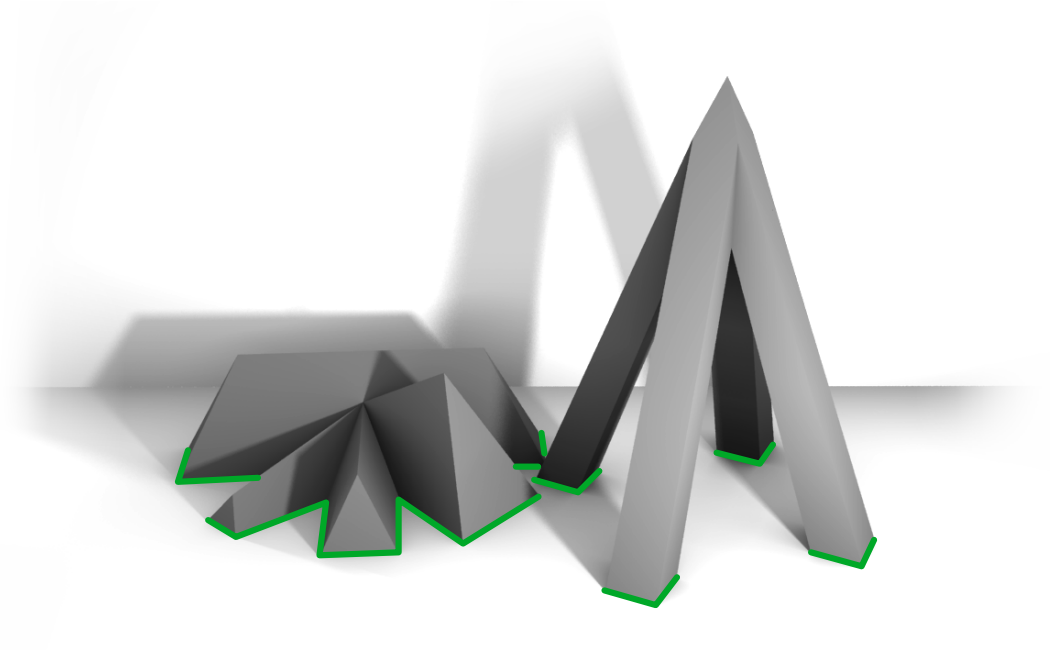

Figure 3.35: *. Left: A complex event in a PWSS, over a plan (green). Right: A MWSS in which four areas merge to become one. Note that the 3D models are the resulting terrains of a skeleton as some MWS skeletons are difficult to illustrate in 2D.*

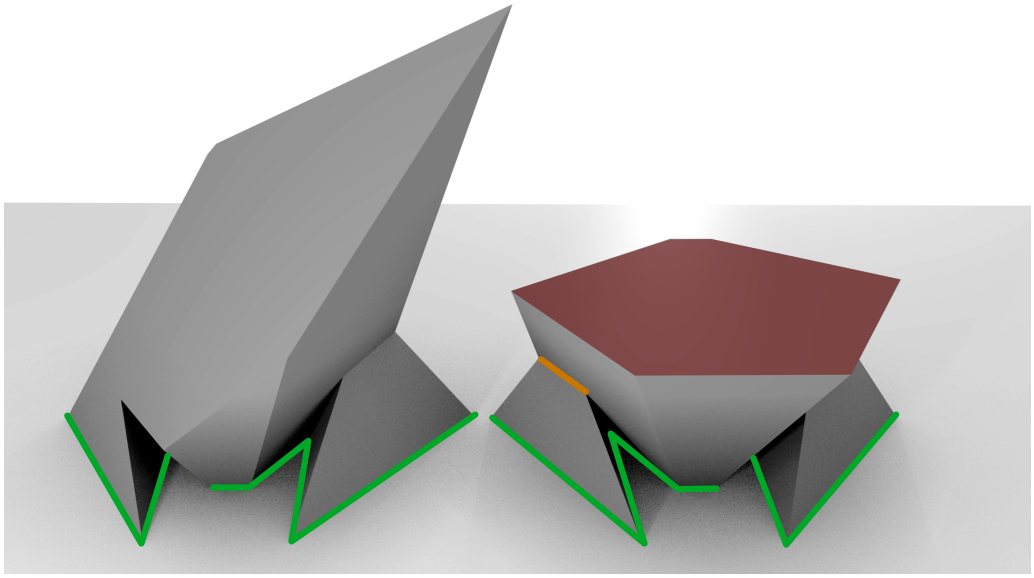

Figure 3.36: *MWSS that are bounded (left) and unbounded (right). The red face grows to an infinite area as the sweep plane rises. A small perturbation to the input plans is the only difference between the input plans, all θ value are equal. The PCE event which occurs along the orange line determines the behaviour of the skeleton.*

We note in passing that MWSS events exist in which no resolution is necessary. The edges intersect only at the event, but not after it. We disregard these *grazing* events in what follows, as they are trivial to test for and may be simply ignored.

Given the additional degrees of freedom available in the MWSS we expect to encounter the degenerate situations observed in the SS and PWSS cases. In addition there are are a new class of *point degeneracies* observable

3.5.1 Point degeneracies

Given the additional degrees of freedom available in the MWSS, it is unsurprising that the GIE solution no longer solves all situations. Fig. 3.37 gives one simple example event in which the GIE causes the active plan to become badly formed.

Indeed every edge of an arbitrary input plan may be coerced to collide at single point by altering the values of θ. A more complex example of a simple event is introduced in Fig. 3.38, which shows a possible event with many edges colliding. Here we can see chains of edges representing bounded, as well as unbounded areas, loops, and chains surrounding other chains, colliding at a simple event.

If all the edges are moving inwards or outwards, as with the PWSS or NWSS, the SS GIE introduced in Sec. 3.2.4 is still suitable. However in the complex degenerate events that may occur with some angles of $\theta > 0$ and some $\theta < 0$, another algorithm is needed. Fig. 3.40 gives one such situation and a number of plausible solutions.

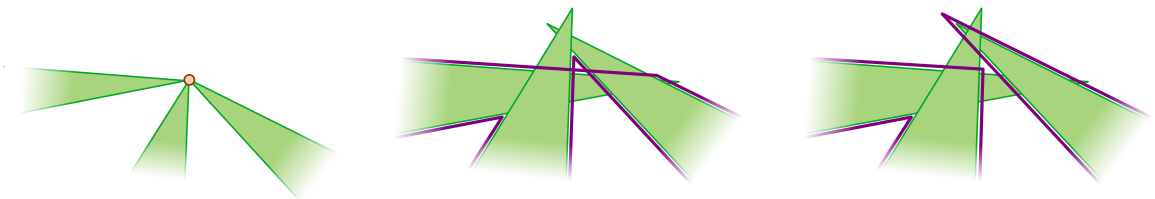

Figure 3.37: *A MWSS topology at (left) and after (middle, right) an event (orange) that is not suitable for the GIE. The GIE output (middle, purple) is self-intersecting, and thus badly formed. A non-intersecting solution does exist (right).*

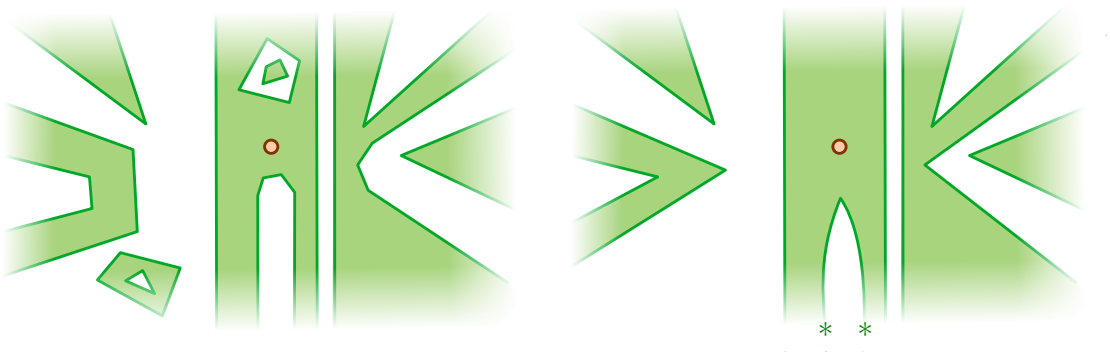

Figure 3.38: *Left: The active plan just before an event. A complex set of chains collide at a single event (orange). Right: after the intra-chain step and one-chain step of the GIE the topology is simplified. Note that the curved edges marked with an asterisk represent the topology of two colinear straight edges.*

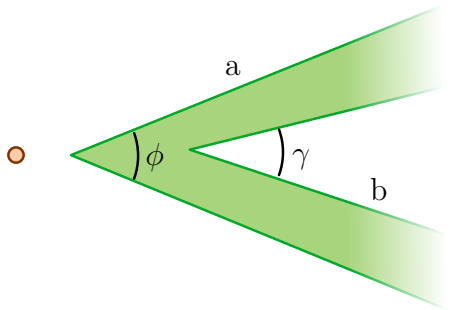

Figure 3.39: *We describe the chain* a *as enclosing chain* b*, as* b *lies inside* a*, and therefore $\phi < \gamma$, $\phi < \pi$ radians. The chains are shown here before a collision at the orange point.*

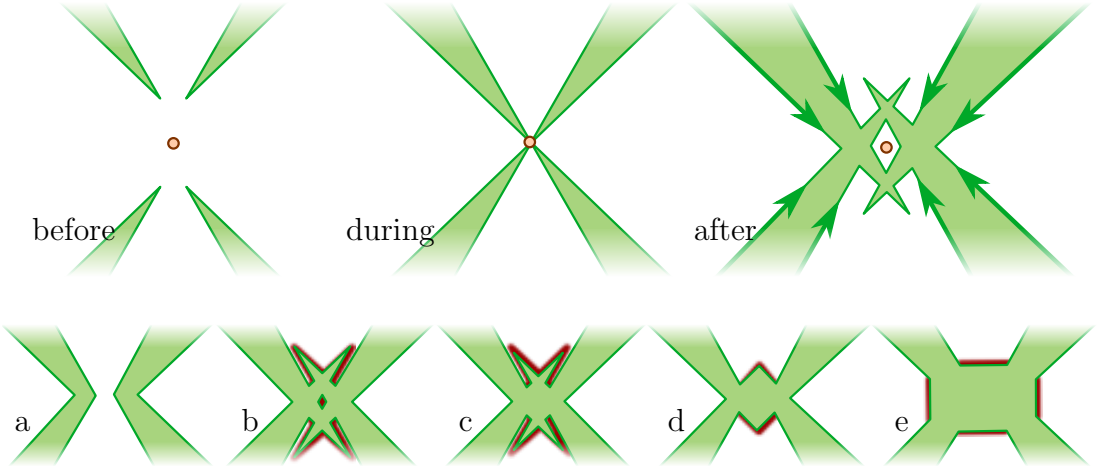

Figure 3.40: *Above: Four chains collide at an event (orange point). The desired plan topology after the event is unclear. We must keep the interface edges (above, right: bold green arrows) in the same locations to remain compatible with the remainder of the plan. Below: There are many possible options for the topology change at the event. (Note that we show the active plan a time after the event). Some solutions use existing edges, others create new zero length edges (below: red shadows). During the event these edges have zero length, but subsequently grow).*

Characteristics that are logical in an algorithm for such events include:

1. The plan remains well formed.
2. Consistency with the SS when all angles are a positive constant.
3. Consistency with the PWSS when all angles are positive.
4. Consistency with the NWSS when all angles are negative.
5. Invariance to rotation of the plan. As with the the straight skeleton the result of an event should not depend on the orientation of the plan.
6. No creation of new zero length edges during the event. The SS, PWSS and NWSS do not introduce additional edges; for consistency, neither should the MWSS.

We have been unable to find a elegant general solution to this problem!

We hypothesise that it is always possible to find a solution in the events we encounter. Fig. 3.41 shows several events and potential solutions, however an algorithm to compute these events has not been discovered. In particular it is condition 6, finding solutions that do not introduce zero length edges, that rules out many obvious algorithms.

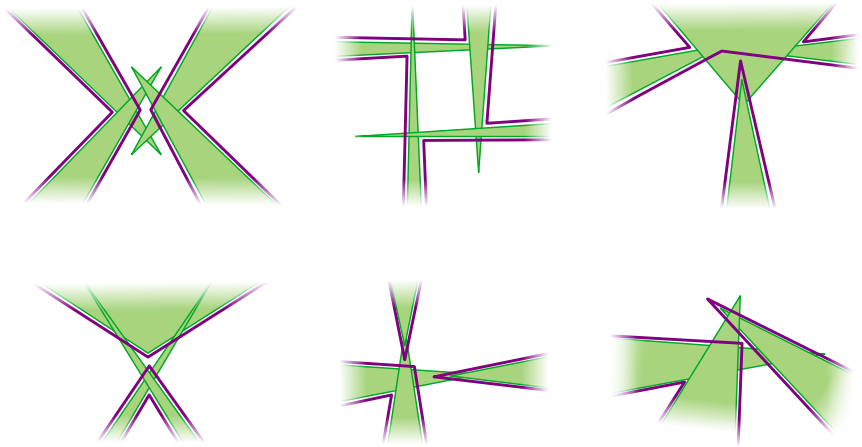

Figure 3.41: *Several example events and solutions that do not require 0-length edges to be introduced into the active plan. The geometry (green area) is shown after the event, and consists of length 2 chains colliding. A good solution for each topology is shown in purple. All examples except that in top, middle, fail when the GIE is used.*

We continue by introducing one further processing step that simplifies these point degeneracies by removing parallel edges. Finally we conclude by introducing a concise description of the unsolved problem, given this simplified event.

3.5.2 Removing Parallel Adjacent Edges

As per the GIE introduced in Sec. 3.2.4 the topology of the event can be simplified by the intra chain and one chain steps. These steps simulate the plan as the sweep plan reaches the height of the event. Zero length edges, including chains that form a closed loop are removed and chains of length 1 are split, leaving a homogeneous topology of chains of length 2.

At an event all the edges involved in the collision approach the location in an ordering defined by the edge's orientation. Fig. 3.42, left, shows the orientation-ordered points for Fig. 3.38. Any edges that do not approach according to their angle must have been removed by an earlier collision, Fig. 3.42, right. This property is known as the $\geq$ *approaching edges* property. This refers to the fact that the angle between consecutive edges around an intersection is equal to, or greater than, zero.

The simplification we would like to perform is the removal of edges which are adjacent and parallel as they approach the event. That is when two parallel edges separated by $0°$ approach an event from the same side. The area between these edges approaches zero near the event. If we connect these adjacent edges together, the event at the other end of the parallel lines will remove the loop in its intra chain stage. Therefore it can

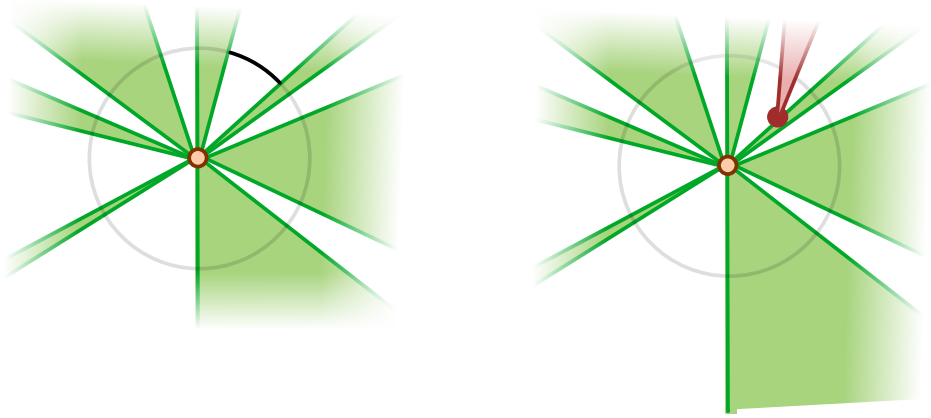

Figure 3.42: *As the chains of edges in the MWSS approach the event (orange) they become ordered (left). If this were not the case (right), they would have intersected during an separate earlier event (red).*

be ignored for the purposes of this event. After we remove these lines, we can say that the event has the $>$ *approaching edges property* as all the angles between adjacent approaching edges are greater than zero.

This basic approach is hampered by the fact that more than two parallel edges may be adjacent at an event. If there are an even number of such edges at one event, the adjacent pairs of edges can be connected together to enclose a region under the sweep plane, as in Fig. 3.43. However if there are an odd number of edges, one edge must be chosen that is not connected to another and remains. This decision should be independent of the order co-heighted events are processed in, and must discard the same edge globally. Here we present two resolutions:

- *interior bias:* The pairs of lines surrounding an interior region of the plan are always connected.
- *exterior bias:* The pairs of lines surrounding an exterior region of the plan are always connected.

The earlier example in Fig. 3.38, is resolved using these two resolutions as shown in Fig. 3.44. Note that although the edges remaining have the same orientation, they may have different speeds. A consequence of the necessity of choosing an interior or exterior bias is that otherwise symmetrical plans may produce an asymmetrical outcome after an event. For example Fig 3.45 shows a plan that before the event is not changing area, but after will either be gaining, or losing area if the interior or exterior biases are chosen respectively.

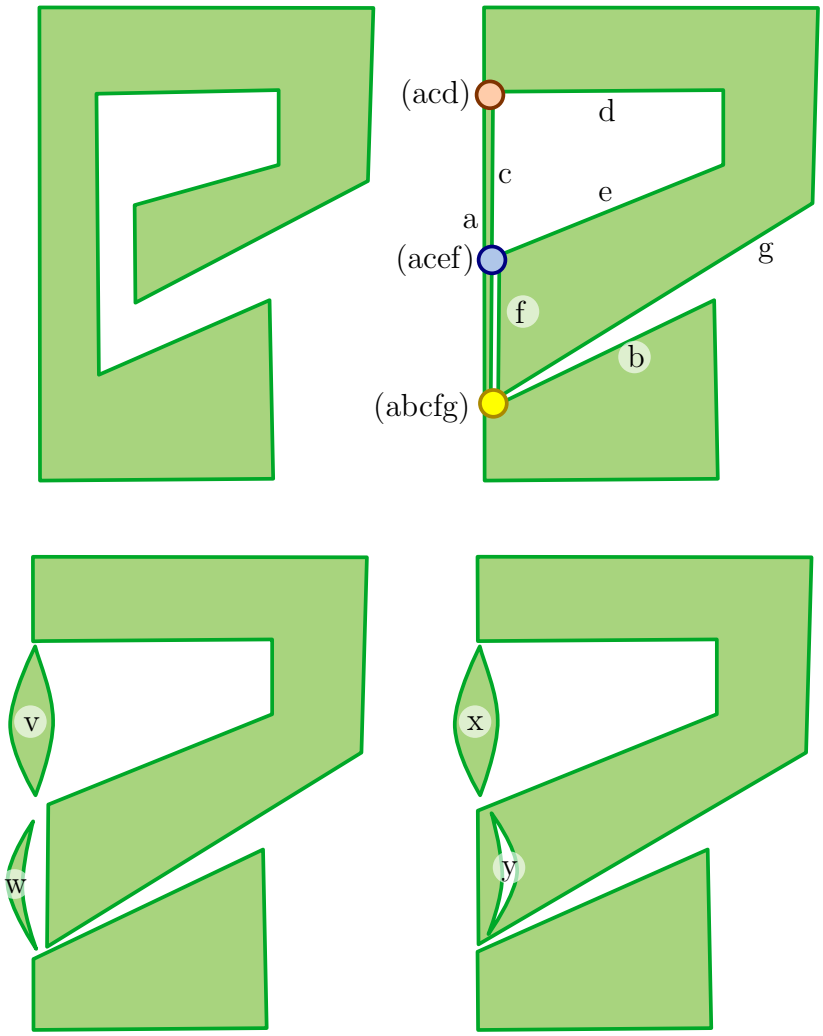

Figure 3.43: *Given a plan before the event (top left) that leads to a number of events with parallel adjacent edges at the same height (top right, red blue and yellow circles), a deterministic and reproducible decision must be made as to which of the parallel edges are connected. The solutions given are to connect the parallel adjacent lines with an interior bias (bottom left) or exterior bias (bottom right). The areas v, w, x and y are all removed by subsequent events.*

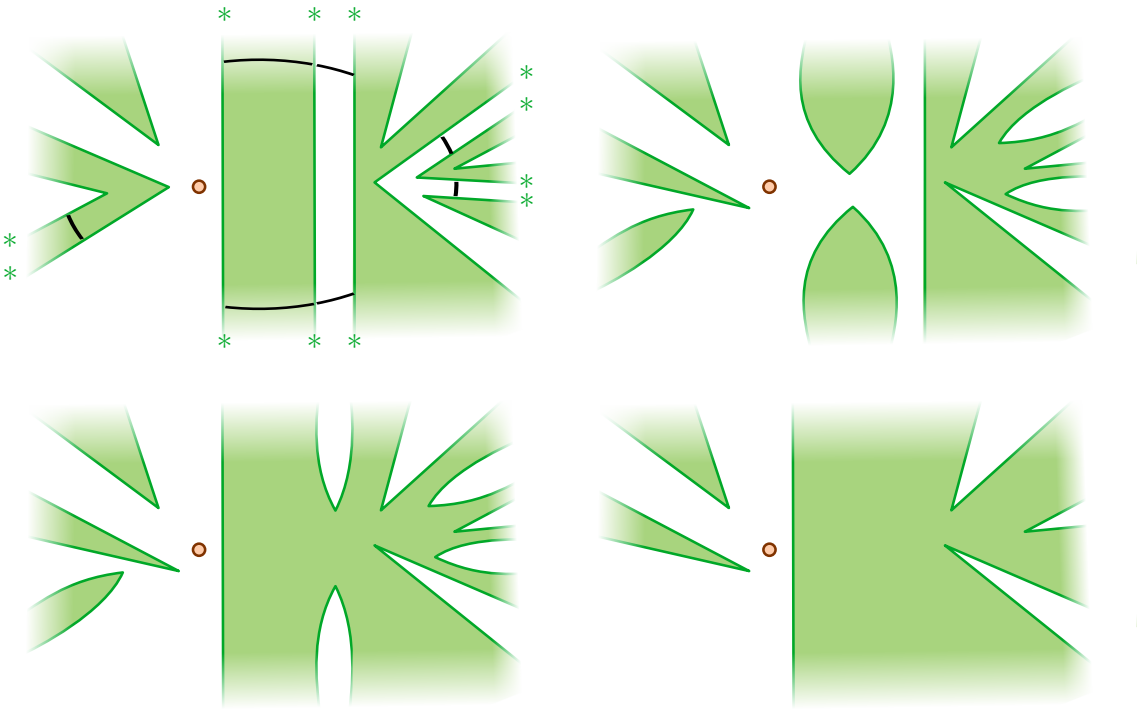

Figure 3.44: *After the intra chain step and one chain steps, we have a simplified topology (top, left). The chains are shown just before the event for clarity. The black lines connect (asterisked) edges which would become adjacent and parallel at the event. We convert these pairs of edges into single chains as shown. We either use the interior bias (top right) or exterior bias (bottom left). After any subsequent events at the same height are processed we are left with simplified topology (bottom right, for exterior bias).*

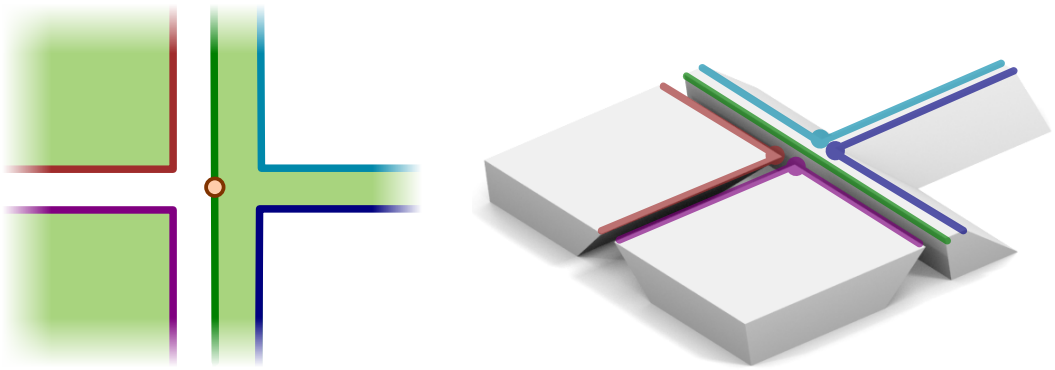

Figure 3.45: *A MWSS event that has unchanging area before the event, but will either grow or shrink after, depending on the resolution strategy.*

3.5.3 The Pincushion Problem

Once an event has been prepared in the above way, we wish to process it in such a way that the plan remains well formed after the event. This is an unsolved problem; this section makes only definitions and observations.

Given a valid event that has been pre-processed such that it has the $>$ approaching edges property, the *pincushion problem* is to devise an algorithm that always finds a solution that does not introduce new zero length edges in to the active plan. First we will show that the plan remains topologically invariant after an event, and then that we can draw a circle around all possible intersections of edges involved in the event. This "pincushion" circle, with "pin" edges leading into it encapsulates the problem of solving a general MWSS event.

As the sweep plane rises towards an event, after it has processed any previous events, the topology of the edges does not change. By definition the plan is well-formed before the event, with no self-intersections. Furthermore we can note that there are no topological changes as the sweep plane approaches the height; such changes would be witnessed by other events. Of more consequence is that topological invariance may also be observed after the event. That is, if we do not handle the event, the geometry after the event only scales, rather than changing topology. We call this the *sector property* of SS events, and is introduced in Fig 3.46. The sector property is summarised in the trivial statement "between events, no events occur".

The sector property follows from two previous definitions:

- The edges move over the plan in a self-parallel manner, at a constant speed.
- The edges involved in an event pass through the event's location at the event

Applying these two definitions allows us to make the trivial observation that all intersections between any pairs of edges move directly away from the intersection point after

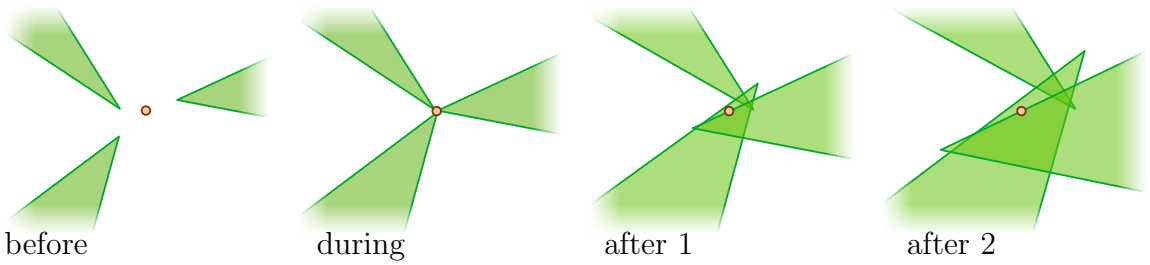

Figure 3.46: *The plan (green triangles) undergoes an event (orange). The sector property states that topology of the edges remains unchanged after the event if we make no attempts at solving it (after 1, 2).*

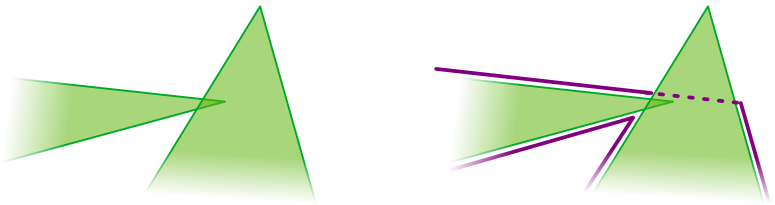

Figure 3.47: *A PWSS event in which the only solution requires the extension of edges (dashed line) from their unmodified post-event topology.*

the event, each with constant speed. Therefore the order of crossings of any subset of involved edges remains invariant, along with the topology.

We may note in passing that there are three topologies of the edges involved in the event - before, at and after. The topology at the event only occurs for a single sweep-plane height, at an instant in time. We define the pincushion problem on the topology after the event.

To find solutions in the MWSS case it is necessary to extend some of the edges. An example where this is required is shown in Fig. 3.47.

Given the invariant topology at some time after the event in question, there are only a finite number of edges involved. If we intersect all the edges we obtain a finite number of possible intersection points that may make up the solution. We discount non-intersections between parallel edges. Therefore we may attempt to encapsulate our problem by drawing a circle that encompasses all these possible intersection points. An example of the resulting *pincushion* diagram is given in Fig. 3.48. From the edge of the circle, an even number of unbounded edge-rays are ordered by angle around the perimeter. Rays are used since we may have to extend some of the line segments. There are an even number of rays, for each edge of the active plan that enters and leaves the circle.

A trivial observation is that for any successful solution only odd-numbered rays may intersect even number rays and vice versa (for any ordering around the perimeter of the pincushion). This matches the intuition that the orientation of the edges within the active plan determines which other edges they may intersect with. To this end we may colour the rays in the diagram with alternating colours; rays may only connect with other rays of the other colour, but may not cross any other rays as in Fig. 3.48 bottom row.

In a valid solution all pairs of rays in the pincushion diagram are connected to form chains of length 2, in such a way that the chains do not cross. We hypothesise that it is *always possible to solve the pincushion problem.* Given a such a solution we can update the active plan in all situations.

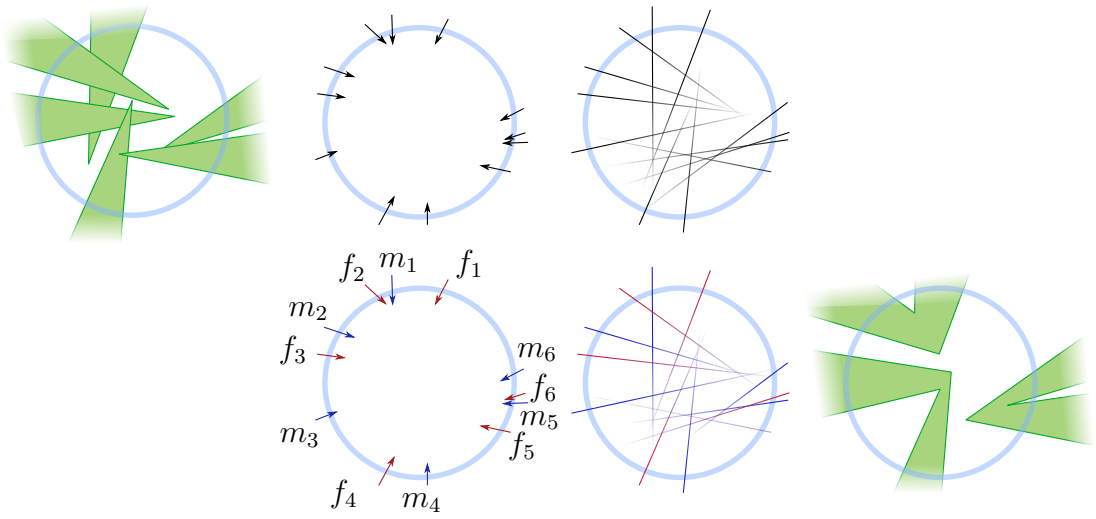

Figure 3.48: *Top Left: It is possible to draw a circle around all possible edges that intersect at an event. Top Middle, Right: Given the sector property, we may summarise the topology as rays entering the pincushion circle. Bottom Left: We may assign alternating colours to rays around the circle. Bottom Middle: A pincushion diagram coloured in this way. Bottom Right: A solution to this pincushion consisting of the intersections* $\{(m_2, f_1), (m_1, f_2), (f_3, m_4), (m_3, f_4), (m_6, f_5)(m_5, f_6)\}$

The solution is not unique, as in Fig. 3.49. Given a number of solutions we may chose to use the criteria of Sec. 3.5 to determine which solution is most suitable for our application.

A brute force search program has been written to search for valid edge pairs to intersect. Fig. 3.50 details an algorithm that applies the intra-chain stage of the GIE to all allowable subsets of edges in the event. This algorithm, together with a visual interface, as in Fig. 3.51, never failed to find a solution to a valid pincushion arrangement. However, without a proof that there is always a solution to the pincushion problem we can not be certain that the brute force approach will always return a valid active plan.

Another approach is a constructive methodology to incrementally add the next pair of rays to an already valid solution, given some arbitrary order of rays. Since we theorise that all such arrangements have a valid solution, such a solution should be possible. However a counter example was found in the "5-star" structure of Fig. 3.52. Attempting to incrementally add rays around the circumference, always keeping a valid solution with those lines already processed, either is not possible, or does not terminate; it is necessary to solve the system globally. In this case the GIE provides such a solution. We therefore believe that a global solution must be found, rather than an iteratively constructed one.

The failures of the GIE, brute force, and incremental approaches to the pincushion

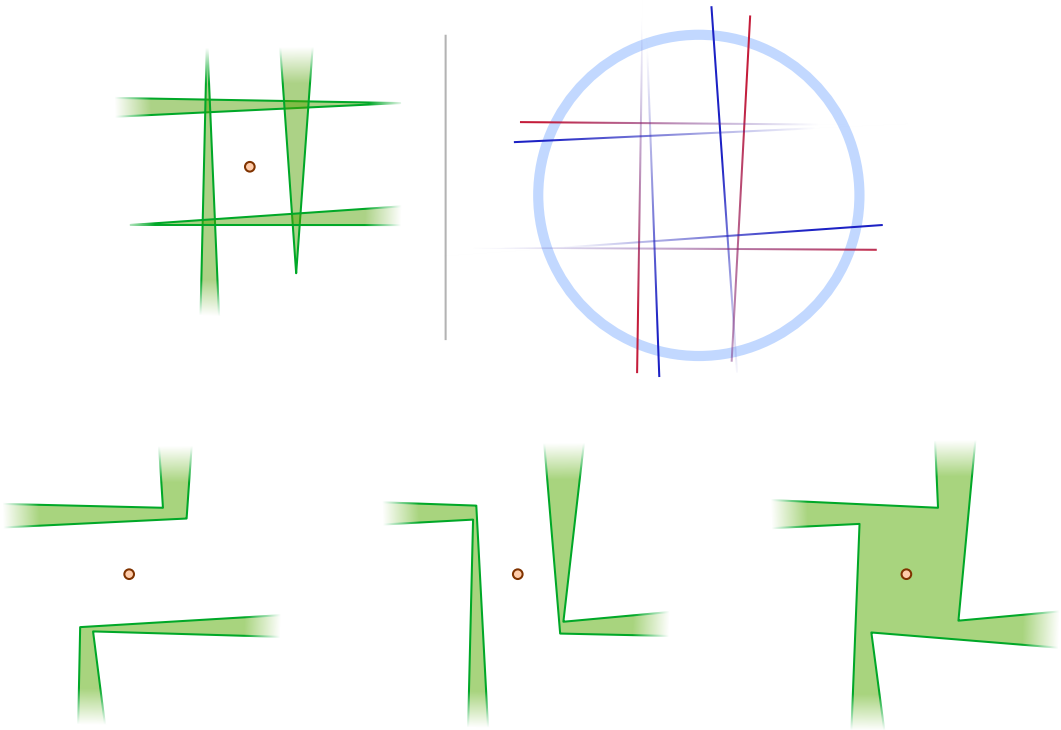

Figure 3.49: *Given the post-event topology (top left), and the corresponding pincushion diagram (top right), there are three different solutions that do not introduce zero length lines (bottom).*

```
BruteForceEvent ( Event event ) begin
    pincusion = preprocess( event );
    Set<Set<Set<Chain>>> combinations = all covering combinations of pincushion.chains();
    foreach Set <Set<Chain>> GIEChains in combinations do
        Set<Chain> resolvedChains = new emptySet();
        foreach Set<Chain> chain in GIEChains do
            resolvedChains.add( interChainStage ( chains ) );
        if noChainsIntersect( resolvedChains ) then
            return resolvedChains;
    return null;
end
```

Figure 3.50: *A brute force approach to the pincusion problem. We hypothesise that it will never return null.*

problem are disappointing. Ultimately the lack of proof that the events of the MWSS have well formed solutions is problematic to the definition of the MWSS. However we may take solace that these are very degenerate situations and solutions that do introduce zero length edges are common.

The pincushion problem was discussed with David Eppstein, author of [65] and Antoine Vigneron, author of [40].

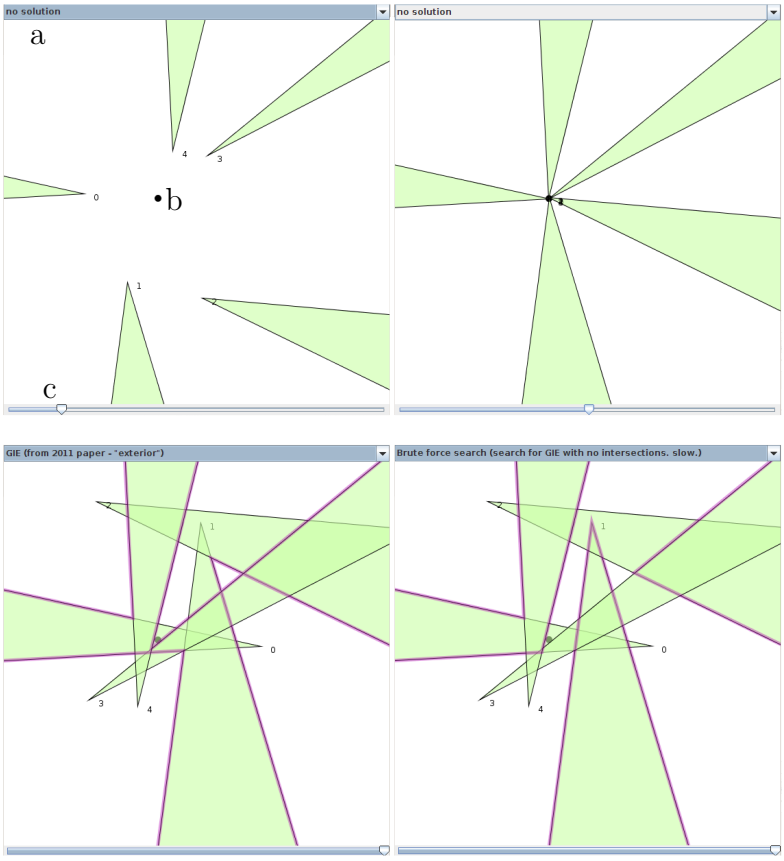

Figure 3.51: *A user interface to the pincusion event solver. Top Left: The users selects a resolution algorithm (a), draws the edges involved in the event around the event location (b), and selects the time relative to the event (c). Top Right: The system simulates the topology at the event. Bottom: The system shows the solutions given by the GIE (Left) and brute force algorithms (Right) in purple after the event.*

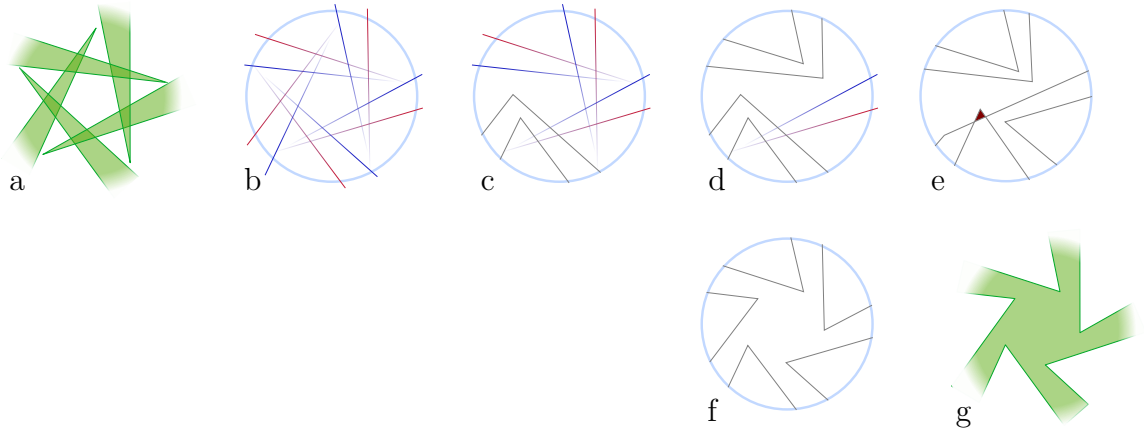

Figure 3.52: *The "5 star" event arrangement of edges, shown after the event (a), and the corresponding pincushion diagram (b). A constructive approach, which takes an arbitrary ordering of edges (c, grey lines) and attempts to maintain a valid solution with each additional line (d), runs into problems when it cannot alter a past result (e). The correct solution in this case (f,g) must be found globally, and happens to be the same as the GIE solution.*

3.6 Summary

In this chapter we have explored a certain class of skeletons, formed by allowing the edges of a 2D shape to move in a self-parallel manner. By observing intersection events as the edges collapse we are able to trace out the arcs of the skeletons. Indeed it is by the simulation of the edge movements that we are able to evaluation skeletons. We may go so far as to describe the skeleton as a "procedural geometric construct". However the fact that we will use such a construct for "procedural modeling" would make such a description less than helpful.

By specifying different constraints over the speed of these edges, distinct classes of behaviour can be witnessed. Four varieties of the straight skeleton have been introduced – the unweighted straight skeleton, the positively weighted skeleton, the negatively weighted straight skeleton, and the mixed weighted straight skeleton. These skeletons form a tree of generalisation as the requirements on the angle of the direction planes are relaxed; SS $\subseteq$ PWSS $\subseteq$ MWSS and NWSS $\subseteq$ MWSS. Of these different geometric constructs only the SS was well previously well described in the literature.

In the non-degenerate case of the of SS, PWSS and NWSS we have simplified existing algorithms by introducing a GIE that specifies a general behaviour given an arbitrary topology of collapsing edges. However each additional generalisation has also brought with it new degenerate cases which we have presented, and found resolution strategies for. These have included the parallel consecutive edge event, many edge degeneracy, point degeneracy and parallel adjcent edges. However in the deepest, most unlikely,

degenerate cases we were unable to suggest a general solution for the MWSS, managing only to formulate the pincushion description. Although we tried, we were unable to create either a proof that the pincushion problem was solvable or not.

The skeletons studied here also contain interesting properties, such as the SS splitting faces into two, the PWSS introducing holes into faces, and the MWSS allowing faces to merge together and split apart. We may also observe that many of the skeletons output resemble fragments of man made structures. The arcs between the faces of the output, the skeleton itself, serves as a polygonal partition of the polygon, influenced by a distance field. We take insipration from this fact in the following Chapter 4, where we use the arcs to partition city blocks into parcels. The offset 2D polygons generated in the shrinking process are reminsicent of man made arches or frames, while the 3D terrain model resembles building's roofs. In addition we find that it is possible to halt the evaluation of the MWSS at any point, creating a new form of extrusion between two plans. It is this observation that will lead us to the ideas in Chapter 5, using the MWSS for solid building modeling.

Chapter 4

Procedural Generation of Parcels

The work in this chapter was based on a collaborative project published in the paper *Procedural Generation of Parcels in Urban Modeling*[252]. I contributed the skeleton parcel subdivision algorithm and implementation, the statistical fitting mechanism and the comparative analyses.

This chapter introduces a method for the procedural generation of city parcels from city blocks. Within an interactive procedural modeling environment the method reproduces parcel subdivisions in a distinct style, given a small number of user specified parameters and no additional user programming. The work was motivated by the real world need of a commercial procedural modeling system, CityEngine[66], a procedural cityscape generator. A fast, robust and realistic block subdivision scheme was required for the product. Given the interesting properties that we observed in the straight skeleton in previous Chapter 3, it seemed a natural choice to solve some of the geometric problems that block subdivision presented.

To create a virtual cityscape a classical "waterfall" urban PGM pipeline utilises discrete stages to first create course features, which specify the inputs to finer elements. A typical pipeline features main roads, between which quarters are divided further by minor roads. Between these small roads, city blocks lie. These are subdivided individual lots, lots into footprints and from footprints, buildings . An overview of these stages is given in Fig. 2.34. In this chapter we address one aspect of this pipeline — the critical problem of creating realistic city lots from blocks within an interactive PGM system.

Here we introduce a novel method of block subdivision. We utilise the geometric self sensitivity of the straight skeleton to generate *Modernist* style parcel subdivisions. We also present a recursive-split approach to create traditional parcel subdivisions, which

is presented here in order to provide a state of the art implementation of a subdivision scheme for comparison. The complete system is able to retain parcel identity under interactive user edits such as moving a street intersection, and is robust enough for integration into a commercial procedural modeling tool. We conclude the chapter by comparing the results of these subdivision techniques against real-world examples.

One of the challenges in procedurally generating parcels is creating geometry that is adaptive to the block shape. In particular identifying the centrelines of rows of parcels within irregular blocks is essential to many observed block subdivisions. We found that the straight skeleton provided a very powerful and stable centreline detection mechanism, that was well suited to interactive modeling.

4.1 Introduction

The urban procedural modeling pipeline has been widely applied to several fields including virtual environments, urban reconstruction and architecture. While there have been numerous systems for the generation of street networks[38], buildings[164] and facades[165], there has been relatively little attention paid to the generation of parcels from city blocks. Those systems which do exist are either not responsive to the block geometry, unrealistic, or are not easily controlled. Increasing the fidelity and speed of parcel subdivision benefits the quality and speed of the entire urban modeling pipeline.

Our high-level approach was to emulate two distinct modes of block subdivision from the urban planning literature. Carmona[36] identifies two such modes:

- *Modernist* patterns position "buildings as separate pavilions freestanding in a more generalised type", examples are given in Fig. 4.1, left. This design often appears "in its pure form when built on greenfield sites", and is generally used in lower density neighbourhoods that are homogeneously planned. The parcels will typically be rectangular, have street access at the front, and neighbour other blocks at the sides.

- *Traditional* patterns of subdivision are characterised by a "generalised highly connected mass" and "*streets and squares* and a small-scale, finely meshed street grid". As demonstrated in Fig. 4.1, right, this design is prevalent in historic cities and unplanned high density areas. The parcels may or may not have street access, with small lanes and courtyards offering access to occupants. Often traditional subdivision patterns emerge in an ad hoc manner, rather than the block being designed, as is common with Modernist patterns.

Figure 4.1: *Clockwise from top left: Glasgow, Shanghai, Param, and Nevada (©Google Maps). Left: Modernist parcel subdivisions. Right: Traditional parcel subdivisions.*

We present an algorithm to model the modernist pattern, and refer the reader to [252] for the details of the traditional subdivision algorithm. As Carmona notes there is something of a continuum between these two ideals – "Indeed, it is not clear at what point *space between buildings* becomes *open space containing buildings*". Both designs are often observed with a uniform structure with rectangular, quadrilateral or sometimes polygonal shape[45].

After discussing the several parcel subdivision schemes in the corpus in the following Sec. 4.2, we will detail the inputs and outputs to our two subdivision systems in Sec. 4.3. The Modernist subdivision style forms the basis for the *skeleton* subdivision algorithm, detailed in Sec. 4.3.2, while the traditional style is approximated by the *oriented bounding box* (*OBB*) algorithm of [252]. Concluding, the application of these techniques to real-world block patterns is presented and evaluated in Sec. 4.4.

4.2 Existing Parcel Subdivision Techniques

The existing literature addressing procedural parcel subdivision comes mostly from computer graphics. Given a city block as a polygon, the task is to subdivide it into a number of non-overlapping parcel-polygons, giving the user control via a number of parameters.

Fig. 4.2 gives several examples of existing automated parcel subdivision techniques. The first approach that the authors are aware of, from within computer graphics, by Parish and Müller[181] (Fig. 4.2, brown), has gained the most traction and variations. The parcel is recursively split into two using straight lines (top, with darker splits created before lighter ones). The variations include different criteria for selecting the line to split a region and the termination criteria, although the literature often gives trivial treatment to the details —

- Parish chooses to split perpendicular to the longest pair of edges that are approximately parallel, until the resulting parcels are below a specified area.
- Weber[260] et al. assume mostly rectilinear parcels and select the longest edge adjacent to a street, before splitting perpendicular to this edge at a randomly displaced midpoint. If the resulting parcels do not have an undesired aspect ratio, they are accepted, otherwise another randomly displaced midpoint is attempted. Once the parcels are below a user specified area the process terminates.
- Vanegas et al.[251] use the population count and number of jobs to estimate the area in their subdivision scheme at which recursion halts.

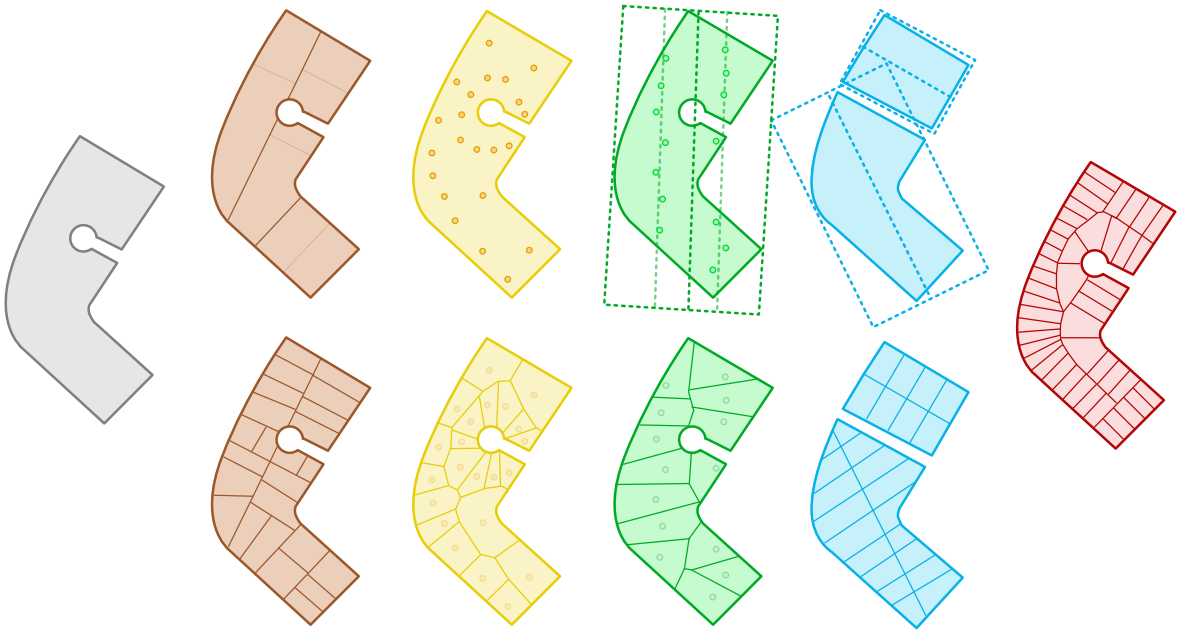

Figure 4.2: *Comparison of the skeleton subdivision approach to existing approaches. From left to right, the input, the parcel subdivision techniques from [181, 122, 12, 265] and our result which gives realistic result of Modernist parcel subdivision on concave blocks.*

Another early approach was to use area division based on a number of sites. The *Voronoi*[253] diagram of a set of sites is a geometrical construct that associates every point on the plane with the nearest site. The area spanned by points associated with a single site is known as a *cell*. These Vornoi cells have been used to generate street networks from a set of sites sampled by population density[229], as well as being used to specify parcel boundaries[122] (Fig. 4.2, yellow). Because the cells boundaries are rarely rectangular, the results are not characteristic of observed parcel subdivisions.

An alternative application of the Vornoi concept is given by Aliaga et al.[12] (Fig. 4.2, green). He observes that blocks often have a centreline dividing two strips of parcels on either side leads. This line is approximated by the fitting of an *oriented bounding box* (OBB), minimising the space between the box (a rectangle) and the block, and using the centreline of the box. Voronoi sites are then positioned on either side of this line and the cells become the parcels. The assumption of a straight line as a centreline fails for concave blocks, as in Fig. 4.2, and still suffers from non-rectangular blocks in some situations.

In general the urban modeling community has performed block subdivision manually according to desired patterns[235, 182]. Those systems that have been created are very limited in their realism and available styles[256, 98, 150]. One such example, [265], again fits an OBB to the block and generates a centreline. As shown in Fig. 4.2, blue, these strips are then divided to approximate a certain parcel width, specified

by a user-defined parameter, and clipped to the block's perimeter. The system also generates additional access roads, a property that we do not wish to emulate since this is an earlier stage of the urban procedural modeling pipeline. This system again fails on concave parcels, and is inflexible to the local geometry of the parcel boundary. The remainder of the work from the urban modeling community has focused on parcel subdivision of coarse raster-grid environments[127, 10, 160], which are not detailed enough to use for visualisation purposes.

If we wish to interactively edit a city we are faced with the further problem of retaining consistency under edits. We wish that changes to the road network, when edited interactively, only minimally affect the associated parcels created. When the changes to the shape of a block are small Lipp[143] utilises mesh-warping techniques to deform the existing parcel subdivision to the new geometry while keeping the topology intact. We are not aware of any techniques in the literature that allow for larger scale interactive editing. The problem of retaining the identity of individual parcels between user edits is also unaddressed.

We find the existing work somewhat limited in the lack of interactive features and ability to deal with planned Modernist parcel subdivisions over concave parcels. We continue by introducing our solutions to these issues.

4.2.1 Evaluating Parcel Subdivisions

Due to both the nature of procedural modeling and its relatively new appearance in the computer graphics world, evaluating any results is often difficult. Typical evaluation techniques are to show the results of the procedural system alongside real world data, such as photographs and plans[165, 226, 39], or to perform subjective studies to explore whether the results of a system correlate to a non-procedural workflow or user intuition[144, 278, 158]. The objective evaluation of procedural content has yet to be addressed in a detailed and consistent way.

Currently a new procedural systems are introduced with a high frequency in very different domains. Therefore there has been little requirement to compare systems within the same domain. In addition, attempting to evaluate content that ideally has the property of being "characteristically similar" to some example, and yet still "varied and unique" is a challenging and somewhat contradictory goal. Evaluating where any given system lies in relation to these two extrema is an interesting problem that has not yet been addressed.

Our literature survey failed to identify any evaluation system for procedurally generated block subdivision. Due to the lack of existing material that evaluates procedural

content in general, and procedural parcel subdivisions in particular, we introduce three per-lot metrics that we will use to evaluate our block subdivisions. These metrics were chosen because of their:

- Objectivity — the statistics are not subject to opinion.
- Ease of computation — because the test data sets are large, each of the heuristics must be fast enough to compute for every lot in a city.
- Clarity — the metrics are all sufficiently simple to implemented quickly by future researchers on the subject.

Therefore the per-lot metrics we have chosen are:

- Area — measured in m^2.
- Aspect ratio — given the smallest bounding box that encloses each lot, this is the ratio of the longest to shortest side.
- Neighbour count — the number of unique lots that the lot shares an edge with. Lots adjacent only at verticies are not counted.

4.3 Block Subdivision

This section introduces the technical background to our parcel subdivision schemes. We first detail the data structures used for the input and output of the system, and the requirements of the output. We continue to discuss both the skeleton and OBB based subdivision algorithms.

4.3.1 Inputs, Outputs and Goals

The input to the system is a set of city blocks, generated by the previous stage in the urban modeling pipeline, while the output is a set of parcel polygons, suitable for the next stage of the pipeline, creating mass models. Our system is able to fulfil these conditions, while delivering statistically similar subdivisions over concave city blocks, controlled interactively by a few parameters.

The previous stage of the urban procedural modeling pipeline delivers a street-network, in our case a planar graph, (V, E), of verticies, V, and edges, E. These verticies lie in the same plane in $\mathbb{R}^2$, at the road intersections. The roads represented by the edges in

E, posses a width, and may be straight or curved. We expect that the graph is planar, and no two roads intersect, giving a 1:1 mapping between the faces of (V, E) and the set of blocks. The topology of city blocks is therefore formed by the faces of (V, E); unbounded faces are not considered at this time.

Taking the geometry of a street (street width, sidewalks, intersections) surrounding the block, B, the street modeling subsystem creates a simple polygon describing the border of the block, $C(B)$. The polygonal border approximates curving streets and any features of the street geometry, such as pavements. This boundary is formed of m verticies $C(B) = \{b_1, b_2, \ldots, b_m\}$ in a counter-clockwise direction. Note that such street modeling is a previous stage in the urban modeling pipeline, and like the following stage of mass-model generation is not addressed here. Every edge in the boundary is associated with a street in E, and a set of parameters. In our implementation we recompute the faces, blocks, and parcels as the street network is edited, or the block parameters adjusted.

The city block, B, is associated with various parameters. Each of these may be specified by the user or extracted from example block subdivisions. The parameters include:

- the algorithm to subdivide the block into parcels, either *skeleton* or *OBB*
- parcel area bounds, (A_{min}, A_{max}): The upper and lower bounds on the area of the resulting parcels.
- minimum parcel width, (W_{min}, W_{max}): The upper and lower bounds on the length of the sides of the oriented bounding box of a parcel.
- split irregularity, ω: The deviation of a split edge from its default position, normalised in $[0, 1]$. Larger values result in the split being further away from the mid-point and a larger variety of parcel areas.
- various algorithm subdivision specific parameters.

The output of the system is a set of polygons describing the new parcels. For every B a set of n parcels, $L = \{l_1, l_2, \ldots, l_n\}$, are created that exactly cover B with no overlap; that is $\bigcup_{i=1}^{n} l_i = B$ and $\forall_{l_i, l_j \in L}(l_i \cap l_j = \emptyset)$. Every parcel, l, is a simple planar polygon.

Modern procedural urban modeling systems make use of non-flat terrain and roads. In this situation, we vertically project the blocks onto the plane before subdivision and re-project the output parcels onto the terrain after. We assume that the terrain is a height field and thus sufficiently flat to preserve the planar and covering properties of the blocks and parcels.

To replicate the two patterns suggested by urban design work (Sec. 4.1) we introduce two independent algorithms to transform each B to a L. Our implementation was in the Java language, within the procedural modeling system provided by CityEngine[66].

The straight skeleton ("SS" or "skeleton") algorithm produces procedural Modernist subdivisions, and is introduced in Sec. 4.3.2. The central assumption of the algorithm is that each parcel has a similar street-frontage. The distance that each parcel occupies behind this frontage is the *parcel depth*. If the depth is shallow, the block becomes a *perimeter block*, with a semi-private *patio* area in the centre of the block. An example of such a block is given at the top left of Fig. 4.1. If the depth is high, there is no patio area, but instead often observe a *centreline* in the subdivision, with a row of parcels on either side. An example of this is shown in the bottom left of Fig. 4.1. The skeleton parcel algorithm uses either a partial or complete application of the straight skeleton to model perimeter and centreline blocks respectively. Typically the result of this algorithm is rectangular blocks on rectilinear street patterns, and "wedge" shaped blocks on curved streets.

4.3.2 Skeleton-based Subdivision

The straight skeleton subdivision algorithm generates Modernist parcel division. Our approach is to generate a contiguous area for a row of parcels along a street (we refer to these areas as *strips*) before slicing these strips along the adjacent street into parcels. This approach ensures that every parcel has street access, and that the length of street-frontage is similar for every parcel.

We observe that both perimeter blocks and centreline blocks contained such strips, and that both can be generated by varying the depth of a block from the street. However determining borders between these strips, both parallel and orthogonal to the street, is an involved problem —

- We observe that at corners of blocks near street intersections one strip will give priority to another to ensure more rectangular blocks
- To control the style of subdivision to be centreline or perimeter, the depth of the blocks from the street must also be generated as specified.
- A special case in our algorithm is the treatment of narrow blocks, in this situation only a single strip is generated. The narrow-block threshold parameter identifies the parcels in which this behaviour is appropriate.

Our insight into this problem came after we observed that the arcs of the partial straight skeleton included a lot of the information that we required to identify the centrelines.

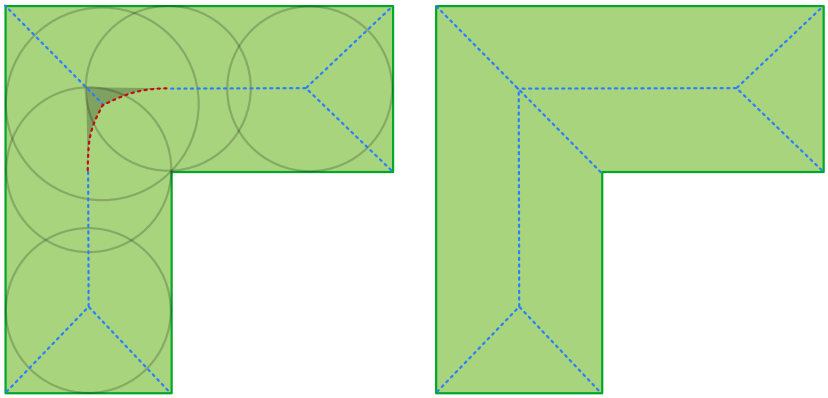

Figure 4.3: *Left: The medial axis (dashed lines) of a polygon (solid green lines) describes points equidistant from the boundaries of the polygon (grey circles). We note that the curved (red) arcs of the medial axis require rasterisation for use in a polygonal environment and that they generate sharp corners in the faces (shaded regions). Right: The equivalent straight skeleton contains no curved arcs, and includes arcs for reflex corners.*

This lead to the solution presented here which uses a partial straight skeleton to specify the depth of the strips, but cleans up the "diagonal edges" generated near the corners to create more realistic rectangular strips.

There were several alternatives to the unweighted skeleton for generating centrelines. One possible alternative was the medial axis. The axis would introduce curved sections into our geometry, Fig. 4.3, leading to awkward "sharp" corners in medial axis faces which would have required intensive filtering to rectify. These sharp corners in faces occur on very simple concave polygons. A further disadvantage to the medial axis was the algorithm's origin as a bitmap image filtering tool [28]. Only recently have algorithms emerged that calculate geometry explicitly [117, 199], however the output of these systems includes parabolic segments. Given that the typical 3D pipeline operates on polygons, parabolic sections would require rasterisation before use in the typically polygonal procedural modeling pipeline. Such rasterisation comes with involved checks for geometric consistency. Finally such medial axis algorithms do not create arcs for reflex verticies, and so are unable to "guide" the splitting of strips in the same manner as skeleton faces.

A further alternative was the weighted straight skeleton. This would have enabled us to move the centreline relative to each of the edges of the block, and to create perimeter blocks with different depths on each road. The weighted straight skeleton proved problematic for two reasons; firstly there was no easy mechanism to assign such depths to each road, and second there were no known commercial weighted skeleton implementations available at the time of publication.

The skeleton subdivision uses the following parameters in addition to those in Sec. 4.3.1.

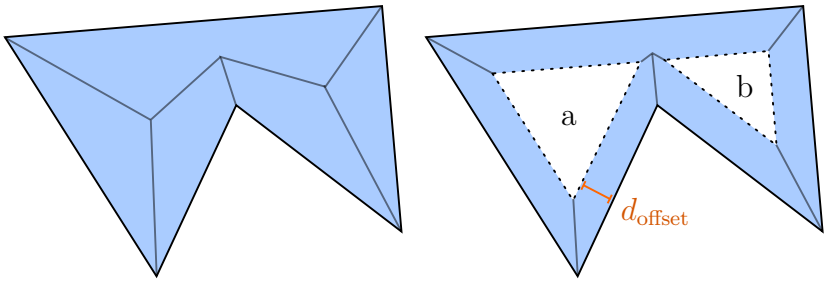

Figure 4.4: *Left: The straight skeleton of a polygon, showing $C(B)$ (black line). Right: A partial application of the straight skeleton computes the offset contour $C'(B)$ (dashed lines) at distant d_{offset}. Note that the contour may split the innermost, or* patio*, region into several portions (a,b). The individual faces of the straight skeleton conform to our definition of a* strip*, and we may take the supporting edges to be portions of the boundary of input polygon. We take these faces to be the initial set of α-strips.*

- The maximum parcel depth, d_{offset}, determining whether the centreline or perimeter styles of subdivision occur.
- A street priority scheme, either *StreetWidth* or *StreetLength*. This specifies the direction in which diagonal edges should be resolved.

Applying the Straight Skeleton

To define the depth of the strips, the user defines a perpendicular distance d_{offset} from the block contour $C(B)$ to an inwards offset contour $C'(B)$. This value corresponds to the maximum depth (distance from the road to the rear) of the parcels. If d_{offset} is sufficiently large (e.g., infinity), then the area enclosed collapses and the rear side of any resulting parcel will be directly adjacent to another parcel, leading to centrelines between rows of parcels. Alternately, if the d_{offset} value is sufficiently small, the partial skeleton application defines a closed inner *patio* region, with no direct access to roads. This inner region may be disconnected if the initial block is concave, as in Fig. 4.4 right, and can be further partitioned using an arbitrary subdivision style. While setting an infinite value for d_{offset} is typical and better complies with the first parcel variety, inner *patios* are not uncommon and we designed our skeleton-based subdivision to also support them. The contour $C'(B)$ is calculated (via the CGAL[1] library) by a partial application of the straight skeleton to $C(B)$ to offset distance d_{offset}, as shown in Fig. 4.4, by computing the intersection of the roof model of [6] with a horizontal plane at a specific height.

The arcs of the skeleton application specify the division of the region between $C(B)$ and $C'(B)$ into a set of strip polygons. We initially refer to these as *α-strips*, to differentiate them from the *β-strips*, from which we have removed some diagonal edges. These strips are an intermediate value in our algorithm, representing a group of parcels with their

primary frontage on the same logical street. Collectively they form a single connected region.

Formally we define a strip, s_i, as a simple polygonal area within B, such that a single connected length of the polygon's boundary forms part of $C(B)$. These lengths are the *supporting edges*, $\psi(s_i)$, of s_i. A block's cyclic list of n strips, $LS(B) = s_1 \dots s_n$, is such that it covers the area between $C(B)$ and $C'(B)$ completely and without overlap. The list $LS(B)$ is ordered counter clockwise, such that the last supporting edge of s_i and first of s_{i+1} are adjacent edges of $C(B)$. Note that we take $i+1$ to mean $(i+1) \bmod n$ in the context of a cyclic list data structure.

We initialise $LS(B)$ from the faces of the straight skeleton used to compute $C'(B)$. We observe that these faces fulfil the strip properties — bounded by the arcs of the skeleton, and supported by an edge of $C(B)$. Any strip in $LS(B)$ may be combined with either of its neighbours and the union retains the strip properties; therefore we may union adjacent faces in $LS(B)$ according to whether they lie on the same logical street, $e \in E$ in our street graph. In this manner we create a single α-strip for every logical street, as in Fig. 4.5, b.

Removing Diagonal Edges

The α-strips computed from the skeleton faces suffer from diagonal edges at the intersection of logical streets as shown in Fig. 4.5, b. As illustrated in Figure 4.5 c-g, we correct these edges, by modifying $LS(B)$ to transfer a near-triangular region from the strip on one side of an offending edge to the strip on the other side. We refer to these corrected strips as β-strips.

Let the shared supporting vertex between each pair of α-strips s_i and s_{i+1}, be designated v_i. The shared boundary of these two strips forms the diagonal edges we are concerned with, one end of which is v_i. We provide a classification $T(v_i) \in \{\textit{Previous, Next, None}\}$, to specify which of the pair of strips will gain the region, and which will lose the same region. A vertex with the property *Previous* (respectively *Next*), will assign a region to the previous (next) strip, given the counter-clockwise vertex ordering. No action is taken with a value of $T(v_i) = \textit{None}$.

The values of $T(v_i)$ may be assigned by one of two *street priority* schemes, determined by a per-block parameter specified by the user. When the angle of the supporting edges at v_i is reflex we always assign $T(v_i) = \textit{None}$. For the remaining v, we choose between the following two schemes:

- *StreetWidth*. If the average width of the street edges associated with the supporting edges of s_i is greater (respectively lesser) than those of s_{i+1} then $T(v_i) =$

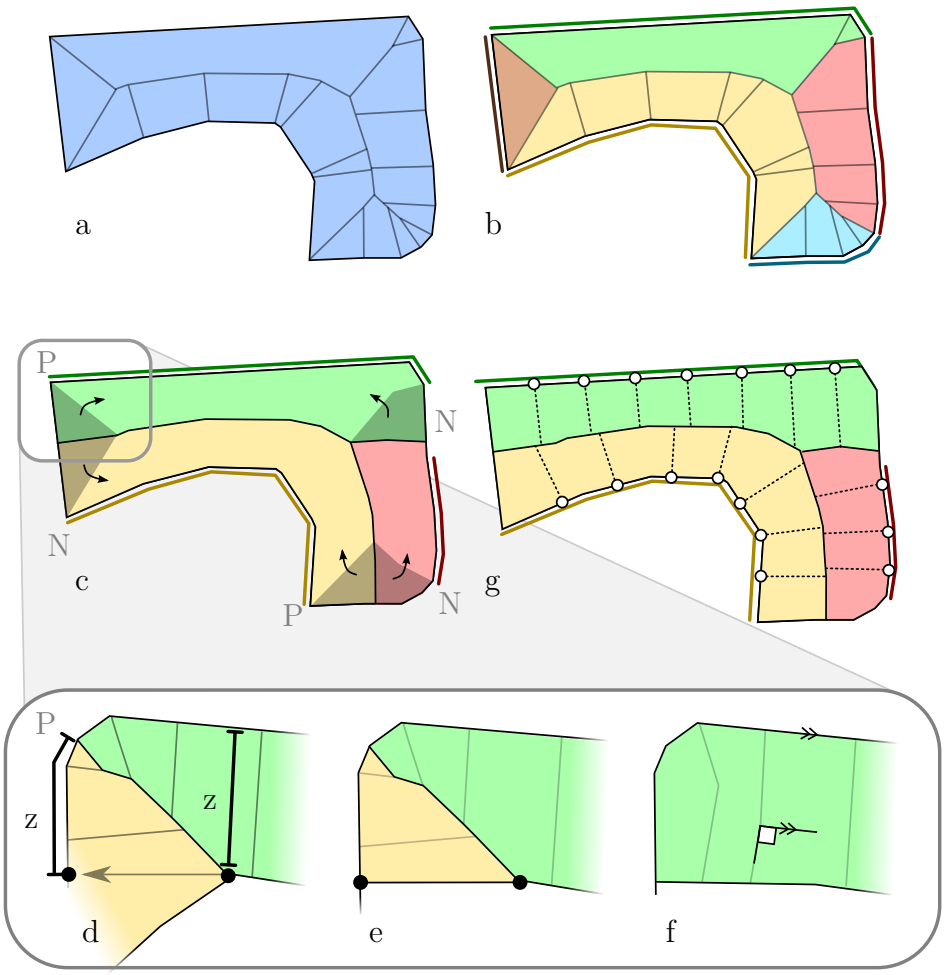

Figure 4.5: *The α-strips (solid colours, b) are recovered from the skeleton (a) and logical streets (bold lines, b). This leaves undesirable diagonal edges, such as that between the brown and green alpha-strips. Given the classification $T(v_i) \in$* None, Previous *(P) or* Next *(N), we reassign regions (shaded, c), to create the set of β-strips. In the example (c-e) we use the classification scheme StreetLength, specifying the direction* Previous. *The subsequent splits are computed over these β-strips (f).*

Previous (*Next*).

- *StreetLength*. If the length of the supporting edges of s_i is greater (respectively lesser) than those of s_{i+1} then $T(v_i)$ =*Previous* (*Next*).

We find that in most most urban environments the parcels face the most important and thus widest street; therefore we use the $StreetWidth$ scheme by default. There are situations in which this assumption is not suited. For example, residential street patterns in which parcels prefer to face the quieter, and longer, residential streets, rather than the wider and busier access-streets. In our experiments it proved difficult to make this distinction automatically, so we allow the user to assign this parameter manually.

Given the parameter $T(v_i)$, we calculate the direction in which to reassign the region, shown in Fig. 4.5, c, creating the set of β-strips. The region is removed from strip s_x, where $s_x = s_i$ if $T(v_i)$ =*Next*, or $s_x = s_{i+1}$ if $T(v_i)$ =*Previous*. The region is removed by cutting between two points. The *primary* point is the location on the boundary of both s_i and s_{i+1} that is furthest, at distance z, from $C(B)$, (Fig. 4.5, d). The *secondary* point is located on $C(B)$ at a distance z from v_i along $psi(s_x)$. The region is then unioned to the strip s_y where $s_y = s_{i+1}$ if $T(v_i)$ =*Next*, or $s_y = s_i$ if $T(v_i)$ = *Previous*. Finally we recompute the skeleton arcs to remain perpendicular to the local edges in $\psi(s_y)$, (Fig. 4.5, f), in order to ensure we are able to guide the subsequent splits in the following stage (Fig. 4.5, g). After processing each pair of adjacent strips in $LS(B)$, we are left with the list of β-strips.

Strips with a small supporting edge are rarely observed, and so are undesirable. If a strip loses area to both neighbouring strips, and the distance between the secondary points is small, we move the secondary points to the same location. A threshold distance of $2W_{min}$ determines whether we move both points to the point closest to their mean location on $\psi(s_y)$. This ensures that the entire strip is reassigned to its neighbours (Figure 4.5b, cyan and brown). Such a strip is removed from LS(B). On small lots this routine may introduce "zig-zag" artifacts, these are resolved as in Fig. 4.6.

Splitting Strips into Parcels

To subdivide the β-strips into parcels, a set of points are sampled approximately equidistantly on $\psi(s_i)$, as shown in Fig. 4.7. Rays from these points, perpendicular to the nearest edges of $\psi(s_i)$, split the β-strip into parcels. We "snap" rays to nearby verticies to create cleaner geometry. The distance between the points is normally distributed around $(W_{min} + W_{max})/2$, with $\sigma^2 = 3\omega$, and clamped to the length of $\psi(s_i)$. This process adds a random displacement to the ray-origin points to create

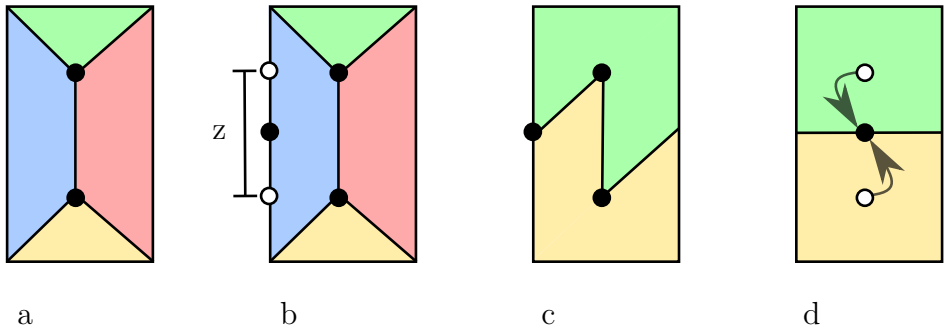

Figure 4.6: *The green and yellow strips take enough area from the blue and red strips to trigger their removal, as z become less than $2W_{min}$ (ab). If we move the secondary point to a mean location, we may be left with "zig-zag" artifacts after the strip is removed (c). In this situation we average the location of the primary points (d). Given that the distance between these primary points is small, we have found that this causes very few problems.*

less uniform parcels. To prevent local perturbations in $\psi(s_i)$ adversely affecting the parcel geometry, we limit the rays to each skeleton face. If the ray crosses a skeleton edge, it follows the edge to the boundary of the strip, as illustrated in Fig. 4.7b.

There are several special cases that are handled independently as post processing steps:

- There are situations in which the block is too shallow to accommodate the two rows of parcels assumed by the algorithm. In this case we group shallow parcels and replace them with parcels generated similarly to the skeleton subsequent split technique.
- Triangular parcels and parcels with small areas are repeatedly unioned with their neighbours until they are either larger than the minimum area (A_{min}), neither small nor triangular, or there is only one remaining parcel. We union such parcels with the adjacent parcel with which it shares the longest boundary.

As illustrated in Fig. 4.8, the diagonal edge removal and the splitting of strips into parcels works in the same way regardless of the value of d_{offset}, that is whether we use a partial or a full skeleton application.

The pseudocode for the complete skeleton subdivision algorithm is given in Fig. 4.9.

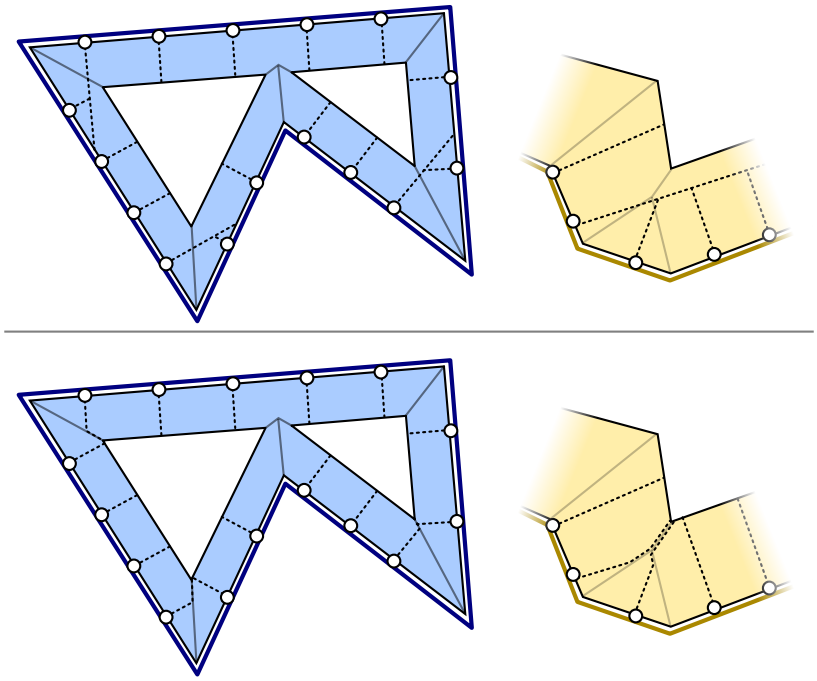

Figure 4.7: *The split operation divides a β-strip's area (solid colour) into parcels with rays (dashed lines). Top: The naive approach leads to unrealistic splitting as an eccentric local normal to the supporting edge (bold lines) may propagate in an uncontrolled manner. Bottom: We constrain split-lines to the skeleton faces they are within to achieve a more realistic effect.*

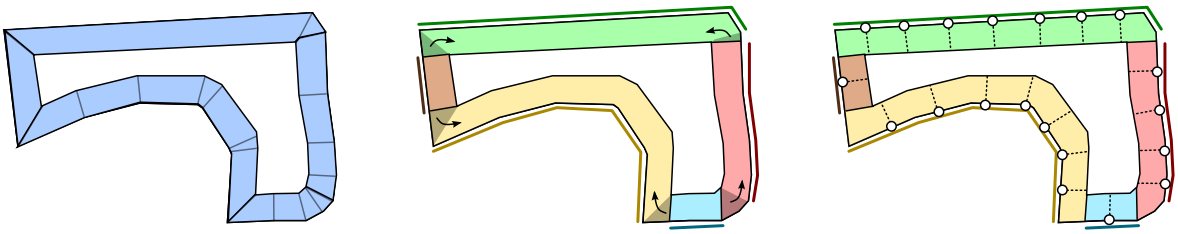

Figure 4.8: *Our algorithm to compute the partial skeleton (left), remove diagonal edges (middle) and split the strips (right) demonstrated on a block with a patio region.*

subdivSkeleton(B)
  $L \leftarrow \emptyset$
  $SS \leftarrow$ *computeSkeletonOffset*$(C(B), d_{\text{offset}})$
  $LS \leftarrow \emptyset$
  for each face $f \in SS$ **do**
    Append convertToStrip (f) *to* LS
  end for
  $LS2 \leftarrow$ mergeOnLogicalStreets (LS)
  $LS3 \leftarrow$ *fixDiagonalEdges* (LS2)
  for each strip s in LS3 **do**
    slice (s)
  end for
  processSmallLargeOrTriangularParcels(LS, A_{min}, A_{max}*)*

---

fixDiagonalEdges(LS)
  for each strip $s_i \in LS$ **do**
    $v_i \leftarrow$ vertex between s_i and s_{i+1}
    $t \leftarrow$ triangular portion at v_i
    if $T(v_i) = Previous$ **then**
      assign t to s_i
    end if
    if $T(v_i) = Next$ **then**
      assign t to s_{i+1}
    end if
  end for
  for each strip $s_i \in LS$ **do**
    if $\psi(s_i) < 2W_{min}$ **then**
      remove s_i from LS
      merge primary verticies
    end if
  end for

---

slice(s)
  $origins \leftarrow$ sample $\psi(s)$ by $n((W_{min} + W_{max})/2, 3\omega)$
  $remainder = \bigcap$ offset faces of s
  for each point $p \in origins$ **do**
    $normal \leftarrow$ average normal of B near p
    Create a ray, r, from p, in direction $normal$
    $[left|right] \leftarrow$ slice $remainder$ by r
    Append $left$ to L
    $remaining \leftarrow right$
    Append $remaining$ to L
  end for

Figure 4.9: *Skeleton parcel subdivision pseudocode.*

4.4 Results

In this section we evaluate the two subdivision algorithms against real-world data. The presented algorithms are able to generate a wide range of styles of subdivision, depending on the block shape and attributes selected. Fig. 4.10 illustrates the effects of altering several parameters over a constant synthetic block. However this level of evaluation is insufficient if we wish to demonstrate the ability to synthesise blocks in a particular style observed in the real world.

The evaluation of PGM is an interesting proposition — we do not wish to produce the same result as the input, but instead to generate a quantity of realistic geometry of a particular style. While there is the question of evaluation against fictional (unobserved) styles for stylistic or inspirational reasons, we came to the conclusion that the most important criteria was realism with respect to real-world data. This was especially true since we desired to evaluate the urban design theory that our algorithms are based upon.

We use an implementation of our algorithms within the CityEngine package to recreate subdivisions over urban areas with known data. Some of the parameters for the algorithms are automatically derived, others were manually set. Several statistical measures were evaluated over the whole area, and per-parcel, to quantify the differences between the observed and procedural subdivisions. These measures are visualised over maps to assist in objective analysis of the quality of block subdivision.

The sources of the observed (ground-truth) parcel subdivisions are given in Fig. 4.11, mainly GIS Government databases. The use of North American cities was due to the ease of accessing parcel data in a suitable format, with the older cities, such as Philadelphia, contrasting with newer cities, such as Pasadena. Neighbourhoods with a consistent and locally representative subdivision style were selected for study within these cities. A number of GIS data irregularities were present, such as overlapping parcels, long thin parcels or small gaps between parcels; these were manually removed.

The workflow consists of the following steps:

1. The road networks and blocks are traced from the GIS data, and street widths manually assigned.

2. Per-block statistics are extracted from the GIS data for the mean and standard deviation of both the parcel area ($\bar{A}$, s_A) and minimum width ($\bar{W}$, s_W). Assuming a rectangular parcel, these figures are sufficient to estimate the average aspect ratio of the parcels within a block.

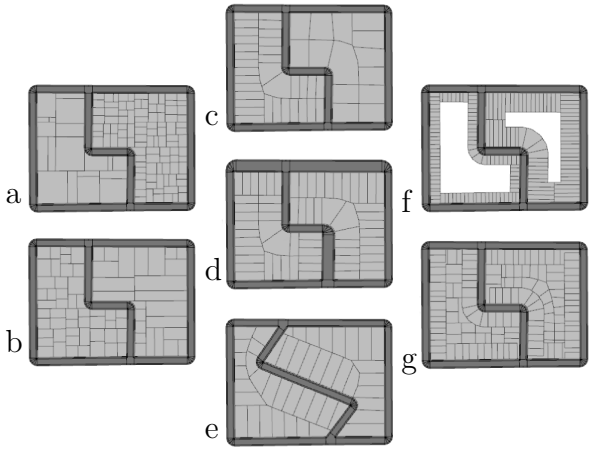

Figure 4.10: *Examples of varying different attributes of OBB (a,b) and skeleton, subdivision (c-g); a large and small difference between A_{min} and A_{max} (a); the effect of enforcing street access (b); low or high parcel-width (c); editing the street widths, to change $T(v_i)$ (d); editing the criteria for shallow-parcel removal (e); low or high value of d_{offset} (f); a higher value of ω, and a variety of subdivision styles in the* patio *region (g).*

Name	Location	Data Source	Algorithm	Figs
Pasadena	California, USA	Propriety Esri dataset	Skeleton	4.12, 4.13
Naperville	Illinois, USA	Esri "Local Govt Basemaps"	Skeleton	4.14, 4.15
Wynnefield	Philadelphia, Pennsylvania, USA	Pennsylvania Dept. of Records	Skeleton & OBB	4.16, 4.17
Germantown	Philadelphia, Pennsylvania, USA	Pennsylvania Dept. of Records	OBB	4.18, 4.19

Figure 4.11: *Data sources used in the evaluation of our system.*

3. The values of block subdivision parameters in the procedural model are set; $A_{min} = \bar{A} - ks_A$, $A_{max} = \bar{A} + ks_A$, $W_{min} = \bar{W} - ks_W$, $W_{max} = \bar{W} + ks_W$, where k is a positive constant that in our examples was set to 2.

4. The algorithm and remaining parameters, including ω, are manually assigned using interactive feedback given from the system.

5. We calculate our statistical measures from the resulting subdivision – i) block area (m^2) ii) block aspect ratio (longest side on a fitted OBB/shortest side) and iii) the number of neighbours each parcel has (a neighbouring block is defined as being within 0.5m of another block's boundary).

The results of this process are shown in Figures 4.12–4.19.

Pasadena is a relatively modern city, and has many areas that are well classified as having a Modernist parcel subdivision. Fig. 4.12 shows the location of area studied, and the aggregate results of observed and procedurally generated lots. The histograms plot the frequency of blocks having certain areas or aspect ratios, while the bar-chart plots a similar measure for the discrete neighbouring parcel count. Note that horizontal axes of the histograms are logarithmic, while the horizontal axes of the bar-chart are linear. The corresponding observed and procedural subdivisions are shown in Fig. 4.13. Per-block shading illustrates each of the three statistical measures for the observed and procedural parcels. Generally we found that our statistical measures agreed with our intuition that the subdivision was generating very similar results. The accuracy of the aggregate statistics was particularly high in this data set.

The example of Naperville was chosen as a good example of a Modernist subdivision with a specific depth, Figs. 4.14 and 4.15. Many of the residential parcels in the observed subdivision neighbour a golf course to the rear leading to fixed-depth offsets. The notable statistical misfit here is that a lower number of procedural parcels were generated than observed, most probably due the changing street-frontage present in the real world data.

To perform a direct comparison of the skeleton and OBB techniques we chose a middle-class neighbourhood in Philadelphia with a range of parcel styles. Figs. 4.16 and 4.17 document the comparison of both subdivision techniques against ground truth. We observe that the aggregate aspect ratio of the straight skeleton subdivision is closer to the observed distribution than that of the OBB. However the parcel level statistics show that both techniques produce reasonable distributions for all three statistical measures. We observe that the OBB technique produces more of the highly irregular patterns present in the larger lots in the top right of the example area, while the

skeleton is able to generate the curving centrelines observed in the small lots to the bottom left.

The final example uses Germantown, Philadelphia, as an example of a traditional lot subdivision. The results are illustrated in Figs. 4.18 and 4.19. Again we observe that the OBB technique generates a flatter aggregate aspect ratio histogram, but in this case this distribution matches the ground data well; this is supported by the per-parcel statistics.

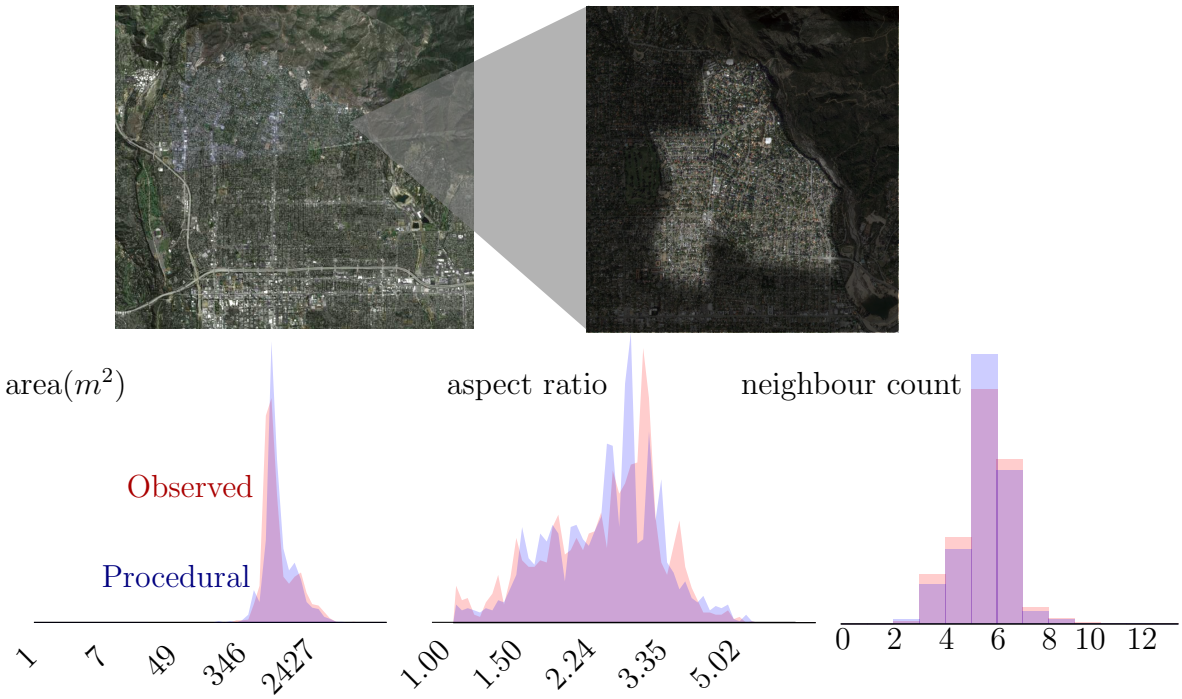

Figure 4.12: *Location and aggregate statistics for the Pasadena data set. Images ©Google Maps.*

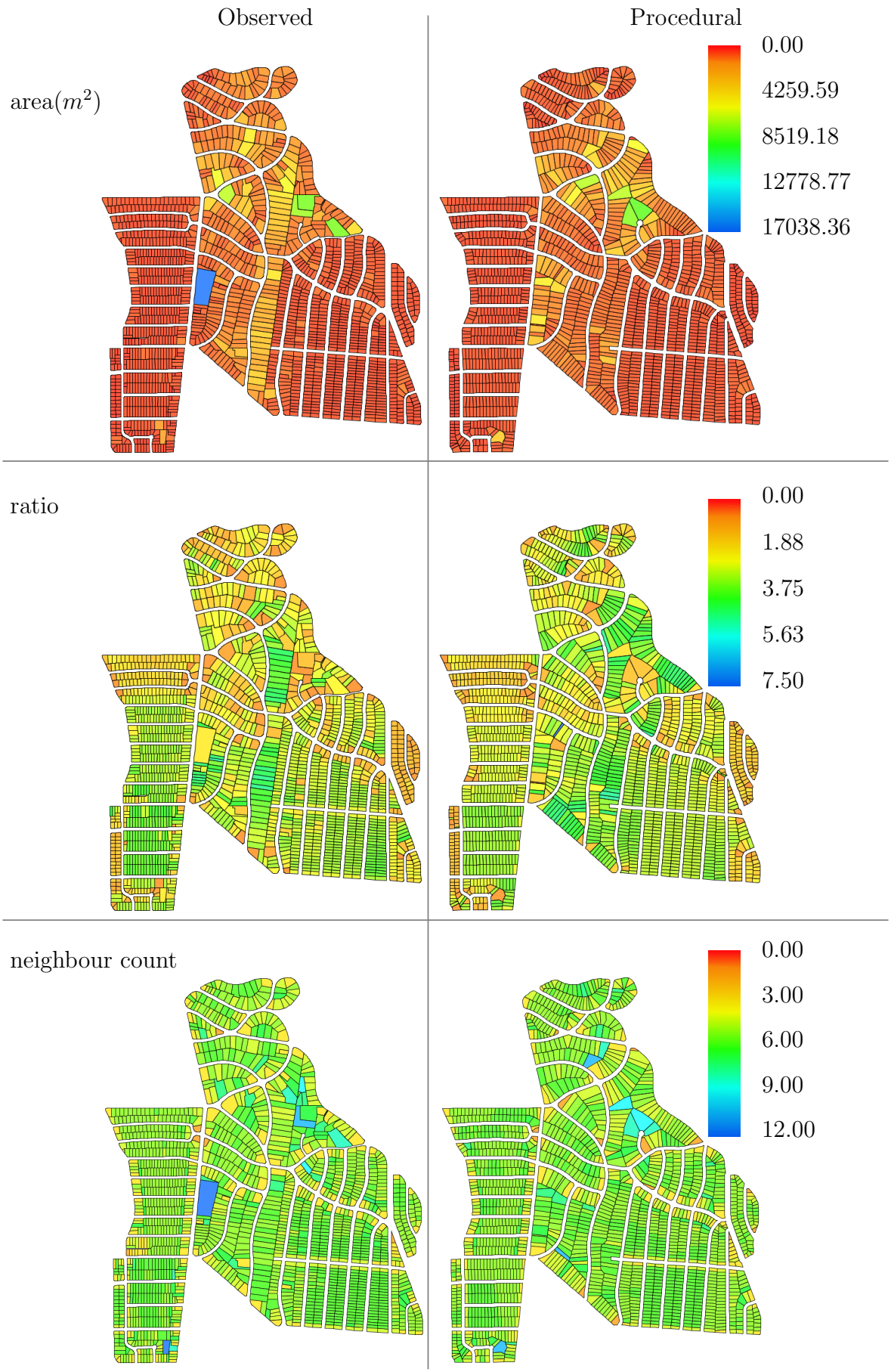

Figure 4.13: *Results for the Pasadena procedural parcels generated using the skeleton algorithm.*

Figure 4.14: *Location and aggregate statistics for the Naperville data set. Images ©Google Maps. Note the truncated* neighbour count *horizontal axis.*

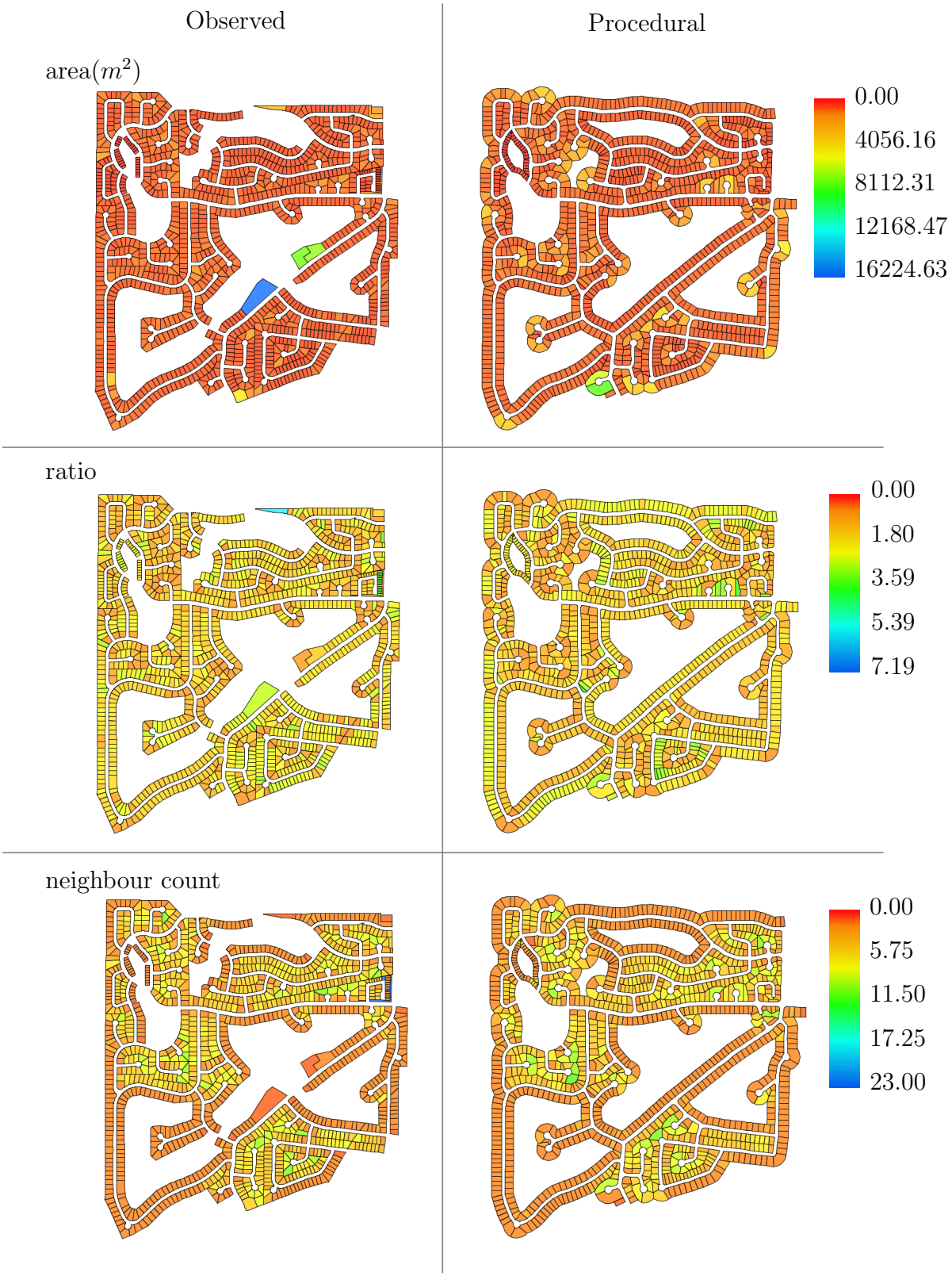

Figure 4.15: *Results for the Naperville procedural parcels generated using the skeleton algorithm.*

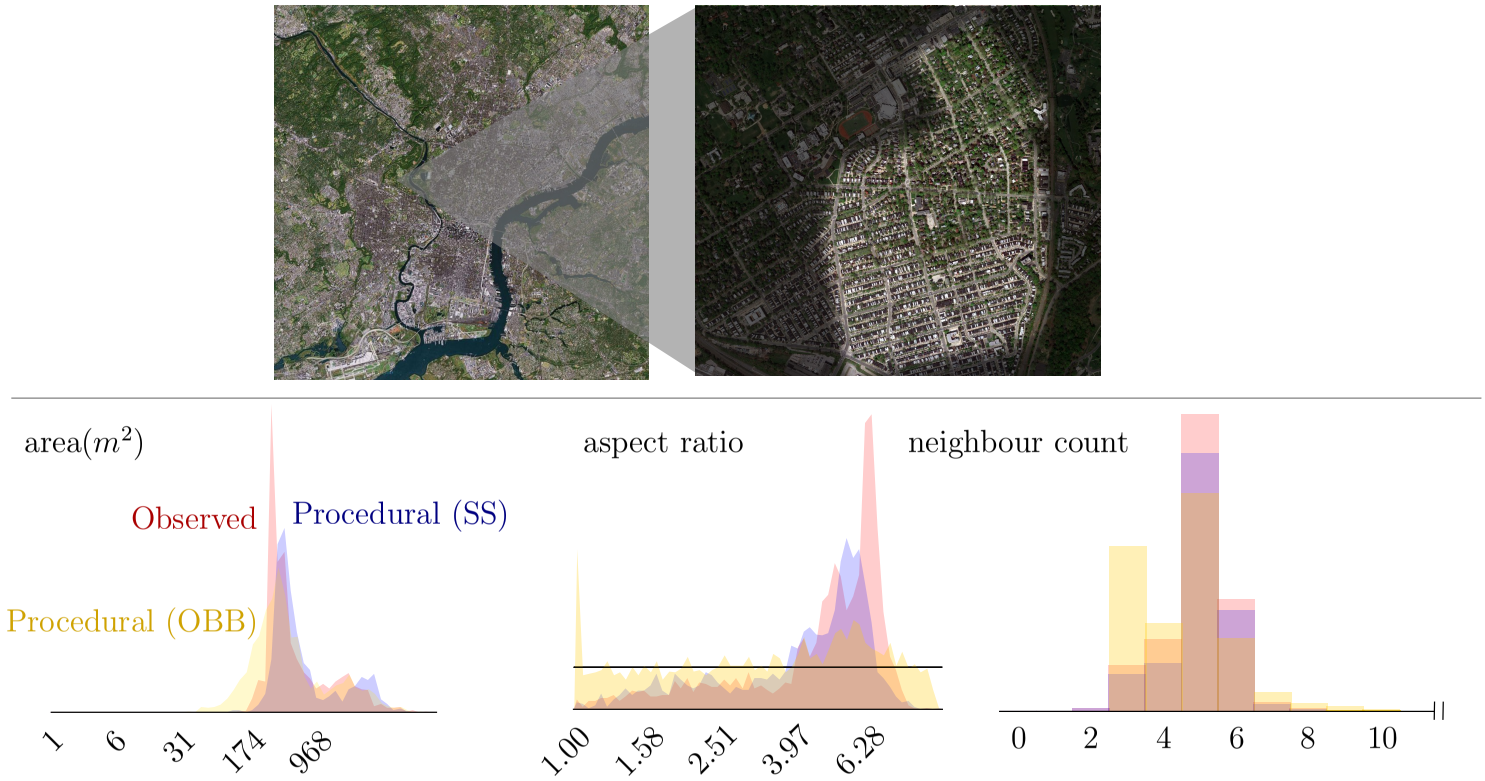

Figure 4.16: *Location and aggregate statistics for the Wynnefield data set. Images ©Google Maps.*

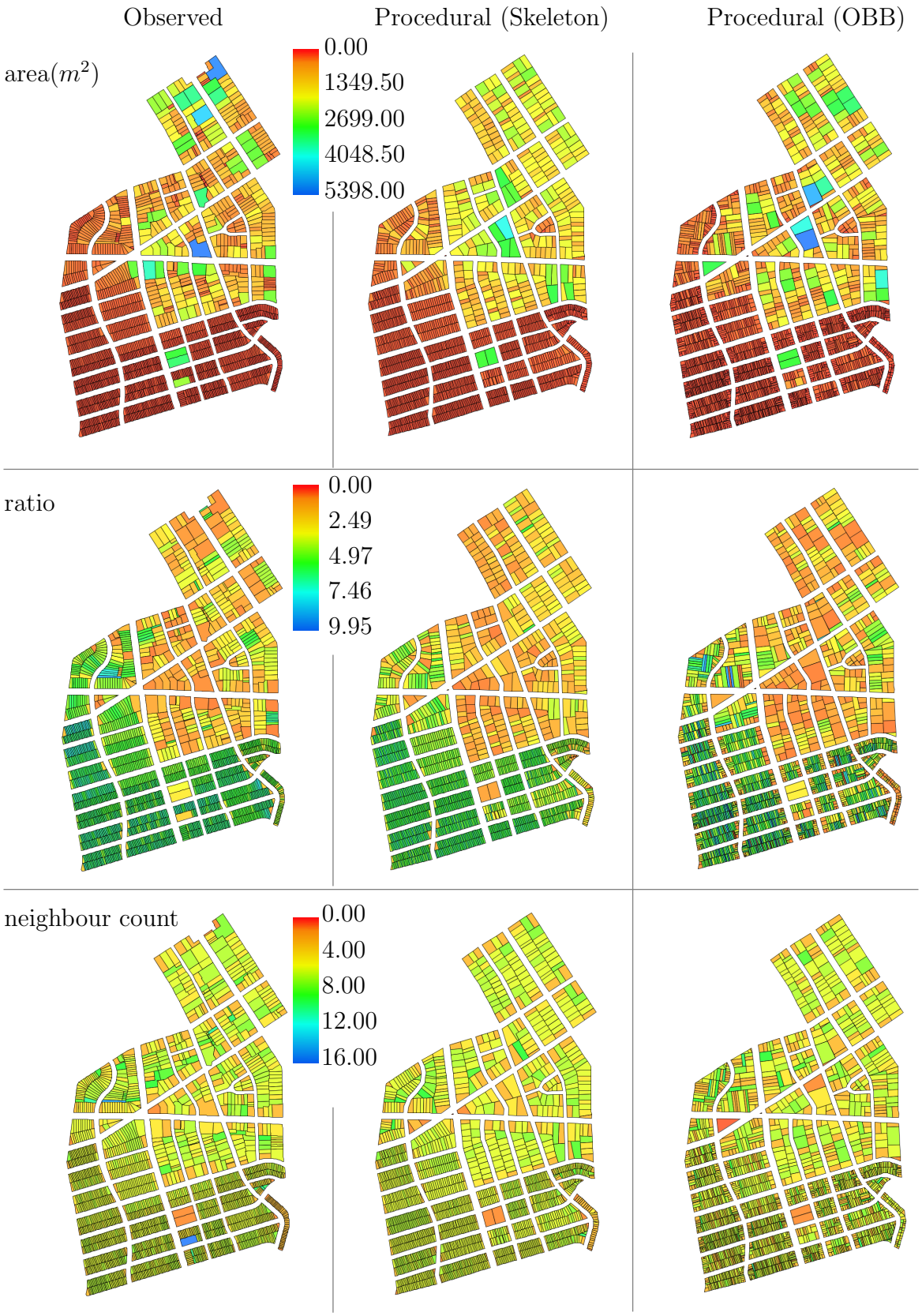

Figure 4.17: *Results for the Wynnefield procedural parcels generated using the skeleton and OBB algorithms.*

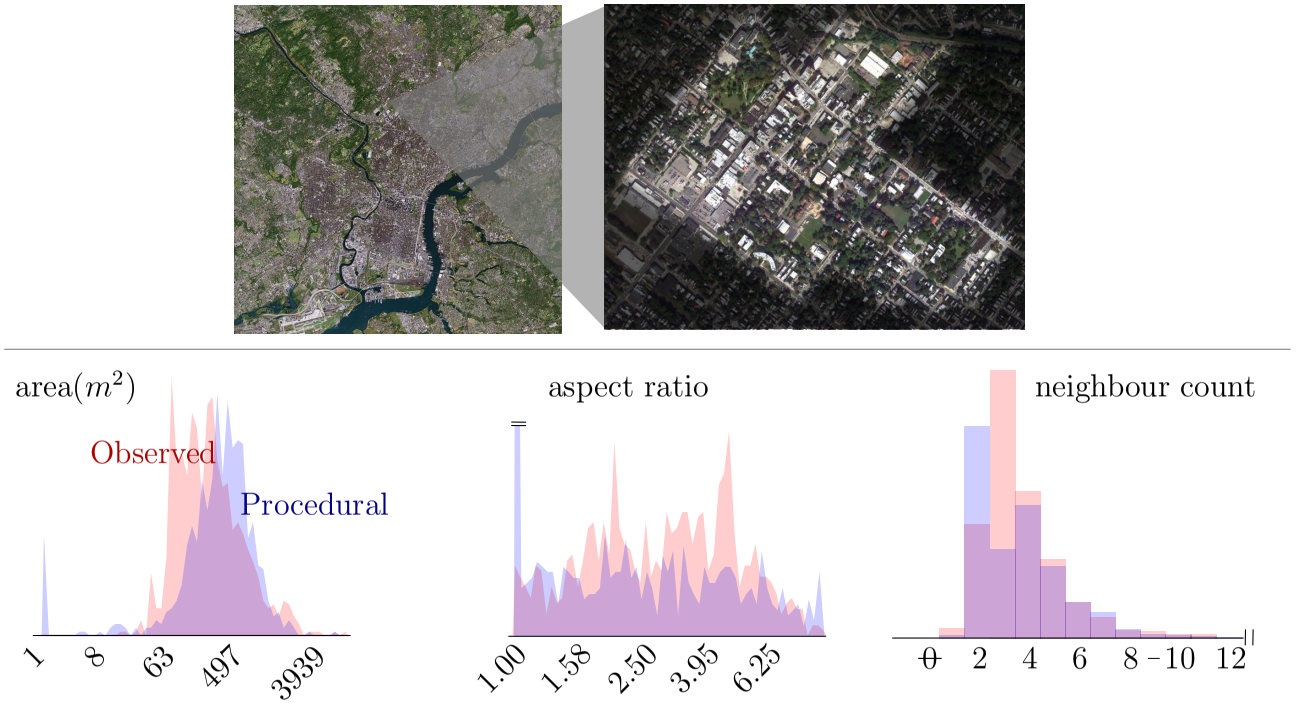

Figure 4.18: *Location and aggregate statistics for the Germantown data set. Images ©Google Maps. Note the vertically truncated procedural aspect ratio.*

Figure 4.19: *Results for the Germantown procedural parcels generated using the OBB algorithm.*

The subdivision methods introduced all successfully imitate real world subdivisions. However certain cases in the above examples demonstrate deficiencies. Fig. 4.20 shows three examples common to all algorithms:

- Left, shows that we do not model parcels with private access roads. The central observed parcel has a lane to the bottom right. Often parcels recorded in GIS data include a narrow stretch of land for access, these deeply concave polygons are not modelled by our system at all. Indeed, both the algorithms do to not include considerations of such polygons.
- Centre, illustrates an artifact related to statistical extraction. The large lot (blue) skews the statistical mean and deviation to cause the subdivision to create larger lots with high variation.
- Right, demonstrates the importance of selecting a suitable algorithm for the shape of block. The OBB subdivision here creates unrealistic interior parcels, and is unable to identify a realistic centreline.

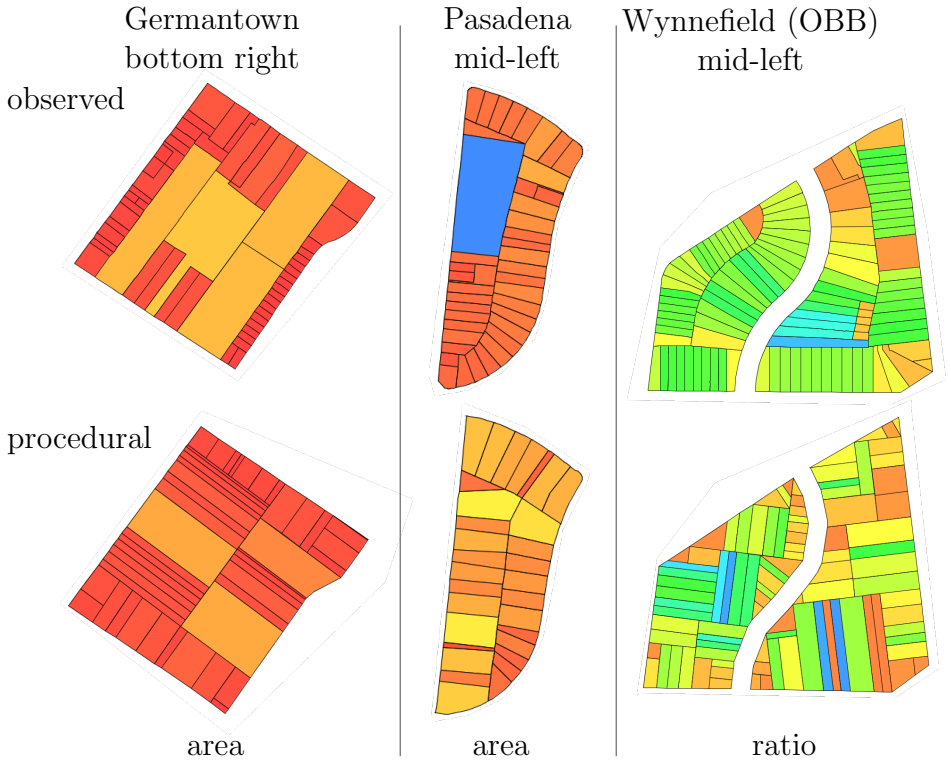

Figure 4.20: *General issues arising from our subdivision algorithms illustrated by cropped portions of earlier images.*

A further feature that we do not take into account is the modeling of non-local features. For example Fig. 4.21 identifies a straight centreline that continues between blocks. Inspection of various maps suggests that this appears to be caused by a power-line running throughout the neighbourhood, dictating the boundary of the parcels. These features are not modeled by our algorithms, and do not form a significant part of the urban planning literature, but seem to be very visible in certain circumstances.

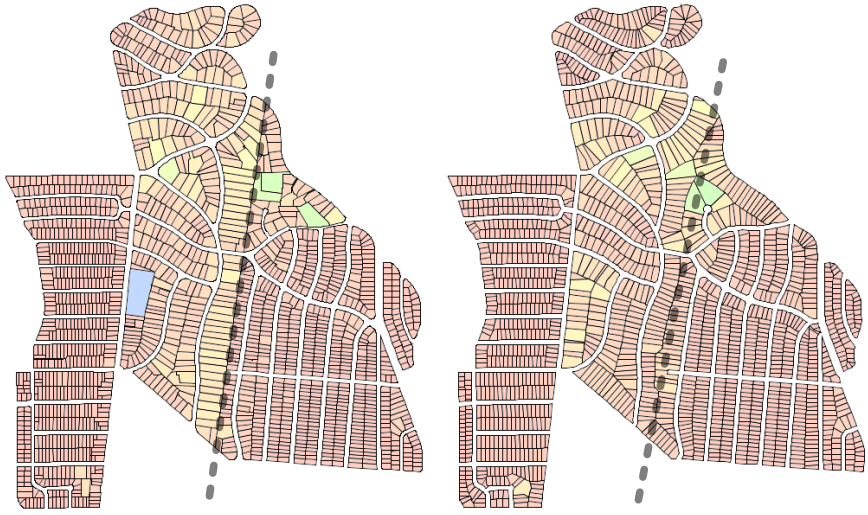

Figure 4.21: *Non-local features are not modeled by our system in the Pasadena data set. Left: observed. Right: modeled (as Fig. 4.13)*

.

The skeleton algorithm in particular provided some very accurate block subdivision, due in part to the additional information available about street priorities. Fig. 4.22 examines various aspects of the skeleton subdivision.

- Column 1 demonstrates that other split-direction heuristics are possible. The observed data in this cases slices strips in a uniform direction, regardless of the local street normal. The parcels of the procedural model adjacent to the right road are also of a peculiar shape. This artifact occurs when diagonal edges do not snap together when there is a small street frontage.
- Column 2 shows a further split-heuristic. The Naperville area statistics make it clear the the designers desired parcels of constant area, unlike our algorithm which attempt to assign equal street frontage. This suggests that another parameter for selecting the split heuristic may be desirable.
- Column 3 shows a complex concave block in which the skeleton subdivision centreline was very faithful to the observed data.
- Column 4 illustrates a complex example from Naperville that was very also similar to observed data, especially when we compare the number of neighbouring parcels.

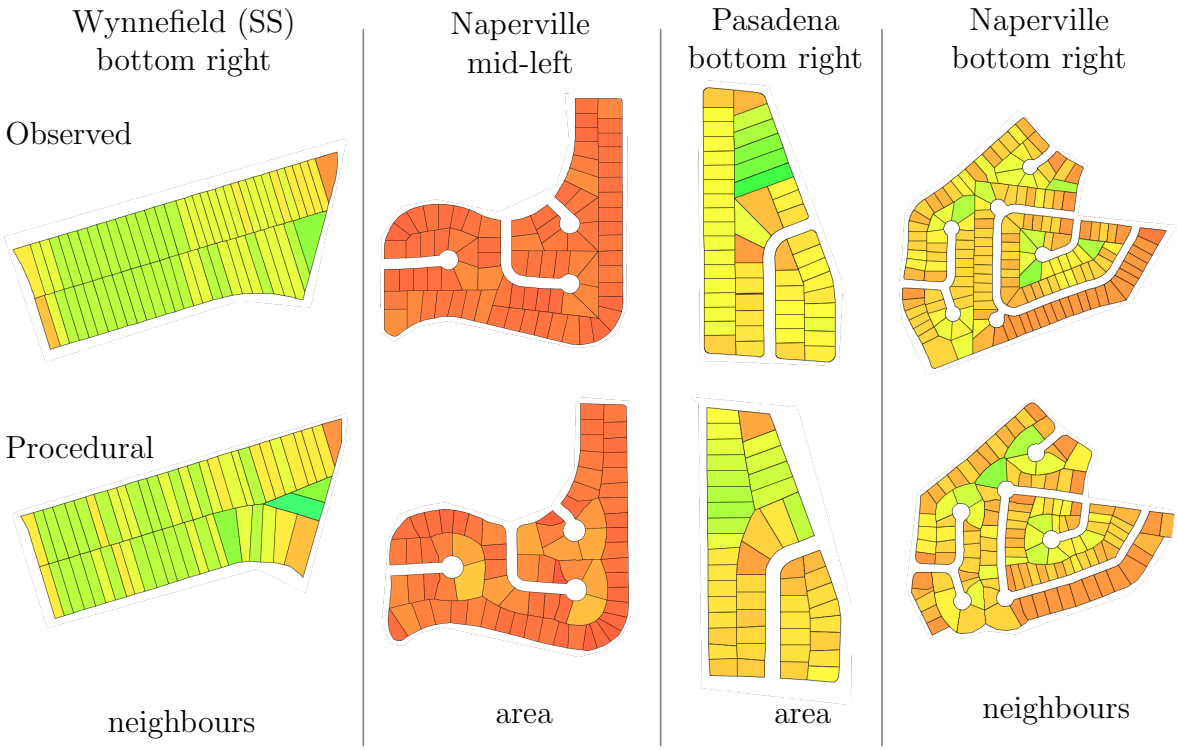

Figure 4.22: *Cropped portions of earlier results images, examining various aspects of the skeleton subdivision.*

4.5 Summary

We have demonstrated the application of the straight skeleton to the generation of city parcel layouts. After examining a number of real world parcel subdivisions we were able to classify them into several distinct types. One of these types, the traditional style, was modelled via extensions to published OBB subdivision algorithms. The second type posed more of a challenge. These modernist block subdivisions were observed to possess a predominant centerline separating two strips lots on either side of a block. In order to model these lines several options were considered. Eventually it was decided to use the straight skeleton to model these centrelines for several reasons. The geometric sensitivity of the skeleton ensured that the entire block was taken into account when calculating centrelines, therefore even complex concave blocks were realistically divided. The presence of robust commercial implementations of the straight skeleton algorithm was also an advantage. In addition, because the skeleton could be intuitively understood by users as the "limit of an offset", we ensured a smooth parametrisation between patio and non-patio lot subdivisions via a single parameter.

We have quantitatively evaluated these two lot subdivision systems over a range of North American real-world data. For four kilometer-scale data sets we generated procedural parcels from GIS-supplied city block data. We were then able to analyse the differences between these parcels by visualising the areas, aspect ratios, and the number of neighbours of both the real and procedural subdivisions. We found that after automatically fitting several parameters, the new procedural models compared favourably across our metrics . The most frequently observed deficit in our system was the inability to simulate concave parcel subdivisions in a manner similar to observed data; we hypothesise that additional simulation elements in the subdivision process may resolve this issue. The presented algorithms allow interactive editing and have proven robust enough for integration into a commercial procedural modeling system.

Future work may include —

- mixing the two subdivision styles within a single block,
- modeling inter-block phenomena, such as a preferred split direction or features such as power cables or administrative boundaries,
- selecting the most appropriate subdivision algorithm automatically from examples; this could be extended to the extraction of all of the parameters, such as street priorities, given examples, or
- adjusting the skeleton subdivision to deliver constant-area, rather than constant-street-access solutions.

Having demonstrated one domain, block subdivision, in which the straight skeleton provides a compelling interactive procedural modeling tool, we continue in the following chapter to examine another domain — that of constructing mass models from floorplans.

Chapter 5

Procedural Extrusions

This section is based on the paper *Interactive Architectural Modeling with Procedural Extrusions*[121], co-authored with Peter Wonka.

5.1 Introduction

Given the contribution of the skeleton to the success of modeling city block subdivision, a natural question is to ask which other urban domains it may contribute to the modeling of?

Recall again the urban procedural modeling pipeline of Fig. 2.34, in which streets subdivide land into blocks, algorithms such as those in the previous chapter divide the blocks into parcels, parcels are converted to footprints, and footprints are used to create mass models of buildings. Here we are interested in the final stage of this waterfall pipeline, creating solid 3D buildings from 2D footprints. To do this procedurally, that is for an arbitrary footprint or plan, without programming is the challenge we address here. To approach this problem we take inspiration from artists' plan and elevation drawings, and the flexibility of the mixed weighted straight skeleton of Chapter 3. The combination of these techniques allows us to interactively create robust 3D procedural models parameterised by the footprints.

We introduce an application of the MWSS to the interactive procedural modeling of architectural forms. The *procedural extrusion* (PE) system procedurally generates solid 3D meshes by extruding building footprints. Such an application of the straight skeleton to the creation of architectural surfaces allows for the generation of difficult architectural surfaces such as curved roofs, overhanging roofs, dormer windows, interior dormer windows, roof constructions with vertical walls, buttresses, chimneys, bay

windows, columns, pilasters, and alcoves. The system comprises of a user interface to specify procedural extrusions manually as well as a tool for the automated generation of large procedural cityscapes from their footprints. Extensions to the the sweep plane algorithm of Chapter 3 are utilised to robustly compute a wide range of two-manifold architectural surfaces.

The procedural extrusion system is both an interactive and procedural modeling tool for such architectural surfaces. Procedural geometric modeling offers several advantages over traditional static modeling of architectural forms. PGM descriptions of objects allow us to edit meshes at a higher semantic level; for example, editing wall angles rather than vertex coordinates, whilst ensuring constraints are enforced, such as polygon planarity. Additionally we can preserve subsequent edits while allowing earlier edits to be modified; such as changing the slope of a roof after a chimney has been created upon it, without adjusting the chimney. Nevertheless, the biggest advantage of procedural modeling over static modeling is the creation of large scale cityscapes, without a proportional increase in designer effort. Many of the current PGM systems, such as CGA Shape[164], require end user programming. In contrast, the PE system provides an interactive graphical tool, instead of a programming language, to specify geometry. This lowers the barriers of entry to PGM, allowing more people to create procedural content.

Architectural surfaces are often deeply concave and contain complex architectural features such as overhanging roofs, dormer windows, interior dormer windows, roof constructions with vertical walls, buttresses, chimneys, bay windows, columns, pilasters, and alcoves. These intricate surfaces have not previously been available as watertight meshes in procedural environments. Systems such as shape grammars[223, 162, 145] have tended to concentrate on the combinatorial, rather than the geometric aspects of architecture generation, and are not able to generate such geometry themselves. Typically these systems rely on pre-existing meshes that are instanced, positioned, and scaled to appropriate locations.

Given buildings, such as in Fig. 5.2, it is not obvious how to construct 3D models of these structures. Procedural extrusions provide a novel parametrisation of such buildings by taking inspiration from architects' drawings consisting of floorplans and elevations.

The first major component of the system is presented in Sec. 5.3 and allows the user to interactively draw a floorplan, and assign an arbitrary profiles to each plan edge. Nested sets of plans and profiles allow features such as dormer windows and alcoves (Fig. 5.2, orange) to be modeled. Interactive modeling via the user interface allows the expressiveness of the system to be explored in depth. We evaluate the interactive

Figure 5.1: *Procedural extrusions allow a footprint (2d plan) to be extruded to form the walls and roof of a house (inset). Meshes and procedural details can then be attached (main).*

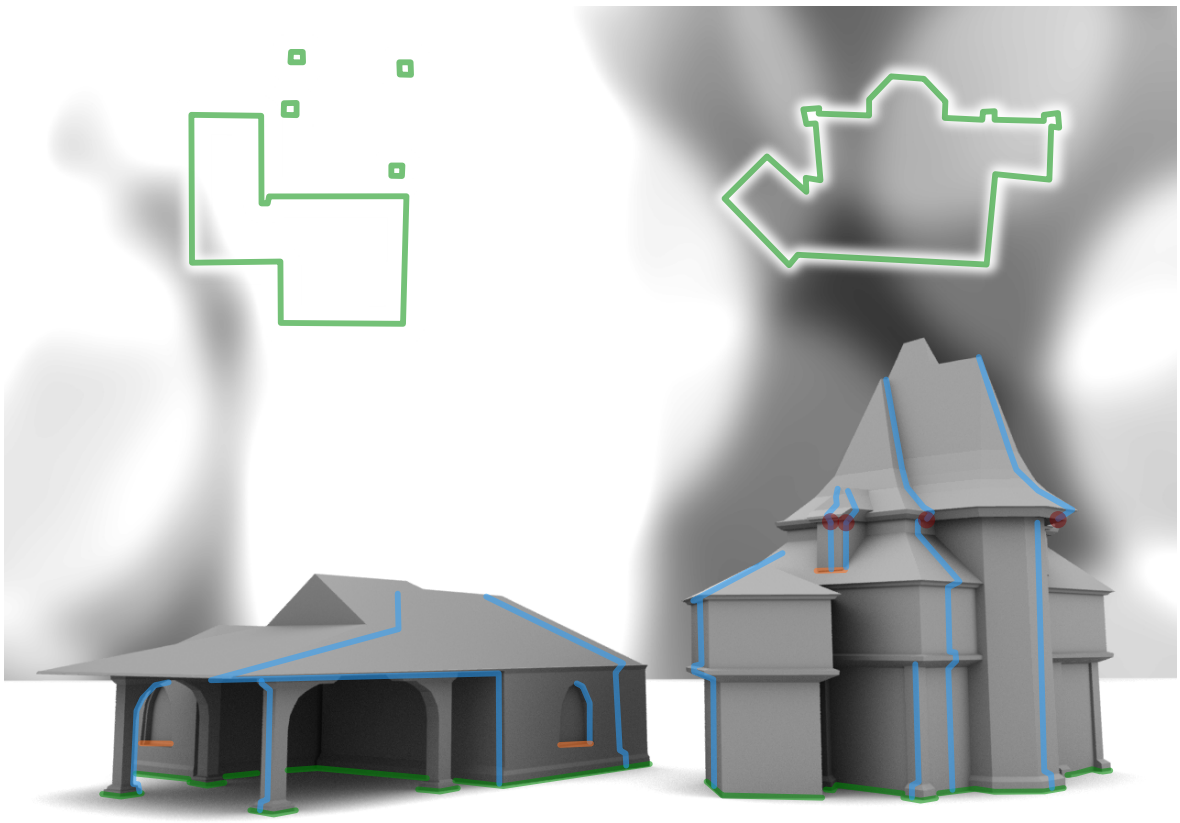

Figure 5.2: *These two examples show architectural surfaces overlayed with the user input. Plans (green), profiles (blue), natural steps (orange) and offset events (red) are specified in the user interface. The output of our system is an architectural shell (grey).*

portion of the PE system in Sec. 5.6 by modeling 50 various structures from a catalogue, as well as seeking opinions from users as to the properties of the system.

In order to combine arbitrary plans and profiles, the second component of the system is a collection of algorithms to construct 3D meshes from the specified plans and profiles. These algorithms utilise a variety of repeated applications of the MWSS (Chapter 3, Sec. 3.5) to create a geometry modeling system. We take the sweep-plane that is used to calculate the MWSS and introduce additional types of user specified events. These algorithms are presented in Sec. 5.5.1. To study the real-world stability of these algorithms we evaluate PEs over a large scale data of 6000 building footprints in Sec. 5.6. Here we note that the computational geometry community emphasises provably correct algorithms and therefore often favours rational arithmetic. In contrast, our work consists of heuristic algorithms that emphasise computational speed and are geared towards a floating point implementation. While our heuristics include various mechanisms to make the results more robust, it is possible that the computations can fail. For example, in the Atlanta data set of 6000 footprints we noted that two roof planes were not computed correctly. The approximate nature of our floating point computation also results in roof planes being moved by millimetres.

We conclude with a description of external applications to which others have successfully applied components of the PE system.

The contributions of our work are:

- the design of the system and tools to enable procedural modeling of complex architectural surfaces.
- the set of tool choices to enable procedural modeling of complex architectural surfaces.
- heuristic algorithms to generate a polygonal mesh from the user specification that is approximately consistent with the input data.
- the evaluation of the system on a collection of examples to verify its practical utility, and to identify configurations that are difficult to model with our tools.

5.2 Related work

In this section we describe and examine some common techniques applied to architectural modeling and analyse some of the properties of the resulting architectural meshes.

Figure 5.3: *In many buildings' geometries, there are many horizontal edges (green). Many faces of such geometry are coplanar to one or two such edges. In this case, only the red faces do not do not have such a horizontal edge.*

We may make the observation that many architectural and man-made objects have a common property: *There are many horizontal edges to the geometry, and the faces between such edges are rectangular and coplanar.* For example Fig. 5.3 shows one building with many horizontal edges and associated faces.

There are several properties that we find desirable in computer models of architectural structures. We assume to use polygonal mesh models, since these are common, somewhat standard in industry, and are those which hardware (GPU) acceleration is designed to accommodate. "Nice" 3D meshes commonly have the following properties:

- Planar faces: Each face lies entirely within a single plane.
- Water-tight: There are no holes in the mesh, all adjacent faces are connected via a shared edge, and all adjacent edges are connected via a shared vertex.
- No self-intersections: No part of the mesh protrudes through another; the only parts of the mesh that touch are adjacent in the mesh data structure.

To describe such meshes, basic 3D modeling tools such as as those introduced in Sec. 2.12 may be used. Tools such as manual vertex modeling, extrusion, lofting, and constructive solid geometry have all been used to model architecture in 3D modeling tools such as Maya[19], Sketchup[240], and Blender[74]. Several examples of buildings created with the Sketchup modeling tool are shown in Fig. 5.4.

- Manual vertex and face specification gives users the tools to create and position verticies in $\mathbb{R}^3$. These tools allow unrestricted mesh creation, but it is possible, and even common, for such tools to create non-planar polygons, non-watertight,

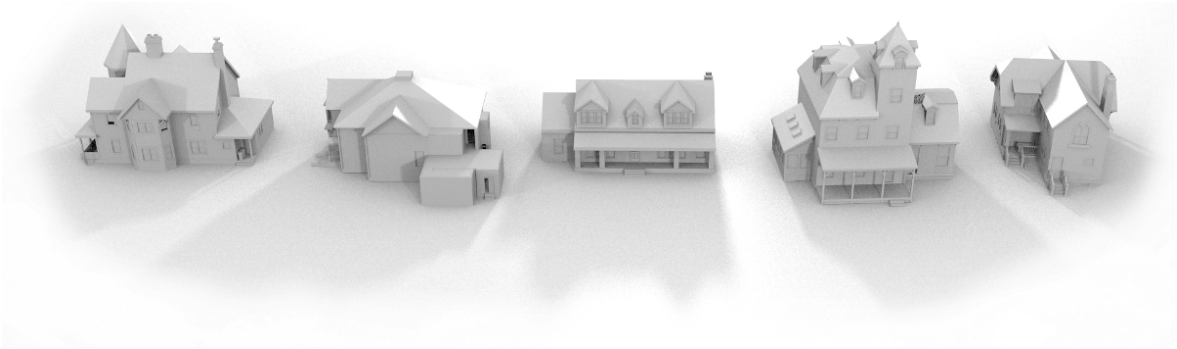

Figure 5.4: *Several typical building meshes created using Sketchup[240], and found in Trimble Warehouse[241] using the search "Victorian house". From left to right the buildings were created by users wiccan, DILBERT, bob1938, Paulwall and bob1938. Buildings have had garden geometry and textures removed to allow comparison with our results. ©2013 Google.*

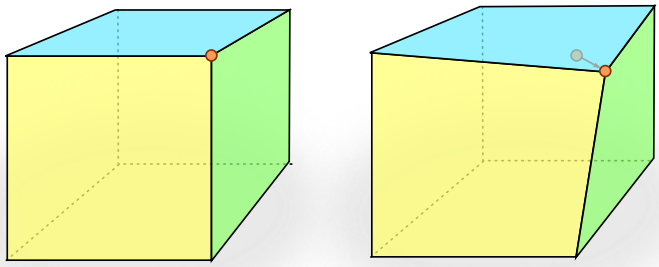

Figure 5.5: *Given a mesh (left), translating a single point(orange) may result in one or more non-planar faces(right).*

or self-intersecting meshes. Often additional post-processing stages must be applied to check for these conditions, and resolving them is left to the user. Fig. 5.5 illustrates how moving a single vertex may result in several non-planar faces.

- Extruding a plan-polygon either in a single direction or along a 3D path, Fig. 5.6, left, is another method to construct meshes with rectangular faces. Careful positioning of the plan and profile can produce meshes with the desired horizontal edge property. An extrusion tool creates an instance of the plan at each vertex of the path. It continues to create a rectangular face between the pairs of corresponding plan edges from adjacent plan-instances.

  However there are some problems with the extrusion tool. If the path rotates, the faces of the resulting geometry may not be planar, Fig. 5.6, centre. Additionally, when modelling walls and roofs, the plans and profiles are not changed in response to the geometry; self-intersections may occur, such as when modeling roofs — the crest of the roof may either fall short, or overshoot as in Fig. 5.6, right. Such

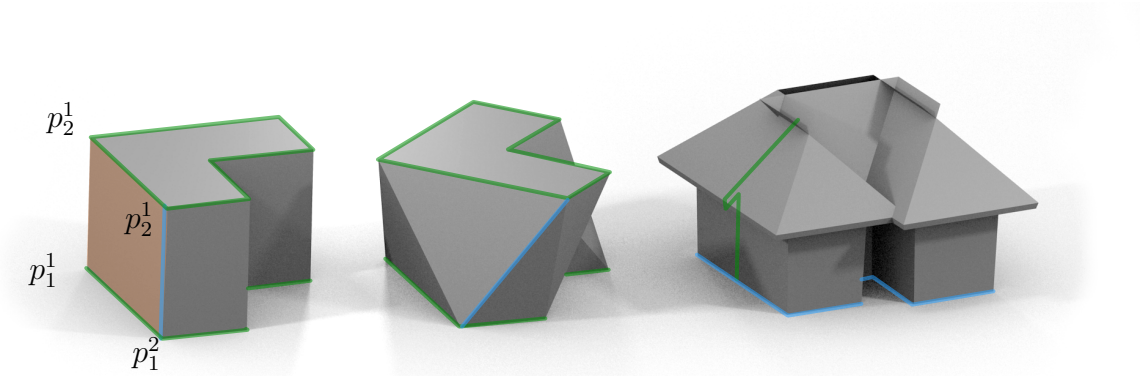

Figure 5.6: *Left: A plan polygon (green) is extruded along a single segment path (blue). Rectangular faces are created between adjacent instances of the polygon. The above verticies p_1^1, p_1^2, from the first instance, and p_2^1 and p_2^2, from the second, form the orange rectangle. Centre: If the path rotates an instance, faces may not be planar. Note that the non-planar quads are depicted here as triangles. Right: Using a more complex path, geometry with strong horizontal lines can be created. However self-intersections and holes in the geometry are evident in this example, such as near the roof line of this mesh, and above the concavity in the plan.*

deficiencies with geometry created by the extrude tool must be identified and removed manually, possible with manual vertex and face edits.

Levelshop[73] is a rapid video game level prototyping tool that uses extrusions, together with user defined 2D plans. Because of the above problems with extrusion, it is limited to relatively simple geometry.

- A modification to the extrusion algorithm allows for different profiles to be used at each vertex on the profile. This *loft tool* allows more user interaction, so that when the geometry does self-intersect, the profiles may be manually edited. Lofts are a modeling primitive extensively used in 3D modeling packages. As when extruding there are no guarantees that the result of a loft will not self-intersect. The manual editing of profiles can be quite involved as it requires the user to specify additional segments for some of the polyline instances as well as specifying corresponding topologies for face creation.

- Another popular method for geometry creation is *constructive solid geometry*[15] to form objects from the addition and subtraction of geometry elements. CSG has been used by several systems since to create urban modeling tools. Sugihara and Hayashi[228] create roofs on orthogonal geometry by unioning roofs after rectangular decomposition. This approach is adapted to building reconstruction in [133], by computing the CSG union of elements from a library of 3D roof-form blocks.

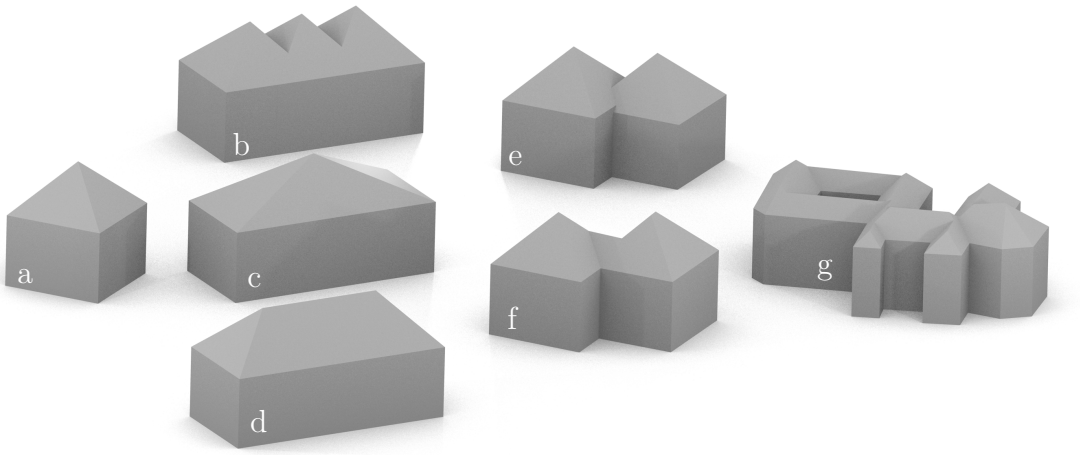

Figure 5.7: *The expressiveness of a constructive solid approach, given a single input primitive (a) is limited. For example, we may wish to elongate the primitive. A CSG union operation could only construct a mesh with several peaks (b), while a scale operation would also adjust the slope of the roof in an unrealistic manner (c), however we probably prefer a result closer to the straight skeleton (d). In a second example, the union (e) is not the same as the SS (f), and introduces unwanted, water collecting, horizontal edges into the roof-line. More complex examples (g) cannot be created at all, since they are not locally similar to the available primitive.*

> The advantages of CSG are that manifold results are guaranteed, and that all the output faces are subsets of the input faces. Thus if the input faces are planar, then so will the result. The disadvantage is, however, that the range of results are limited by the available CSG primitives, as illustrated in Fig. 5.7.

As introduced in Chapter 2 there are a wide range of languages and grammars for specifying geometry. Many of these systems, such as CGA Shape[164], are concerned with the combinatorial and positional aspects of the modeling, rather than the geometric elements. For example, CGA may specify the location of the roof, but would rely on extrude operations to specify the mass model and other geometric routines to calculate the roof geometry.

Several systems exist to deform existing architectural meshes into new configurations [93, 35, 77], additional detail is given in Chapter 2. For example, in [93] Habbecke and Kobbelt introduce a mesh deformation tool that constrains specified edges to remain, for example, coplanar, horizontal or vertical. The system constructs a linear system that may be deformed in real time. These deformation tools, however, do not solve the problem of creating geometry to be deformed in the first place.

Previous systems have applied the straight skeleton to the modeling of architectural roofs. Laycock and Day[173] use the SS to define roofs over arbitrary floorplans, and adjust the positions of the verticies to create Gable roofs. Havemann[105] uses an

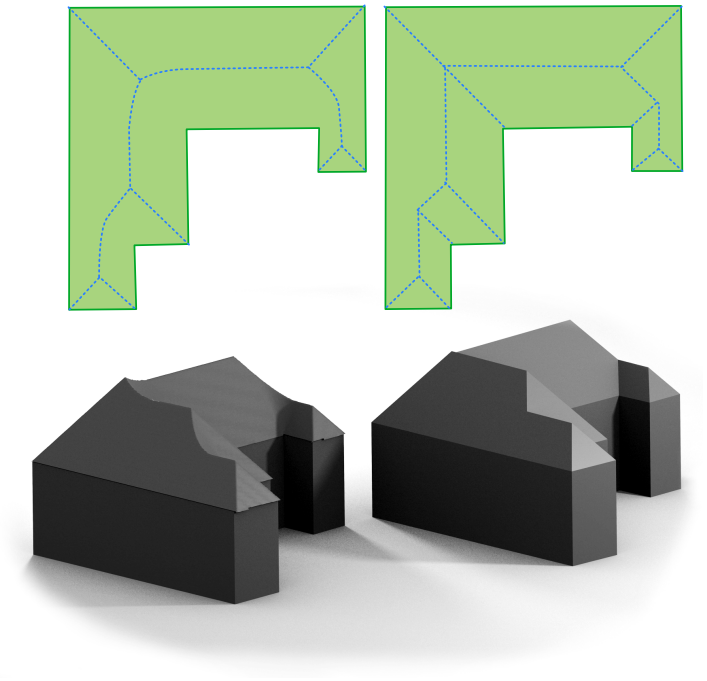

Figure 5.8: *A comparison of modeling roofs with the medial axis, left, and the straight skeleton, right. The corresponding 2D geometries are shown above.*

application of the SS with uniform negative weights, followed by an application with uniform positive weights to create overhanging roofs. Our goals are similar to these approaches and we contribute new extensions to the straight skeleton to avoid the need for Laycock's vertex adjustment and to extend the skeleton beyond roof modeling to an interactive procedural modeling system for entire architectural meshes.

An alternative to the SS for offsetting areas is the medial axis[28]. As discussed in Sec. 4.3.2, there are several technical limitations to using the medial axis in the polygonal domain. In addition we may wish to study the aesthetic reasons for not using the medial axis; we can ignore these technical limitations to create a model such as demonstrated in Fig. 5.8. In this model we observe that there are many unrealistic curved roof ridges, both when viewing the model from the top or the sides. These unrealistic curved edges make the medial axis much less suitable for modeling the roofs of buildings than the straight skeleton. In addition we note that the method used to visualise the medial axis for Fig. 5.8 created 65,000 polygons, compared to the 80 polygons created by the SS algorithm. This large difference in model complexity was caused by the terrain used to model the roof from a 2D bitmap image of a medial axis computation. It may be possible to create such 3D models using the medial axis with fewer polygons, but we are unaware of any such published techniques.

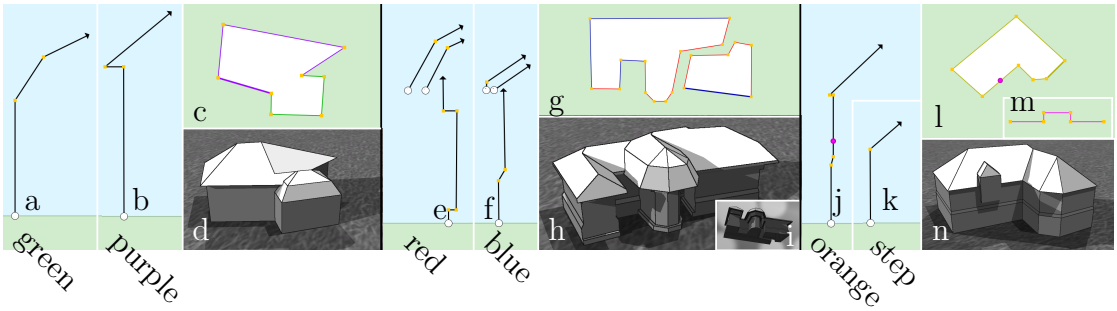

Figure 5.9: *Three example buildings constructed in our user interface. We demonstrate multiple profiles on a simple plan (abcd), modeling overhangs (efghi) and anchors (jklmn). Simple profiles (ab) are applied to the green and purple edges of the plan (c) to create the geometry (d). Overhangs are defined using an additional pair of profile polylines associated with every edge (ef) to create typical roof geometry (hi). Anchors (magenta circles) are defined on the profile (j) and the plan (l) to position features. In this example the anchors position a rectangular natural step (m) with a profile (k) that creates a roof-window (n).*

5.3 User Interface Description

To control the underlying application of MWSS instances, the PE system utilises a graphical user interface. This section introduces the interface, and how it can be used to model single instances of complex watertight architectural meshes, we call *shells*. The MWSS algorithms are largely motivated by the desirable user interface commands, and so the user interface provides a motivation for the technicalities in the following sections. These new event types specified by the UI are explained in Sec. 5.5.

5.3.1 Overview

Our UI originates from the observation that simple roofs can be defined by a aerial plan, and an angle for the roof. We combined this line of enquiry with the study of architect's drawings that combine plan drawings from above, and elevation images from the four sides. The plan specifies the footprint of the structure, while the observed roof angle is often present in the elevations. Exploring this observation, one may extract angles and heights from other locations on the profile in an architectural elevation, such as the height of the walls. However, architects typically produce a small number of elevations, typically one for each cardinal direction, and this provides insufficient detail for reconstruction. For example when the footprint of the house contains concavities, cardinal elevations under-constrain the resulting solid shape. The premise of the PE system is to create solid geometry from a *plan* and per plan-edge *profiles*, as in Fig. 5.2.

The plans and profiles are evaluated by a rising sweep plane algorithm, in a manner

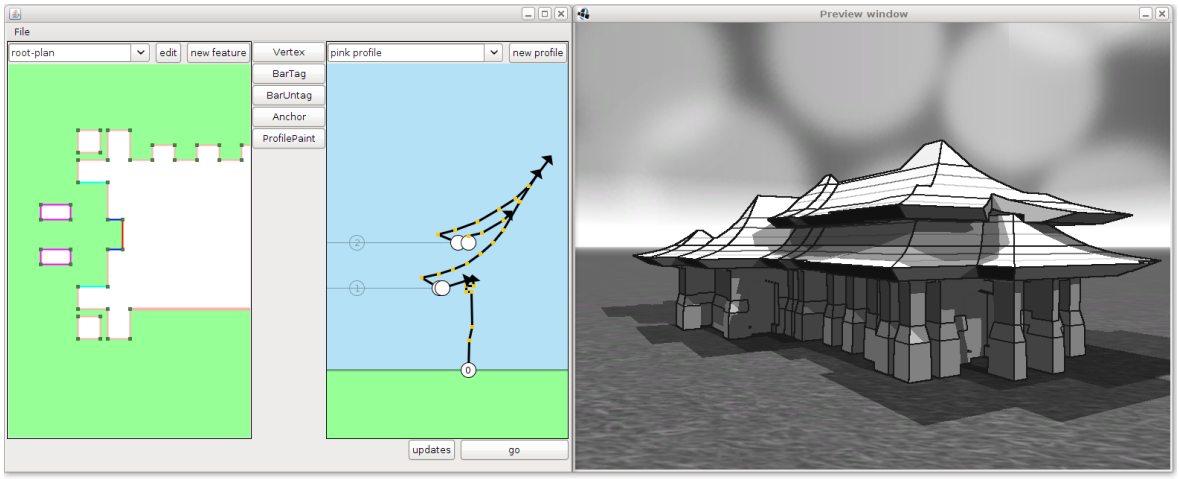

Figure 5.10: *The interactive interface during the design of a temple. The right window contains the output preview whilst the left window contains the plan and the profile editors.*

similar MWSS, of Sec. 3.5. As the sweep plane rises, it carries with it an *active plan* which combines the different profiles to create a solid polygonal mesh.

The complete UI, including the MWSS implementation, is available online[120].

5.3.2 Plans and Profiles

The complete user interface, as illustrated in Fig. 5.10 and provides:

- the current plan,
- the current profile,
- a 3D preview of the current architectural shell,
- tools to add, remove and move verticies in the plan and profile,
- tools to associate profiles with plan edges,
- options to add and remove profiles
- options to add *events* to the profile and plan using anchors. There are several different types of discrete UI events, introduced below, which are enacted as the sweep plane rises past them.
- Finally the UI also provides standard save, load, and export functionality.

We shall continue to use the definition of a plan introduced in Sec. 3.2.1 — a linked list of verticies that define the counter-clockwise boundaries of enclosed regions. In

the PE system, every edge in the plane is also associated with a *profile*. A profile is a collection of polyline segments that define a cross-section of the building through the associated plan edge. As the user edits the plan or profile, the system shows the resulting architectural shell in a 3D preview window. The following Sec. 5.5.3 will introduce *edge direction events* into the sweep plane algorithm, each of which is specified by a profiles vertex.

Fig. 5.9, c, shows an example of a plan and two profiles, a & b. In the 2D plan, different colours show the association between the plan-edges and profiles. Each profile is automatically assigned a colour upon creation, and the plan-edge is drawn with this colour.

Because of the underlying sweep-plane algorithm we must constrain the profiles to be monotonic in the vertical (z) direction; horizontal polylines are allowed as a special case. The underlying procedural extrusions grow architecture upwards from an input-plan. Therefore, a downwards moving line-segment is meaningless. In order to creating buildings with overhanging roofs, such as the temple of Fig. 5.10, there were two design directions that could have been taken:

1. Allow the user to draw arbitrary polylines as profiles that can go up or down in the vertical direction. These would be automatically decomposed into monotonic profiles;

2. Force the user to explicitly model profiles as multiple polylines where each polyline must be monotonic in the vertical direction.

Given several examples, it became clear that when design 1 was used it was difficult to coordinate different profiles, each with an overhang, to occur at the same height. This case is relatively common, so design 2 was chosen. All the polylines in a profile are, therefore, monotonic; polylines that represent overhangs on different profiles all start from the same height. The height is marked in the user interface by a white circle, as in Figs. 5.10 & 5.9 e & f. The height of all overhangs starting from the same elevation can be changed by moving the position of this circle.

We will explain the process of modeling overhangs using the second example in Fig. 5.9 efhg & i. The user creates the input floor plan shown in (g). The edges in this plan are colour coded as either red or blue. A red edge will be extruded according to the red profile (e) and the blue edges will be extruded according to the blue profile (f). The final architectural shell is shown in (h) and (i). The red profile and the blue profile each consist of three polylines. Each of these polylines is monotonic in the vertical direction. In the red profile we can see that one of the polylines has two segments that

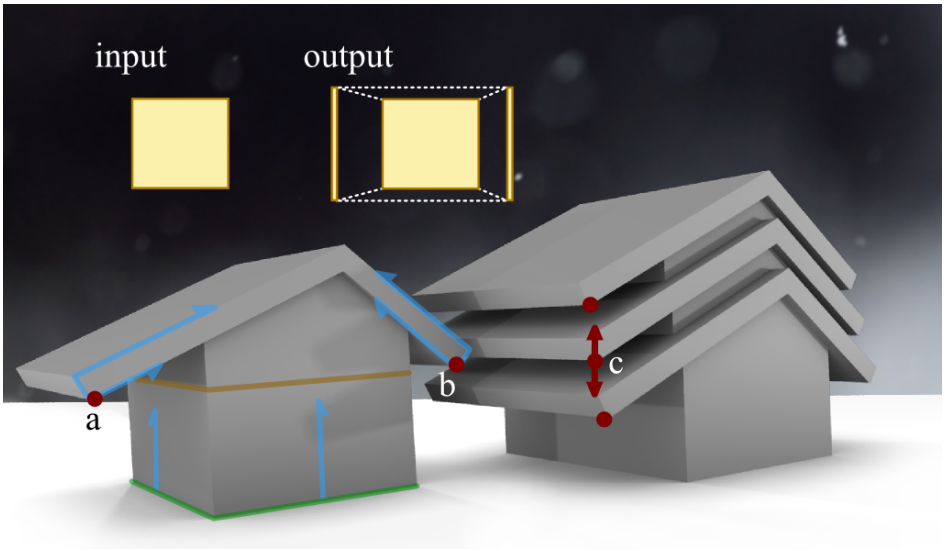

Figure 5.11: *A profile offset event simulates a non-monotonic profile by manipulating the active plan at the height of the event and adding an additional overhanging region (top left). In this example the front and back edges of the roof have been disabled from taking part in the offset. One profile offset event (a,b) may define a shared starting height for one roof with two different angles. Coordinating this offset event between profiles allows for a single parameter to control the roof height (c; several heights shown).*

are completely horizontal. Modeling horizontal segments is transparent to the user, but will be handled as special case later in the implementation. Modeling overhangs is an explicit operation. The overhang is modeled by inserting two new polylines into both profiles at a certain height. In the user interface this is one atomic insertion operation. When the user adds an overhang to one profile, via a right-click menu, then all profiles will obtain two new polylines at the same height. These two polylines bound the inside and outside of the overhanging area in the active plan. The user can independently edit the new polylines for each profile, whilst only the starting height remains synchronised. The interface allows users to disable edges so that they do not contribute to the offset boundary, an example of which is shown in Fig. 5.11. The profile associated with edges adjoining such disabled edges is specified once for the entire offset. Both the edge disable option and adjoining edge profile are manipulated via the right-click menu.

Computing these non-monotonic sections of the profiles is somewhat involved as the user interface does not specify the offset region in absolute coordinates, but rather relative to current edges in the active plan. Sec. 5.5.6 will introduce these *profile offset events*, and a solution to computing the corresponding 3D meshes via sub-applications of the WSS to the current active plan outline.

5.3.3 Anchors

There are several categories of UI operation that perform actions at specific locations on the 3D architectural model being constructed. For example we may wish to position a decorative mesh at a specific location, make local change to the active plan in order to induce dormer windows into a roof, or we may wish to divide the active plan into separate parts at a certain height. The difficulty here is that these locations must be persistent to changes in the input plan, profile changes and re-calculations of the architectural shell. This is called the *persistence problem* in procedural systems[145], and we introduce *anchors* as a partial solution in our system.

An anchor is created, after specifying the event type, by selecting a point on the plan, or on the corresponding profile polylines. In Fig. 5.9 (jklm & n), the anchors are shown as magenta circles on a floor plan edge and a profile edge. A plan anchor and profile anchor together specify the location of a feature, in this case a roof window. Fig. 5.12 shows how an anchor on the plan (a), and the profile (b), may be combined to specify a location (c). A profile anchor alone specifies an event at a the specified height, for example splitting the active plan into two halves. In either case, if the corresponding profile anchor is no longer associated with an edge in the active plan at the specified height, then it will not be instanced. Furthermore, if the edge on which an anchor was placed has been split, then the event may occur two or more times.

5.3.4 Plan Edits

Editing the active plan at a specific location allows a wide range of local features to be created on the architectural shell. These edit-events are *plan edits*; they are specified by a plan-edit-plan and profile, a plan/profile anchor pair to position the edits, and a *step type*. The step type specifies one of two options for inserted edges into the active plan, with different advantages:

- *Forced steps* insert an arbitrary set of edges into the plan.
- *Natural steps* offer a range of simple shapes that can be inserted, and come with a guarantee not to cause self-intersecting geometry.

The details of the differences between these two step types are discussed later. Fig. 5.9 (jklm & n) show a plan edit with a forced step being used to create a roof window.

Fig. 5.13 illustrates that, as well as adding additional regions into the plan, plan edits may also remove regions. Here we use a plan edit to specify a square portion of the roof to be removed. This square is replaced by a square plan region, and associated

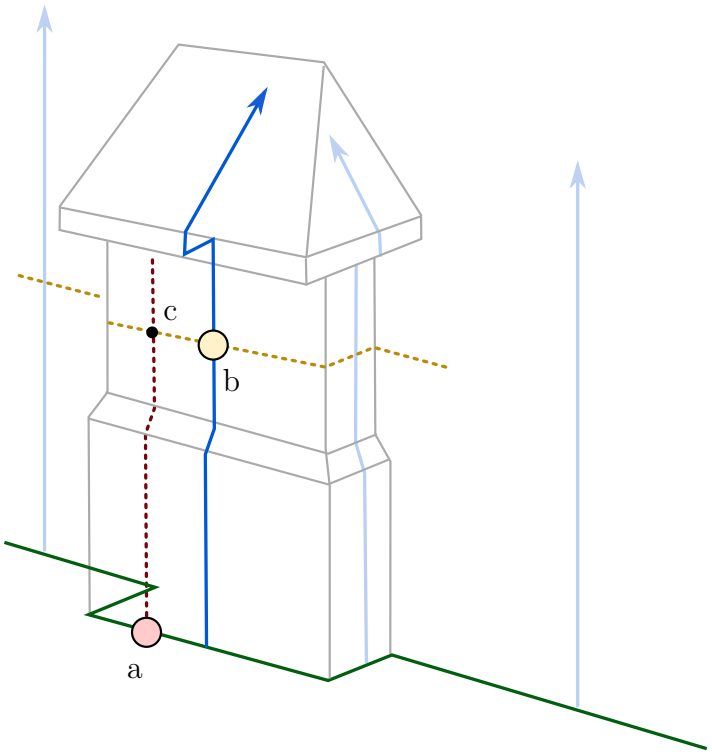

Figure 5.12: *Positioning a feature, c, using plan anchor a and profile anchor b on the complex surface of a bay window.*

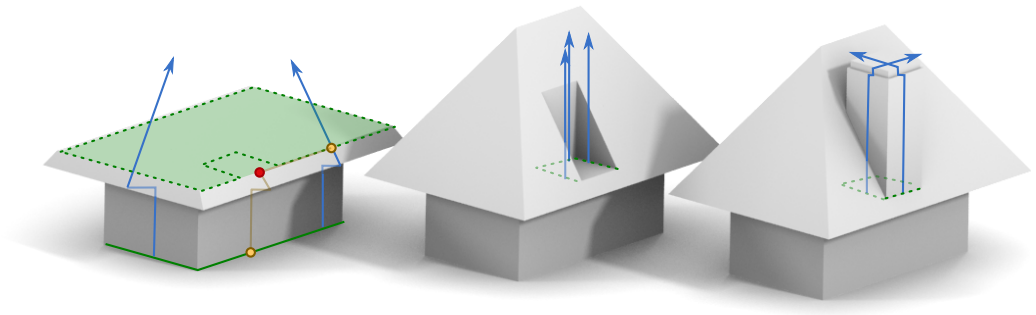

Figure 5.13: *Left: The plan (solid green line) and profiles (blue lines) define the shape of the structure. The anchors (orange) locate the chimney (red). A natural step is inserted into the building at the anchored location (dashed green lines). Middle: The finished 3d geometry, showing the profiles for the new edges. Right: Alternative natural step which adds an additional rectangle into the plan (dashed green lines) to specify a chimney.*

profiles, such that a chimney is formed as the sweep plane rises. If the input plan has several repeated elements, such as bay windows or buttresses, plan edits give a convenient tool for defining the repeated plan and profile once, whilst repeating it at a number of different anchored locations; for example the creation of the buttresses of Fig. 5.34.

5.3.5 Positioning Decorative Details

Another application of anchors is to specify the location of architectural details. Sets of anchors can be used to mark the location of anchor points of decorative meshes. For example the top and bottom elements in a grid of windows of Fig. 5.14. This figure also provides an example of re-using plan and profile anchors to ensure that the decorative meshes are positioned in a regular pattern. By using a pair of anchors to specify the top and bottom of each window mesh on the facade, the user specifies that the windows have a particular height. In general, we may use tuples of anchors to specify the position of control bones to provide a variety of deformations to decorative meshes. The mesh deformation takes place using per-bone vertex weights[136], imported into the PE system in the MD5 file format. Typically these are created using an external modeling tool; the examples in this chapter were created with Blender[74].

A user interface parameter allows the users to specify the scale of the decorative meshes on the architectural shell. This is useful when working with decorative meshes from a library with varying scales.

While pairs of anchors can be used to specify points on the architectural shell, individual faces of the shell can be identified by adding *tags* to the appropriate profile segment. These are shown as small triangles in the user interface, a cyan coloured example is shown in Fig. 5.15. After the complete manifold is computed, the faces that were generated from the specified profile segment are post-processed in a particular way, for example to add tiles to the roof.

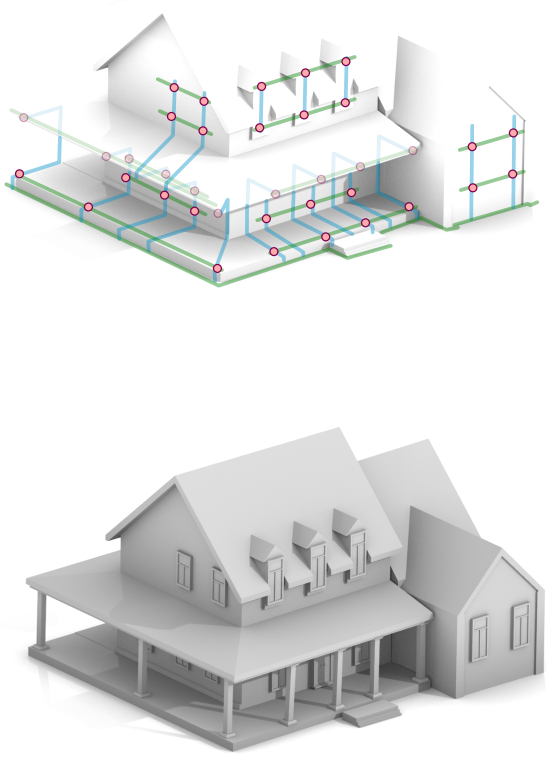

Figure 5.14: *Above: Plan (blue) and profile (green) anchors define the attachment points (purple) for decorative meshes. By sharing plan and profile anchors, the attachment points may be constrained to the same horizontal or vertical line. Below: The window and pillar meshes are deformed by the attachment points to increase the variety in the model.*

5.4 Splitting the active plan

A *subdivision event* splits the area enclosed by the active plan into several sections at a particular height. It is used to model buildings that rely on an internal structures, such as "saw tooth" roofs. The user defines a set of offsets, which bound the newly created regions on the active plan. As with profile offset events, the challenge in implementing subdivision events is in creating a robust result for all possible active plan topologies; again a second application of PE are used to define these offset region boundaries.

When creating a subdivision event the user specifies the following using the interface of Fig. 5.15:

- A height for the subdivision event, specified by a profile anchor.
- A map that defines the new profiles in the subdivision application of procedural extrusions, from the existing profiles.
- A set of tags applied to these new profiles which specify the new regions of the subdivided plan.
- A map that specifies new profiles for the new regions.

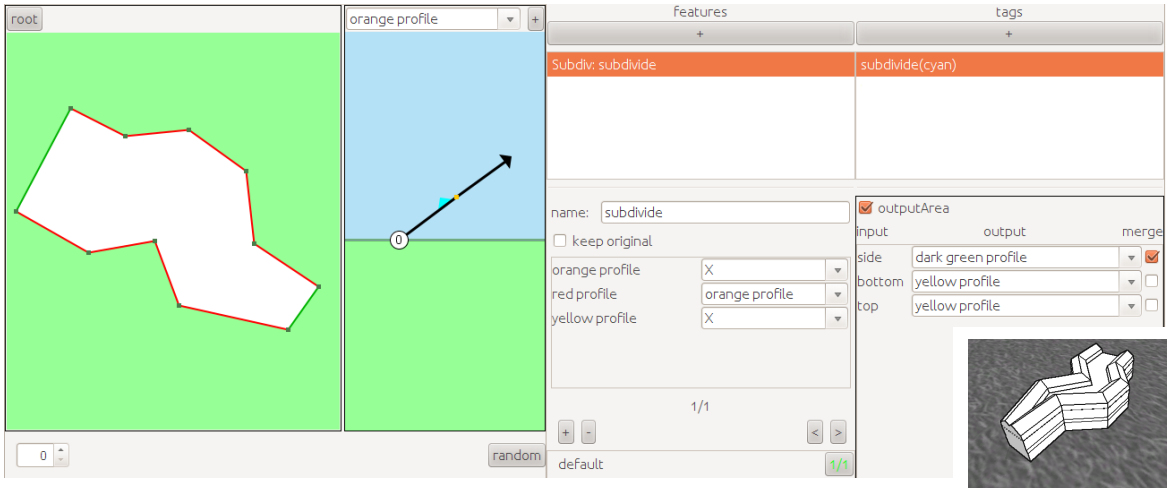

Figure 5.15: *The subdivision event UI. Left: The plan and subdivision profile. Right: The UI for specifying the new profile map, and tags for specifying the new regions and associated profiles for their side, bottom and top edges. Inset: The resulting 3D model.*

5.5 Computing Procedural Extrusions

Given the UI input, this section details the procedural extrusion system which generates the output geometry. It begins by defining the terminology used, the inputs and the outputs of the main algorithm. The section continues with a description of the different events generated automatically and by the user, and how each event type is computed.

5.5.1 Definitions

We shall use the terminology of Chapter 3, briefly introducing it again, and extending it where appropriate. Broadly, the inputs are the plans and profiles defined, for example, by the UI, while the output of the system is an architectural shell in 3d Euclidean space with a xyz world coordinate system. The up direction is along the z axis.

A *(floor) plan* is a planar subdivision (a straight line planar embedding of a planar graph) that divides a plane into *inside* and *outside* regions. A plan has corners and oriented edges. A plan is embedded in a plane parallel to the xy-plane (the ground plane), so that all corners of a plan have the same z (height) value. We require that the boundaries of a plan are a non-intersecting collection of oriented polygons. The inside is on the left-hand side of each oriented polygon edge. The polygons are oriented counter-clockwise, but polygons describing holes are oriented clockwise. Additional bounded regions may be recursively located inside a hole. The jth polygon is described by n^j polygon corners $c_i^j \in \mathbb{R}^3$ with $1 \leq i \leq n^j$. Each corner c_i^j is connected to the next corner (according to the polygon orientation) by an implicitly defined *edge*, e_i^j. In the following, indices should be treated cyclically, such that a polygon with corners c_1^j, c_2^j,

and c_3^j, the corner c_4^j means c_1^j.

Each edge in a plan is associated with a *direction plane*, dp_i^j, which contains the edge. Since we will be using it to evaluate a MWSS, it is defined by an angle θ such that $-\pi/2 \leq \theta \leq \pi/2$. A vertical direction plane has $\theta = 0$, whilst a direction plane oriented towards the inside (outside) satisfies $\theta > 0$ ($\theta < 0$ respectively). The angle is measured between the direction plane and a vertical plane that also contains the edge, as in previous Fig. 3.28.

A *profile* is a set of polylines that is used to control the direction plane of an edge. A polyline is modeled in a local 2d wz-coordinate system and consists of a list of m points t_i. The location of point i is $(t_i.w, t_i.z)$ and we require, for monotonicity, that $t_i.z \leq t_{i+1}.z$. The polyline defines $m-1$ angles, $\theta_1..\theta_{m-1}$. The angle θ_i is calculated as the clockwise angle between a vertical line and the line t_i to t_{i+1}. The angle lies in the range $-\pi/2 \leq \theta_i \leq \pi/2$, and the final angle is constrained such that $\theta_{m-1} > 0$. This final condition ensures that the MWSS terminates.

5.5.2 Overview

This section describes the input, output, and an outline of the PE algorithm.

Input

The input of the algorithm is a (floor) plan, called the *input plan*, profiles associated with the edges of the input plan, profile offset events, and anchor events. Anchor events specify the location of plan edits, a mesh instance or subdivision event.

Output

The main output of the algorithm is an *architectural shell* (3d mesh) in the xyz world coordinate system. In the non-degenerate case the shell is watertight and two-manifold. The architectural shell is a polygonal mesh stored in a half-edge data structure. The half-edge data structure stores a set of vertices in $\mathbb{R}^3$, a set of input edges and skeleton arcs between the vertices, and a set of planar faces which may contain holes. Faces are defined by a counter-clockwise ordering of arcs.

Outline

The algorithm is an extension of the MWSS algorithm introduced in Chapter 3. As well as the automatic events that occur in the MWSS, the event queue also contains

user interface events. As before, the core algorithm repeatedly takes the next event from the queue, allowing it to update the *active plan* as well as insert additional events into the queue if necessary. Fig. 5.16 gives the algorithm in pseudocode form.

```
Main begin
    Q = new priority queue;
    sweepZ = 0;
    foreach corner c in active plan do
        CreateGIEEvents ( c, Q );
    CreateUserEvents( queue Q)
    while !Q.empty() do
        event = FindNextEvent(Q);
        event.updateActivePlan();
        event.updateEventQueue(Q);
    foreach edge e in input plan do
        ReconstructFace (e);
end
CreateUserEvents( queue Q ) begin
    foreach Profile p in user profiles do
        foreach ProfileOffsetEvent poe in p do
            Q.insert (new ProfileOffsetEvent(poe) );
        foreach vertex v in p do
            Q.insert (new EdgeDirectionEvent(p, v) );
    foreach AnchorEvent ae in user anchor events do
        Q.insert (new AnchorEvent(ae) );
end
```

Figure 5.16: *Pseudo-code for main loop of the PE algorithm, an extension of Fig. 3.14*

The priority queue orders events by their z height, thus simulating the rising sweep plane. By allowing additional edges to be added by the user to the rising active plan, the MWSS is extended to describe a wide range of architectural forms. Therefore the PE algorithm is equivalent to a succession of MWSS skeletons stacked on top of each other, along the z axis.

Once all the events in the priority queue have been processed the algorithm terminates. The skeleton faces defined by the events are post processed and output. This post processing involves identifying holes, positing decorative meshes and applying the textures specified by user tags.

Data structures

The first significant data structure is the *plan data structure*, which encodes the active plan on the sweep plane, as in [69] and Chapter 3. This structure is a doubly linked list of corners. Each corner has a pointer to the next corner, the previous corner, and a pointer to its previous and next direction planes, Fig. 5.17. At the beginning of the

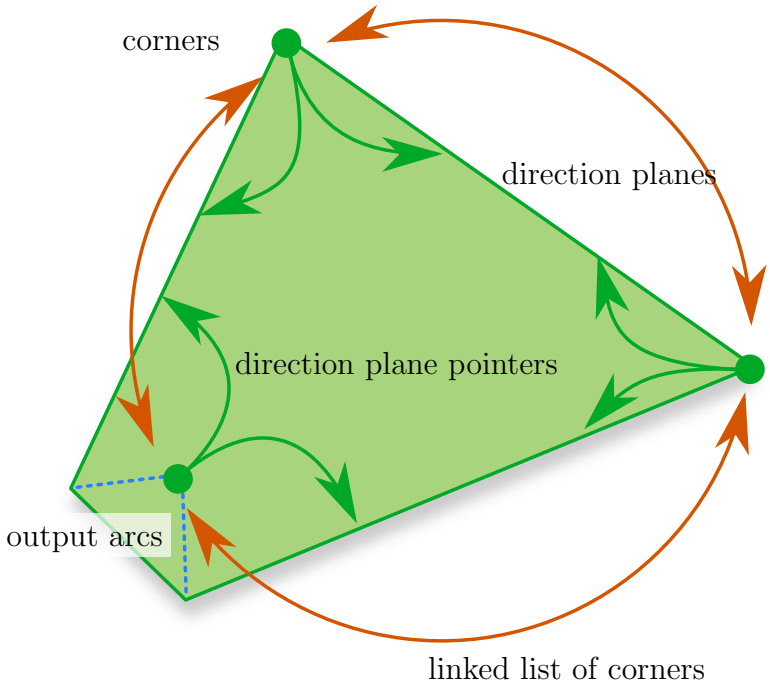

Figure 5.17: *The plan data structure, shown part way through the sweep. A linked list of corners describes each enclosed region. In addition every corner has a reference to the previous and next direction planes, each associated with an edge on the active plan. Skeleton arcs are output by events, and are used to reconstruct the 3D architectural shell.*

algorithm the input plan is specified by the building floorplan. During the algorithm, the sweep rises from the input plan and this data structure is updated to encode any changes to the active plan.

The second important data structure is a priority queue, Fig. 5.16 Q, that sorts events by ascending height. GIE events are automatically created, while user events (edge direction events, profile offset events and anchor events) are defined by the user.

5.5.3 Description of Events

As the sweep plane ascends it encounters several different types of events, introduced in this section. The two major classes of events are those automatically inserted to ensure the area on the active plan remains well formed, and those specifically inserted by the user.

The automatic events are the general intersection events — our generalisation of split, edge[69] and vertex events[65], as introduced in Sec. 3.2.4. These events are created whenever a new event is added to the active plan.

The user events are specified in various portions of the user interface. There are five types of UI event:

- *Edge direction events* occur at profile polyline verticies. Such an event updates the direction plane associated with a set of edges in the active plane
- *Profile offset events* occur at heights specified by user edits. Intuitively, a profile offset event results in additional inside regions being added to the active plan at the specified height.
- *Anchor events* come in a further three varieties:
  - *Plan edit anchors* modify the active plan to insert architectural features such as chimneys, or dormer windows into the shell.
  - *Mesh anchors* specify attachment points for decorative meshes.
  - *Subdivision event anchors* divide the active plan into a number of pieces. They occur over the entire active plan at a height given by the anchor.

We continue to detail each of these event types.

5.5.4 Generalised Intersection Event

The GIE is an automatic type of event, introduced previously in Sec. 3.2.4. Here we introduce the implementation details required for a robust implementation in a floating point environment. We chose a double-precision floating point environment, instead of an exact computation paradigm, such as CGAL[1], as it was both simpler to work with, and faster — a benefit for the rapid computation of large environments. The main robustness tool we use are epsilon tolerances.

Generalised intersection events perform topological changes on the active plan to ensure that it never self-intersects as the sweep plane ascends. These events are automatic, and inserted whenever new edges are added to the active plan. For example, all user specified events that add edges to the output, will also check for potential GIE events involving those new edges.

Chapter 3 introduces the limitations of the GIE. Indeed there are many MWSS situations in which the GIE does succeed in forcing the active plan to remain well formed. Despite this we found the GIE a remarkably robust solution to the complex events created by architectural plans and profiles.

Input: The input of a generalised intersection event is a point $l \in \mathbb{R}^3$, and a set of three or more direction planes, f, whose associated direction planes intersect at l. The point l is calculated as the centre of the clustered volume.

Output: The output of a generalised intersection event is an updated active plan. This represents the bounded region on the sweep plane after the event.

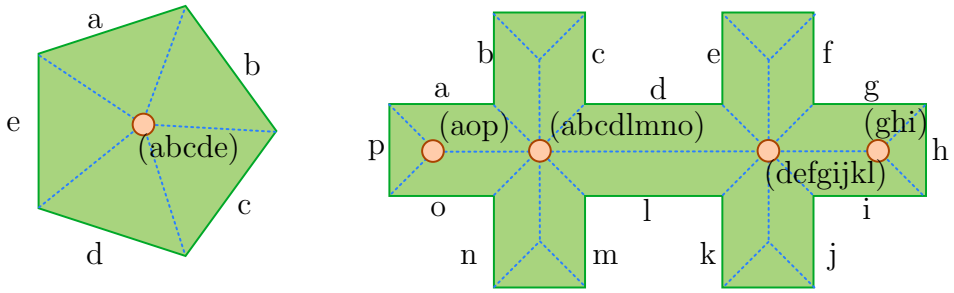

Figure 5.18: *Left: Five faces forming an intersection event. Right: Events can interfere with each other if they have the same height, in this case the four points that share a roof ridge.*

Epsilon Tolerances

As part of the GIE we remove any *out of bounds* edges from the edge set, f. It is possible for the line defined by the intersection of the direction plane and the sweep plane to pass close to l, however the line-segment defined by the associated active plan edge may not. Because the intersections are detected using unbounded direction planes, there may be edges in f that do not approach l on the active plan. Such edges are removed from f.

A small epsilon range, ϵ_1, expands the active plan edge and ensures that collisions occur reliably over the floating point precision range. On our inputs of footprints measured in meters around the origin we found $\epsilon_1 = 10^{-5}$ a sufficient margin. If ϵ_1 becomes too large, the chances of the extended edges intersecting with unintended geometry increases.

In addition, we use expanded bounds for intersection location clustering. This addresses two stability problems:

- In symmetrical inputs made up of regular polygons, such as often found in architectural plans, it is very common for more than three direction planes to meet at a point. To avoid degenerate output in a floating point situation it is necessary to identify intersections whose locations are close together, and treat these as a single event. Fig. 5.18, left, illustrates an example of such a building footprint.

- Second, direction plane intersections that are far apart from each other can interfere if they are close to one other in height, Fig. 5.18, right. It is also necessary to detect and handle these events at the same height to resolve the parallel consecutive edge degeneracies.

To address the two previously mentioned event detection problems, we cluster the events in both vertical and horizontal directions. We poll the priority queue to collect

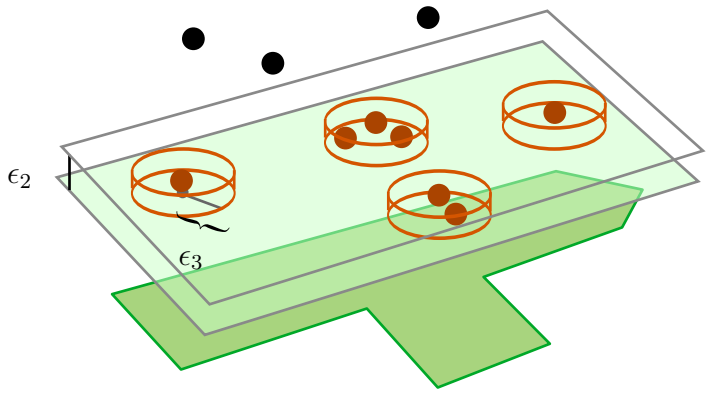

Figure 5.19: *When an event is processed we simultaneously extract all intersection events within a height of ϵ_2. Then we cluster all events that are within a cylinder of radius ϵ_3 and height ϵ_2.*

all intersection events whose height, z, is within some threshold, ϵ_2, of the initial event. Second, we cluster all the events according to their location after projection onto the xy sweep plane. The clustered volume is therefore a cylinder of radius ϵ_3 and height ϵ_2. Fig. 5.19 illustrates this clustering step. We found that values of $\epsilon_2 = 10^{-4}$ and $\epsilon_3 = 10^{-6}$ gave the best reliability. There are certain pathological inputs which cause this clustering stage to fail. An example would be a row of events, each within ϵ_2 of another, which could contain an arbitrary number of events.

PCE resolution

As introduced in Sec. 3.3.2, the MWSS is poorly defined in several situations. Different modeling choices lead to different ambiguous-case resolution strategies, Fig. 5.20. In particular when modeling architecture the parallel consecutive edge degeneracies need to resolved in an architecture viable way. We found that the *volume maximising* approach tended to be the most desirable default for architecture situations; we take the lowest valued θ when resolving the PCE. We hypothesise that this case is observed most commonly since it maximises the space inside the building.

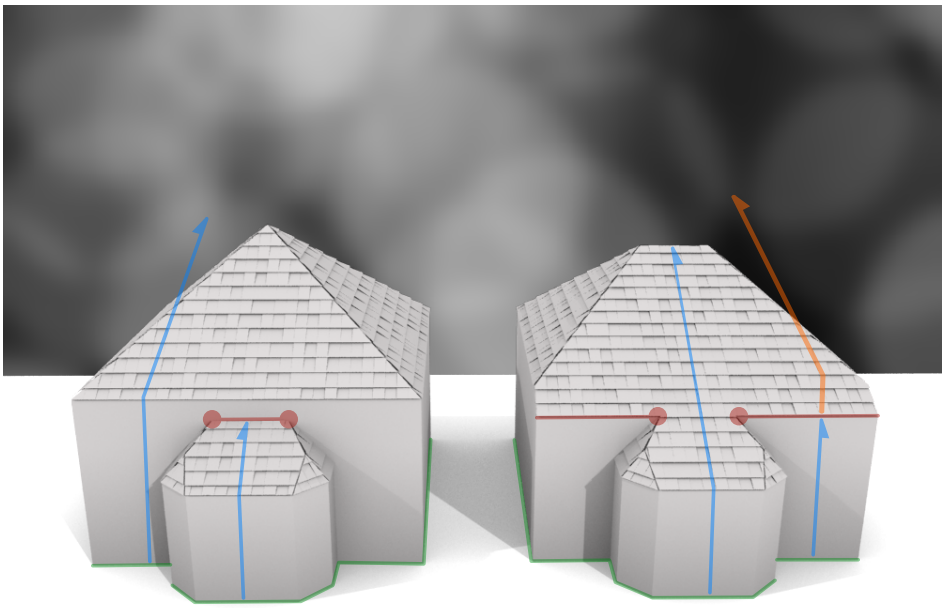

Figure 5.20: *Two identical bay windows that lead to the same two events (red circles) involved in a degenerate PCE situation (red line). To resolve the PCE situation, a single edge must be chosen to replace the others. The building on the left (right) resolves the ambiguity using the volume maximising (respectively minimising) priority technique. The resulting unused section of the original profile is shown in orange. Note that in each case, two ambiguous events occur at the same height, and must create globally consistent output.*

5.5.5 Edge Direction Events

A set of edge direction events are created for each profile. An edge direction event updates the angle and direction planes of a set of edges. There are two types of edge direction event, *standard* and *near horizontal*. Standard edge direction events are constructed from a single angle in the plan, while a near horizontal edge direction event is constructed from two consecutive angles and a distance. These values are calculated from the profile polyline.

Standard edge direction events

Input: A set of edges, f, in the active plan, each associated with the same profile and a single new angle for all the edges, γ.

Output: A new active plan which replaces the original.

For each of these edges $e_i^j \in f$, we update the associated direction plane by setting its angle, θ_i^j to γ. The implicit edge, e_i^j, continues to propagate over the sweep plane with a new speed, as defined by the new angle.

Near horizontal edge direction events

When the angle associated with an edge, θ, approaches $\pm\pi/2$, standard edge direction events face a problem as two parallel (horizontal) direction planes do not intersect to form a line. Additionally, as the angle approaches these limits the algorithm computes the intersections of near coplanar planes, causing numerical instability. To resolve this issue, as illustrated in Fig. 5.21, we use a secondary application of a MWSS to calculate the horizontal section of the profile. To do this we first increase the angles according to the length of the horizontal profile segment, then calculate the secondary MWSS, and finally project the result onto the original sweep plane.

Input: A set of edges in the active plan, f, associated with the profile, a distance, d, a direction angle, γ, and a following angle, ζ. The angle $\gamma \approx \pi/2$ ($\gamma \approx -\pi/2$) specifies the direction of the horizontal as towards the inside (respectively outside) of the active plan. ζ specifies the angle of the following non-horizontal edge event.

Output: A new active plan which replaces the original.

First we create a temporary plan as a copy of the active plan. For each edge in the original plan, e_i^j, and associated angle θ_i^j, the temporary plan has an edge E_i^j, and associated angle Θ_i^j. Secondly we update the angles in the temporary plan according to the following mapping:

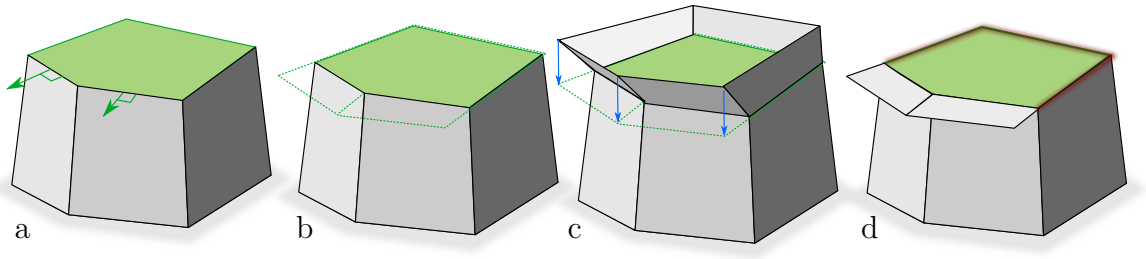

Figure 5.21: *The horizontal section desired (b) can be created by a secondary application of a MWSS to calculate the offset in the given direction. After flattening (c) unchanged edges (red, d) are ignored.*

$$\Theta_i^j = \begin{cases} \tan^{-1}(d) & \text{if } e_i^j \in f \text{ and } \gamma > 0 \\ -\tan^{-1}(d) & \text{if } e_i^j \in f \text{ and } \gamma < 0 \\ 0 & \text{otherwise} \end{cases}$$

The secondary MWSS extrudes the temporary plan for a height of one unit. The temporary active plan is projected onto, and replaces, the active plan in the original procedural extrusion instance. That is, e_i^j is replaced by E_i^j if it exists in the updated plan, otherwise e_i^j is removed from the active plan. The location of E_i^j is projected onto the original active plan. Finally the values of θ in the original skeleton are updated using the mapping:

$$\theta_i^j = \begin{cases} \zeta & \text{if } e_i^j \in f \\ \theta_i^j & \text{otherwise} \end{cases}$$

Occasionally multiple edge direction events occur at the same height. In this situation the direction events are sequenced by the order of user creation.

5.5.6 Profile Offset Events

Profile offset events specify the start of overhangs. The difficulty of specifying and handling profile offset events comes from the procedural definition. While it is easy to specify overhangs for a given region, the geometry must produce good results for a wide range of building footprints, and adjust itself according to the user editing the plan. Our technique must procedurally perform changes to the active plan without creating badly formed self-intersections.

At a profile offset event, an additional inside region, called an *offset region*, is inserted into the active plan (see Fig. 5.22). Two offset boundaries are grown from the active plan to enclose the new offset region. We introduce new edges and corners into the active plan to represent this newly enclosed region on the sweep plane. The new edges are classified as inside, outside, or side, depending if the edge stems from the first

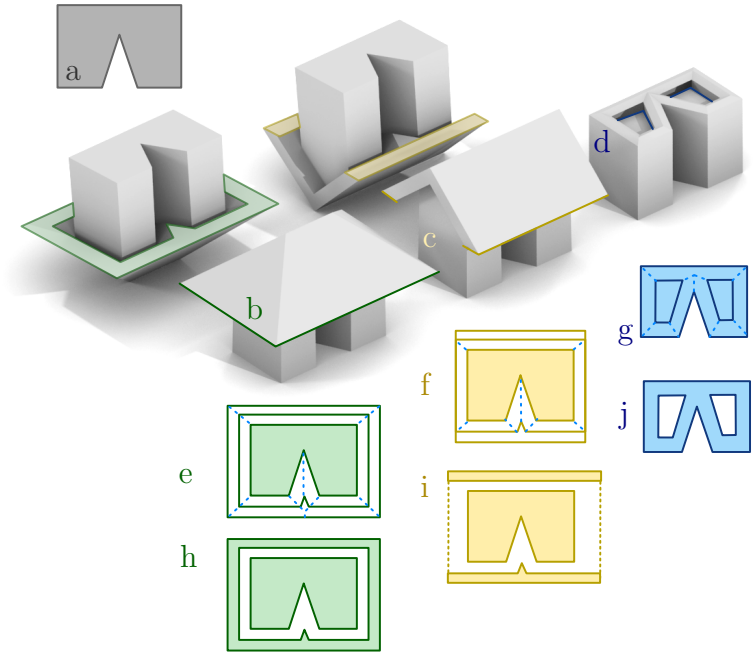

Figure 5.22: *Some meshes that can be computed from an input plan (a) using profile offset events. Buildings b and c are shown in two orientations. By creating two offset boundaries (e) that define an offset region (h), an overhanging roof (b) can be generated from an arbitrary plan (a). If two edges are disabled in the profile offset event, open-ended roofs can be created (c,f,i). Finally, by offsetting inside the active plan, walled roofs can be created (d,g,j).*

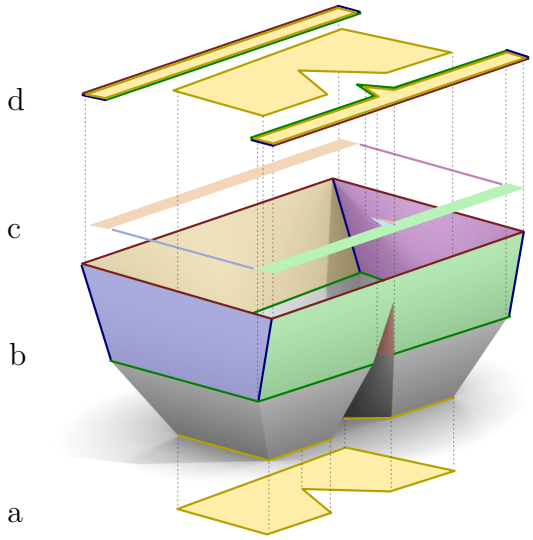

Figure 5.23: *The recursive application of procedural extrusions (b) to a plan (a) from Fig. 5.22 (c). The faces between $z = 1$ and $z = 2$ are projected onto the primary active plan (c), before being merged (d). Zero area faces (blue and purple) are removed, and profiles assigned based on the origin of the edge. In (d) green edges are assigned $profile\_inside$, red $profile\_outside$ and blue $profile\_side$.*

boundary, the second boundary, or are at the side-edge of an offset region.

Input: A map for each edge in the active plan, e_i^j to a tuple, $t_i^j = \{disabled_i^j, dist\_inside_i^j, dist\_outside_i^j, profile\_inside_i^j, profile\_outside_i^j\}$ and a single $profile\_side$. The variable $disabled_i^j$ is a Boolean value that specifies if the offset region associated with this edge is present in the output; $dist\_inside_i^j$ and $dist\_outside_i^j$ are real values that define distance and direction from the active plan of the inside and outside offset boundaries; $profile\_inside_i^j$, $profile\_outside_i^j$ and $profile\_side$ are profiles. We require that all values of $dist\_inside_i^j$ and $dist\_outside_i^j$ have the same sign; a positive (negative) sign indicates an offset (respectively inset) of the active plan. To ensure proper topology on the active plan, the distance, $dist\_inside$, is constrained to be non-zero.

Output: The output of an offset event is an updated active plan, typically with the additional region defined either inside or outside of the input active plan.

We create a temporary plan as a copy of the primary (input) active plan. For each edge in the primary plan, e_i^j, the temporary plan has an edge E_i^j, and an associated profile, $profile\_recursive_i^j$. Edge E_i^j is constructed by projecting e_i^j onto the plane $z = 0$. The profile $profile\_recursive_i^j$ defines the angles $\Theta_i^j = tan^{-1}(dist\_inside_i^j)$ at $z = 0$, and $\Theta_i^j = tan^{-1}(dist\_outside_i^j)$ at $z = 1$. We execute a recursive application of procedural extrusions using the temporary plan as input. It is executed from height 0 to 2, to

create a temporary output shell. Before continuing we correct the orientation to ensure that counter-clockwise loops enclose an inside region; the orientation of each face in the shell is reversed (the counter-clockwise ordering of vertices in the half edge data structure is reversed to a clockwise ordering). Faces of the shell between the planes $z = 1$ and $z = 2$ are projected onto the primary active plan, forming the offset region. This process is illustrated in Fig. 5.23.

The projection associates each tuple, t_i^j, with an offset region in the primary active plan. The entire offset region is bounded by the projected edges, r. Additionally the projection defines a 1:1 mapping between the new edges, $e_l^k \in r$, and a subset of the temporary shell's arcs A_l^k. We remove from the primary active plan any edges in r that enclose an offset region of area 0 or that are associated with a tuple containing a value of $disabled_i^j = true$. We update the profile, $profile_i^j$, associated with each edge, e_i^j, in the primary active plan according to the function:

$$profile_i^j = \begin{cases} profile_i^j & \text{if } e_i^j \notin r \\ profile\_inside_i^j & \text{if } A_i^j \text{ lies in the plane } z = 1 \\ profile\_outside_i^j & \text{if } A_i^j \text{ lies in the plane } z = 2 \\ profile\_side & \text{otherwise} \end{cases}$$

Finally we merge adjacent parts of the offset region to avoid self-intersections. We remove the corresponding edges and corners from the active plan.

5.5.7 Anchor events

Anchors define the location of features, such as plan edits, decorative meshes, or subdivision events. The plan and profile anchors specified in the user interface are used in different combinations to define either an event that happens at a certain height, or an event that happens at a particular point on the mesh. Subdivision events are triggered at a certain height by a profile anchor on an active profile. In contrast, plan edits and decorative meshes are placed at points by both a profile and plan anchor.

Finding parametrised locations on a surface that are robust to subsequent edits in the floor plan is challenging. The manifold of the structure may not reach any given point in space because, for example, the anticipated active plan edge may have been removed by previous events. Therefore, to position features in a manner robust to plan and profile edits the user positions a pair of two dimensional anchors, Fig. 5.12.

The profile anchor defines a plane parallel to the sweep plane, at the anchor's z height. When the sweep plane reaches this height we trigger height-events. If there is an

associated plan anchor, it is evaluated upon the current active-plan to give the xy coordinates.

We allow the user to select from two types of plan anchor — relative and absolute. A *relative anchor's* location is a fraction of its length on the active plan edge, Fig. 5.24 middle row, left. If the edge is represented in the active plan at the specified height, the feature is instanced. *Absolute anchors* are defined on an input plan edge, and define a plane perpendicular to this edge, Fig. 5.24 bottom row, left. The intersection of this plane and the corresponding edge in the active plan at the height specified by the profile anchor defines the instance location. Because an active plan edge may grow, it is possible to position absolute anchors beyond the ends of the input plan edge.

Relative and absolute anchors each define a different co-ordinate system on faces of the architectural shell, Fig. 5.24 centre column. Each system is a more natural way to express certain patterns with different geometric properties:

- Relative plan edge anchors: if an edge is present at the height, the operation will occur at least once. If a split event has taken place on the corresponding edge, it may take place more than once, 5.24, middle row, right. This makes relative anchors suitable for features that must always exist, however having multiple instances of certain features may be inconvenient.

- Absolute plan edge anchors: these may occur once or zero times at a certain height. At a certain height the corresponding plan anchor may no longer define a perpendicular plane that intersects the corresponding edge in the active plan. Hence the absolute anchors may not be suitable for referencing features that must exist, 5.24, bottom row, right.

It is also desirable to be able to position features on the surfaces created by plan edits, introduced in the following section. In this situation we may define plan anchors for the new edges introduced by the plan edits, Fig. 5.25. We translate instances of the profiles associated with the plan event by the height of the event. This also moves the associated profile anchors. These anchors may define additional plan edits, leading to a possibly recursive sequence of plan edits.

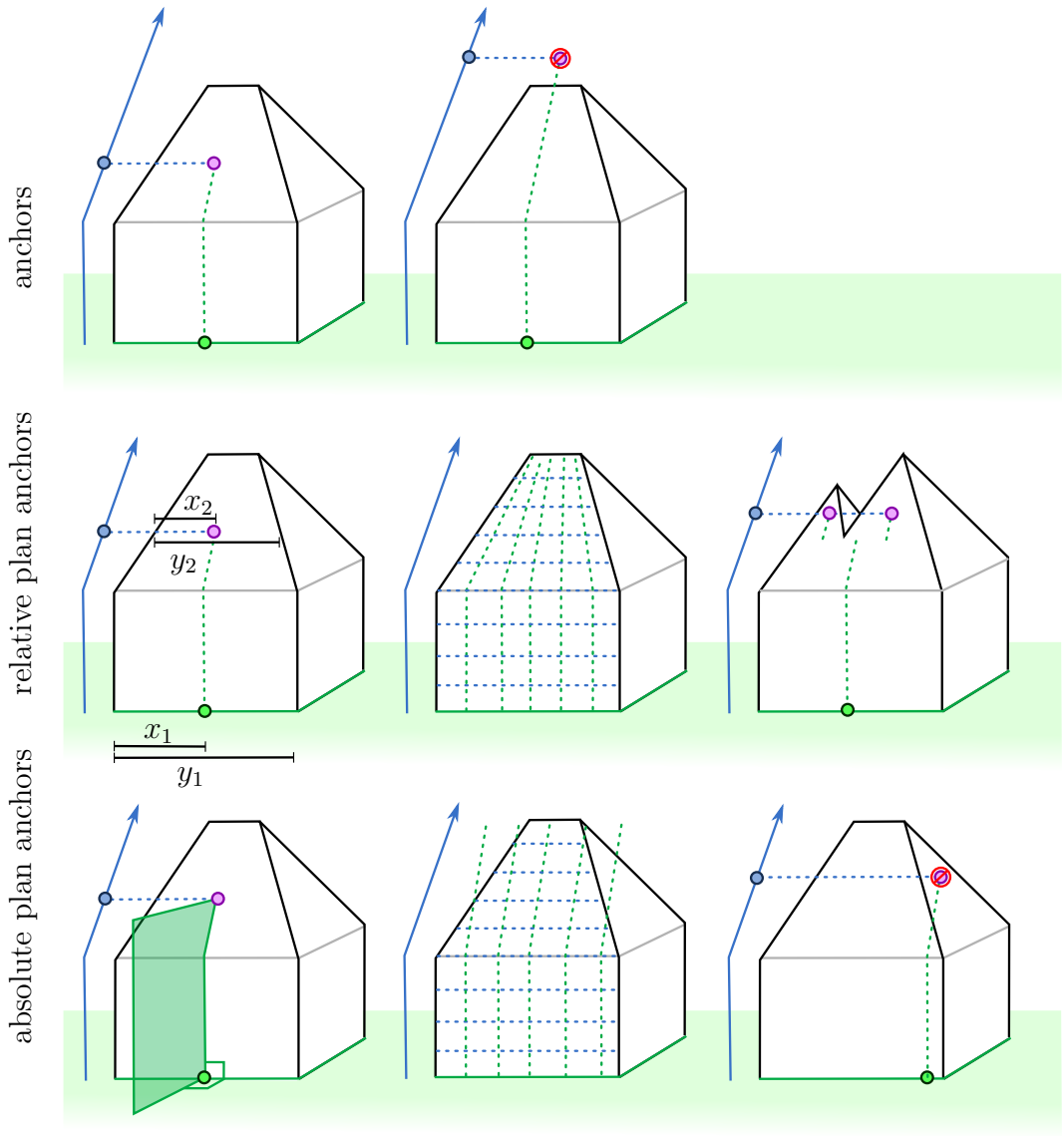

Figure 5.24: *Top row: plan anchors (green) and profile anchors (blue) combine to locate a feature (purple). If the edge is not in the active plan at a given height, the feature may not be instanced (red). Middle row: Relative plan anchors define a proportional coordinate system relative to the input plan edge's length, $\frac{x_1}{y_1} = \frac{x_2}{y_2}$ (left). However some features may be repeated (right). Bottom row: Absolute plan anchors define a rectilinear grid over the shell, however they may not be always instanced (red).*

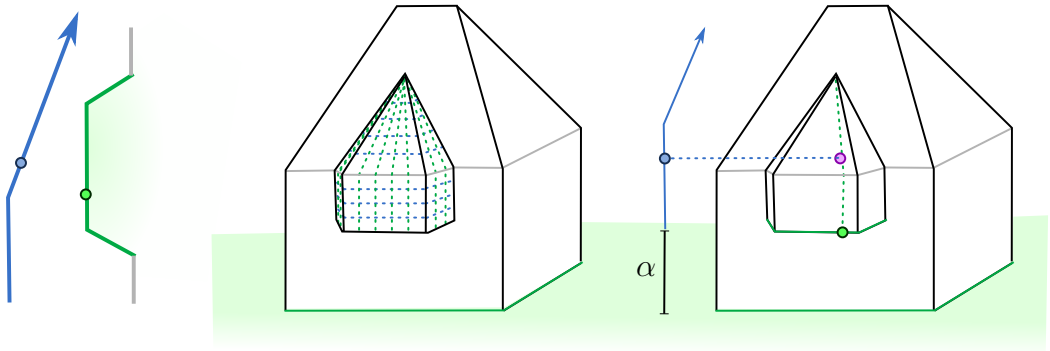

Figure 5.25: *A plan edit may be defined by a plan segment and a profile (left). The geometry arising from the edit may be parametrised in several ways, here we show the use of relative plan anchors (middle). The profiles associated with the plan event are offset by some value, α, such that feature locations are positioned relative to the start of the plan event (right).*

5.5.8 Plan Edit Events

Plan edits introduce discrete changes to the active plan at specified heights. We describe how plan edits operate efficiently and detail two methods to define them.

Input: Plan and profile anchors defines the location, or locations of the step. In addition the step type (natural or forced), and step geometry is specified. Natural steps have an additional distance parameter.

Output: The output of a plan edit event is an updated active plan, with its boundary altered by the step.

When performing a plan edit, some edges are deleted, some edges are moved, and some edges are inserted, Fig. 5.26. The new edges are at the height of the current sweep plane.

Our user interface offers two types of plan edits. Inserting an arbitrary shape gives the largest variety of geometric designs. However these *forced steps* offer no guarantees that the resulting active plan will not self intersect and create an invalid topology. The challenge comes again from the procedural nature of our approach and the fact that the edit has to work for all input plans. *Natural steps* offer a solution to this problem by using a recursive application of procedural extrusions to insert edges into the active plan.

Natural steps are calculated on the active plan at a given height by amending a small (typically 10^{-3} by 10^{-3}) protrusion. This is offset by a recursive application of procedural extrusions such that it does self intersect, Fig. 5.27, similar to the edge direction events of Sec. 5.5.5. This recursive PE application is constructed by assigning $\theta = 0$ to all edges not part of the feature, and a user defined θ to those edges in the protru-

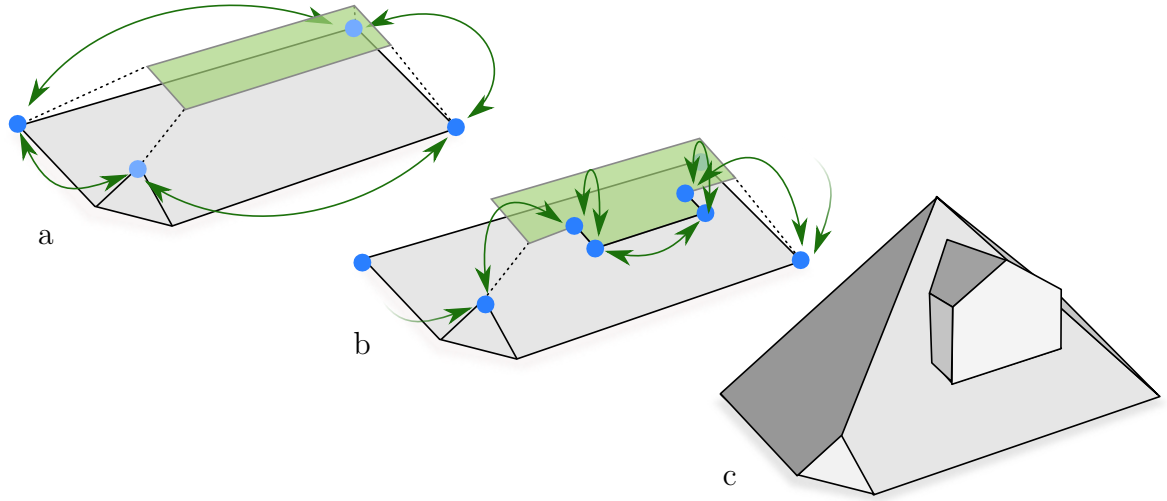

Figure 5.26: *Inserting a plan edit into the active plan during execution. a) The plan data structure (blue dots, green arrows) implicitly defines the active plan (cyan). b) To insert new edges into the active plan, corresponding edges are linked into the plan data structure. c) The resulting architectural shell.*

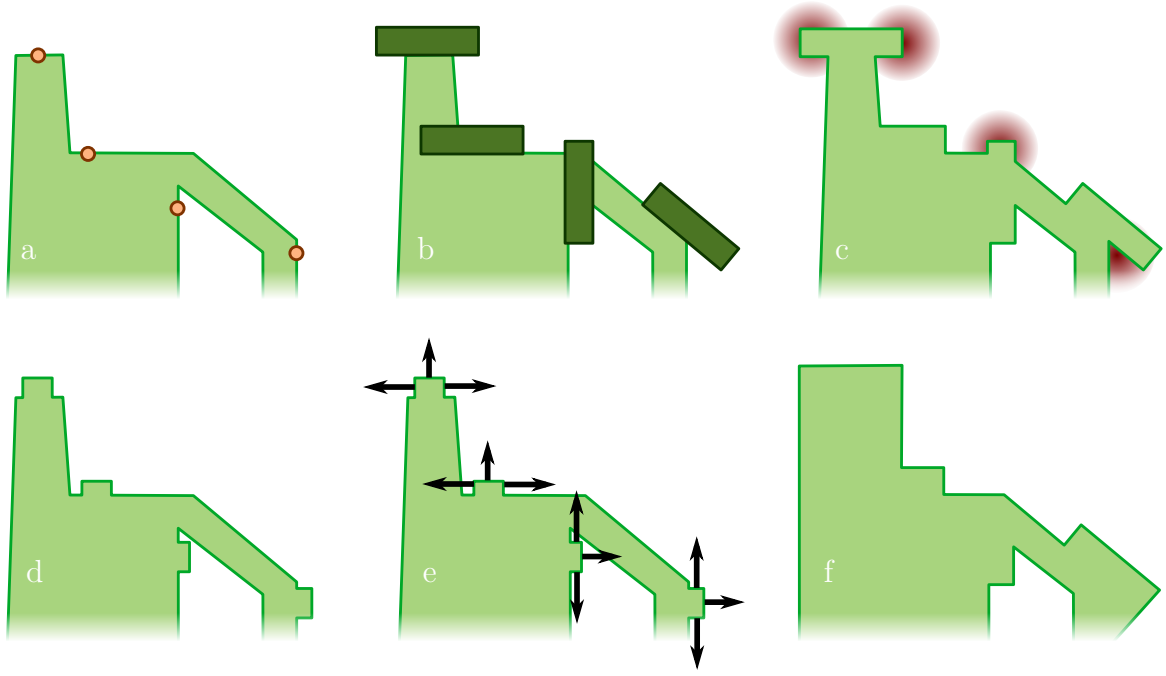

Figure 5.27: *Given an intricate plan, calculating a robust perturbation is challenging. Forced steps are positioned at the location of the anchors (a, orange). These are combined with the boundary. However many geometry artifacts are undesirable (c, red) in an architectural situation. Given natural steps at certain positions (a, orange), small changes to the boundary are made (d), which are then grown (e) using a recursive application of procedural extrusions, to create more natural geometry (f).*

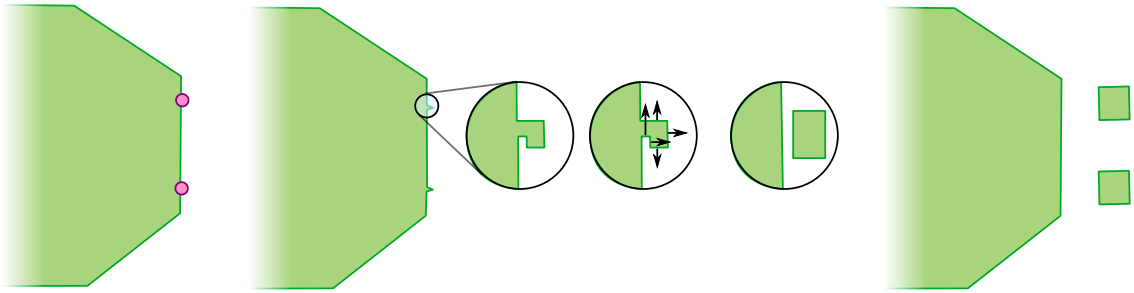

Figure 5.28: *Given a natural step feature location, a, we may insert a small protrusion, d, intro the active plan. It is possible to assign weights (black arrows) to the edges in such a way that the geometry becomes disconnected. This changes the genus of the active plan, and creates a suitable footprint for a buttress or similar (d).*

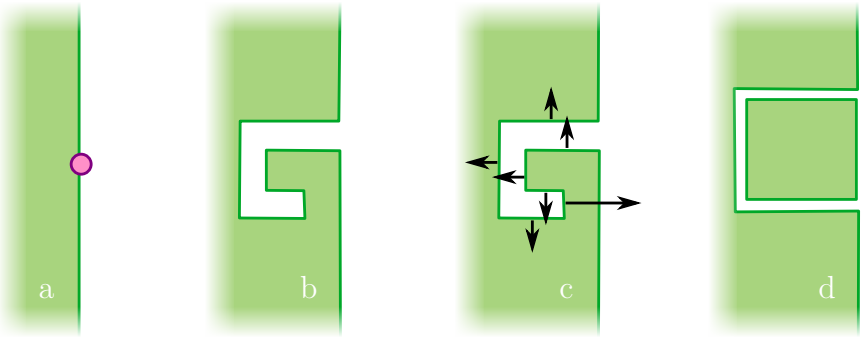

Figure 5.29: *If we combine an step towards the interior of the active plan with a genus change, we can create a suitable plan edit to represent a chimney or similar. Note that the length of the black arrows indicates the relative speeds of the natural step offset.*

sion. The resulting temporary active plan is calculated at a specific height, and this is incorporated into the original active plan. The new edges in the active plan have the relevant profiles assigned to them.

We have discovered that natural steps can create a wide range of geometry in this robust manner. Buttresses and other disjoint regions can be created by growing the protrusion in such a manner that it disconnects itself, Fig. 5.28. The chimney plans of Fig. 5.13, can be grown by combining this disjoint region with an inwards step, Fig. 5.29.

5.5.9 Mesh Anchors

In order to add intricate details to the architectural shells, anchors may also be used to position decorative meshes. A range of simple parametrisations is given by positioning

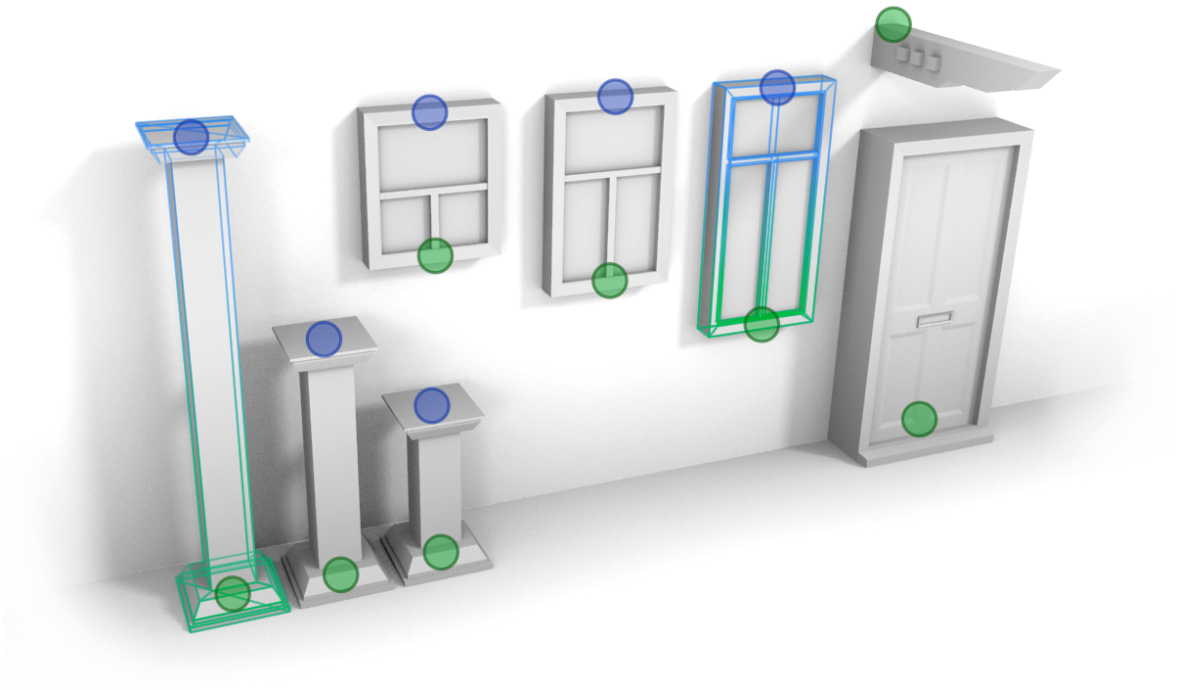

Figure 5.30: *The four example meshes used in the evaluation. The meshes are parametrised via control points (blue and green circles) and can be instanced to different sizes.*

a number of bones which deform the mesh. For example we can increase the height of a pillar without deforming the capitals, as in Fig. 5.30, left.

Input: A mesh with n bones, a scale factor, g, and n anchor locations, where $n \geq 1$.
Output: As the sweep plane passes, the location and orientation of each anchor is recorded. During the post processing stage, if all n anchors are recorded, the mesh is instanced with the scale factor g applied to each bone.

5.5.10 Subdivision Events

We may also wish to subdivide a given primary active plan into a number of discrete areas. Like profile offset events these occur over the entire active plan at a specific height, but are specified in the UI using profile anchors rather than the profile polylines. A recursive PE application is again used to ensure a robust manipulation of the active plan, Fig. 5.31. The boundaries of these new *subdivision regions* are then assigned profiles corresponding to a combination of their originating primary active plan edge profiles and their classification as top, bottom or *side* edges in the subdivision output shell.

Input: A map from each profile present on the active plan to a *subdivision profile*, m, and a set of tags, $t_x \in t_0..t_tmax$, attached to subdivision profile segments

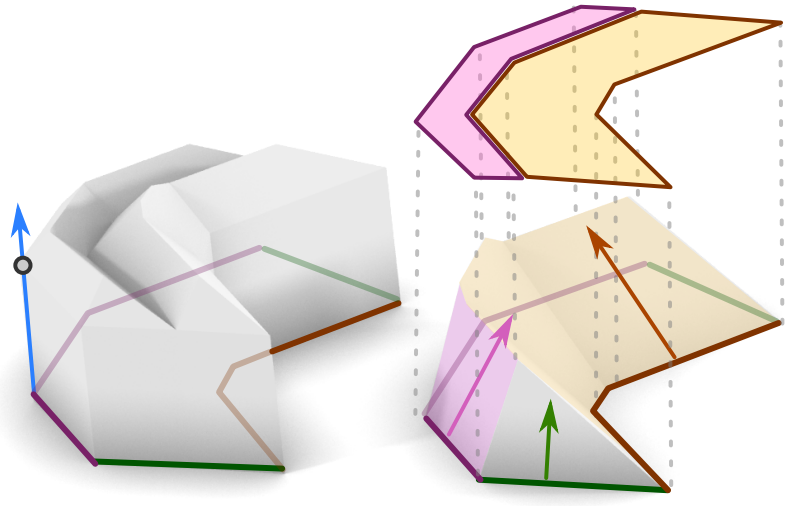

Figure 5.31: *The subdivision of the primary active plan is triggered at height by a profile anchor (left: grey circle) into two new regions to create a sawtooth roof. Given the primary profiles (left: purple green orange), the map m specifies the subdivision profiles, (right, arrows), from which we can calculate the subdivision PE (right). The result is projected back to the original active plan, replacing the original geometry, and assigned new profiles. Finally the original sweep plane continues to rise, creating the final mesh (left).*

with properties, $(profile\_bottom, profile\_top, profile\_side, merge\_bottom, merge\_top, merge\_side)_x$. The map is specified such that $m(profile_1) = profile_2$, where $profile_1$ is a profile in the primary active plan before the subdivision event, and $profile_2$ is a subdivision profile. The Boolean values, *merge_bottom*, *merge_top*, *merge_side*, specify whether the subdivision region should be merged with the corresponding abutting region. The tags, t_x, are optionally assigned to a set of polyline segments in the subdivision profiles to mark faces in the subdivision shell, Fig. 5.31. The profiles, $profile\_bottom, profile\_top$ and $profile\_side$ are assigned to the newly created subdivision regions in the primary plan.

Output: The output of a subdivision event is a new primary active plan.

Each edge in an output shell can be classified as *top*, *bottom* or *side* according to to how it was created. Horizontal edges created by the input plan or edge direction events are classified as *top* or *bottom*, depending on their orientation, while all other edges in the output shell are classified as *side*.

We create a new, recursive application of procedural extrusions, the *subdivision* application. Initially this is a copy of the primary active plan, translated to height 0. We update the profile associated with each edge in the subdivision active plan according to the map, m. We then execute this instance of procedural extrusions to create a 3d shell. Each face in the subdivision shell may have a subdivision tag, t_x associated with

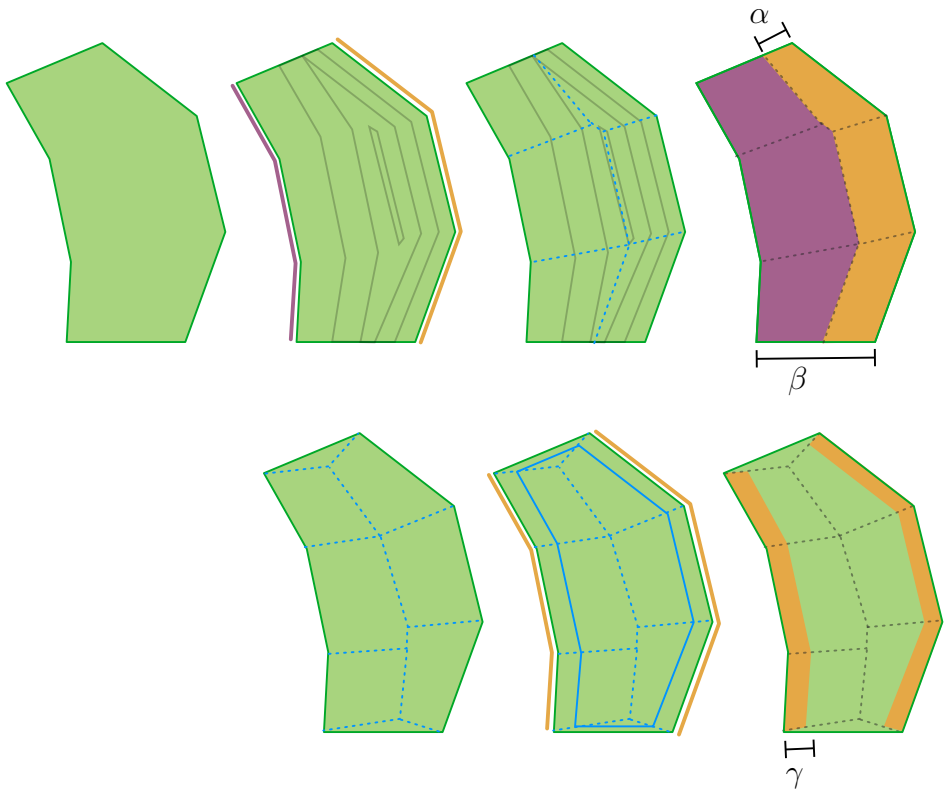

Figure 5.32: *We may use different profiles to divide an irregular plan into regions defined by relative or absolute measures. Above: by assigning the angle on the profile of one edge to be twice the speed (red) of another (purple) we may create a region of relative size* $\frac{1}{3} = \frac{\alpha}{\beta}$ *(top left, pink). Below: By only using the lower section of a profile curve, an absolute subdivision of* γ *units may be created.*

it, which specifies how it is merged into the primary active plan, and which profiles the new edges have.

Each secondary PE face is projected it onto the primary active plan, possibly combining with adjacent regions according to the *merge* tags associated with t_x. The profiles of these new regions on the active plan are given by the $profile\_bottom, profile\_top$ and $profile\_side$ members of the tuple.

We note that subdivision events are a generalisation of profile offset events. That is, it is possible to create a profile offset event using a subdivision event. However subdivision events cannot be easily incorporated into the user interface profile curves, and are much more involved for the user because of the specification of m and t_x.

Subdivision events are a flexible method of creating relative or absolute portions of a plan. By assigning profiles with angles of a certain ratio, we can split the active plan into relatively sized areas, Fig. 5.32 top. Alternately we can only use a certain polyline segment of the profile to create an area of absolute dimension, Fig. 5.32 bottom. By combing both these techniques, a wide range of shapes can be created. Fig. 5.33 gives an example of a relative subdivision event in a modeling context.

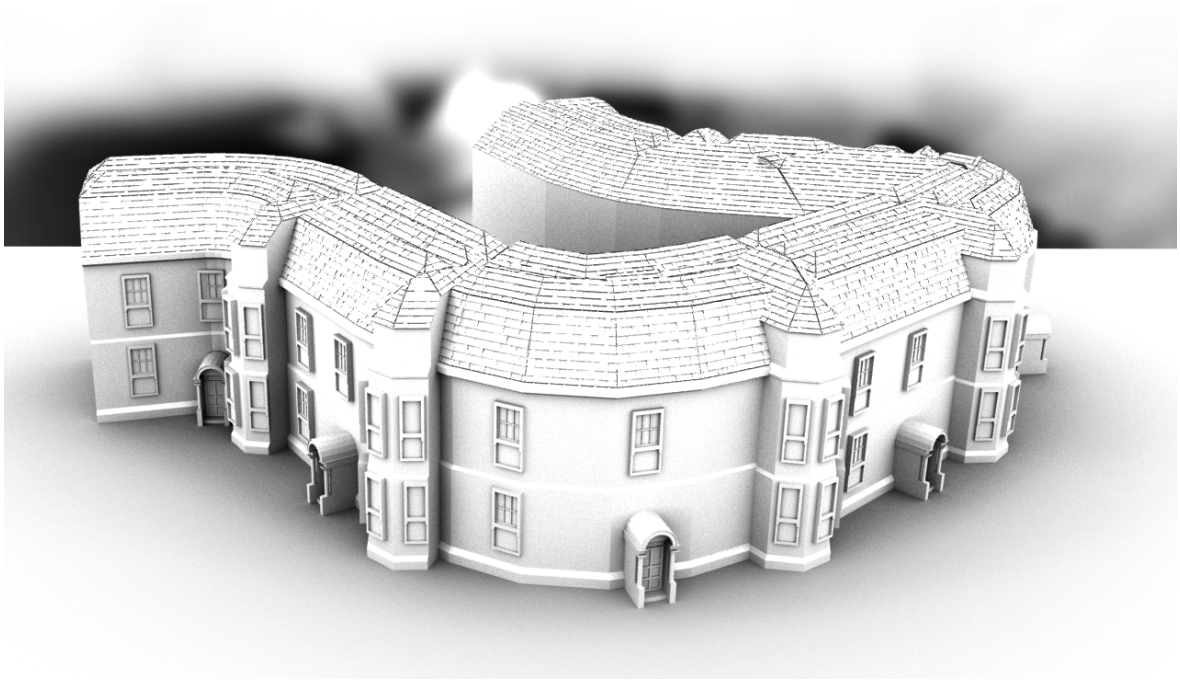

Figure 5.33: *A procedural model that creates a row of houses from a spline. In this case the street was generated by four points defining the street's curve. Seed points were grown using another application of the skeleton to create the building footprints. Relative subdivision events were used to split the roof plan into three areas.*

5.6 Evaluation

Given the PE system consisting of the user interface, and the algorithms to process the user specified events into an architectural shell, we continue to evaluate the usefulness of the system. Initial results such as Fig. 5.34 shows many typical architectural shells that are not possible using just the straight skeleton, or extrude operations alone. The earlier Fig. 5.33 also illustrates how we may generate architecture along a curved street, a challenge for systems such as CGA Shape. We can also create buildings with horizontal roof overhangs, such as Fig. 5.35. The alcoves and columns illustrate how disconnected regions can merge together and interact. This is possible because the MWSS can grow as well as shrink, unlike the SS, which can only shrink.

More eccentric uses of the PE system can also be imagined. Many other designed forms contain the strong horizontal edges that inspired this SS approach. By rotating the plan, such that the sweep plane moves horizontally rather than vertically, we may model objects such as windows or moldings, Fig. 5.36. As an illustration of the ability to compute extrusions on complex plans we may use a thresholded image as a plan, as in Fig. 5.37, to create artistic representations of images.

However, in order to perform a more objective evaluation of the PE system, three different approaches were taken. Firstly, Sec. 5.6.1 we examine the use of PEs as an

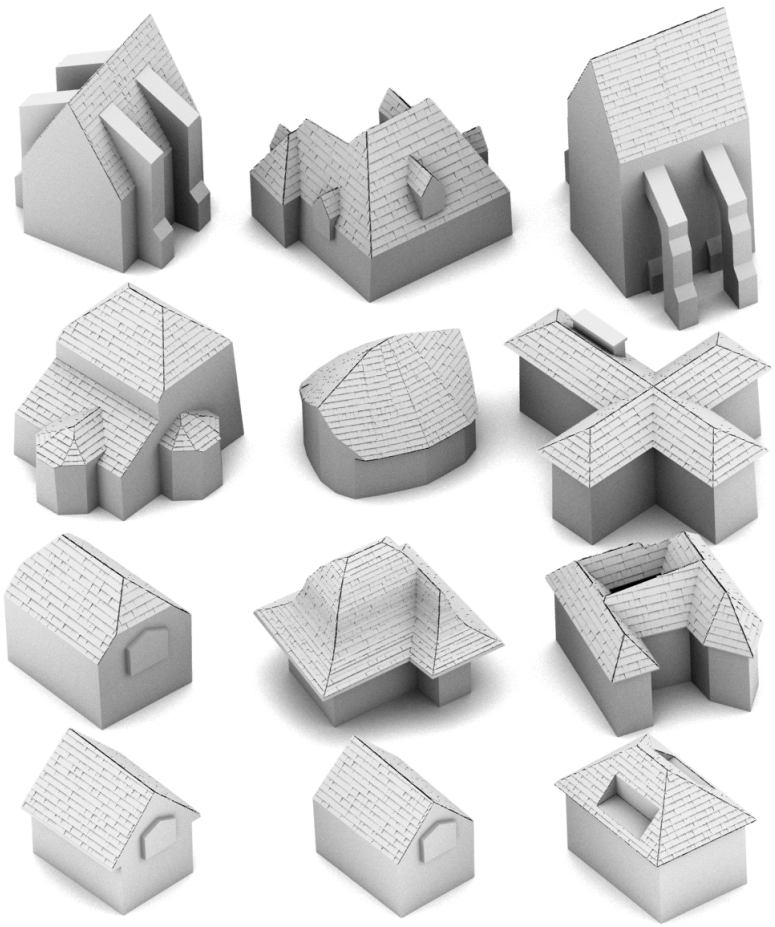

Figure 5.34: *From top, left: buttress, dormer windows, flying buttress, bay windows, curved plan, eight faces meeting on a symmetrical footprint with a chimney, hipped roof, curved roof, a horizontal overhang, an overhanging gable, standard gable and interior dormer windows*

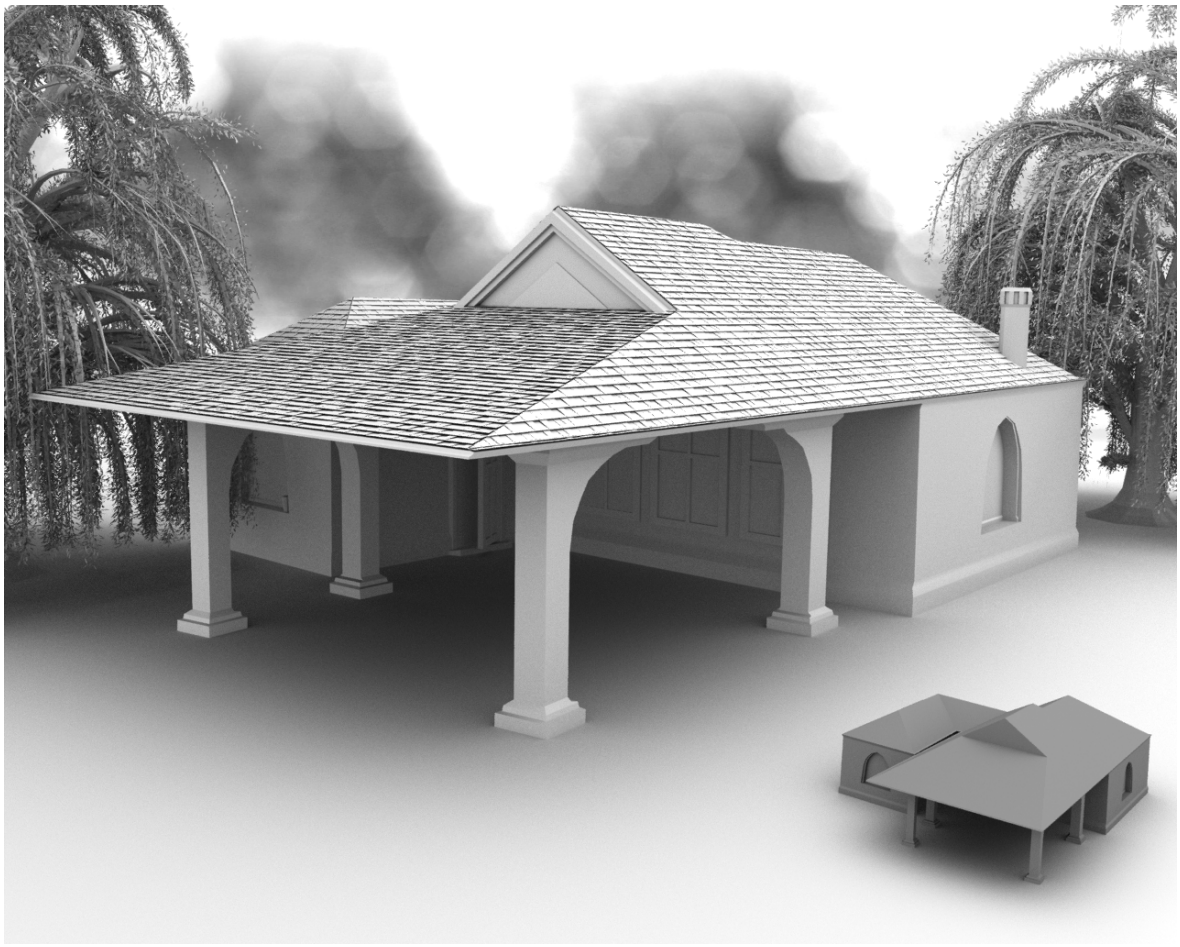

Figure 5.35: *Inset: the output of our procedural extrusions using a complex footprint, horizontal sections and plan edits. We are able to create pillars, covered parking and alcoves respectively. Main: A procedural condo with roof texture surrounded by procedural trees*

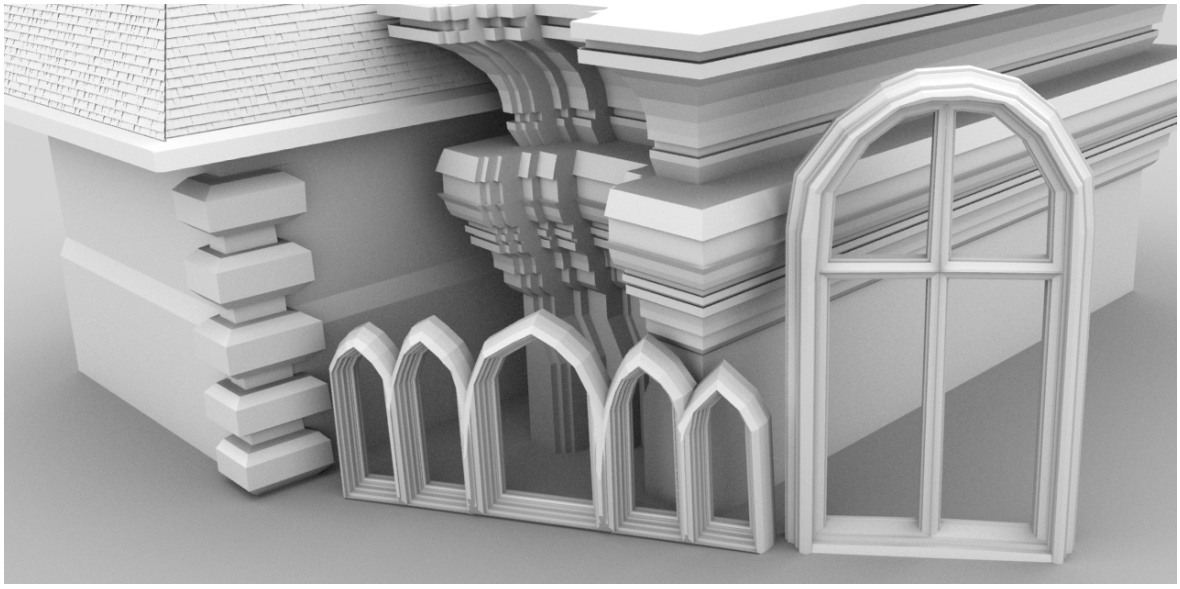

Figure 5.36: *Using a creative set of profiles, a wide range of architectural features can be modelled. By setting the input in a vertical plane, and carefully designing perpendicular profiles these windows and details may be extruded.*

Figure 5.37: *A thresholded image (inset) was used as the plan, with one of two profiles randomly assigned, to create this artistic image.*

automated GIS procedural modeling system, secondly Sec. 5.6.2 describes our experiences of PEs as an interactive tool. Finally Sec. 5.6.3 describes the use of the PEs by artists, and documents their opinions of the system.

5.6.1 GIS Evaluation

In order to evaluate the usefulness of the PE system for procedural modeling, we developed and evaluated a tool that generates 3D meshes given a *Geographic Information System* data-set of building footprints.

GIS User Interface

To generate and apply appropriate profiles to the footprints, we developed a secondary GIS UI. The graphical interface allows users to to apply sets of profiles and anchors to existing plans semi-automatically. Given a set of floorplans from a GIS or similar database, Fig. 5.38, the user can specify a *machine* to assign profiles and anchors to each building plan. Each machine defines a certain style of building, such as Victorian, industrial or Dutch. The tools to assign machines are:

- Directly: this sets the assigned machine to all the selected plans.
- Painting: after selecting a set of plans to paint, the user selects a machine type from a palette, a brush size, and is then able to assign the machines to profiles by painting over the centrum of each plan with the brush.
- By size: After selecting a set of plans, the user can execute a program that assigns machines based on the area enclosed by the floorplans. For example, the smallest buildings may become garden sheds and the largest become factories.
- Randomly: The user is given an option to select a fraction of the currently selected plans randomly. This allows, for example, 10% of the plans in a particular area of the city are assigned machines to create Victorian properties.

Each machine utilises several items of meta-data from the GIS database to enable the assignment of profiles to each edge and other features described by the anchors. The most important datum is an orientation label applied to each edge. This is assigned by an angle computed by orienting the building to the nearest street and mapping the normal vectors of the footprint edges to the unit disk. We assign labels for the *front, left, right* and *back* of the building, Fig. 5.40. Furthermore *short* edges at the front

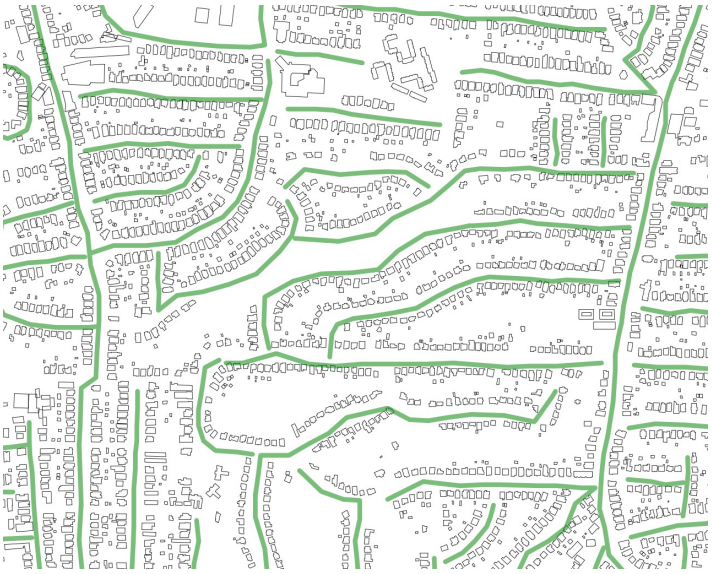

Figure 5.38: *Typical GIS data. In this case this is a subset of the floorplans of buildings in Atlanta (black), which have subsequently been marked up with road data(green).*

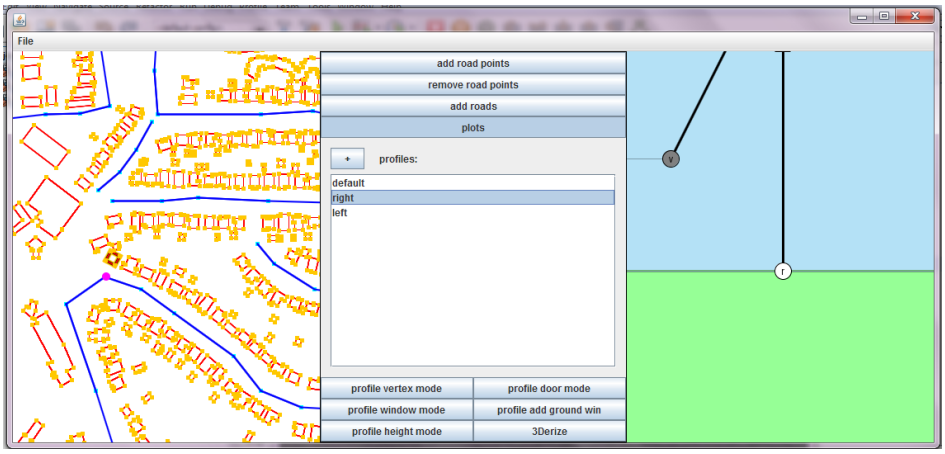

Figure 5.39: *The GIS UI allows different sets of profiles (right) to be assigned to different footprints (left). Users are able to edit the sets of profiles that are used to generate the architectural shells.*

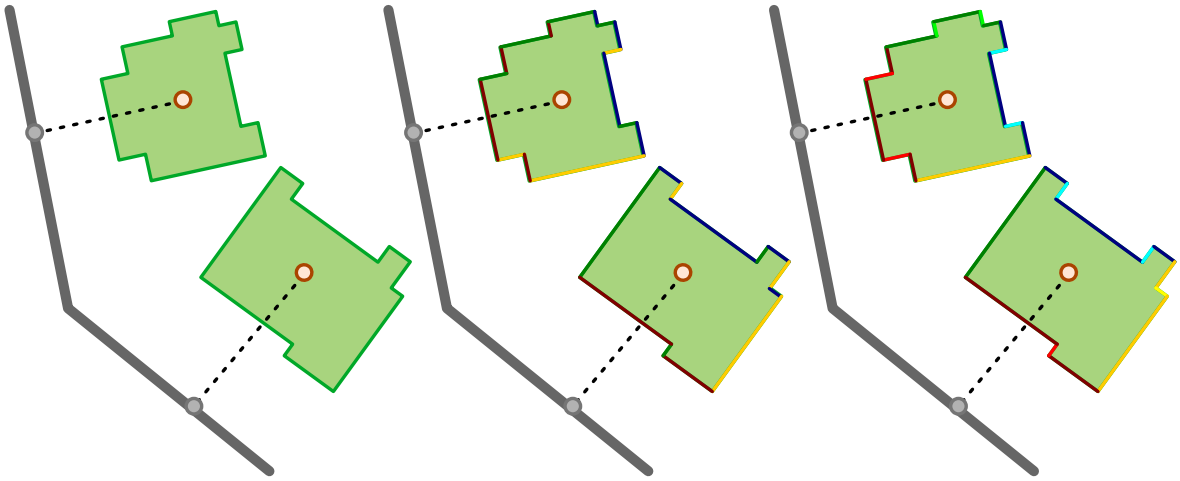

Figure 5.40: *Left: Given a plan (solid green) and a road (thick grey line), we assign a set of different profiles (red: front, blue: back, green: right, yellow left, with light and dark shades specifying long and short edges). Centre: the naive ordering assigns a label based on the orientation. Right: the long and short labels are assigned by considering triples of consecutive edges. If the first and last edge of the triple have the same orientation, and the second has a shorter length than the first or third, then the assignment of the second edge is changed to a short edge of the same orientation as the first.*

and side of the building are assigned the appropriate profile for their direction. These labels are then mapped by each machine onto profiles.

The positioning of anchors representing machines is also delegated by these labels. Profile anchors are specified on the associated profiles, while the plan-anchors are positioned by short Java programs which specify an interval to repeat anchors at — for example to create a row of windows, or a door and several windows.

GIS results

Using our GIS UI tool we were able to apply PEs to a large scale cityscape. We created a procedural model using about 6000 footprints from Atlanta (see Fig. 5.41). We used our interactive system to apply 4 different machines to generate different styles of architecture to the footprints.

The resulting geometry has three million polygons, 4 different building styles, took 20 minutes user modeling time, 10 minutes to compute the procedural extrusions, and 15 minutes to render. The automated system used GIEs, horizontal and normal edge direction events, as well as anchor events. One limitation was that we were not able to find a rendering infrastructure to render such a detailed model. We therefore had to omit the decorative meshes from all but the nearest structures. The PE system was implemented in Java and we measured the running times of our system on a 64bit

Figure 5.41: *We present an interactive procedural modeling system that is able to model difficult architectural surfaces, such as roof constructions. This figure shows procedural extrusions applied to 6000 floorplans synthesised from a GIS database of Atlanta. Procedural trees were added for decoration.*

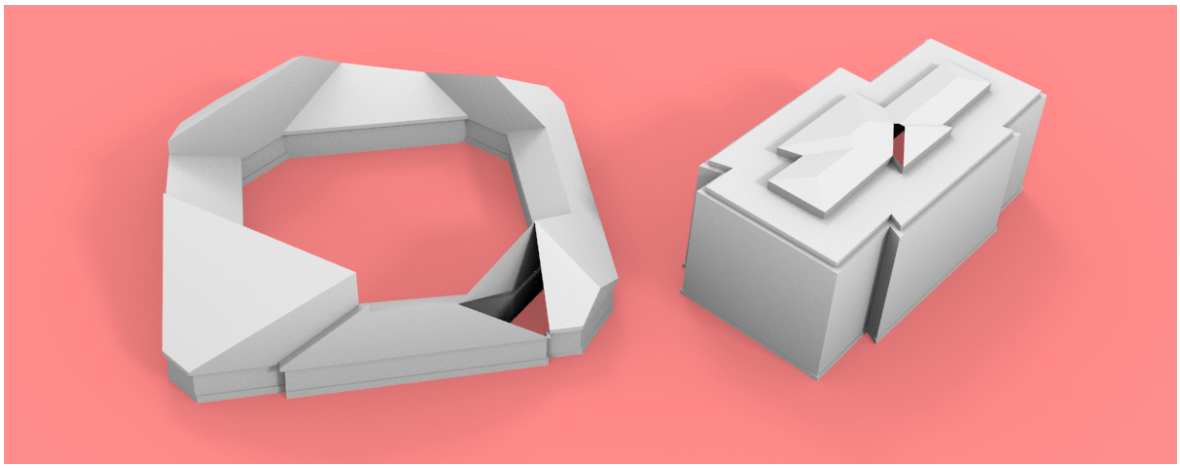

Figure 5.42: *The two observed examples of missing geometry. Note the missing roof sections in both buildings.*

2.6GHz CPU.

The system efficiently created a large quantity of architectural geometry. However, we were able to identify several geometry failures by manual inspection, as in Fig. 5.42. It is likely that these cases were caused by floating point errors, or our use of GIE for event resolution. Typically these errors expressed themselves as missing sections of roof, or very tall, self-inverted roof lines.

5.6.2 Interactive Evaluation

While procedural evaluation of the PE shows the algorithmic stability and potential for large scale cityscapes, it does not explore the range of forms that can be created. To this end we performed an evaluation of the range of forms that our user interface was able to successfully model. In order to do this we modeled 50 buildings, and recorded the issues encountered.

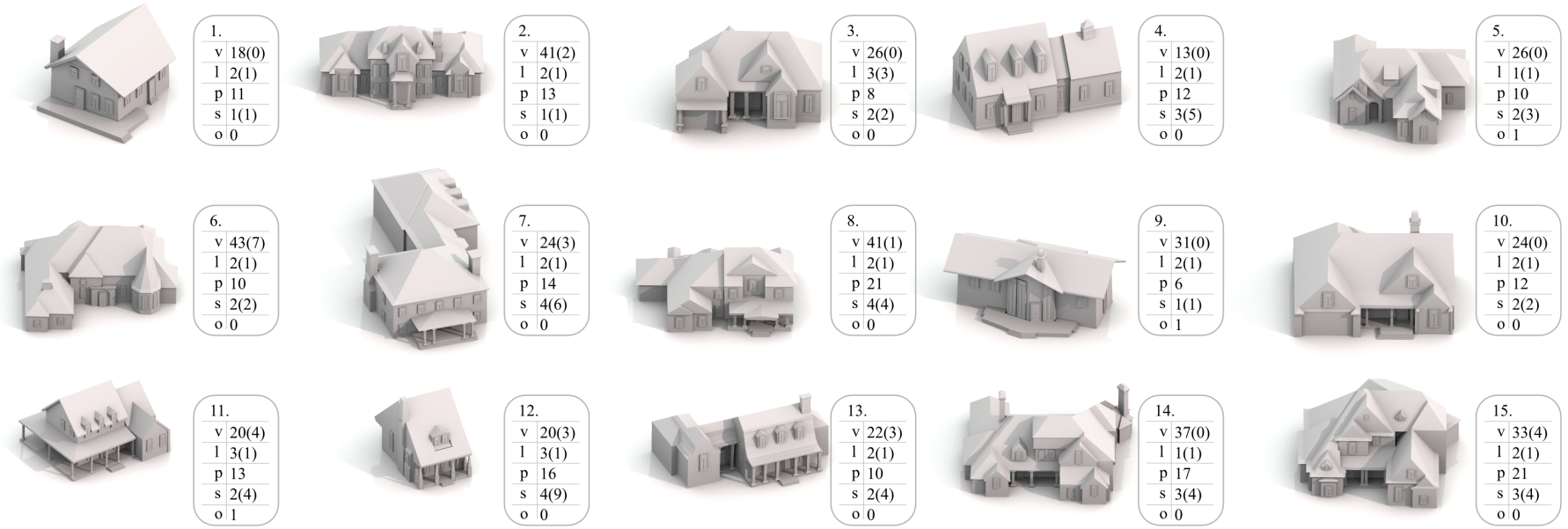

Figure 5.43: *The example cases and modeling statistics.* v *Vertices in modeled plan (additional vertices);* l *Polygons in modeled plan (polygons in library plan);* p *Number of profile sections in model;* s *Number of natural steps designed (number of natural step applications);* o *Number of offset events.*

Figure 5.44: *Examples continued from Fig. 5.43.*

Figure 5.45: *Examples continued from Fig. 5.44.*

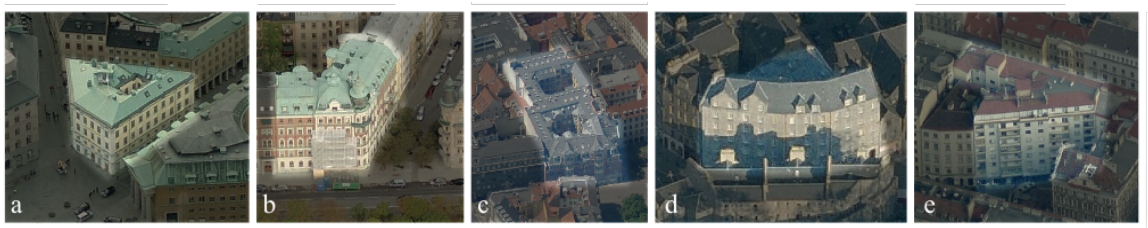

Figure 5.46: *Sample aerial photographs of buildings used for modeling examples 46 to 50 in Fig. 5.30. a,b) Stockholm, c) Copenhagen, d) Edinburgh, e) Vienna. ©2013 Google.*

Each building was modeled from a plan and a perspective image. A set of four simple meshes were used to add detail to the structures, these meshes are illustrated earlier in Fig. 5.30. The events used for modeling were edge direction events, profile offset events, natural steps and decorative mesh anchors.

We undertook the evaluation with the goal that all major geometric features from the elevation drawings should be present, although smaller details (such as cornices, plumbing and decorative windows) were excluded. We traced the plans into the interactive system directly, or via aerial views of the property. The construction of profiles and positioning of features was performed "by eye" by the author of this thesis.

The first 45 buildings were taken from a library of ready designed architectural styles for family homes[102], Appendix A. We modeled the first example in each of the categories in the library. These categories included styles as diverse as *ranch* or *Dutch* (Fig. 5.43, examples 13 and Fig. 5.44 32 respectively), however much of the stylistic content was dependent on architectural details that were replaced with our simple meshes.

Because the library plans were generic American templates, they had predominantly 90° and 45° degree angles between floorplan edges. That is, the design was not constrained by environmental features. To provide more challenging examples, we chose an additional five buildings from European cities that had irregular plans (Fig. 5.45, examples 46-50). These buildings were modeled from satellite and aerial views, Fig. 5.46.

The modeling times ranged from 20 to 120 minutes with a mean time of 63 minutes. Features on the input plan smaller than approximately 30cm were not modeled. We also recorded a number of additional metrics for each building: the number of vertices in the input plan and in the model; the number of corner-loops in the input and in the model; the number of profiles in the model, the number of offset events, the number of natural step templates and the number of instances of those steps. These statistics are given in Fig. 5.43–5.45.

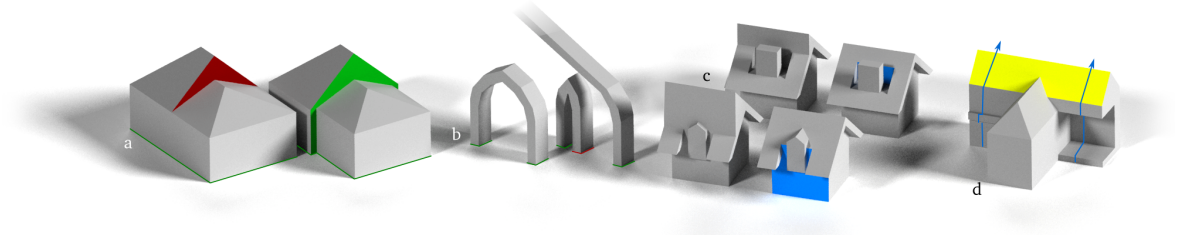

Figure 5.47: *a) The red roof face is not described in the input polygon(left). By creating a small change to the input polygon we can create the desired face (green). b) left: edges can be expected to collide at a certain height (green polygons), right: however when these edges are involved in other events (such as those from the red polygon), there may be undesired consequences, here a non-terminating polygon. c) Some structures (such as dormer windows and chimneys) do not obey the volume-maximising resolution to the ambiguous case, in this situation we have to lower the ambiguous case priority of some edges (blue) to get the desired result. d) A face (yellow) may be shared between two profiles (blue lines), defining co-planar profile sections requires patience on behalf of the user.*

Observations

It was possible to model all the buildings using the PE system, although the long modeling times reflect the fact that constructing some roof lines was complex. The results are of a similar detail and use cases as those taken from Trimble Warehouse in Fig. 5.4, when compared without textures or surrounding garden geometry. We continue to describe some of the problems encountered, and conclude with a breakdown of the modelling of a single building.

The most common issue when modeling was the construction of structures that contained edges not specified in the input plan, as shown in Fig. 5.47 a. In these circumstances it was necessary to add extra edges to model these features. These would either be added in the plan, leading to the difference between the vertices in the input plans and the model in several of the examples, or by natural steps at certain heights.

In several circumstances one face relies upon another, spatially separated, face to halt its propagation at the correct time; that is, an edge is fated to meet another, as in Fig. 5.47, b. When another feature blocks, or changes the course of one of these faces, the other may not terminate, or collide in an unexpected location. These fated edges lead to potentially undesirable intermediate outputs while editing.

Modeling circular arches was difficult because any adjustment in the width of the arch, would have to be accompanied by a re-scaling of the profiles. Modeling techniques such as shape grammars are able to retain such semantic information to automate such a process, and it is possible to imagine a similar system for the procedural extrusions.

It is not convenient to model a roof that is held only by a large number of pillars,

because it is not easy to model the transition from pillars to the roof. For example, *pergolas*, such as those in Fig. 5.44, example 31, contain no walls to allow the plan to generate a roof. These were not a large part of our data set, and were approximated by walled structures of similar volume.

It was occasionally necessary to override our default of a volume maximising priority in the ambiguous case. For example, in the case of a chimney stack or a dormer window of Fig. 5.47, c. To do this we used tags to specify high priority and low priority profile segments. This approach proved simple compared to the alternative of specifying a priority for every pair of segments.

It was relatively easy to split one edge into two by inserting a step event in the edge. In contrast, we found the reverse case quite tricky; allowing two profiles to merge to one. This situation is illustrated in Fig. 5.47, d. We see this architectural feature as two different profiles to merge at the top of a shorter roof in Fig. 5.43, example 3, and Fig. 5.44, example 20. To design a profile with a face co-planar to another is difficult, especially if the second edge starts from an edge parallel, but not colinear to the first.

Natural steps proved very versatile for inserting edges into the polygons. For example, Fig. 5.44 example 34, required a new edge internal to the plan for the back-facing wall of the tower. By positioning a wide square natural step on the end of the building, it was possible to split the polygon into two. One partition became the tower, and the other the remainder of the roof structure.

Most small edits to the plans and profile lead to small changes in the geometry and topology of the output mesh. However while modeling these example buildings there were noticeable situations where there were *discontinuities* — small user edits causing large changes such as altering the number of output faces, or their connectivity. From a geometric perspective these occur in the MWSS when two or more reflex verticies (or a non-reflex vertex with negative weights) pass each other. From a user perspective we have identified several situations where such discontinuities have affected the modeling process.

The first type of discontinuity arise from the PCE degeneracy of Sec. 3.2.3. When two adjacent edges, which are nearly parallel have different θ values, the behaviour of the resulting roof can be erratic as the angle between the edges is set to slightly greater than, or less than zero. In practice these edges do not appear often in architecture. When they do, it is often possible to add a perpendicular edge to lessen the chaotic behaviour, illustrated in Fig. 5.47, a. Another class of discontinuity emerges when an overhanging roof suddenly merges with some adjacent geometry, as in Fig. 5.48, left. In this situation, moving a single vertex a short distance can cause the active plan to gain or lose several verticies. Finally, we observed the discontinuities in the straight skeleton

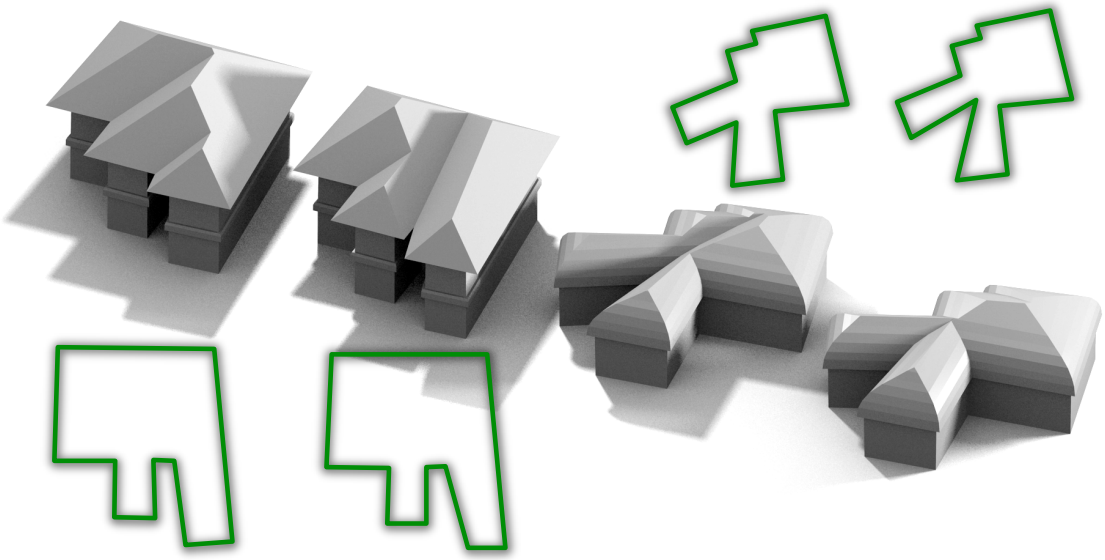

Figure 5.48: *Small changes in the plans can cause large changes in the results. Left: One such discontinuity caused by two portions of an overhanging roof merging. Right: Reflex skeleton arcs can also cause discontinuities.*

identified by Eppstein in [65], illustrated here by Fig. 3.21, in several configurations while constructing models. A simplified version of such a case is illustrated in Fig. 5.48, right.

While modeling we typically encountered one or two of these cases in each of the examples. However, given the interactive feedback of the system, it was relatively simple to adjust verticies to understand, and so avoid the degeneracy.

The Modeling Process

After a number of models were created, several distinct phases of modeling became clear. A description of these stages during an 80 minute modeling workflow for a model similar to number 34 follows:

1. 5 minutes — Planning and creation of a rough mass model with a single profile, consisting of only 2 segments, on all plan edges. The plan is traced from the given example plan, and the profile is heavily edited to achieve the best fit.

2. 10 minutes — Massive features requiring natural steps were inserted, in the case of model 34, this was the tower over the garage, but in other models features such as overhangs without matching footprints are created at this stage.

3. 5 x 5 Minutes — For each major edge in the plan, the profile was updated to match the example images. Once the new profile was created it was copied to

other edges with similar profiles in the plan. Often a profile could be re-used or edited, because similar profiles were found around a building. Portions of the profile could also be shared. For example, the bottom of a façade without an adjoining roof may be re-used on another edge of the profile that does require a roof. This stage was iterated through five times, each time making smaller additions, corrections, and taking into account previous changes.

4. 10 minutes — Additional smaller edges were added to the profile. Again, interactive feedback enables feedback as to the result of each change.

5. 15 minutes — Smaller natural steps were positioned for decorative elements such as roof elements and chimneys. It was possible to re-use main-plan profiles for several of the new plan edges introduced by the steps.

6. 15 minutes — The meshes were positioned using anchors. This was complicated by concave faces, with the need to switch between different anchor types. In addition, the user interface required manually selecting the file to apply, and selecting the appropriate anchors for each window. For grids of windows this was time consuming, but could be easily automated in future work.

These 6 stages were typical of many of the 50 models. However there where exceptions; in one example it was necessary to re-start after it became clear that a feature that was modeled by a stage in a profile polychain, would have to be modelled by a natural step instead. In another example, a deviation from this workflow was caused by problematic discontinuities becoming a problem in stage 5, which meant that the user had to return to stage 1.

After stage one, a reasonable low-quality model was almost always present. While the resemblance to the given example model was sometime dubious, the results at this stage were obviously "house-like". In general, throughout the modeling process, the 3D output that the user worked was obviously a building, and the mesh was mostly watertight. When modeling in a non-domain-specific tool, such as with Blender in Sec. 2.12, this is rarely the case. These tools often leave non-planar faces, gaps in geometry and intermediate geometry visible throughout the workflow to distract the user from the object being constructed.

A particularly useful feature of the UI is the fast iteration that it allows in all workflow stages. For example, in stage 1 it was useful to quickly examine the results of several different profiles in quick succession, and make a decision as to which was best. In stage 3 it was useful to be able to slowly reduce the scale of edits, converging in on a solution with each iteration. Finally fast interactive iteration also helps negates some

of the problems with discontinuities that may occur; it is easy to quickly backtrack and explore the geometry which causes a particular discontinuity, whether it is desired or not.

5.6.3 Artistic Evaluation

The final evaluation technique was intended to investigate the usability of the system by those unfamiliar with procedural modeling. We employed two artists to use the system part time for four weeks. These users reported that it took between 5 hours and 3 weeks to become competent with the tool, given a short three page user guide. Brief telephone calls were made with the artists, and no direct tutoring occurred.

During this training the artists were able to create a number of interesting forms, Fig. 5.49. Finally they were asked to create some complex example meshes, Fig. 5.50. To create these complex examples the artists created their own custom meshes to attach. This took the total modeling time to 30 hours for both artists, although the time spend using the procedural extrusion system ranged from 5-10 hours. The time saved compared to standard mesh modeling techniques was estimated by the artists to be between 5 and 15 hours.

Whilst this approach only gives a coarse qualitative metric, it shows the applicability of the procedural extrusions in the real world. The final interviews with the artists are recorded in Sec. B. Both artists commented that the PE system was faster to use than commercial generic mesh modeling packages.

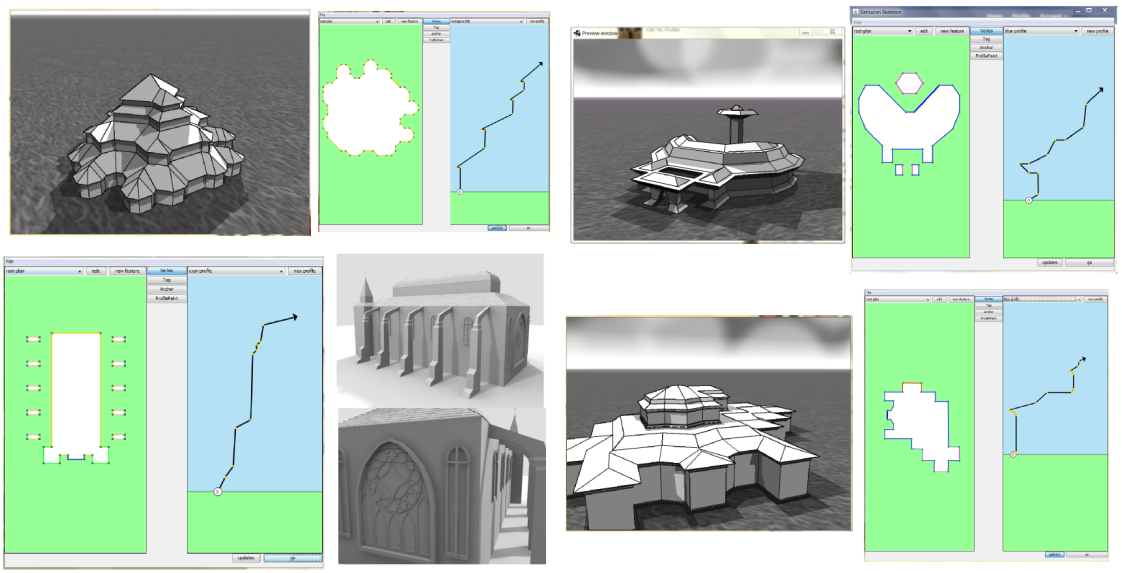

Figure 5.49: *The artists' example work while learning to use procedural extrusions. Note the wide range of roof shapes easily expressed in the system.*

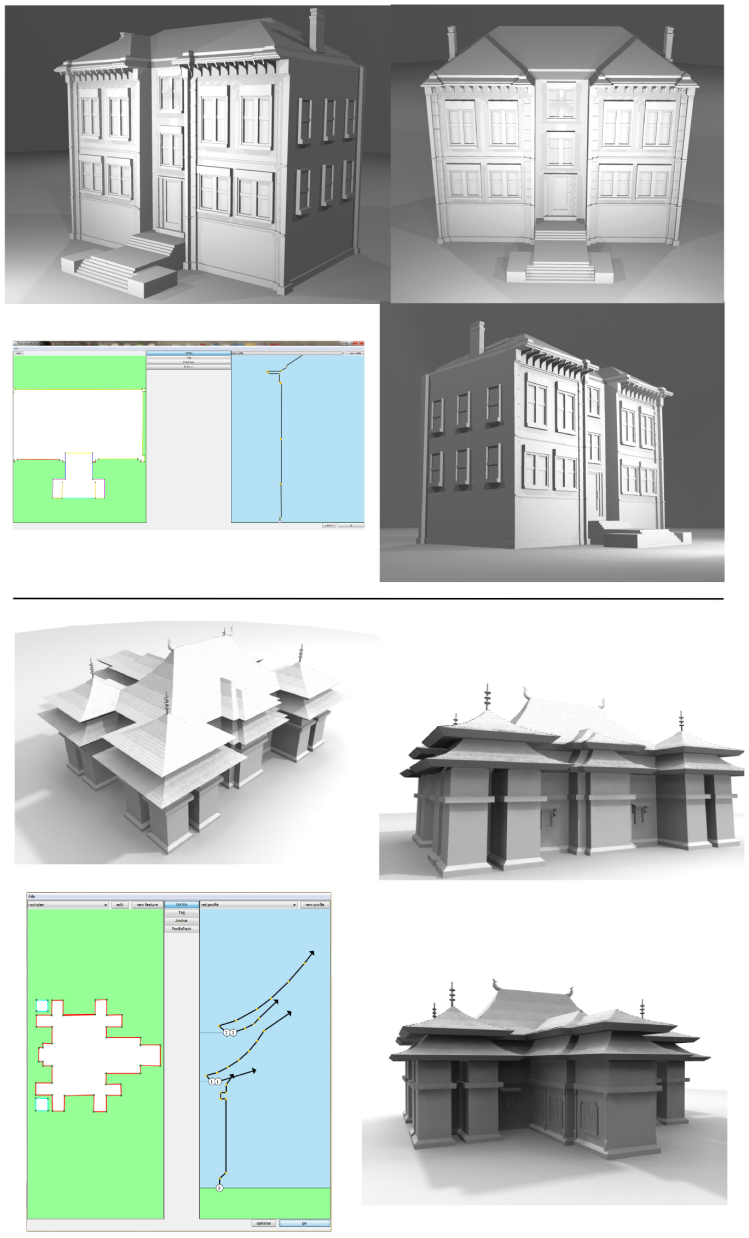

Figure 5.50: *The final projects from user 1 (above) and user 2 (below). These took "10 hours" and "5-10" of work with the PE system.*

5.6.4 Notable external applications

Procedural extrusions have been used in external academic and commercial projects.

Fig. 5.51 illustrates the intended use of procedural extrusions in the video game *Clockwork Empires*[79]. This project, which is still in development, extends on the work presented here by including texturing, and forced termination at specified height — "caps", stop the user creating run-away geometry that may become very tall.

In an academic project, our PE library has been integrated into the skylineEngine[201], implemented in Houdini3D[219]. This project allows basic plans and profiles to be defined inside the Houdini environment, as in Fig. 5.52.

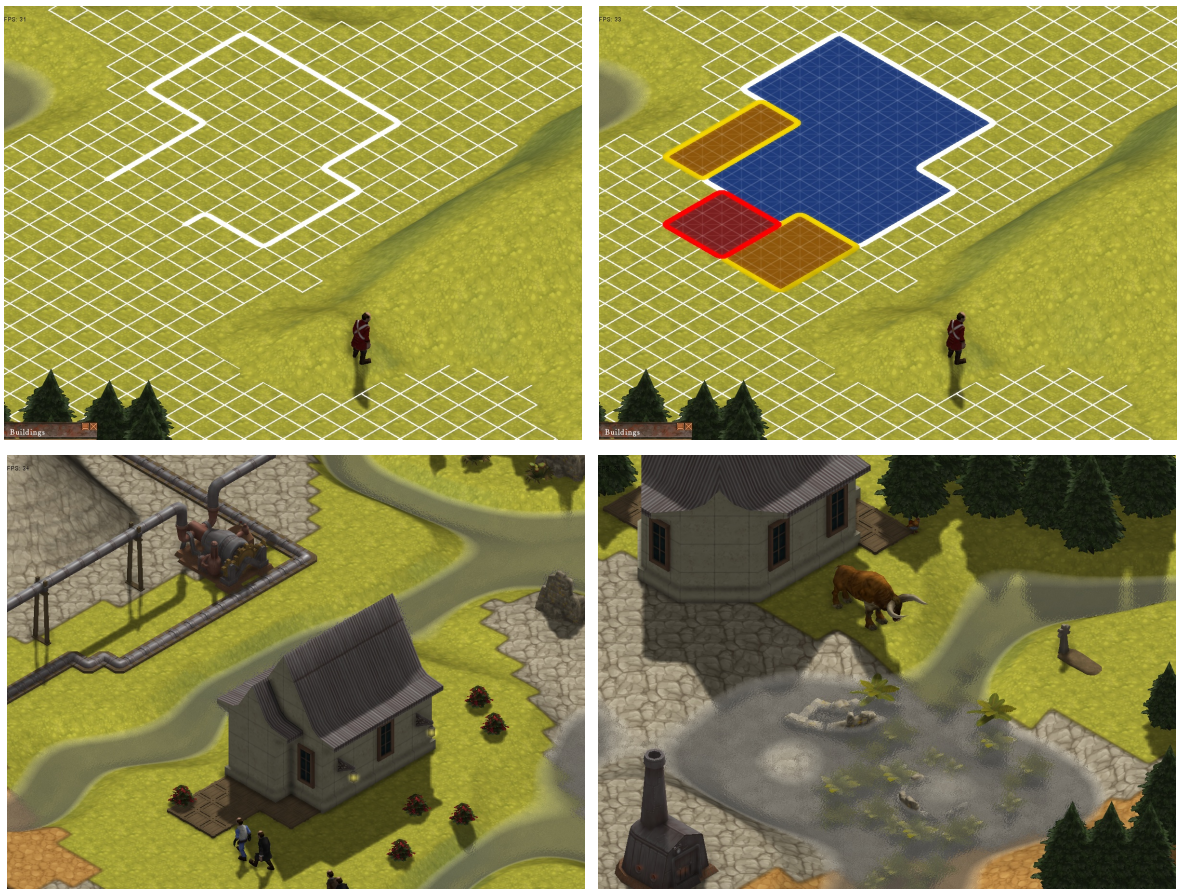

Figure 5.51: *©2012, 2013, Gaslamp Games. Clockwork Empires[79] uses procedural extrusions to generate buildings from user specified footprints. Top: The user designs a footprint. Bottom Left: the resulting mesh. Bottom Right: Another in-game building in context.*

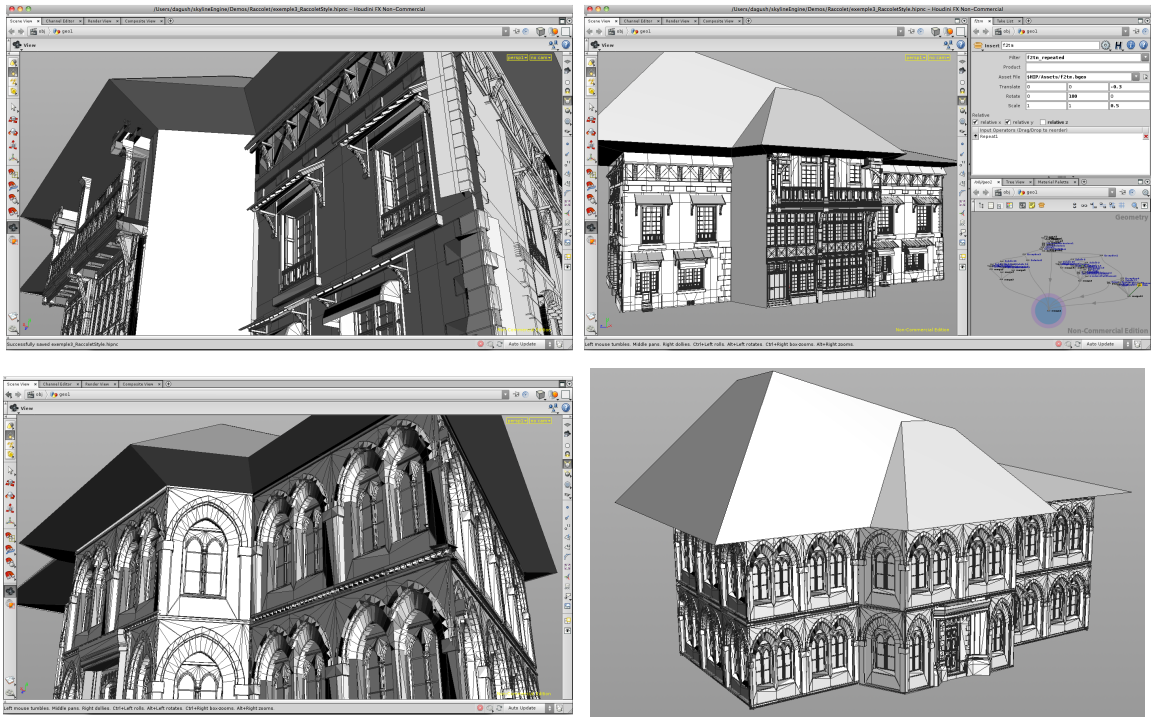

Figure 5.52: *©Gustavo Patow 2012. The integration of our PE implementation with Houdini. Top: Two views of a Raccolet style house, and the graph that generates it. Bottom: Two views of a "sea view" style house.*

5.7 Comments

A significant decision made early on in the development of the PE system was to choose between an exact arithmetic or a floating point implementation. Our floating point implementation is well suited to interactive modeling applications because it prioritises interactive update speeds over high precision. An exact arithmetic approach may be important to give theoretical guarantees and such an alternative implementation would be very valuable. Posing a particular problem to such a rigorous approach is the lack of a solution for a generic MWSS – the pincushion problem of Sec. 3.5.3.

An informative perspective on the PE system is to consider the MWSS as a system for automated and domain-appropriate information loss. The user inserts data into the system, in the form of UI specified events, and the MWSS removes it in an architecturally appropriate manner. As the sweep plane rises, MWSS events such as split and edge events remove edges (and information) from the active plan. Concurrently the input plan, edge direction events, profile offset events and subdivision events insert additional information into the active plan. This contrast invites the description of PE as an *automated information loss* system. The user specifies the places to insert additional data, while the MWSS is utilised to remove it in an architecturally-meaningful

Figure 5.53: *Left: Straight skeleton; Middle: Straight Skeleton with angle changes; Right: Procedural extrusions*

manner. An example is given in Fig. 5.54.

An interesting challenge is that it is possible, and indeed probable, that the façades generated the PE system are not rectangular. The large variety of shapes that a façade can take leads to issues integrating the PE system with other approaches which expect shapes to be rectangular, such as CGA Shape. While the system of deformable meshes and anchors has been successful in positioning elements, describing a repeating facade over an irregular polygon is still a matter for research. This problem has been particularly evident when integrating PEs with Houdini.

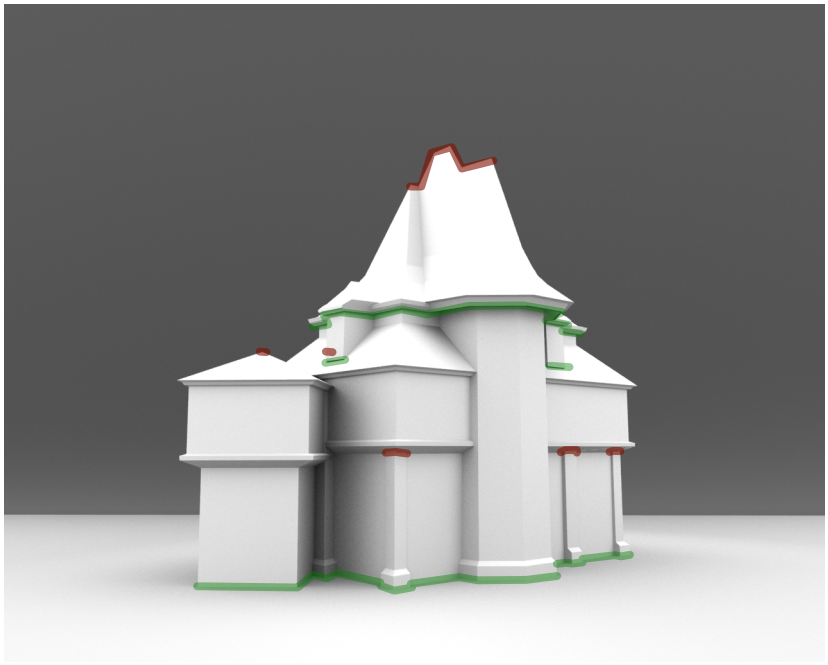

Figure 5.54: *A procedural extrusion model of a haunted house. The green lines show where data is inserted into the rising sweep plane, and the red lines show where an user event removes data.*

5.8 Summary

In contrast to the previous chapter, which used the straight skeleton for modeling parcel subdivisions, this chapter has introduced an application of the MWSS to the modeling of complex architectural shells.

We took inspiration from the range of man-made objects that contain offset surfaces, and observed that the strong horizontal edges in many common architectural forms can be generated by offsetting the plan of such a building. This lead us to the same conclusion of many architects: that plans and elevations (profiles) are a very effective way of representing a wide range of structures. Given the theoretical foundations of straight skeletons in Chapter 3, and the success in implementing a block subdivision scheme in Chapter 4, it was possible to envisage a system where the geometric self-sensitivity and expressive power of the MWSS was exploited to combine a plan and multiple profiles into a 3D mesh. The 3D terrain model of the MWSS itself proved very capable at creating mass models of many complex buildings, and in particular roof structures.

Existing modeling techniques, such as the extrude operation and Havemann's[105] roof modeling constrain the direction of the extrudes to angles above the sweep plane. By using profile offset events and horizontal edge direction events, the PE system can simulate arbitrary non-monotonic elevations. This dramatically increases the range of

shapes possible. Theoretically it is possible to encode an arbitrary mesh into a system of PEs, with an arbitrary sweep plane direction. This is, however, future work.

There were several limitations of this basic approach, which necessitated various innovations. In order to create overhanging and even hollow roofs, we used various sub-applications of the straight skeleton to define the required geometry in a procedural manner. Another issue was that the façades of the output geometry were not rectangular, making it difficult for conventional systems, such as split shape grammars, to position windows and doors. To resolve this issue we introduced several types of anchors, giving different parametrisations of skeleton faces. To model the windows and doors themselves we resorted to a bone based technique which could deform and position decorative meshes across buildings.

Because the entire PE input was geometrically defined, it was possible to describe the system entirely with a graphical editor for plans and profiles. We were able to illustrate that the complete PE system is both usable and useful to people without significant programming experience. The expressibility of the system was successfully evaluated by modeling a large number of sample buildings from a catalogue with our user interface. We were eventually able to model all of our sample buildings using our UI.

In addition to demonstrating that the PE system is suitable for interactive architectural modeling, we also illustrate that it is suitable for kilometer scale procedural cityscape visualisation. We built a framework to generate large scale geometry given a set of floorplans provided from a GIS source. In this system we observed minimal errors and proved that the PE system was robust enough for large scale procedural geometry creation.

The theoretical problems underlying the specification of MWSS events have had minimum impact on the usefulness of the PE system. While a few failures cases were encountered in the large scale GIS test case, this issue has not caused significant problems during software development or evaluation.

We believe that the PE system is the first to provide a solution for the procedural modeling of walls, roofs, and complex architectural elements from arbitrary building footprints. The main contribution of this chapter is the design of a set of tools that extend the basic extrude operation into one that is geometrically self-sensitive. These tools are able to model a wide range of architectural surfaces that may have not been expressible with previous PGM systems.

Chapter 6

Conclusion

6.1 Summary of Objectives

In this dissertation we examined the straight skeleton as a procedural modeling technique. We proposed that the straight skeleton is a powerful PGM primitive that is useful in a variety of situations to users who are unable or unwilling to write classical computer programs. In particular we suggested that skeletons are able to create highly realistic results within the domain or urban procedural modeling.

To pursue this goal, Chapter 2 studied the wide variety of geometric modeling tools available, forming a spectrum of proceduralisation. We saw a strong correlation between this spectrum and the requirement that users must write computer programs. Those systems that required programming were the most general and expressive, while those that didn't were easier to use and more specialised. This led to the realisation that the concept of a "procedural system" was poorly defined between these two extremes. Eventually we took the stance that the "most procedural" systems lay in the middle of this spectrum, those that gave the most expressive power, with the simplest possible interaction. When we examined a variety of man-made objects, it became clear that some generalised offset mechanism may be able to describe many features of man-made geometry.

This offset mechanism was formalised in Chapter 3, which introduced the protagonist of this dissertation, the straight skeleton. A theoretical diversion at this point led us to examine the types of events that occur in generalisations of the straight skeleton. This line of enquiry led to both positive and negative outcomes. We discovered a novel skeleton with unique categories of events that would prove to be usefully applied to urban modelling, but at the same time we showed that there were some situations in which we could not define this new skeleton well. This mixed weighted straight

skeleton, however, proved to be a very flexible and powerful modeling primitive.

The SS was applied to two urban PGM scenarios. We were not able to apply our techniques to a wider range of applications due to time limitations. The first application was given in Chapter 4 and described how to use the straight skeleton to subdivide city blocks into parcels. The direction of this work was heavily motivated by the requirements of the commercial CityEngine PGM system. This lead to a real-time system with an emphasis on robust results for application to industry requirements.

Chapter 5 introduced the second application of the SS, in particular the mixed weighted straight skeleton, to the modeling of buildings themselves. This work was strongly motivated by our offset observations, and the relationships between the straight skeleton and the classical form of buildings' roofs. As we explored the modeling possibilities of the MWSS we found several varied and related techniques for its application to architectural modeling. Given our emphasis on procedural modeling we showed how cities could be reconstructed from their floorplans using this approach.

Both the systems we have applied the MWSS to have proven robust and flexible enough to generate kilometer-scale geometry procedurally. The block subdivision system was shown to reproduce particular subdivision styles over several expansive real-world examples, whilst the procedural extrusion system was able to generate a cityscape of multiple building styles from given building footprints. In both systems additional variation could be added without programming – either by changing parameters, or by editing polylines. Importantly, in both systems a wide range of inputs were shown to create domain-meaningful output; a wide range of inputs created output with an urban appearance.

These systems utilising the straight skeleton take a position in the spectrum of proceduralisation, of Chapter 2, that would otherwise require a written programming. While the urban modeling domain of applications in this dissertation pushes the skeleton based systems towards the specific end of the spectrum of generality; both the parcel subdivision and procedural extrusion systems have shown —

- self sensitivity: Usually reserved for very general procedural modeling system, the SS is a geometrically self-sensitive construct. Because any part of the perimeter of the polygon may affect the resulting skeleton, the skeleton responds to any change in the perimeter. This is particularly true of the MWSS used in the PE system.

- themselves capable of producing a wide range of results within their domain: Both systems were tested on a wide range of input data, and were able to create

realistic procedural approximations in the parcel subdivision and architecture domains.

- that they are useful without programming: The systems require no end user programming. The procedural extrusion system was demonstrated to be useful to users with no programming expertise, while the parcel subdivision was shown to be able to extract the required parameters automatically.

In addition the SS and MWSS proved to be intuitive geometric elements in the interactive systems. Users were able to understand the logic behind the centreline position in the parcel subdivision system, and were satisfied with the way it moved when the block's boundary was interactively edited. Similarly, users of the procedural extrusion system were able to control the MWSS, without understanding the underlying geometry, or algorithms, involved. Even when chaotic configurations were encountered, users were able to interactively modify the plans to explore and understand what was causing the instability.

6.2 Contributions

The general intersection event

Chapter 3 introduced our contributions to straight skeleton theory.

The SS is formed by shrinking a polygon, and allowing each edge to move towards the interior with a constant speed. By generalising SS we encounter the *positively weighted straight skeleton*. In this case each individual edge could move with an independent, if positive speed. For this case we introduced novel degeneracies as well as a simplification of existing events for computing the PWSS. This *general intersection event* was able to calculate the result of all PWSS events encountered, with fewer special cases.

This unification of existing skeleton events allows for both more general events and more general skeletons, such as the PWSS. In addition the resulting algorithm is simpler and easier to implement.

The mixed weighted straight skeleton

When we again generalised the PWSS we discovered the *mixed weighted straight skeleton*, a novel skeleton which allowed the edges to move either towards the interior of the plan, or toward the exterior. These new skeletons had interesting geometric features

such as splitting faces into two, introducing holes into faces, or allowing faces to merge together and split apart.

The degeneracies in the MWSS were quite involved, including one category of events which appeared to have no "nice" solution. We introduced the *pincushion problem* as a description of this situation.

This mixed weighted skeleton is relevant to many modeling tools which extrude 3D surface geometry. In addition we continue to use and evaluate the MWSS as a powerful PGM tool in Chapter 5.

A city block-to-lot subdivision system and evaluation

We introduced a system for city block to lot subdivision in Chapter 4.

Within this system we used the SS to model the block centrelines. The geometric sensitivity of the skeleton ensured that the entire block was taken into account when calculating centrelines, therefore even complex concave blocks were realistically divided. The presence of commercial robust implementations of the straight skeleton algorithm was also an advantage. In addition, because the skeleton could be intuitively understood by users as the "limit of an offset", we ensured a smooth parametrisation between patio and non-patio lot subdivisions via a single parameter. Users were able to modify a small number of parameters to change the characteristics of the subdivision, or automatically extract such statistics from existing subdivisions.

We quantitatively evaluated two block subdivision systems over a range of North American real-world data. Analysis of the generated parcels was performed by visualising the areas, aspect ratios, and the number of neighbours of both the real and procedural subdivisions. We found that after automatically fitting several parameters, the new procedural models compared favourably across our metrics. In addition, we found local lot arrangements that were very close to the baseline data.

The most frequently observed deficit in our subdivision system was the inability to model parcel subdivisions with external patterns in a manner similar to observed data. For example power-lines or rivers create divisions between sets of lots that our subdivision schemes are unable to model. We hypothesise that additional simulation elements in the subdivision process may resolve this issue. Another issue was the inability to move the centreline closer to either one side of the block or the other, this would have created better matches when the strips of a lot were of different depths. Selecting the corner priority was a further weakness in the system; we did not develop a mechanism to extract the priority of the streets at the corners from the example data automatically.

This application and evaluation of the skeleton to modeling block subdivision is the first within computer graphics, and presents a baseline for future work in this area. In addition our integration of the system within a commercial product allows a high level of robustness and interoperability with other GIS systems. For example the product has been used by commercial special effects houses and architects worldwide.

A method for the modeling of architectural shells using the MWSS

Our final contribution is the procedural extrusion architectural shell modeling system of Chapter 5.

By applying the 3D interpretation of the MWSS to this problem, we created the procedural extrusion system. It proved very capable at creating mass models of many complex buildings, and in particular roof structures.

The procedural extrusion system applies the MWSS in a variety of ways to create procedural models. Basic buildings without overhangs can be assembled by stacking truncated MWSS geometry. In order to create over-hangs or hollow roofs we use a sub-application of the MWSS to robustly create the offsets. Lastly, to introduce new features at a certain height, plan events can use the MWSS to create a robust perturbation of the buildings geometry. To model the windows and doors themselves we resorted to a deformable bone-based system which could "stretch" decorative meshes across models. These meshes were external to our system, and had to be created using an external 3D package.

Because the entire PE input is geometric, it is possible to describe the system entirely with a graphical editor for plans and profiles. We were able to evaluate the system and show that it is both usable and useful to people without significant programming experience. The expressibility of the system was successfully evaluated by modeling a large number of sample buildings from a catalogue with our user interface. In addition, we also illustrated that PEs are suitable for kilometer scale procedural cityscape visualisation. We built a framework to generate large scale geometry given a set of floorplans provided from a GIS source. In this framework we observed minimal geometric errors and proved that the PE system was useful for robust large scale procedural geometry creation.

There were several limitations of the basic approach. One is that conventional programming was used to position the decorative meshes on the large scale evaluation project. Ideally this could be specified graphically, in a per-plan-edge manner. However, accounting for different ways of repeating elements over varied geometry is challenging. Another issue was that the façades of the output geometry were not rectangular, making it difficult for conventional systems, such as split shape grammars, to position

windows and doors. To resolve this issue we introduced several types of anchors, giving different parametrisations of façades. Finally our evaluations also showed that our floating point implementation of the MWSS had some numerical issues, and would occasionally fail to generate a polygon. An arbitrary precision implementation would lessen these issues, at the expense of execution time.

The ease of use of the PE system, combined with its proven expressivness and suitability to large-scale geometry creation are rare. Because of these features, concepts from the procedural extrusion system have been adopted by commercial video game creators and a research PGM system. Finally, the system provides a concrete application and validation of our theoretical work on the MWSS.

6.3 Future Work

There is a wide variety of work still to be undertaken in understanding the application of the SS to procedural modeling. The most obvious direction to undertake would be to attempt to combine the work of Chapter 4 and Chapter 5. Given the wide range of polygon subdivision results in Sec. 5.5.10, we may ask "is there a general language of offsets?" Such a language may be applicable to parcel subdivision, footprint extrusion, and other urban modeling situations. When we consider the objects in the home, it may be that a large number of the frames, borders, skirting boards and other features can be created using such a system.

More specific future work might attempt to combine the techniques documented in this dissertation with the more mainstream shape grammar modeling systems. In particular extending CGA Shape[164] to work intuitively with non-rectangular façades, such that the MWSS can become a primitive within the large existing libraries of CGA Shape operations. We suspect that it is possible to construct such an irregular façade only using some language of skeletons.

With the PE system it would be most advantageous to be able to generate unique plans and profiles, or even position and repeat the anchors. This problem is quite challenging, and solutions may involve shape grammars, pattern synthesis or even by-example modeling.

One further avenue for future work is to question whether the techniques introduced in this dissertation are applicable to other domains. Geometric techniques to simulate other types of skeleton, such as the medial axis, with the straight skeleton[233] offer the promise of being able to model more curved forms in unison with the human-designed appearance of the SS. In particular exploring 3D growth mechanisms, such the 3D WSS, offer some interesting avenues of research into the modeling the growth of flora

and fauna. However, it becomes clear quite quickly that the first stumbling block of the 3D WSS is the degeneracy caused by a valency four mesh vertex — an imaginative solution would be required!

An early problem in our studies was that of evaluating procedural content. This dissertation has used several different methods for evaluation — comparing statistical measures against ground truth with the lot subdivision project, examining the ability to recreate the ground truth exactly in the PE UI demonstration, or subjective analysis of procedural output as in the PE GIS evaluation. Because PGM has no requirement to reconstruct such a ground truth, only create a novel, yet characteristically valid geometry, objective evaluation is difficult. The trade off between producing realistic or novel geometry is probably something the user wants to control very closely. The "best" solution probably changes for each application of procedural technology and is thus highly subjective. It may depend on the amount of user input desirable, the required speed or the level of detail required. Future work in this direction would be very useful, although there is a question as to whether we need better, more photo-realistic procedural systems for it to begin.

One extreme application of the WSS may be in the classification of data points, from the field of machine learning. In 2D we can imagine using a skeleton to "colonise" the space around each data point. The area composed of skeleton faces would form a classification boundary. This would be somewhat similar to a weighted Voronoi diagram, but with the potential to change the propagation weights based on direction, propagation distance, or a property of the data point. The initial problem is how to generalise the skeleton higher dimensions efficiently.

Appendix A

Appendix - input for interactive UI evaluation

Figure A.1: *The input plans and profiles to Fig. 5.43—5.45. ©2012 ePlans.*

Appendix B

Appendix - artists' comments on the procedural extrusions system

Please note that the artists refer to the procedural extrusion system as "the skeleton program" or similar.

B.0.1 User 1

In less than 3 sentences, describe your artistic training (eg: university course and any relevant work experience you've done) My artistic training consists of a bachelors of fine arts degree in 3-D Imaging and Animation from Arizona State University, as well as a certificate in computer gaming. Relevant work experience includes creating all artistic assets for a stroke patient rehabilitation interactive videogame for the Arizona State University Biomedical Research Facility.

How much programming experience have you had (eg: none? max-scripting? c++?) My personal programming experience consists of one meager class in flash programming for videogames that I was not extremely successful at.

How long did it take you to become competent at using the tool? After being given a list of hot keys and experimenting with the program, it took roughly three weeks to become comfortable with multiple profiles and floor plan pieces while using the program.

Was the skeleton program easy to use (compare to using Max/Maya/Sketchup)? Compared to Max or Maya the program has a much softer learning curve, from interface aspects to object creation. For the sole purpose of creating buildings and architecture, the skeleton program appears more expedient than the normal modeling programs due to automated steps it takes in completing and triangulated the meshes.

How long did it take you to create you current projects (the mansion or the oriental house). How much of this time was creating the meshes. How much of this time was using the skeleton program? To create my brick mansion and final renders took roughly twenty to twenty five hours. Creating my meshes (windows, door, cornice, chimney) only took about four to five hours in Maya. It took about 10 hours using the skeleton program to create the mansion mesh itself, but that was due to changing it repeatedly and experimenting with 10+ profiles and how they align. The latter 10 hours or so was spent in Maya first creating textures, then a 10 piece lighting unit, and then creating quality renders for the paper.

Would it have taken longer to create these models without the skeleton program? Yes, it would have taken quite a while longer to create the mesh in Maya, and I can assume that the triangulation and face count wouldn't be as low either. It probably would take at least twice the amount of time due to the roof most of all, to create all the angles seamlessly and uniformly.

Would the tool be a useful addition to current 3D modeling packages? The tool would be very useful for a 3-D Environment modeling package. Being able to export an OBJ file, it would be very easy to populate the background of an environment with buildings that differed just enough that they didn't look like duplicates, but not so high poly that it would slow down a game engine.

Any other comments about the skeleton program? Overall the program has quite a lot of potential, if only for a specific set of uses. The only suggestions I had is to find a way to make the measurements more exact than just the align to grid system, whether it's just a soft grid in the background, or an actual numerical system that can be manipulated. This goes for the profile view as well. One thing that makes it very easy in Maya is you can always move things in exact, straight lines, which is very useful for low poly creation. Occasionally I would find that my building swelled at the top compared the bottom, or one side was actually just a shade shorter than the other even though they look identical on the floor plan.

B.0.2 User 2

In less than 3 sentences, describe your artistic training (eg: university course and any relevant work experience you've done): I have taken a number of traditional art classes including Drawing, Painting, Sculpture, Color Theory as well as 2D and 3D Design. I have also completed 4 classes in 3D Modeling and Animation, and have been using 3D programs for over 5 years.

How much programming experience have you had (eg: none? max-scripting? c++?) I have taken introductory courses in Visual Basic, C++, Java and Action Script. I am also familiar with HTML and CSS.

How long did it take you to become competent at using the tool? With only the Note document it took me about 5 hours to get a decent understanding of the program. I think that a video guide would cut down on this time quite a bit, as well as give a user a much better grasp of the program.

Was the skeleton program easy to use (compare to using Max/Maya/Sketchup)? Yes, the skeleton program was easy to use compared to Max and Maya.

How long did it take you to create you current projects (the mansion or oriental house). How much of this time was creating the meshes. How much of this time was using the skeleton program? I would say that it took be about 20 to 30 hours to get the oriental house to where it is now. I would say the majority of this time was spent creating the meshes, 15 to 20 hours and 5 to 10 hours using the skeleton program.

Would it have taken longer to create these models without the skeleton program? I think that it would have taken me longer to get my model to the same level of completion without the skeleton program. I would say traditional modeling techniques would add at least 5 hours of work.

Would the tool be a useful addition to current 3D modeling packages? This would be a great addition to Max or Maya, the speed with which it allows you to create buildings

Any other comments about the skeleton program? Overall I think that the core idea behind the skeleton program is really great, and for the most part the execution of the program is equally great. The ease with which you can create a building and then tweak it until it is exactly what you are looking for is extremely useful. In its current state, I think the meshes are the weakest part of the Skeleton program. The main reason I say this is because as it currently stands, the application of meshes doesnt really save you that much time compared to creating and attaching them within a separate 3D program. If I were using this program in the industry my preferred pipeline would be something along the lines of the below.

- Use the Skeleton program to create the basic shape of a building
- Create any dormer-window like protrusions (if implemented again)
- Apply roof tiles where appropriate within the skeleton program

- Export the building as an .obj file
- Import building into Max or Maya
- Build the detail meshes for the building on top of the imported building
- Duplicate, rotate, and transform the meshes to flesh out all the desired details.

This only difference between the above pipeline and the current pipeline is that currently I build a mesh, skin it, export it, and then attach it within the skeleton program. I think that the removal of the need to skin and weight the meshes makes up for the need to manually duplicate, rotate, and transform them.

Ultimately, in a perfect software, I would love to be able to create meshes and then apply them to my models in a 3D environment instead of the two 2D environment the Skeleton program uses. In other words, I would want the ability to create the anchor points directly on the mesh in the 3D view of the Skeleton program.

Bibliography

[1] CGAL, Computational geometry algorithms library. www.cgal.org, February 2008.

[2] G. Abram and L. Treinish. An extended data-flow architecture for data analysis and visualization. In *Proceedings of the 6th conference on Visualization'95*, page 263. IEEE Computer Society, 1995.

[3] M Agarwal and J Cagan. A blend of different tastes: the language of coffeemakers. *Environment and Planning B: Planning and Design*, 25(2):205–226, March 1998.

[4] S. Agarwal, N. Snavely, I. Simon, S.M. Seitz, and R. Szeliski. Building rome in a day. In *Computer Vision, 2009 IEEE 12th International Conference on*, pages 72–79. Ieee, 2009.

[5] O. Aichholzer, D. Alberts, F. Aurenhammer, and B. Gärtner. Straight skeletons of simple polygons. In *Proc. 4th Internat. Symp. of LIESMARS*, pages 114–124, 1995.

[6] O. Aichholzer, F. Aurenhammer, D. Alberts, and B. Grtner. A novel type of skeleton for polygons. *Journal of Universal Computer Science*, 1(12):752–761, 1995.

[7] Oswin Aichholzer and Franz Aurenhammer. Straight skeletons for general polygonal figures in the plane. In *Computing and Combinatorics*, pages 117–126. Springer-Verlag, 1996.

[8] S. Al-Kheder, J. Wang, and J. Shan. Fuzzy inference guided cellular automata urban-growth modelling using multi-temporal satellite images. *International Journal of Geographical Information Science*, 22(11-12):1271–1293, 2008.

[9] Christopher Alexander, Sara Ishikawa, and Murray Silverstein. *A Pattern Language: Towns, Buildings*. Oxford University Press, later printing edition, August 1977.

[10] K. Alexandridis, B.C. Pijanowski, and Z. Lei. Assessing multiagent parcelization performance in the mabel simulation model using monte carlo replication experiments. *Environment and Planning B: Planning and Design*, 34(2):223, 2007.

[11] Daniel G. Aliaga, Paul A. Rosen, and Daniel R. Bekins. Style grammars for interactive visualization of architecture. *IEEE Transactions on Visualization and Computer Graphics*, 13(4):786–797, 2007.

[12] Daniel G. Aliaga, Carlos A. Vanegas, and Bedřich Beneš. Interactive example-based urban layout synthesis. *ACM Transactions on Graphics*, 27(5):1–10, 2008.

[13] Fabricio Anastacio, Przemyslaw Prusinkiewicz, and Mario Costa Sousa. Sketch-based interfaces and modeling (sbim): Sketch-based parameterization of l-systems using illustration-inspired construction lines and depth modulation. *Computer Graphics*, 33(4):440–451, 2009.

[14] R. Anderl and R. Mendgen. Modelling with constraints: theoretical foundation and application. *Computer-Aided Design*, 28(3):155–168, 1996.

[15] Peter R Atherton. A scan-line hidden surface removal procedure for constructive solid geometry. *SIGGRAPH Computer Graphics*, 17(3):73–82, 1983.

[16] Franz Aurenhammer. Weighted skeletons and fixed-share decomposition. *Computer Geom. Theory Appl.*, 40(2):93–101, 2008.

[17] Autodesk. ArcGIS. www.esri.com/software/arcgis, accessed (14/8/12).

[18] Autodesk. AutoCAD. www.autodesk.co.uk/autocad, accessed (14/8/12).

[19] Autodesk. Autodesk Maya. usa.autodesk.com/maya, accessed (14/8/12).

[20] Autodesk. Mudbox. http://www.autodesk.com/mudbox, accessed (14/8/12).

[21] Shai Avidan and Ariel Shamir. Seam carving for content-aware image resizing. *ACM Transactions on Graphics*, 26(3):10, 2007.

[22] S. Becker. Generation and application of rules for quality dependent façade reconstruction. *ISPRS journal of photogrammetry and remote sensing*, 64(6):640–653, 2009.

[23] T. Beier and S. Neely. Feature-based image metamorphosis. *Computer Graphics*, 26(2):35–42, 1992.

[24] B. Beneš, O. Šťava, R. Měch, and G. Miller. Guided procedural modeling. In *Computer Graphics Forum*, volume 30, pages 325–334. Wiley Online Library, 2011.

[25] Bentley. Generative Components. www.bentley.com/en-GB/Products/GenerativeComponents/, accessed (14/8/12).

[26] J. Bloomenthal. Medial-based vertex deformation. In *Proceedings of the 2002 ACM SIGGRAPH/Eurographics symposium on Computer animation*, pages 147–151. ACM, 2002.

[27] Jules Bloomenthal. Modeling the mighty maple. *SIGGRAPH Computer Graphics*, 19(3):305–311, 1985.

[28] Harry Blum. A transformation for extracting new descriptors of shape. *Models for the Perception of Speech and Visual Form*, pages 362–380, 1967.

[29] M. Bokeloh, A. Berner, M. Wand, H.P. Seidel, and A. Schilling. Symmetry detection using feature lines. In *Computer Graphics Forum*, volume 28, pages 697–706, 2009.

[30] M. Bokeloh, M. Wand, and H.P. Seidel. A connection between partial symmetry and inverse procedural modeling. *ACM Transactions on Graphics*, 29(4):104, 2010.

[31] Martin Bokeloh, Michael Wand, Vladlen Koltun, and Hans-Peter Seidel. Pattern-aware shape deformation using sliding dockers. *ACM Transactions on Graphics*, 30:123:1–123:10, December 2011.

[32] Martin Bokeloh, Michael Wand, Hans-Peter Seidel, and Vladlen Koltun. An algebraic model for parameterized shape editing. *ACM Transactions on Graphics*, 31(4):XXX, August 2012.

[33] P. Borrel and D. Bechmann. Deformation of n-dimensional objects. In *Proceedings of the first ACM symposium on Solid modeling foundations and CAD/CAM applications*, pages 351–369. ACM, 1991.

[34] G.H. Buck-Sorlin, O. Kniemeyer, and W. Kurth. Barley morphology, genetics and hormonal regulation of internode elongation modelled by a relational growth grammar. *New Phytologist*, 166(3):859–867, 2005.

[35] M. Cabral, S. Lefebvre, C. Dachsbacher, and G. Drettakis. Structure-preserving reshape for textured architectural scenes. In *Computer Graphics Forum*, volume 28, pages 469–480. Wiley Online Library, 2009.

[36] M. Carmona. *Public places, urban spaces: the dimensions of urban design*. Architectural Press, 2003.

[37] HH Chau, X. Chen, A. McKay, and A. de Pennington. Evaluation of a 3d shape grammar implementation. *Design computing and cognition*, 4:357–376, 2004.

[38] Guoning Chen, Gregory Esch, Peter Wonka, Pascal Muller, and Eugene Zhang. Interactive procedural street modeling. *ACM Transactions on Graphics*, 27(3), 2008.

[39] Guoning Chen, Gregory Esch, Peter Wonka, Pascal Müller, and Eugene Zhang. Interactive procedural street modeling. *ACM Transactions on Graphics*, 27(3):103:1–9, 2008.

[40] S.W. Cheng and A. Vigneron. Motorcycle graphs and straight skeletons. In *Proceedings of the thirteenth annual ACM-SIAM symposium on Discrete algorithms*, pages 156–165. Society for Industrial and Applied Mathematics, 2002.

[41] N. Chomsky. Three models for the description of language. *Information Theory, IRE Transactions on*, 2(3):113–124, January 1956.

[42] N. Chomsky. On certain formal properties of grammars*. *Information and control*, 2(2):137–167, 1959.

[43] M.F. Cohen, J. Shade, S. Hiller, and O. Deussen. Wang tiles for image and texture generation. *ACM Transactions on Graphics*, 22(3):287–294, 2003.

[44] Complexity zoo, January 2011. [online] `http://qwiki.stanford.edu`, retrieved 1/1/12.

[45] G. Curdes. *Stadtstruktur und Stadtgestaltung*. Kohlhammer, 1997.

[46] Scott Davidson. Grasshopper. http://www.grasshopper3d.com/, accessed (14/8/12).

[47] AL Davis and RM Keller. Data flow program graphs. *Computer*, pages 26–41, 1982.

[48] AL Davis and SA Lowder. A sample management application program in a graphical data driven programming language. *Digest of Papers Compcon Spring*, 81:162–167, 1981.

[49] M. Davis, R. Sigal, and E.J. Weyuker. *Computability, complexity, and languages: fundamentals of theoretical computer science*. Morgan Kaufmann, 1994.

[50] MD de Jong and CL Hankin. Structured data flow programming. *ACM SIGPLAN Notices*, 17(8):18–27, 1982.

[51] Phillippe de Reffye, Claude Edelin, Jean Françon, Marc Jaeger, and Claude Puech. Plant models faithful to botanical structure and development. In *SIGGRAPH '88: Proceedings of the 15th annual conference on Computer graphics and interactive techniques*, pages 151–158, New York, NY, USA, 1988. ACM.

[52] Paul E. Debevec, Camillo J. Taylor, and Jitendra Malik. Modeling and rendering architecture from photographs: a hybrid geometry- and image-based approach. In *Proceedings of the 23rd annual conference on Computer graphics and interactive techniques*, SIGGRAPH '96, pages 11–20, New York, NY, USA, 1996. ACM.

[53] F. Dellaert, S.M. Seitz, C.E. Thorpe, and S. Thrun. Structure from motion without correspondence. In *Computer Vision and Pattern Recognition, 2000. Proceedings. IEEE Conference on*, volume 2, pages 557–564. IEEE, 2000.

[54] J. Dennis. First version of a data flow procedure language. In *Programming Symposium*, pages 362–376. Springer, 1974.

[55] A.R. Dick, PHS Torr, and R. Cipolla. Modelling and interpretation of architecture from several images. *International Journal of Computer Vision*, 60(2):111–134, 2004.

[56] J.J. Dolado and F.J. Torrealdea. Formal manipulation of forrester diagrams by graph grammars. *Systems, Man and Cybernetics, IEEE Transactions on*, 18(6):981 –996, nov/dec 1988.

[57] P. Dosch, K. Tombre, C. Ah-Soon, and G. Masini. A complete system for the analysis of architectural drawings. *International Journal on Document Analysis and Recognition*, 3(2):102–116, 2000.

[58] K. Dylla, B. Frischer, P. Mueller, A. Ulmer, and S. Haegler. Rome reborn 2.0: A case study of virtual city reconstruction using procedural modeling techniques. *Computer Graphics World*, 16:25, 2008.

[59] A.A. Efros and T.K. Leung. Texture synthesis by non-parametric sampling. In *Computer Vision, 1999. The Proceedings of the Seventh IEEE International Conference on*, volume 2, pages 1033–1038. Ieee, 1999.

[60] Alexei A. Efros and William T. Freeman. Image quilting for texture synthesis and transfer. In *Proceedings of ACM SIGGRAPH 2001*, pages 341–346, 2001.

[61] H. Ehrig and H.J. Kreowski. Parallel graph grammars. In *Automata, Languages, Development*, pages 425–442. Amsterdam: North Holland, 1976.

[62] H. Ehrig, M. Pfender, and H.J. Schneider. Graph-grammars: An algebraic approach. In *Switching and Automata Theory, 1973. SWAT'08. IEEE Conference Record of 14th Annual Symposium on*, pages 167–180. IEEE, 1973.

[63] Michael Eigensatz, Martin Kilian, Alexander Schiftner, Niloy J. Mitra, Helmut Pottmann, and Mark Pauly. Paneling architectural freeform surfaces. *ACM Transactions on Graphics*, 29:45:1–45:10, July 2010.

[64] D. Eppstein. Subgraph isomorphism in planar graphs and related problems. In *Proceedings of the sixth annual ACM-SIAM symposium on Discrete algorithms*, pages 632–640. Society for Industrial and Applied Mathematics, 1995.

[65] David Eppstein and Jeff Erickson. Raising roofs, crashing cycles, and playing pool: applications of a data structure for finding pairwise interactions. In *SCG '98: Proceedings of the fourteenth annual symposium on Computational geometry*, pages 58–67, New York, NY, USA, 1998. ACM.

[66] Esri. Esri CityEngine. www.esri.com/software/cityengine/index.html, accessed (14/8/12).

[67] Esri. Swiss village for masdar city. http://www.esri.com/software/cityengine/resources/casestudies/swiss-village accessed (3/5/13).

[68] P. Felkel and S. Obdržálek. Straight skeleton implementation. In *Proceedings of Spring Conference on Computer Graphics*, pages 210–218, 1998.

[69] Petr Felkel and Stepan Obdrzalek. Straight skeleton implementation. In *Proceedings of Spring Conference on Computer Graphics*, pages 210–218, 1998.

[70] Dieter Finkenzeller. Detailed building facades. *IEEE Computer Graphics and Applications*, 28:58–66, 2008.

[71] M.A. Fischler and R.C. Bolles. Random sample consensus: a paradigm for model fitting with applications to image analysis and automated cartography. *Communications of the ACM*, 24(6):381–395, 1981.

[72] U. Flemming. More than the sum of its parts: the grammar of queen anne houses. *Environment and Planning B*, 14:323–350, 1987.

[73] Harvey Fong. Levelshop: From grid paper to playable. Game Developers Conference, 2011.

[74] Blender Foundation. Blender. www.blender.org, accessed (14/8/12).

[75] T. Funkhouser, M. Kazhdan, P. Shilane, P. Min, W. Kiefer, A. Tal, S. Rusinkiewicz, and D. Dobkin. Modeling by example. In *ACM Transactions on Graphics*, volume 23, pages 652–663. ACM, 2004.

[76] T. Funkhouser, P. Min, M. Kazhdan, J. Chen, A. Halderman, D. Dobkin, and D. Jacobs. A search engine for 3d models. *ACM Transactions on Graphics*, 22(1):83–105, 2003.

[77] Ran Gal, Olga Sorkine, Niloy Mitra, and Daniel Cohen-Or. iWIRES: An analyze-and-edit approach to shape manipulation. *ACM Transactions on Graphics (proceedings of ACM SIGGRAPH)*, 28(3):1–10, 2009.

[78] Bay 12 Games. Dwarf fortress. http://www.bay12games.com/dwarves/, accessed (10/8/13).

[79] Gaslamp Games. ClockworkEmpires. http://www.gaslampgames.com/2012/08/27/clockw
empires-the-press-release/ accessed (10/10/12).

[80] M. Gardner. The fantastic combinations of john conway's new solitaire game "life". *Scientific American*, 223:120–123, October 1970.

[81] Björn Gerth, René Berndt, Sven Havemann, and Dieter W. Fellner. 3d modeling for non-expert users with the castle construction kit v0.5. In *VAST 2005: 6th International Symposium on Virtual Reality, Archaeology and Intelligent Cultural Heritage*, pages 49–58, November 2005.

[82] Y. Gingold, T. Igarashi, and D. Zorin. Structured annotations for 2d-to-3d modeling. *ACM Transactions on Graphics*, 28(5):148, 2009.

[83] Y. Gingold and D. Zorin. Shading-based surface editing. In *ACM Transactions on Graphics*, volume 27, page 95. ACM, 2008.

[84] J. Gips. Computer implementation of shape grammars. In *NSF/MIT Workshop on Shape Computation*, 1999.

[85] Google. Google Blockly. code.google.com/p/blockly, accessed (14/8/12).

[86] J. Gosling and H. McGilton. The java language environment: A white paper. 1995. *Sun Microsystems*, 1996.

[87] H. Göttler. Attributed graph grammars for graphics. In *Graph-Grammars and their Application to Computer Science*, pages 130–142. Springer, 1983.

[88] H. Göttler. *Graphgrammatiken in der Softwaretechnik: Theorie und Anwendungen*, volume 178. Not Avail, 1988.

[89] T. Grasl and A. Economou. Palladian graphs. In *Future cities: proceedings of the 28th Conference on Education in Computer Aided Architectural Design in Europe, September 15-18, 2010, Zurich, Switzerland, ETH Zurich*, page 275. vdf Hochschulverlag AG, 2010.

[90] N. Greene. Voxel space automata: modeling with stochastic growth processes in voxel space. In *SIGGRAPH '89: Proceedings of the 16th annual conference on Computer graphics and interactive techniques*, pages 175–184, New York, NY, USA, 1989. ACM.

[91] Herbert Gttler. Graph grammars, a new paradigm for implementing visual languages. In Nachum Dershowitz, editor, *Rewriting Techniques and Applications*, volume 355 of *Lecture Notes in Computer Science*, pages 152–166. Springer Berlin / Heidelberg, 1989.

[92] Herbert Gttler, Joachim Gnther, and Georg Nieskens. Use graph grammars to design cad-systems! In Hartmut Ehrig, Hans-Jrg Kreowski, and Grzegorz Rozenberg, editors, *Graph Grammars and Their Application to Computer Science*, volume 532 of *Lecture Notes in Computer Science*, pages 396–410. Springer Berlin / Heidelberg, 1991.

[93] M. Habbecke and L. Kobbelt. Linear analysis of nonlinear constraints for interactive geometric modeling. *Proceedings Eurographics.*, XXX 2012.

[94] A. Habel, R. Heckel, and G. Taentzer. Graph grammars with negative application conditions. *Fundamenta Informaticae*, 26(3):287–313, 1996.

[95] P.E. Haeberli. Conman: a visual programming language for interactive graphics. In *ACM SIGGRAPH Computer Graphics*, volume 22, pages 103–111. ACM, 1988.

[96] S. Haegler, P. Müller, and L. Van Gool. Procedural modeling for digital cultural heritage. *Journal on Image and Video Processing*, 2009:4–4, 2009.

[97] Evan Hahn, Prosenjit Bose, and Anthony Whitehead. Persistent realtime building interior generation. In *sandbox '06: Proceedings of the ACM SIGGRAPH symposium on Videogames*, pages 179–186, NY, USA, 2006. ACM.

[98] Jan Halatsch, Antje Kunze, and Gerhard Schmitt. Using shape grammars for master planning. In John S. Gero and Ashok K. Goel, editors, *Design Computing and Cognition '08*, pages 655–673. Springer Netherlands, 2008.

[99] Feng Han and Song-Chun Zhu. Bottom-up/top-down image parsing by attribute graph grammar. In *ICCV*, pages 1778–1785, Washington, DC, USA, 2005. IEEE Computer Society.

[100] J.S. Hanan and P. Adviser-Prusinkiewicz. *Parametric L-systems and their application to the modelling and visualization of plants*. The University of Regina (Canada), 1992.

[101] C.L. Hankin and HW Glaser. The data flow programming language cajole-an informal introduction. *ACM Sigplan Notices*, 16(7):35–44, 1981.

[102] Hanley Wood, LLC. eplans.com, sept 2010. http://www.eplans.com.

[103] Sarah Harries. Man of steel: Procedural city building and destruction, 2013.

[104] John C. Hart and Brent Baker. Structural simulation of tree growth and response. In *In: Proceedings International Conference on Shape Modeling and Applications*, pages 7–11. Springer-Verlag, 1996.

[105] S. Havemann. *Generative Mesh Modeling*. PhD thesis, TU Braunschweig, 2005.

[106] Sven Havemann and Dieter Fellner. Generative parametric design of gothic window tracery. *Shape Modeling and Applications, International Conference on*, 0:350–353, 2004.

[107] B. Hohmann, U. Krispel, S. Havemann, and D. Fellner. Cityfit: High-quality urban reconstructions by fitting shape grammars to images and derived textured point clouds. In *Proceedings of the 3rd ISPRS Workshop*. Citeseer, 2009.

[108] M. Honda, K. Mizuno, Y. Fukui, and S. Nishihara. Generating autonomous time-varying virtual cities. In *Cyberworlds, 2004 International Conference on*, pages 45–52. IEEE, 2004.

[109] Y. Horry, K.I. Anjyo, and K. Arai. Tour into the picture: using a spidery mesh interface to make animation from a single image. In *Proceedings of the 24th annual conference on Computer graphics and interactive techniques*, pages 225–232. ACM Press/Addison-Wesley Publishing Co., 1997.

[110] P. Hudak, S. Peyton Jones, P. Wadler, B. Boutel, J. Fairbairn, J. Fasel, M.M. Guzmán, K. Hammond, J. Hughes, T. Johnsson, et al. Report on the programming language haskell: a non-strict, purely functional language version 1.2. *ACM SigPlan notices*, 27(5):1–164, 1992.

[111] T. Igarashi, T. Moscovich, and J.F. Hughes. As-rigid-as-possible shape manipulation. In *ACM Transactions on Graphics*, volume 24, pages 1134–1141. ACM, 2005.

[112] M. Ilčík, S. Fiedler, W. Purgathofer, and M. Wimmer. Procedural skeletons: kinematic extensions to cga-shape grammars. In *Proceedings of the 26th Spring Conference on Computer Graphics*, pages 157–164. ACM, 2010.

[113] National Instruments. Labview. www.ni.com/labview, accessed (14/8/12).

[114] International Business Machines Corporation. *General information manual; programmer's primer for FORTRAN automatic coding system for the IBM 704 data processing system*. IBM Corporation, pub-IBM:adr, 1957.

[115] A. Irschara, C. Zach, M. Klopschitz, and H. Bischof. Large-scale, dense city reconstruction from user-contributed photos. *Computer Vision and Image Understanding*, 2011.

[116] Nianjuan Jiang, Ping Tan, and Loong-Fah Cheong. Symmetric architecture modeling with a single image. *ACM Transactions on Graphics*, 28(5):113:1–113:8, December 2009.

[117] R Joan-Arinyo, L Pérez, and J Vilaplana. Computing the medial axis transform of polygonal domains by tracing paths. 1999.

[118] Evangelos Kalogerakis, Siddhartha Chaudhuri, Daphne Koller, and Vladlen Koltun. A probabilistic model for component-based shape synthesis. *ACM Transactions on Graphics*, 31(4):XXX, August 2012.

[119] Yoichiro Kawaguchi. A morphological study of the form of nature. In *SIGGRAPH '82: Proceedings of the 9th annual conference on Computer graphics and interactive techniques*, pages 223–232, New York, NY, USA, 1982. ACM.

[120] Tom Kelly. Siteplan. https://code.google.com/p/siteplan/.

[121] Tom Kelly and Peter Wonka. Interactive architectural modeling with procedural extrusions. *ACM Transactions on Graphics*, 30(2):14:1–14:15, April 2011.

[122] Tom W A Kelly. City architecture generation. Master's thesis, University of Bristol, 2006.

[123] B. Kerautret, X. Granier, and A. Braquelaire. Intuitive shape modeling by shading design. In *Smart Graphics*, pages 923–923. Springer, 2005.

[124] J.W. Klop and R. de Vrijer. *Term rewriting systems*. Cambridge Univ Pr, 2003.

[125] T. W. Knight. The generation of hepplewhite-style chair-back designs. *Environment and Planning B*, 7(2):227–238, 1980.

[126] D.E. Knuth. Semantics of context-free languages. *Theory of Computing Systems*, 2(2):127–145, 1968.

[127] D.W. Ko, H.S. He, and D.R. Larsen. Simulating private land ownership fragmentation in the missouri ozarks, usa. *Landscape ecology*, 21(5):671–686, 2006.

[128] H Koning and J Eizenberg. The language of the prairie: Frank lloyd wright's prairie houses. *Environment and Planning B: Planning and Design*, 8(3):295–323, 1981.

[129] L. Krecklau and L. Kobbelt. Procedural modeling of interconnected structures. In *Computer Graphics Forum*, volume 30, pages 335–344. Wiley Online Library, 2011.

[130] R. Krishnamurti. The arithmetic of shapes. *Environment and Planning B: Planning and Design*, 7(4):463–484, 1980.

[131] R. Krishnamurti. The construction of shapes. *Environment and Planning B*, 8:5–40, 1981.

[132] R. Krishnamurti and CF Earl. Shape recognition in three dimensions. *Environment and Planning B: Planning and Design*, 19(5):585–603, 1992.

[133] F. Lafarge, X. Descombes, J. Zerubia, and M. Pierrot-Deseilligny. Structural approach for building reconstruction from a single dsm. *Pattern Analysis and Machine Intelligence, IEEE Transactions on*, 32(1):135–147, 2010.

[134] G. Lee, R. Sacks, and C.M. Eastman. Specifying parametric building object behavior (bob) for a building information modeling system. *Automation in construction*, 15(6):758–776, 2006.

[135] J. Lee and T. Funkhouser. Sketch-based search and composition of 3d models. In *Eurographics Workshop on Sketch-Based Interfaces and Modeling*, pages 97–104. The Eurographics Association, 2008.

[136] J.P. Lewis, M. Cordner, and N. Fong. Pose space deformation: a unified approach to shape interpolation and skeleton-driven deformation. In *Proceedings of the 27th annual conference on Computer graphics and interactive techniques*, pages 165–172. ACM Press/Addison-Wesley Publishing Co., 2000.

[137] R. Lewis and C. Séquin. Generation of 3d building models from 2d architectural plans. *Computer-Aided Design*, 30(10):765–779, 1998.

[138] Y. Li, X. Wu, Y. Chrysathou, A. Sharf, D. Cohen-Or, and N.J. Mitra. Globfit: consistently fitting primitives by discovering global relations. In *ACM Transactions on Graphics*, volume 30, page 52. ACM, 2011.

[139] Yuanyuan Li, Eugene Zhang, Yoshihiro Kobayashi, and Peter Wonka. Editing operations for irregular vertices in triangle meshes. *ACM Transactions on Graphics*, 29:153:1–153:12, December 2010.

[140] Jinjie Lin, Daniel Cohen-Or, Hao Zhang, Cheng Liang, Andrei Sharf, Oliver Deussen, and Baoquan Chen. Structure-preserving retargeting of irregular 3d architecture. *ACM Transactions on Graphics*, 30(6):183:1–183:10, December 2011.

[141] A. Lindenmayer and G. Rozenberg. Parallel generation of maps: Developmental systems for cell layers. In *Graph-grammars and their application to computer science and biology*, pages 301–316. Springer, 1979.

[142] Aristid Lindenmayer. Mathematical models for cellular interactions in development ii. simple and branching filaments with two-sided inputs. *Journal of Theoretical Biology*, 18(3):300–315, March 1968.

[143] M. Lipp, D. Scherzer, P. Wonka, and M. Wimmer. Interactive modeling of city layouts using layers of procedural content. In *Computer Graphics Forum*, volume 30, pages 345–354. Wiley Online Library, 2011.

[144] Markus Lipp, Peter Wonka, and Michael Wimmer. Interactive visual editing of grammars for procedural architecture. *ACM Transactions on Graphics*, 27(3):1–10, 2008.

[145] Markus Lipp, Peter Wonka, and Michael Wimmer. Interactive visual editing of grammars for procedural architecture. *ACM Transactions on Graphics*, 27(3):102:1–10, 2008. Article No. 102.

[146] Hua Liu, Qing Wang, Wei Hua, Dong Zhou, and Hujun Bao. Building Chinese Ancient Architectures in Seconds. In *International Conference on Computational Science*, pages 248–255, 2005.

[147] Yang Liu, Helmut Pottmann, Johannes Wallner, Yong-Liang Yang, and Wenping Wang. Geometric modeling with conical meshes and developable surfaces. *ACM Transactions on Graphics*, 25(3):681–689, 2006.

[148] R. Lovejoy. Turtle graphics implementation using a graphical dataflow programming approach(M. S. thesis). Master's thesis, Navel Postgraduate School, 1992.

[149] F. Ludolph, Y.Y. Chow, D. Ingalls, S. Wallace, and K. Doyle. The fabrik programming environment. In *Visual Languages, 1988., IEEE Workshop on*, pages 222–230. IEEE, 1988.

[150] S. Marshall. *Cities design and evolution*. Urban design and planning. Routledge, 2009.

[151] M. Mathias, A. Martinovic, J. Weissenberg, and L.V. Gool. Procedural 3d building reconstruction using shape grammars and detectors. In *3D Imaging, Modeling, Processing, Visualization and Transmission (3DIMPVT), 2011 International Conference on*, pages 304–311. IEEE, 2011.

[152] S. Matwin and T. Pietrzykowski. Prograph: a preliminary report. *Computer Languages*, 10(2):91–126, 1985.

[153] J.P. McCormack and J. Cagan. Supporting designers' hierarchies through parametric shape recognition. *Environment and Planning B*, 29(6):913–932, 2002.

[154] H. Meinhardt and M. Klingler. A model for pattern formation on the shells of molluscs. *Journal of Theoretical Biology*, 126(1):63–89, 1987.

[155] E. Mendez, G. Schall, S. Havemann, D. Fellner, D. Schmalstieg, and S. Junghanns. Generating semantic 3d models of underground infrastructure. *Computer Graphics and Applications, IEEE*, 28(3):48–57, 2008.

[156] Paul Merrell. Example-based model synthesis. In *I3D '07: Proceedings of the 2007 symposium on Interactive 3D graphics and games*, pages 105–112, New York, NY, USA, 2007. ACM.

[157] Paul Merrell and Dinesh Manocha. Continuous model synthesis. *ACM Transactions on Graphics*, 27(5):1–7, 2008.

[158] Paul Merrell, Eric Schkufza, Zeyang Li, Maneesh Agrawala, and Vladlen Koltun. Interactive furniture layout using interior design guidelines. *ACM Transactions on Graphics*, 30:87:1–87:10, July 2011.

[159] N. J. Mitra, L. Guibas, and M. Pauly. Partial and approximate symmetry detection for 3d geometry. In *ACM Transactions on Graphics*, volume 25, pages 560–568, 2006.

[160] F. Morgram and D. O'Sullivan. Using binary space partitioning to generate urban spatial patterns. In *4th International Conference on Computers in Urban Planning and Urban Management*, 2009.

[161] F. Morsdorf, E. Meier, B. Kötz, K.I. Itten, M. Dobbertin, and B. Allgöwer. Lidar-based geometric reconstruction of boreal type forest stands at single tree level for forest and wildland fire management. *Remote Sensing of Environment*, 92(3):353–362, 2004.

[162] Müller, Wonka, Haegler, Ulmer, and Van Gool. Procedural modeling of buildings. *ACM Transactions on Graphics*, 25(3):614–623, 2006.

[163] Pascal Müller, T Verneenooghe, Andy Ulmer, and Luc Van Gool. Spatial relations and grammars. In *International Workshop on Recording, Modeling and Visualization of Cultural Heritage*, pages 287–297, 2005.

[164] Pascal Müller, Peter Wonka, Simon Haegler, Andreas Ulmer, and Luc Van Gool. Procedural modeling of buildings. *ACM Transactions on Graphics*, 25(3):614–623, 2006.

[165] Pascal Müller, Gang Zeng, Peter Wonka, and Luc Van Gool. Image-based procedural modeling of facades. *ACM Transactions on Graphics*, 24(3):85, 2007.

[166] P. Musialski, P. Wonka, D.G. Aliaga, M. Wimmer, L. van Gool, W. Purgathofer, N.J. Mitra, M. Pauly, M. Wand, D. Ceylan, et al. A survey of urban reconstruction. In *Eurographics 2012-State of the Art Reports*, pages 1–28. The Eurographics Association, 2012.

[167] Radomír Měch and Przemyslaw Prusinkiewicz. Visual models of plants interacting with their environment. In *SIGGRAPH '96: Proceedings of the 23rd annual conference on Computer graphics and interactive techniques*, pages 397–410, New York, NY, USA, 1996. ACM.

[168] P. Mller, T. Vereenooghe, P. Wonka, I. Paap, and L. Van Gool. Procedural 3d reconstruction of puuc buildings in xkipch. In *Eurographics Symposium on Virtual Reality, Archaeology and Cultural Heritage (VAST)*, pages 139–146. EG, 2006.

[169] M. Nagl. Formal languages of labelled graphs. *Computing*, 16(1):113–137, 1976.

[170] M. Nagl, G. Engels, R. Gall, and W. Schäfer. Software specification by graph grammars. In *Graph-Grammars and Their Application to Computer Science*, pages 267–287. Springer, 1983.

[171] J. Nakielski. Tensorial model for growth and cell division in the shoot apex. *Pattern Formation in Biology, Vision and Dynamics*, pages 252–267, 2000.

[172] A. Nealen, T. Igarashi, O. Sorkine, and M. Alexa. Fibermesh: designing freeform surfaces with 3d curves. In *ACM Transactions on Graphics*, volume 26, page 41. ACM, 2007.

[173] Laycock University Of, R. G. Laycock, and A. M. Day. Automatically generating roof models from building footprints, 2003.

[174] R. Ohbuchi, M. Nakazawa, and T. Takei. Retrieving 3d shapes based on their appearance. In *Proceedings of the 5th ACM SIGMM international workshop on Multimedia information retrieval*, pages 39–45. ACM, 2003.

[175] M. Ovsjanikov, W. Li, L. Guibas, and N.J. Mitra. Exploration of continuous variability in collections of 3d shapes. In *ACM Transactions on Graphics*, volume 30, page 33. ACM, 2011.

[176] S. Owada, F. Nielsen, and T. Igarashi. Copy-paste synthesis of 3d geometry with repetitive patterns. In *Smart Graphics*, pages 184–193. Springer, 2006.

[177] P. Paczkowski, M.H. Kim, Y. Morvan, J. Dorsey, H. Rushmeier, and C. OSullivan. Insitu: sketching architectural designs in context. *ACM Transactions on Graphics*, 30(6):182, 2011.

[178] P. Palfrader, M. Held, and S. Huber. On computing straight skeletons by means of kinetic triangulations. *Algorithms–ESA 2012*, pages 766–777, 2012.

[179] Wojciech Palubicki, Kipp Horel, Steven Longay, Adam Runions, Brendan Lane, Radomír Měch, and Przemyslaw Prusinkiewicz. Self-organizing tree models for image synthesis. *ACM Transactions on Graphics*, 28(3):1–10, 2009.

[180] Yoav I. H. Parish and Pascal Müller. Procedural modeling of cities. In *SIGGRAPH '01: Proceedings of the 28th annual conference on Computer graphics and interactive techniques*, pages 301–308, New York, NY, USA, 2001. ACM.

[181] Yoav I. H. Parish and Pascal Müller. Procedural modeling of cities. In Eugene Fiume, editor, *Proceedings of ACM SIGGRAPH 2001*, pages 301–308. ACM Press, 2001.

[182] D.G. Parolek, K. Parolek, and P.C. Crawford. *Form-based codes: a guide for planners, urban designers, municipalities, and developers*. J. Wiley & Sons, 2008.

[183] G. Patow. User-friendly graph editing for procedural modeling of buildings. *Computer Graphics and Applications, IEEE*, 32(2):66 –75, march-april 2012.

[184] Mark Pauly, Niloy J. Mitra, Johannes Wallner, Helmut Pottmann, and Leonidas J. Guibas. Discovering structural regularity in 3d geometry. In *SIGGRAPH '08: ACM SIGGRAPH 2008 papers*, pages 1–11, New York, NY, USA, 2008. ACM.

[185] A. Peytavie, E. Galin, J. Grosjean, and S. Merillou. Arches: a framework for modeling complex terrains. In *Computer Graphics Forum*, volume 28, pages 457–467. Wiley Online Library, 2009.

[186] J.L. Pfaltz and A. Rosenfeld. Web grammars. In *Proceedings of the 1st international joint conference on Artificial intelligence*, pages 609–619. Morgan Kaufmann Publishers Inc., 1969.

[187] Pixologic. ZBrush. http://www.pixologic.com/zbrush, accessed (14/8/12).

[188] A. Plas, D. Comte, O. Gelly, and JC Syre. Lau system architecture: A parallel data driven processor based on single assignment. In *Proceedings of the International Conference on Parallel Processing*, pages 293–302, 1976.

[189] M. Pollefeys, L. Van Gool, M. Vergauwen, F. Verbiest, K. Cornelis, J. Tops, and R. Koch. Visual modeling with a hand-held camera. *International Journal of Computer Vision*, 59(3):207–232, 2004.

[190] H. Pottmann, Y. Liu, J. Wallner, A. Bobenko, and W. Wang. Geometry of multilayer freeform structures for architecture. In *ACM Transactions on Graphics*, volume 26, page 65. ACM, 2007.

[191] Helmut Pottmann, Qixing Huang, Bailin Deng, Alexander Schiftner, Martin Kilian, Leonidas Guibas, and Johannes Wallner. Geodesic patterns. *ACM Transactions on Graphics*, 29:43:1–43:10, July 2010.

[192] Helmut Pottmann, Alexander Schiftner, Pengbo Bo, Heinz Schmiedhofer, Wenping Wang, Niccolo Baldassini, and Johannes Wallner. Freeform surfaces from single curved panels. *ACM Transactions on Graphics*, 27(3):76:1–76:10, August 2008.

[193] P. PRUSINKIEWICZ. Graphical applications of l-systems. In *Canadian Information Processing Society Graphics Interface 1986*, pages 247–253, 1986.

[194] P. Prusinkiewicz and A. Lindenmayer. *The Algorithmic Beauty of Plants*. Springer Verlag, 1991.

[195] P. Prusinkiewicz, A. Lindenmayer, and J. Hanan. Development models of herbaceous plants for computer imagery purposes. In *ACM SIGGRAPH Computer Graphics*, volume 22, pages 141–150. ACM, 1988.

[196] Przemyslaw Prusinkiewicz, Mark James, and Radomír Měch. Synthetic topiary. In *SIGGRAPH '94: Proceedings of the 21st annual conference on Computer graphics and interactive techniques*, pages 351–358, New York, NY, USA, 1994. ACM.

[197] S. Pu and G. Vosselman. Knowledge based reconstruction of building models from terrestrial laser scanning data. *ISPRS Journal of Photogrammetry and Remote Sensing*, 64(6):575–584, 2009.

[198] M.J. Pugliese and J. Cagan. Capturing a rebel: modeling the harley-davidson brand through a motorcycle shape grammar. *Research in Engineering Design*, 13(3):139–156, 2002.

[199] M. Ramanathan and B. Gurumoorthy. Constructing medial axis transform of planar domains with curved boundaries. *Computer-Aided Design*, 35(7):619 – 632, 2003.

[200] M. Resnick, J. Maloney, A. Monroy-Hernández, N. Rusk, E. Eastmond, K. Brennan, A. Millner, E. Rosenbaum, J. Silver, B. Silverman, et al. Scratch: programming for all. *Communications of the ACM*, 52(11):60–67, 2009.

[201] R Ridorsa and G Patow. skylineEngine. http://ggg.udg.edu/skylineEngine/, accessed (10/1/13).

[202] N. Ripperda. Determination of facade attributes for facade reconstruction. *International Archives of Photogrammetry, Remote Sensing and Spatial Information Sciences*, 37(B3a):285–290, 2008.

[203] N. Ripperda and C. Brenner. Application of a formal grammar to facade reconstruction in semiautomatic and automatic environments. In *Proceedings of the 12th AGILE Conference on GIScience*, 2009.

[204] G. Rozenberg and A. Salomaa. *Handbook of formal languages: Beyond words*, volume 1. Springer Verlag, 1997.

[205] Adam Runions, Brendan Lane, and Przemyslaw Prusinkiewicz. Modeling trees with a space colonization algorithm. In *Eurographics Workshop on Natural Phenomena*, 2007.

[206] S. Said and M.R. Embi. A parametric shape grammar of the traditional malay long-roof type houses. *International Journal of Architectural Computing*, 6(2):121–144, 2008.

[207] T.W. Sederberg and S.R. Parry. Free-form deformation of solid geometric models. *ACM Siggraph Computer Graphics*, 20(4):151–160, 1986.

[208] A. Sharf, M. Alexa, and D. Cohen-Or. Context-based surface completion. In *ACM Transactions on Graphics*, volume 23, pages 878–887. ACM, 2004.

[209] B. Shizuki, M. Toyoda, E. Shibayama, and S. Takahashi. Smart browsing among multiple aspects of data-flow visual program execution, using visual patterns and multi-focus fisheye views. *Journal of Visual Languages and Computing*, 11(5):529–548, 2000.

[210] I. Shlyakhter, M. Rozenoer, J. Dorsey, and S. Teller. Reconstructing 3d tree models from instrumented photographs. *Computer Graphics and Applications, IEEE*, 21(3):53–61, 2001.

[211] P.G. Sibley, P. Montgomery, and G.E. Marai. Wang cubes for video synthesis and geometry placement. In *ACM SIGGRAPH 2004 Posters*, page 20. ACM, 2004.

[212] DC Simmonds. The design of the delta land-use modelling package. *Environment and Planning B*, 26:665–684, 1999.

[213] Loic Simon, Olivier Teboul, Panagiotis Koutsourakis, Luc Van Gool, and Nikos Paragios. Parameter-free/pareto-driven procedural 3d reconstruction of buildings from ground-level sequences. In *Computer Vision and Pattern Recognition*. IEEE, 2012.

[214] S.N. Sinha, D. Steedly, R. Szeliski, M. Agrawala, and M. Pollefeys. Interactive 3d architectural modeling from unordered photo collections. In *ACM Transactions on Graphics*, volume 27, page 159. ACM, 2008.

[215] Jeffrey Smith, Jessica Hodgins, Irving Oppenheim, and Andrew Witkin. Creating models of truss structures with optimization. *ACM Transactions on Graphics*, 21(3):295–301, July 2002.

[216] R.S. Smith, S. Guyomarc'h, T. Mandel, D. Reinhardt, C. Kuhlemeier, and P. Prusinkiewicz. A plausible model of phyllotaxis. *Proceedings of the National Academy of Sciences of the United States of America*, 103(5):1301–1306, 2006.

[217] D.B. Smythe. A two-pass mesh warping algorithm for object transformation and image interpolation. Technical report, ILM Computer GRaphcis Department, Lucasfilm, 1990.

[218] CNC Software. AutoCAD. www.mastercam.com, accessed (14/8/12).

[219] Side Effects Software. Houdini. http://www.sidefx.com/index.php, accessed (10/1/13).

[220] O. Šťava, B. Beneš, R. Měch, D.G. Aliaga, and P. Krištof. Inverse procedural modeling by automatic generation of l-systems. In *Computer Graphics Forum*, volume 29, pages 665–674. Wiley Online Library, 2010.

[221] J.S. Steyer, M. Boulay, and S. Lorrain. 3d external restorations of stegocephalian skulls using zbrush: The renaissance of fossil amphibians. *Comptes Rendus Palevol*, 9(6-7):463–470, 2010.

[222] G. Stiny. Ice-ray: A note on the generation of chinese lattice designs. *Environment and Planning B*, 4:89–98, 1977.

[223] G Stiny. Introduction to shape and shape grammars. *Environment and Planning B Planning and Design*, 7(3):343–351, 1980.

[224] G. Stiny. Spatial relations and grammars. *Environment and Planning B: Planning and Design*, 9(1):113–114, 1982.

[225] G Stiny and W J Mitchell. The palladian grammar. *Environment and Planning B: Planning and Design*, 5(1):5–18, January 1978.

[226] G. Stiny and W. J. Mitchell. The grammar of paradise: on the generation of mughal gardens. *Environment and Planning B*, 7:209–226, 1980.

[227] George Stiny and James Gips. Shape grammars and the generative specification of painting and sculpture. In *Segmentation of Buildings for 3DGeneralisation. In: Proceedings of the Workshop on generalisation and multiple representation , Leicester*, 1971.

[228] Kenichi Sugihara and Yoshitugu Hayashi. Automatic generation of 3d building models with multiple roofs. *Tsinghua Science and Technology*, 13(Supplement 1):368 – 374, 2008.

[229] J. Sun, X. Yu, G. Baciu, and M. Green. Template-based generation of road networks for virtual city modeling. In *Proceedings of the ACM symposium on Virtual reality software and technology*, pages 33–40. ACM, 2002.

[230] W.R. Sutherland. *On-line graphical specification of computer procedures*. PhD thesis, MIT, 1966.

[231] K. Takayama, R. Schmidt, K. Singh, T. Igarashi, T. Boubekeur, and O. Sorkine. Geobrush: Interactive mesh geometry cloning. In *Computer Graphics Forum*, volume 30, pages 613–622. Wiley Online Library, 2011.

[232] J.O. Talton, Y. Lou, S. Lesser, J. Duke, R. Měch, and V. Koltun. Metropolis procedural modeling. *ACM Transactions on Graphics*, 30(2):11, 2011.

[233] Mirela Tănase and Remco C. Veltkamp. A straight skeleton approximating the medial axis. 3221:809–821, 2004.

[234] S.L. Tanimoto and M.S. Runyan. Play: an iconic programming system for children. In *Visual Languages*, pages 191–205. Plenum Press: New York, 1986.

[235] D.A. Thadani, L. Krier, and A. Duany. *The language of towns & cities: a visual dictionary*. Rizzoli, 2010.

[236] J. M. Thijssen, H. J. F. Knops, and A. J. Dammers. Dynamic scaling in polycrystalline growth. *Phys. Rev. B*, 45(15):8650–8656, Apr 1992.

[237] D. Thompson, J. Braun, and R. Ford. *OpenDX: Paths to Visulization: Material Used for Learning OpenDX-the Open Derivate of IBM's Visualization Data Explorer*. Visualization an imagery solutions, 2001.

[238] RB Tilove and A.A.G. Requicha. Closure of boolean operations on geometric entities. *Computer-Aided Design*, 12(5):219–220, 1980.

[239] A. Toshev, P. Mordohai, and B. Taskar. Detecting and parsing architecture at city scale from range data. In *Computer Vision and Pattern Recognition (CVPR), 2010 IEEE Conference on*, pages 398–405. IEEE, 2010.

[240] Trimble. SketchUp. www.sketchup.com, accessed (14/8/12).

[241] Trimble. Trimble (formally google) warehouse. www.sketchup.google.com, accessed (14/8/12).

[242] K. Tuite, N. Snavely, D.Y. Hsiao, N. Tabing, and Z. Popovic. Photocity: Training experts at large-scale image acquisition through a competitive game. In *Proceedings of the 2011 annual conference on Human factors in computing systems*, pages 1383–1392. ACM, 2011.

[243] TurboSquid. Turbosquid.com. www.turbosquid.com, accessed (14/8/12).

[244] A. M. Turing. The chemical basis of morphogenesis. *Philosophical Transactions of the Royal Society of London. Series B, Biological Sciences*, 237(641):37–72, 1952.

[245] Alan M. Turing. On computable numbers, with an application to the Entscheidungsproblem. *Proceedings of the London Mathematical Society*, 2(42):230–265, 1936.

[246] N. Umetani, T. Igarashi, and N.J. Mitra. Guided exploration of physically valid shapes for furniture design. *ACM Transactions on Graphics*, 31(4):86, 2012.

[247] S. Upstill. *The renderman companion*. Addison-Wesley Reading, MA, 1990.

[248] C.A. Vanegas, D.G. Aliaga, and B. Benes. Building reconstruction using manhattan-world grammars. In *Computer Vision and Pattern Recognition (CVPR), 2010 IEEE Conference on*, pages 358–365. IEEE, 2010.

[249] C.A. Vanegas, D.G. Aliaga, B. Benes, and P. Waddell. Visualization of simulated urban spaces: Inferring parameterized generation of streets, parcels, and aerial imagery. *Visualization and Computer Graphics, IEEE Transactions on*, 15(3):424–435, 2009.

[250] C.A. Vanegas, D.G. Aliaga, P. Wonka, P. Müller, P. Waddell, and B. Watson. Modeling the appearance and behaviour of urban spaces. In *Computer Graphics Forum*, volume 29, pages 25–42. Wiley Online Library, 2010.

[251] Carlos A. Vanegas, Daniel G. Aliaga, Bedřich Beneš, and Paul A. Waddell. Interactive design of urban spaces using geometrical and behavioral modeling. *ACM Transactions on Graphics*, 28:111:1–111:10, December 2009.

[252] Carlos A. Vanegas, Tom Kelly, Basil Weber, Jan Halatsch, Daniel G. Aliaga, and Pascal Mller. Procedural Generation of Parcels in Urban Modeling. *Computer Graphics Forum*, 31(2):681–690, 2012.

[253] G Voronoi. Nouvelles applications des paramtres continus la thorie des formes quadratiques. *J. reine angew. Math.*, 133:97–178, 1907.

[254] E. Vouga, M. Höbinger, J. Wallner, TU Graz, TU Wien, and H. Pottmann. Design of self-supporting surfaces. *ACM Transactions on Graphics*, 31(4):XXX, August 2012.

[255] Paul Waddell. Urbansim: Modeling urban development for land use, transportation and environmental planning. In *Journal of the American Planning Association*, volume 68, pages 297–314, 2002.

[256] D. Walker and T. Daniels. *The Planners Guide to CommunityViz: The Essential Tool for a New Generation of Planning*. Orton Family Foundation Books. American Planning Association, 2011.

[257] He Wang and Taku Komura. Manipulation of flexible objects by geodesic control. *Computer Graphics Forum*, 31(2pt2):499–508, May 2012.

[258] Y. Wang, K. Xu, J. Li, H. Zhang, A. Shamir, L. Liu, Z. Cheng, and Y. Xiong. Symmetry hierarchy of man-made objects. In *Computer Graphics Forum*, volume 30, pages 287–296. Wiley Online Library, 2011.

[259] Ian Watson and John Gurd. A prototype data flow computer with token labelling. *Managing Requirements Knowledge, International Workshop on*, 0:623, 1979.

[260] Basil Weber, Pascal Mueller, Peter Wonka, and Markus Gross. Interactive geometric simulation of 4d cities. *Computer Graphics Forum*, April 2009.

[261] Li-Yi Wei and Marc Levoy. Fast texture synthesis using tree-structured vector quantization. In Kurt Akeley, editor, *Proceedings of ACM SIGGRAPH 2000*, pages 479–488. ACM Press, 2000.

[262] J. Wernecke. Open inventor c++ reference manual. *United States of America*, 1994.

[263] T. Werner and A. Zisserman. New techniques for automated architectural reconstruction from photographs. *Computer Vision ECCV 2002*, pages 808–809, 2002.

[264] Emily Whiting, John Ochsendorf, and Frédo Durand. Procedural modeling of structurally-sound masonry buildings. *ACM Transactions on Graphics*, 28(5):112:1–112:9, December 2009.

[265] Rohan Wickramasuriya, Laurie A. Chisholm, Marji Puotinen, Nicholas Gill, and Peter Klepeis. An automated land subdivision tool for urban and regional planning: Concepts, implementation and testing. *Environmental Modelling & Software*, (0):–, 2011.

[266] Wikipedia. Masdar city. http://en.wikipedia.org/wiki/Masdar-City accessed (3/8/13).

[267] S. Wolfram and M. Gad-el Hak. A new kind of science. *Applied Mechanics Reviews*, 56:B18, 2003.

[268] Stephen Wolfram. Statistical mechanics of cellular automata. *Rev. Mod. Phys.*, 55:601–644, Jul 1983.

[269] Peter Wonka, Michael Wimmer, François Sillion, and William Ribarsky. Instant architecture. In *SIGGRAPH '03: ACM SIGGRAPH 2003 Papers*, pages 669–677, New York, NY, USA, 2003. ACM.

[270] M. Woo, J. Neider, T. Davis, D. Shreiner, and OpenGL Architecture Review Board. *OpenGL Programming Guide*. Addison Wesley, 1999.

[271] K. Xu, H. Zheng, H. Zhang, D. Cohen-Or, L. Liu, and Y. Xiong. Photo-inspired model-driven 3d object modeling. In *ACM Transactions on Graphics*, volume 30, page 80. ACM, 2011.

[272] Kai Xu, Hao Zhang, Daniel Cohen-Or, and Baoquan Chen. Fit and diverse: Set evolution for inspiring 3d shape galleries. *ACM Transactions on Graphics*, 31(4):XXX, August 2012.

[273] Weiwei Xu, Jun Wang, KangKang Yin, Kun Zhou, Michiel van de Panne, Falai Chen, and Baining Guo. Joint-aware manipulation of deformable models. *ACM Transactions on Graphics*, 28(3):35:1–35:9, July 2009.

[274] Yong-Liang Yang, Yi-Jun Yang, Helmut Pottmann, and Niloy J. Mitra. Shape space exploration of constrained meshes. *ACM Transactions on Graphics*, 30:124:1–124:12, December 2011.

[275] X. Yin, P. Wonka, and A. Razdan. Generating 3d building models from architectural drawings: A survey. *Computer Graphics and Applications, IEEE*, 29(1):20–30, 2009.

[276] T. Yokomori. Stochastic characterizations of e0l languages. *Information and Control*, 45(1):26–33, 1980.

[277] S. Yoshizawa, A. Belyaev, and H.P. Seidel. Skeleton-based variational mesh deformations. In *Computer Graphics Forum*, volume 26, pages 255–264. Wiley Online Library, 2007.

[278] Lap-Fai Yu, Sai-Kit Yeung, Chi-Keung Tang, Demetri Terzopoulos, Tony F. Chan, and Stanley J. Osher. Make it home: automatic optimization of furniture arrangement. *ACM Transactions on Graphics*, 30:86:1–86:12, July 2011.

[279] K. Yue, R. Krishnamurti, and F. Gobler. Computation-friendly shape grammars. *Proceedings of CAAD futures*, 2009.

[280] Q.Y. Zhou and U. Neumann. Fast and extensible building modeling from airborne lidar data. In *Proceedings of the 16th ACM SIGSPATIAL international conference on Advances in geographic information systems*, page 7. ACM, 2008.